AD-A089 965 RENSSELAER POLYTECHNIC INST TROY NY MICROWAVE ACOUST--ETC F/G 17/2
SIGNAL PROCESSING USING SURFACE ACOUSTIC WAVE DEVICES AND ITS A--ETC(U)
DEC 79 D R ARSENAULT, L B MILSTEIN, P DAS DAAG29-77-G-0205
UNCLASSIFIED RPI-MA-ARO-10 ARO-15004.14-EL NL

1 of 4

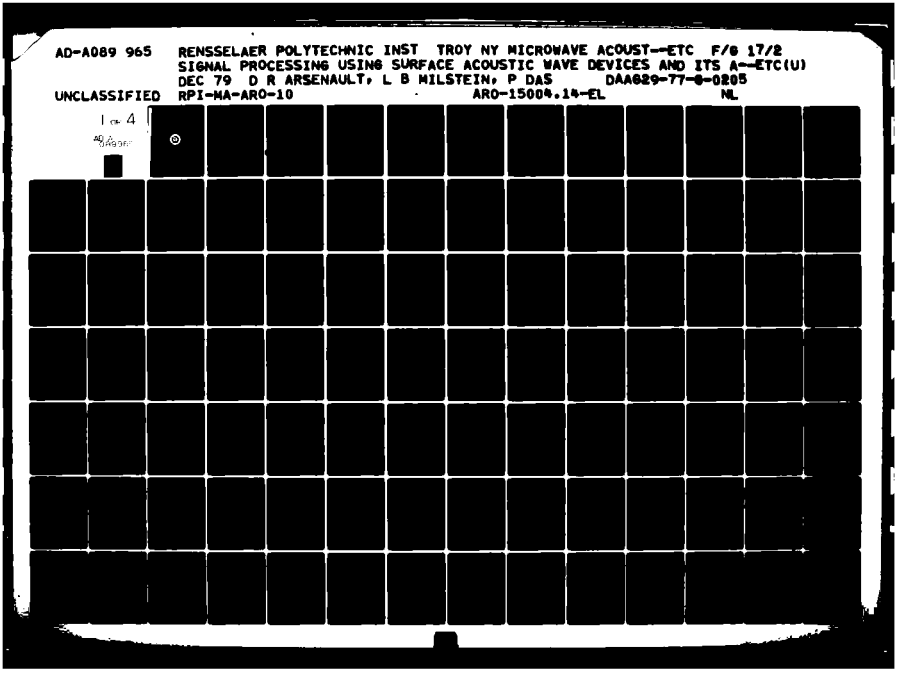

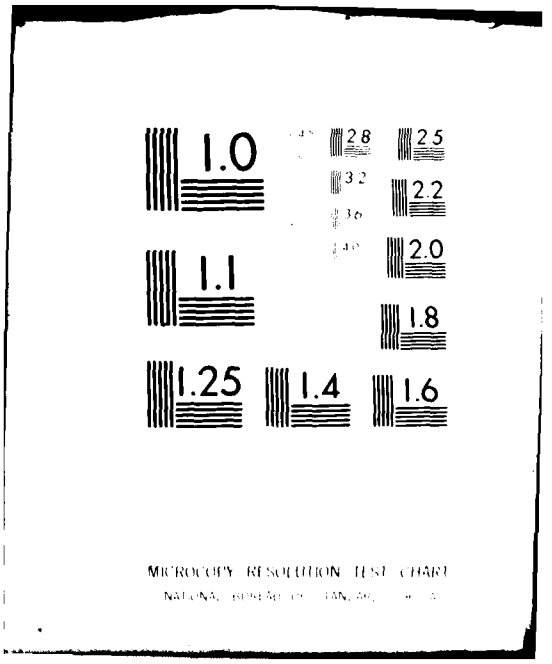
1.0
2.8
2.5
3.2
2.2
3.6
2.0
4.0
1.1
1.8
1.25
1.4
1.6
MICROCOPY RESOLUTION TEST CHART

ARO 15004.14-EL

(12)

SIGNAL PROCESSING USING SURFACE ACOUSTIC WAVE DEVICES AND ITS APPLICATION TO SPREAD SPECTRUM COMMUNICATION SYSTEMS

TECHNICAL REPORT MA-ARO-10

BY

D. R. ARSENAULT, L. B. MILSTEIN AND P. DAS

DECEMBER 13, 1979

U. S. ARMY RESEARCH OFFICE
GRANT DAAG-29-77-G-0205

ELECTRICAL AND SYSTEMS ENGINEERING DEPARTMENT
Rensselaer Polytechnic Institute
Troy, New York 12181

APPROVED FOR PUBLIC RELEASE;
DISTRIBUTION UNLIMITED.

SECURITY CLASSIFICATION OF THIS PAGE (When Data Entered)

REPORT DOCUMENTATION PAGE

READ INSTRUCTIONS BEFORE COMPLETING FORM

1. REPORT NUMBER: MA-ARO-10	2. GOVT ACCESSION NO.: AD-A089965
3. RECIPIENT'S CATALOG NUMBER:	
4. TITLE (and Subtitle): SIGNAL PROCESSING USING SURFACE ACOUSTIC WAVE DEVICES AND ITS APPLICATION TO SPREAD SPECTRUM COMMUNICATION SYSTEMS	5. TYPE OF REPORT & PERIOD COVERED: Technical Report
	6. PERFORMING ORG. REPORT NUMBER:
7. AUTHOR(s): D. R. Arsenault, L. B. Milstein and P. Das	8. CONTRACT OR GRANT NUMBER(s): DAAG-29-77-G-0205, NSF-ENG77-23652
9. PERFORMING ORGANIZATION NAME AND ADDRESS: Electrical and Systems Engineering Department, Rensselaer Polytechnic Institute, Troy, NY 12181	10. PROGRAM ELEMENT, PROJECT, TASK AREA & WORK UNIT NUMBERS: 11 13 Dec 79
11. CONTROLLING OFFICE NAME AND ADDRESS: U. S. Army Research Office, Post Office Box 12211, Research Triangle Park, NC 27719	12. REPORT DATE: December 13, 1979
	13. NUMBER OF PAGES: Three hundred seventeen (317)
14. MONITORING AGENCY NAME & ADDRESS(if different from Controlling Office): DAAG 29-77-G-0205, 14-EL	15. SECURITY CLASS. (of this report): UNCLASSIFIED 324
	15a. DECLASSIFICATION/DOWNGRADING SCHEDULE:

16. DISTRIBUTION STATEMENT (of this Report)

Approved for public release; distribution unlimited

17. DISTRIBUTION STATEMENT (of the abstract entered in Block 20, if different from Report)

18. SUPPLEMENTARY NOTES

The findings in this report are not to be construed as an official Department of the Army position, unless so designated by other authorized documents

19. KEY WORDS (Continue on reverse side if necessary and identify by block number)

spread spectrum communication system, adaptive, SAW technology, SAW convolver, signal processing, matched filter, correlator, Fourier transformer

20. ABSTRACT (Continue on reverse side if necessary and identify by block number)

Three Surface Acoustic Wave (SAW) devices, the separated-medium convolver, the memory correlator and the chirp filter are analyzed for signal processing applications. Emphasis is placed on convolution/correlation and Fourier transformation processes. The chirp filter theory is more general and applied equally well to chirp filters fabricated by alternate techniques.

In the SAW convolver there is a piezoelectric delay line. Two surface waves are introduced onto the delay line surface by interdigital transducers at its

DD FORM 1 JAN 73 1473 EDITION OF 1 NOV 65 IS OBSOLETE 41 0 427

UNCLASSIFIED

SECURITY CLASSIFICATION OF THIS PAGE (When Data Entered)

opposing ends. The two waves overlap beneath a semiconductor spaced above the surface and their fields interact with its charge carriers. A non-linear potential is produced and averaged over the semiconductor. From its back contact is obtained the time-compressed convolution of the two signals.

The memory correlator is similar to the convolver except that the semiconductor possesses a charge-storage mechanism. Also additional transducers are required for recovery of stored information.

One implementation of a SAW chirp filter consists of a piezoelectric crystal with grooves etched onto its surface. A surface wave, launched by an interdigital transducer, is selectively reflected to a second interdigital transducer situated alongside the first. The groove spacing for this Reflective Array Compressor (RAC) varies quadratically and a surface wave is reflected at a time linearly proportional to its carrier frequency producing a device impulse response having a quadratic phase variation.

The generation of three-dimensional ambiguity functions using a convolver is described with the criteria for its implementation. The equations for specific functions are given and these and others are generated experimentally by this technique. The basic process is the generation of a 'slow chirp' by applying a 'slow ramp' to a VCO. The 'slow chirp' modifies the signal center frequency and the 'slow ramp' is summed to the convolver output before display. The design for a specific range/Doppler response by modification of the waveform while monitoring the ambiguity function is demonstrated.

Chirp transformation using a convolver is also described. The relationships for its realization are derived and experimental Fourier transforms are shown. Inverse transformation results are given where signals are corrupted by monochromatic noise and time gating of their transforms prior to inversion eliminates the noise from the signals.

A general formulism is developed for the memory correlator where the device outputs and stored charge are related to the interaction between surface waves, stored charge and applied fields. The convolution/correlation type relationships are developed from which the duality of output convolution versus stored correlation arises. Some experimental results with surface states and PN diodes are given where a modified device package required for uniformity and ease of sample substitution is described. An application whereby an ambiguity function is generated using a stored reference is demonstrated.

Chirp transformation with chirp filters is analyzed in detail. Chirp-generated Fourier transform modification is also discussed. The transformation capability of these systems is demonstrated by showing actual waveforms. More complex systems, correlating receivers, where autocorrelations are obtained by inverse transforming transform products, are demonstrated. Probability-of-error data is used to assess the performance of a particular correlating receiver. Outputs from a correlating receiver capable of operating on contiguous data are shown.

An appendix covering chirp-transformation-related topics has been included. There is an extensive analysis of the Fresnel transform and a discussion on the generation of other transforms using these devices.

Preface

This technical report was prepared by the Microwave Acoustics Laboratory, Electrical and Systems Engineering Department of Rensselaer Polytechnic Institute, Troy, New York. The partial support for this work came from Army Research Office Grant No. DAAG-29-77-G-0205 (monitored by Dr. W. Sander, ARO) and National Science Foundation Grant No. ENG 77-23658 (monitored by Dr. J. Harris).

This report summarizes the work related to the real time signal processing and other applications of devices based on the acousto-electric interaction and chirp impule response using SAW. Part of this work has already been published in references (Arsenault, 1977), (Arsenault, 1978), (Das, 1976), (Das, 1977), (Das, 77 Ultrason. Symp.), (Das, 1977 NTC), (Das, 1978), (Milstein, 1978), (Milstein, 1977), (Milstein, 1978 NTC) and other parts will be published in the near future. The objective of this report is to present all the information in one place coherently.

Mr. R. T. Webster, Mr. Colin Lanzl and many students in the Laboratory have provided help in experimental set-up from time to time. Finally, most of this report forms the Ph.D. Thesis of Mr. D. R. Arsenault whose present address is Lincoln Laboratory, MIT, Lexington, MA.

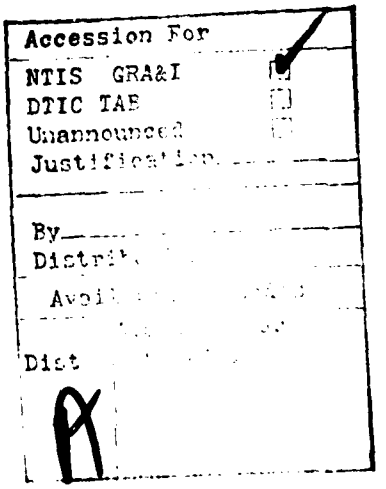

ABSTRACT

Three Surface Acoustic Wave (SAW) devices, the separated-medium convolver, the memory correlator and the chirp filter are analyzed for signal processing applications. Emphasis is placed on convolution/correlation and Fourier transformation processes. The chirp filter theory is more general and applies equally well to chirp filters fabricated by alternate techniques.

In the SAW convolver there is a piezoelectric delay line. Two surface waves are introduced onto the delay line surface by interdigital transducers at its opposing ends. The two waves overlap beneath a semiconductor spaced above the surface and their fields interact with its charge carriers. A non-linear potential is produced and averaged over the semiconductor. From its back contact is obtained the time-compressed convolution of the two signals.

The memory correlator is similar to the convolver except that the semiconductor possesses a charge-storage mechanism. Also additional transducers are required for recovery of stored information.

One implementation of a SAW chirp filter consists of a piezoelectric crystal with grooves etched onto its surface. A surface wave, launched by an interdigital transducer, is selectively reflected to a second interdigital transducer situated alongside the first. The groove spacing for this Reflective Array Compressor (RAC) varies quadratically and a surface wave is reflected at a time linearly proportional to its carrier frequency producing a device impulse response having a quadratic phase variation.

The generation of three-dimensional ambiguity functions using a convolver is described with the criteria for its implementation. The equations for specific functions are given and these and others are generated experimentally by this technique. The basic process is the generation of a 'slow chirp' by applying a 'slow ramp' to a VCO. The 'slow chirp' modifies the signal center frequency and the 'slow ramp' is summed to the convolver output before display. The design for a specific range/Doppler response by modification of the waveform while monitoring the ambiguity function is demonstrated.

Chirp transformation using a convolver is also described. The relationships for its realization are derived and experimental Fourier transforms are shown. Inverse transformation results are given where signals are corrupted by monochromatic noise and time gating of their transforms prior to inversion eliminates the noise from the signals.

A general formulism is developed for the memory correlator where the device outputs and stored charge are related to the interaction between surface waves, stored charge and applied fields. The convolution/correlation type relationships are developed from which the duality of output convolution versus stored correlation arises. Some experimental results with surface states and PN diodes are given where a modified device package required for uniformity and ease of sample substitution is described. An application whereby an ambiguity function is generated using a stored reference is demonstrated.

Chirp transformation with chirp filters is analyzed in detail. Chirp-generated Fourier transform modification is also discussed. The transformation capability of these systems is demonstrated by showing

actual waveforms. More complex systems, correlating receivers, where autocorrelations are obtained by inverse transforming transform products, are demonstrated. Probability-of-error data is used to assess the performance of a particular correlating receiver. Outputs from a correlating receiver capable of operating on contiguous data are shown.

An appendix covering chirp-transformation-related topics has been included. There is an extensive analysis of the Fresnel transform and a discussion on the generation of other transforms using these devices.

PART I

INTRODUCTION AND HISTORICAL REVIEW

Convolution and Fourier transformation are utilized extensively for the analysis of signals and the design of systems employed specifically for communications and radar applications. For instance, the Fourier transform of the impulse response of a linear time-invariant system is its transfer function. The Fourier transform of the output of the linear system is the Fourier transform of the input multiplied by this transfer function. In the time domain this output is the convolution of the input signal with the system impulse response. In general, when two signals are convolved in the time domain their Fourier transforms are multiplied in the Fourier (or frequency) domain and, due to symmetry, when two signals are multiplied in the time domain their Fourier transforms are convolved in the Fourier domain. Since a system input is convolved with the system impulse response, it may be more desirable to multiply, in the frequency domain, the Fourier transform of the input signal with the system transfer function. The Fourier transform of a signal contains the magnitudes and phases of infinite duration sines and cosines which, when summed together, produce this signal exactly. When the signal is written as this infinite sum of sines and cosines, each component can be treated independently in a linear system since the output of this system is due to the superposition of every input component. The transfer function of a system is essentially its frequency response, from which both the magnitude and phase response of the system for every frequency component can be found. The Fourier transformation of a linear differential equation describing some linear

system produces an algebraic equation that is much easier to solve. Convolution is the basic principle behind the technique of matched filtering, whereby a signal is convolved with its time complement to produce a maximum output when the two signals are fully correlated. This technique is heavily relied upon in spread spectrum systems and radar receivers where large correlation gains make it possible to transmit signals that are imperceptable and high range and Doppler resolution can be obtained with moderate signal power levels. Furthermore, the shape of the output correlation (i.e. convolution for which one of the signals is time reversed) from a correlating receiver as a function of Doppler shift produces a three-dimensional figure whose form indicates the range and Doppler resolution capability of the signal utilized for the particular radar application. For these reasons and many others, convolution and Fourier transformation form the backbones for the analysis of most systems utilized for the processing of information (Papoulis, 1968) (Papoulis, 1977) (Skolnik, 1970) (Cook, 1967) (Rihaczek, 1969).

Due to the importance of convolution and Fourier transformation as signal processing tools and in particular due to the versatile properties of the Fourier transform (namely its symmetry, conjugation, scaling, modulation, shifting, moment, derivative, energy and convolution theorems), it would be highly desirable to possess the capability to perform these functions in real time with relatively small devices at high frequencies using a minimum of power and back-up equipment. Up until now the computer has been the main mechanism for their realization. Although computers are continually increasing in speed while decreasing in size, they are just beginning to perform fast enough for real-time applications. It will

furthermore be quite a while before such units are developed to the point where they are small in size as well as in power consumption. Also, they are inherently complex units and it will take a while before they can perform satisfactorily in the microwave domain. Charge-coupled devices (CCD's) are demonstrating the potential for meeting all the desirable requirements although they are still essentially baseband devices, are complicated at the initial design stage and are inherently active devices. There are, however, devices that can meet all the criteria and are the result of the growing surface acoustic wave (SAW) technology. In particular, the process of convolution is directly performed by the so-called SAW separated-medium convolver which is one of the devices that is examined in detail in this thesis. The second device, generally called a chirp filter, is the basic element in the realization of the signal processing techniques utilized in most of the remaining portion of this work. This device, an example of which is the SAW reflective array compressor (or RAC), is heavily relied upon for the realization of the Fourier transform. The bulk of this work is essentially dedicated to the analysis of these two surface wave devices and attempts to demonstrate their potential as invaluable signal processing elements.

SAW devices consist of crystals having at least one surface upon which a surface wave can propagate. A surface wave is a special type of wave where the mechanical energy of the wave is confined to within a few wavelengths of the crystal surface. This type of wave can be compared to earthquake-propagating waves and most of the analytical foundation has evolved from work done in this area. The crystals used for surface wave devices are typically anisotropic and in such crystals

there are only so many directions in which the surface wave and its energy will propagate along the same path (i.e. normal mode directions). Although surface waves may be excited on virtually any crystalline surface, it is the piezoelectric substrates that are easiest to use and possess the most desirable characteristics. This is due to the ease in which surface waves can be made to propagate on these substrates using interdigital transducers. These transducers initiate SAW propagation by impressing time varying electric fields having alternating polarities between the individual transducer fingers onto the substrate. The surface waves on these crystals possess electric fields that propagate with the waves and evanesce above the piezoelectric substrate surface. The electrical energy is small in comparison to the mechanical energy and is dependent and proportional to the coupling constant of the material (i.e. .0241 for YZ $LiNbO_3$ used for many applications due to its large coupling constant) which is given by the ratio of the change in velocity of the surface wave when a metal (shorting) plane is deposited on the surface (with negligible damping due to mass loading) to the unshorted intrinsic velocity of the surface wave on the bare crystal surface. The shorted velocity is always slower since piezoelectricity always tends to stiffen the elastic surface. The velocity of a surface wave is typically 10^5 times slower than the equivalent electromagnetic wave (3488 m/sec for YZ $LiNbO_3$). The attenuation of these waves is small in comparison to electromagnetic wave attenuation for the equivalent number of wavelengths of propagation (i.e. ≈ .01 dB per 3 μ sec of propagation or about 1 cm for YZ $LiNbO_3$ at 100 Mhz which is eq ivalent to a 34.9 μm wavelength or about 300 wavelengths per cm). The attenuation of the waves increases

dramatically, however, up into the Ghz range (i.e. ≈ 1 dB per cm for YZ $LiNbO_3$ at 1 GHz) and the wavelength becomes too small for efficient transducer deposition (done photolithographically using ≈ 2000 Å of aluminum) whose fingers are a quarter wavelength wide (i.e. ≈ .87 μm for YZ $LiNbO_3$ at 1 GHz). Although devices have been fabricated in this range, the typical limit is somewhere in the lower Ghz range due to the above limitations.

The basic usage for these devices is that of piezoelectric delay lines. By designing special transducers utilizing variable finger lengths or withdrawn fingers, virtually any desirable finite impulse response filter can be designed having extremely linear phase characteristics. By varying the spacings between the transducer fingers, variable phase responses can be built into these filters so that Linear-FM or chirp filters can be realized. Due to bulk wave distortions, however, a better mechanism for realizing chirp filters utilizes surface wave reflections from gratings etched into the surface of the delay line (i.e. the reflective array compressor or RAC). This technique has also been used to fabricate high Q (in the tens of thousands) resonant cavity devices (or resonators). Then there are the devices, of which the separated-medium convolver is an example, that produce an output by the interaction of the SAW electric fields with the carriers in a slice of semiconductor adjacent to the piezoelectric delay line surface or the carriers within a piezoelectric/semiconductor substrate. These are the so-called acousto-electric devices of which the SAW amplifier is also representative. A variety of other types of devices have been conceived and fabricated utilizing these surface wave techniques

(Matthews, 1977) (Kino, 1976) (Oliner, 1978). The signal processing area has benefitted greatly due to the advent of SAW technology (Kino, 1971) (Maines, 1976) (Ash, 1978) (Hays, 1976). Many devices have been devised and implemented for use in radar applications (Maines, 1977) and for spread spectrum communications (Collins, 1976) (Unkauf, 1977). The excellent performance of chirp transformation anti-jam receivers (Arsenault, 1978) (Milstein, 1978) and the potential for the integration of SAW with CCD's (Whitehouse, 1973) open-up new avenues for the processing of information.

The SAW convolver has undergone several stages of development over the past years up to its presently accepted form, although its predecessors are again being investigated as devices having the potential for low cost production. The first of such devices utilized the non-linearities in the crystal itself to obtain a second order mixing between two counter-propagating surface waves. This second order output was typically integrated over by a metallic plate or an interdigital type of contact at twice the periodicity of the difference in frequency between the two waves. The device is essentially an 'elastic convolver' (Quate, 1970) (Luukkala, 1971) (Kino, 1973). The output of such a device was quite small and led to the investigation of an enhanced non-linearity mechanism. (The 'elastic convolver', however, is being reinvestigated (Becker, 1979), since surface waves can be concentrated into higher power-density modes, thereby increasing the second order non-linearity. By proper guiding structures such devices have been shown to perform almost as efficiently as the separated-medium convolver.) It was found that the second order non-linearity was greatly enhanced (in the absence

of beam concentration) by the interaction of the SAW fields with charge carriers in a semiconductor and led to the piezoelectric-semiconductor convolvers (Wang, 1972) (Turner, 1971) and the separated-medium convolvers (Wang, 1972) (Yamanishi, 1972) which are the subject of an appreciable portion of this thesis. The theory for the SAW separated-medium convolver has undergone significant development over the past years (Otto, 1976) (Gautier, 1977). Section 2.1 of this report is an attempt to organize the theory in a way that allows one to visualize the interaction between two information bearing surface waves and thereby witness the evolution of a device-characteristically-weighted output convolution amidst a series of distortion terms. This theory does not attempt to materialize the individual spatial and frequency dependent functions describing wave propagation and the physics of the device (which can be found in one form or another in the literature) but attempts to show where and how these functions relate to the total device output and the spectral symmetry relationships that these functions must obey for a physically realizable device. The output of the device obtained in this follow-through fashion is then compared with the output obtained by a converse technique whereby a function is assumed to exist that describes the weighting between any two frequency components of the two convolver input signals. Fourier transformation theory and moment expansions are utilized extensively throughout this section along with the approximation that spatially varying device characteristics vary much more slowly than the spatial frequencies of the surface waves and are therefore separable functions. Most of the functions describing various aspects of device physics can be derived from numerous sources investigating specific phenomena such as

the accumulation of charge at the silicon surface facing the surface of the piezoelectric delay line (Smith, 1973). Note that another convolver structure has also been developed and should be mentioned based upon the tapped delay line structure (Reeder, 1973). The discrete device utilizes individual diodes at each tap (i.e. interdigital transducers) along the piezoelectric delay line surface to perform the non-linearity. The diode outputs are summed to produce the convolution between two surface waves.

The realization of convolvers by utilizing the principles of surface wave propagation has presented the possibility for a wide variety of applications. Ambiguity function generation was demonstrated by Das (Das, 1974) utilizing the separated-medium convolver. The process is improved upon in this thesis, whereby the ambiguity functions are shown to be easily displayed in three dimensions (amplitude vs. frequency or Doppler shift vs. time or range) utilizing a 'slow ramp' and chirp. The analysis of this process is presented along with analytical and experimentally generated ambiguity functions. Some experimental results are given that specifically demonstrate the dynamic design capability of such a convolver implementation (Das, 1978). Another powerful convolver application is the generation of Fourier transforms based upon the chirp transformation algorithm (Otto, 1972). In Section 2.5 of this report an analysis for the implementation of the convolver chirp transform is presented. In Section 3.1 experimental results are given showing some chirp-modulated output Fourier transforms from such a system. Also shown are results demonstrating the time-gating of the Fourier transform resulting in a filtered output obtained by inverse-Fourier transforming the gated Fourier transform. Literature related to these results have

been published concerning the topics of non-destructive testing (NDT) for distortion elimination (Tiemann, 1976) and the implementation of adaptable receivers (Das, 1975) (Milstein, 1977) both of which are based upon the utilization of the SAW convolver and the chirp transform. A modification to the convolver structure is utilized to produce the memory correlator. This convolver has the capability for signal storage by some form of charge storage mechanism along the surface of the semiconductor in a separated-medium convolver structure. The preliminary work in this area consisted of utilizing semiconductor surface states (Bers, 1974). Some experimental results obtained using the surface states found in untreated slices of 40 Ω-cm silicon are shown in Section 3.1 of this report. The storage times were found to be quite small (≃ 25 μs) for these states which led to the use of diode arrays whereby charge is stored through the imposition of a forward biasing field and then held for tens of milliseconds (and seconds at cryogenic temperatures) by the high back resistance of the diodes. This report presents some results obtained using PN diode vidicon arrays in a convolver package intended to facilitate vidicon array removal and possess the capability to maintain uniform interactions. These results demonstrated the ability to generate ambiguity functions with a stored reference. Section 2.3, furthermore, presents a general formalism for the operation of the convolver in the presence of a charge storage mechanism and with fields imposed within the interaction region by potentials applied directly to the semiconductor. The form of the direct output signals, the spatially stored signals and those recalled at a later time are all presented within this framework. This analysis

is based upon the results obtained over the years in conjunction with the memory correlator. Not only has work been done utilizing PN diodes (Defranould, 1976) (Das, 1977), but Schottky diodes are now being extensively used (Ingebrigtsen, 1975) due to their faster response times and structural simplicity. Theories detailing the influence of the device physics on its output are evolving in this area (Kino, 1976) and devices such as the coherent integrator, whereby the signal to noise ratio of a repetitive signal is improved by the integration in storage and the integrating correlator in which signals thousands of times the length of the convolver interaction time can be integrated producing a piece of the correlation of duration equal in length to the interaction time (Ralston, 1977) are now beginning to leave the laboratory and enter the applications stage. Most of these new devices are utilizing third and higher order convolver interactions in order to reduce the background spurious components stored along with the desired information.

The surface wave chirp filter and its implementation in the generation of real-time Fourier transforms is studied extensively in the remainder of this report. Chirp filters evolved from phase weighted interdigital transducer devices (Gerard, 1973) (Gerard, 1977) to devices utilizing selective reflections from quadratically spaced arrays of grooves (Williamson, 1973) (Williamson, 1977). These latter devices called reflective array compressors or RAC's were greatly influenced by research related to the development of the IMCON's (IMpedance CONtrol devices) at Andersen Laboratory (Martin, 1973) (Martin, 1976). The IMCON is a chirp filter that utilizes groove array reflections, but the wave is a bulk wave in a thin metal sheet. Due to the close similarity

in the operation of these devices to that of RAC devices, the analysis of their implementation for signal processing applications is identical in either case. IMCON's were used for the demonstration of chirp filter principles in this report due to their ready availability. (They were supplied on loan by Andersen Laboratory.)

The chirp filter is finding wide applications in the area of signal processing (Nudd, 1975). Systems utilizing these devices have been demonstrated, such as a variable bandwidth filter (Maines, 1975), a variable delay line (Dolat, 1976) and a programmable pulse compression filter (Gerard, 1977). One application that utilizes the Fresnel transformation input/output relationship of the chirp filter has been demonstrated in Section 3.2 of this report whereby any desirable portion of a continuous signal is selectively time-inverted (Arsenault, 1977). The Fresnel aspect of chirp filters has essentially evolved from the work related to this thesis. A detailed documentation of the Fresnel transform, its properties and relationships, was derived specifically for this work and is found in its complete form in Appendix A. Although no such analysis technique has been developed to date, this Fresnel analysis was performed with the intention of developing a chirp system analysis technique similar in form to the applicability of Fourier analysis to the general design and analysis of linear systems.

A very important application of the chirp filter is its utilization in a chirp transformation system (Atzeni, 1975) (Hays, 1975). A useful application of the Fourier transforms obtained using these

devices has been demonstrated in this thesis by the selective time gating of monochromatic noise from an NDT (non-destructive testing) reflection (Das, 1978) and by implementating the process into a variety of correlating receiver structures (Das, 1977) (Arsenault, 1978) (Milstein, 1977) (Milstein, 1978). The basic transformation process was demonstrated elsewhere in the literature (Otto, 1976) where it has also been utilized for network analysis (Jack, 1976). Continuous transformation has been demonstrated in this work and although the continuous transform streams in the receiver demonstrated in Section 3.3 of this report were not separated into real and imaginary components, the system demonstrated the ability to perform three Fourier transformations, two to obtain the product-of-transforms and one to take the inverse transform of this product and thereby obtain the correlation of the input signal with a reference. This system represented the incorporation of techniques developed in a variety of receiver structures that are also documented in Section 3.3. The chirp filter chirp transformation process is discussed at length in Section 2.4 and the effect upon a signal by the modification of its chirp-generated Fourier transform is discussed in Section 2.6. Finally, the ability to generate a wide variety of other transforms utilizing the convolver and chirp filter is discussed in the Appendix. In this appendix the techniques for generating a number of the more popular transforms (Sneddon, 1972) are dwelled upon. Much of the discussion is based upon time scaling which has already been utilized for the generation of the Mellin transform in the area of optical signal processing (Casasent, 1977).

PART 2

THEORY

2.1 The SAW Separated Medium Convolver Input/Output Relationship

A signal f(t) is applied to one input of the convolver and a signal g(t) is applied to the other. Before producing an output from this device both signals must pass through input transducer matching networks (which may be only single inductors) after which they are transformed by their respective transducers into surface waves that propagate toward one another. The electric fields that propagate with these traveling surface waves interact non-linearly (when the waves overlap) with the charge carriers in the semiconductor (that is supported above the piezoelectric delay line) so as to produce a time and space varying current density within this semiconductor that is proportional, at any point in time and space, to the product of the fields of the two contrapropagating signals at that point in time and space. This non-linear current density produces a potential that is related linearly to the current through the average semiconductor conductivity and is also a function of time and space. The back ohmic contact of the semiconductor averages out this spatially varying potential at every point in time and the resultant time varying signal is transmitted through the output matching network of the convolver whereby it is sensed as the output of the device.

The two convolver inputs can be written as infinite sums of cosines as follows (where the $1/2\pi$ will be ignored in all the equations)

$$f(t) = \int_0^\infty A_f(\omega)\cos(\omega t + \phi_f(\omega))d\omega \qquad (1.1)$$

$$g(t) = \int_0^\infty A_g(\omega)\cos(\omega t + \phi_g(\omega))d\omega \qquad (1.2)$$

Since both these signals are undoubtedly real, then from Fourier analysis

$$A(\omega) = A(-\omega) \ , \quad \phi(\omega) = -\phi(-\omega) \tag{1.3}$$

so that Eqs. (1.1) and (1.2) can be rewritten as

$$f(t) = \int_{-\infty}^{\infty} A_f(\omega)e^{j\phi_f(\omega)} \ e^{j\omega t} \ d\omega \quad = \int_{-\infty}^{\infty} F(\omega)e^{j\omega t} \ d\omega \longleftrightarrow F(\omega) \tag{1.4}$$

and

$$g(t) = \int_{-\infty}^{\infty} A_g(\omega)e^{j\phi_g(\omega)} \ e^{j\omega t} \ d\omega \quad = \int_{-\infty}^{\infty} G(\omega)e^{j\omega t} \ d\omega \longleftrightarrow G(\omega) \tag{1.5}$$

where

$$F(\omega) = \int_{-\infty}^{\infty} f(t)e^{-j\omega t} \ dt = A_f(\omega)e^{j\phi_f(\omega)} = F^*(-\omega) \tag{1.6}$$

and

$$G(\omega) = \int_{-\infty}^{\infty} g(t)e^{-j\omega t} \ dt = A_g(\omega)e^{j\phi_g(\omega)} = G^*(-\omega) \tag{1.7}$$

are the Fourier transforms of f(t) and g(t), respectively.

The transducers and their matching networks have impulse responses $m_f(t)$ and $m_g(t)$ for the f(t) and g(t) inputs, respectively. These responses are surface waves injected onto the surface of the delay line. (Impulses applied to the transducers produce surface wave displacements $m_f(t)$ and $m_g(t)$ at points on the surface immediately following the transducers.) Therefore, the signals injected onto the delay line at each transducer can be written as*

$$f_1(t) = f(t) * m_f(t) = \int_{-\infty}^{\infty} f(\tau)m_f(t-\tau)d\tau$$

$$= \int_{-\infty}^{\infty} F(\omega)M_f(\omega)e^{j\omega t} \ d\omega \tag{1.8}$$

and

$$g_1(t) = g(t) * m_g(t) = \int_{-\infty}^{\infty} g(\tau)m_g(t-\tau)d\tau$$

* Capital letters denote Fourier Transform. For example the Fourier Transform of $m_f(t)$ is $M_f(\omega)$.

$$= \int_{-\infty}^{\infty} G(\omega)M_g(\omega)e^{j\omega t}\, d\omega \tag{1.9}$$

If the direction of propagation is the z direction and $f_1(t)$ and $g_1(t)$ are injected at $z = -\delta_f$ and $z = L + \delta_g$, respectively, where δ_f and δ_g are the distances between each transducer and its nearest semiconductor edge and L is the length of the semiconductor, then

$$f_1(t) = f_1(t, z = -\delta_f) \tag{1.10}$$

and

$$g_1(t) = g_1(t, z = L + \delta_g) \tag{1.11}$$

If the intrinsic loss of the piezoelectric delay line (loss in the absence of any close-proximity perturbing medium such as the semiconductor) is given by α_o, then $f_1(t)$ and $g_1(t)$ will decay by a_f and a_g, respectively, after propagating to their nearest semiconductor edges where

$$a_f = e^{-\alpha_o \delta f} \tag{1.12}$$

and

$$a_g = e^{-\alpha_o \delta g} \tag{1.13}$$

and diffraction effects are ignored (perfectly parallel wave fronts assumed). The signals at the semiconductor edges can be written as

$$f_2(t, z = 0) = a_f \int_{-\infty}^{\infty} F(\omega)M_f(\omega)e^{-jk_o\delta f}\, e^{j\omega t}\, d\omega \tag{1.14}$$

and

$$g_2(t, z = L) = a_g \int_{-\infty}^{\infty} G(\omega)M_g(\omega)e^{-jk_o\delta g}\, e^{j\omega t}\, d\omega \tag{1.15}$$

where

$$k_o = \omega/v_o \tag{1.16}$$

and

v_o = free surface (intrinsic) SAW velocity .

If x is the direction parallel to the wave fronts, diffraction effects could have been included by utilizing weighting functions at z = 0 and z = L that are functions of both x and ω. Since surface waves beneath the semiconductor tend to remain collimated by the waveguiding properties of the semiconductor/ground plane combination and even the semiconductor support rails (if they are used), all spatial variations will typically be slowly varying functions of space in comparison to the spatial wavelength of the signal. These spatial variations due to waveguide moding and diffraction will therefore be included in the spatial functions $S_f(x,z,\omega)$ and $S_g(x,z,\omega)$ for f(t) and g(t), respectively. In other words, if it is assumed that the spatial dependences of any CW component of the signals f(t) or g(t) at frequency ω in the x and z directions is forced to be constant for that component by the waveguiding action of the semiconductor piezoelectric convolver structure (which forces the component to propagate in a well defined mode that may or may not be a function of frequency), then each component of the signal can be multiplied by a constant spatial function in x and z for that particular frequency where any spatial variation will be assumed slow compared to the spatial frequency of that component beneath the semiconductor.

Beneath the semiconductor, besides being weighted by the spatial functions $S_f(x,z,\omega)$ and $S_g(x,z,\omega)$, the surface wave components at any point have undergone attenuation, from the time they have entered beneath the semiconductor, that is frequency dependent due to the presence of the semiconductor. This attenuation factor is given by the sum of the

intrinsic piezoelectric attenuation and a frequency dependent term, namely

$$\alpha(\omega) = \alpha_o + \alpha_1(\omega) \tag{1.17}$$

Furthermore, any component at any point z beneath the semiconductor is delayed by an amount $\delta_f/v_o + z/v(\omega)$ for f(t) and $\delta_g/v_o + (L-z)/v(\omega)$ for g(t) where $v(\omega)$ is the velocity of that component which is also frequency dependent due to the presence of the semiconductor.

Incorporating this information, the signals seen at any point z beneath the semiconductor can be written as

$$f_3(x,z,t) = a_f \int_{-\infty}^{\infty} F(\omega)M_f(\omega)S_f(x,z,\omega)e^{-jk_o(\delta_f+z)}\ e^{-j\beta(\omega)z}\ e^{j\omega t}\ d\omega \tag{1.18}$$

and

$$g_3(x,z,t) = a_g \int_{-\infty}^{\infty} G(\omega)M_g(\omega)S_g(x,z,\omega)e^{-jk_o(\delta_g+L-z)}$$

$$e^{-j\beta(\omega)(L-z)}\ e^{j\omega t}\ d\omega \tag{1.19}$$

where

$$\beta(\omega) = k_1(\omega) - j\alpha(\omega) \tag{1.20}$$

$$k(\omega) = k_o + k_1(\omega)$$

$$= \omega/v(\omega) \tag{1.21}$$

and

$$v(\omega) = v_o - v_1(\omega) \tag{1.22}$$

since the piezoelectrically 'stiffened' surface wave velocity is decreased due to the presence of the semiconductor representing an increase in the spatial frequency $k(\omega)$. Note that

$$\frac{k_1(\omega)}{k_o} = \frac{v_1(\omega)}{v_o - v_1(\omega)} \simeq \frac{v_1(\omega)}{v_o} \tag{1.23}$$

so that the ratio of the change in spatial frequency to the intrinsic value

is approximately given by the ratio of the change in velocity to the intrinsic velocity at any frequency ω since the change in velocity is typically quite small. The signal equations given by Eqs. (1.18) and (1.19) represent the signal seen at any point (x,z) beneath the semiconductor at the surface of the piezoelectric delay line as a function of time and written in component form. Although to this point these signals could have been representative of any mechanical or electrical component of the surface waves, it will now be assumed that they represent the electric potential ϕ of the waves. The electric field and the charge density deviation inside the semiconductor can both be found from the potential functions for both signals.

The decay of the potential of a surface wave away from the surface of the piezoelectric delay line, which will be considered as the positive y direction, in the absence of the semiconductor, is purely exponential having a decay constant proportional to the spatial wavelength of the wave. The introduction of the semiconductor at a small distance h above the delay line surface (at $y = 0$) greatly perturbs this behavior so that the actual behavior inside the semiconductor (of width d) is much more complicated. Typically the solution for the variation of the potential in the y direction away from the delay line surface and inside the semiconductor consists of a summation of complex terms. In other words, a component of the potential at the surface of the delay line having frequency ω and magnitudes and phases given in Eqs. (1.18) and (1.19) will appear, at any point (x,y,z) inside the semiconductor, to consist of a summation of components whose amplitudes decay independently into the semiconductor (or the y direction) and, furthermore, some of these compon-

ents take on the characteristics of potential waves propagating into the semiconductor. When solved in detail, there are typically four components that are the solutions of a fourth order differential equation. Therefore, this type of variation can be included in the equations for the potential by utilizing the complex function $D(y,\omega)$ that is typically a summation of four complex components. Not all of the four components are necessarily complex. Those components that are complex represent potential waves independently decaying and propagating into the semiconductor at the point (x,z). Real components represent time varying replicas of each signal component at the point (x,z) that simply decay independently into the semiconductor and do not appear to propagate at this point. In the absence of the semiconductor there is only one real component so that, along any line in the y direction, the potential simply decays exponentially and varies temporally with the signal. When written in component form, the potential at any point inside the semiconductor, for the two signals, would be of the form

$$f_4(x,y,z,t) = a_f \int_{-\infty}^{\infty} F(\omega)M_f(\omega)S_f(x,z,\omega)D(y,\omega)e^{-jk_o(\delta_f+z)} e^{-j\beta(\omega)z} e^{j\omega t} d\omega \tag{1.24}$$

and

$$g_4(x,y,z,t) = a_g \int_{-\infty}^{\infty} G(\omega)M_g(\omega)S_g(x,z,\omega)D(y,\omega)e^{-jk_o(\delta_g+L-z)} e^{-j\beta(\omega)(L-z)} e^{j\omega t} d\omega \tag{1.25}$$

where the summation is over the N components of the y variation and

$$D(y,\omega) = \sum_{n}^{N} D_n(y,\omega) = \sum_{n}^{N} |D_n(y,\omega)| e^{j\arg(D_n(y,\omega))} \tag{1.26}$$

In actuality the function $D(y,\omega)$ is an extremely weak function of the spatial directions x and z. The differential equation describing the potential interaction of which $D(y,\omega)$ is the solution includes the spatial variations along these directions. However, due to the fact that the x and z direction variations are much slower than the spatial variations of the surface wave, where $k(\omega)$ is the spatial frequency of the component of frequency ω, these variations can be neglected, as is typically done in practice, with very little error.

This discussion assumes idealized uniformity along the length of the device. If the device were not only perfectly uniform but symmetric with respect to the center of the slice of semiconductor, both surface waves, from their points of injection, would undergo the same amount of diffraction before reaching their closest semiconductor edges. Furthermore, since both waves would essentially 'see' the same structure, then the same restrictions would be imposed upon them by the waveguiding action of the device. Under these conditions, therefore, it can be expected that $S_f(x,z,\omega)$ and $S_g(x,z,\omega)$ would be space inverted images of one another, i.e.

$$S_f(x,z,\omega) = S_g(-x,L-z,\omega) \tag{1.27}$$

where the width of the semiconductor extends from $x = -a$ to $x = a$. Smoothly varying device non-uniformities can be included in these terms without forcing $D(y,\omega)$ into becoming a function of the x and z spatial variables, if these non-uniformities are not due to appreciable changes in semiconductor to piezoelectric air gap, material dimensions or other material characteristics. What is constituted as an appreciable change is dependent on

how great a change influences the parameters of the differential equation for the y variation of potential. If some such non-uniformities are included in these terms, then Eq. (1.27) would not in general hold. In particular for this discussion, it is being assumed that $\delta_f \neq \delta_g$ so that the x variation of a component at one semiconductor edge, injected from that end, would be different from the x variation of the same component along the other edge, if injected from this other end, since the wave will undergo a differing amount of diffraction in the two cases. Therefore, $S_f(x,z,\omega)$ and $S_g(x,z,\omega)$ will be assumed independent of one another for the remainder of this discussion.

Equations (1.24) and (1.25) for the potential of any point inside the semiconductor can be rewritten as

$$f_4(x,y,z,t) = f(t - \frac{z}{v_o} - \frac{\delta_f}{v_o}) * f_D(x,y,z,t) \tag{1.28}$$

and

$$g_4(x,y,z,t) = g(t + \frac{z}{v_o} - \frac{\delta_g}{v_o} - \frac{L}{v_o}) * g_D(x,y,z,t) \tag{1.29}$$

where

$$f(t - \frac{z}{v_o} - \frac{\delta_f}{v_o}) \longleftrightarrow F(\omega)e^{-jk_o(\delta_f+z)} \tag{1.30}$$

$$g(t + \frac{z}{v_o} - \frac{\delta_g}{v_o} - \frac{L}{v_o}) \longleftrightarrow G(\omega)e^{-jk_o(\delta_g+L-z)} \tag{1.31}$$

$$f_D(x,y,z,t) \longleftrightarrow a_f M_f(\omega) S_f(x,z,\omega) D(y,\omega) e^{-j\beta(\omega)z}$$

$$= F_D(x,y,z,\omega) \tag{1.32}$$

and

$$g_D(x,y,z,t) \longleftrightarrow a_g M_g(\omega) S_g(x,z,\omega) D(y,\omega) e^{-j\beta(\omega)(L-z)}$$

$$= G_D(x,y,z,\omega) \qquad (1.33)$$

Equations (1.29) and (1.30) state that the potentials at any point (x,y,z) inside the semiconductor are given by the time convolution of surface waves derived from the original undistorted input signals with time signals that are functions of position inside the semiconductor. Essentially $f_D(x,y,z,t)$ and $g_D(x,y,z,t)$ can be considered as distortion terms. The functions f(t), g(t), $f_D(x,y,q,t)$ and $g_D(x,y,z,t)$ are band limited functions with a finite bandwidth around the center frequencies ω_1 and $_2$. Within these bandwidths the distortion functions and their Fourier transforms can be expanded into a series of progressively decreasing terms which facilitate numerical computation (Arsenault, 1979).

The potentials produce time and space varying fields and charge densities. The electric field at every point in conjunction with the charge density produces a current density at that point. This current density in turn produces a potential through the average resistivity of the semiconductor. Since only the potential in the y direction is utilized for the convolver output, then only the currents propagating in this direction are of any interest. The current at any point (x,z) produces a potential across the semiconductor at this point by propagating in the y direction through the distributed resistance resulting from the unperturbed resistivity of the semiconductor

at this point. In general this resistivity is a function of the y spatial variable due to surface depletion, accumulation and inversion. The time varying resistivity due to the time varying charge density produced by the two surface waves merely represents a perturbation to the semiconductor resistivity so that the convolver output across this semiconductor can be assumed entirely due to charge propagation through the unperturbed resistivity. The y component of the current density is produced by the product of the y component of electric field and the charge density at every point (x,y,z). Since there are two y components of electric field present; namely, one due to the input signal, f(t), and the other due to the other input signal, g(t), and since, in addition to the average (unperturbed) charge density at every point in the semiconductor, these signals, as surface waves, also produce time varying components of charge density, then there is in actuality a sum of current density components at every point. Although every one of these y components of current density will produce a potential across the semiconductor, it is only the non-linear components due to the cross products of the electric fields and charge densities of the two propagating surface waves that will produce an output proportional to the convolution of these two signals. The interactions of the electric field of a propagating surface wave with its own induced time varying charge density and with the unperturbed semiconductor charge density (represented as a very large constant value) do not result in potential distributions with zero spatial frequencies as do the interactions between the fields and charge densities of the two surface waves due to the contrapropagation of these two waves. In this manner the convolution output is due entirely to the cross interactions that don't integrate to zero. Finally, it must also be noted that, due to surface effects on heavily

accumulated semiconductors, the mobility, μ, required in the calculations of current density, will also be a function of y. The mobility can change by a factor of two from the surface to the bulk of heavily accumulated silicon. This has been verified by acousto-electric current interactions with the silicon surface under heavy accumulation (Cafarella, et al, 1972).

Since the surface waves propagate typically five orders of magnitude slower than electromagnetic waves in air, the electrostatic approximation, by which the field components are the negative qradients of the potential in their respective directions, can be utilized in order to obtain the y-components of electric field for the two signals inside the semiconductor. These components are given by

$$E_{fy}(x,y,z,t) = - \frac{\partial}{\partial y} f_4(x,y,z,t) \tag{1.34}$$

and

$$E_{gy}(x,y,z,t) = - \frac{\partial}{\partial y} g_4(x,y,z,t) \tag{1.35}$$

The charge density variations at every point inside the semiconductor can be found using Poisson's equation which states that the charge deviation is proportional to the negative Laplacian of the potential. From this the charge density variations due to the two surface waves are given by

$$\rho_f(x,y,z,t) = - \varepsilon_s \nabla^2 f_4(x,y,z,t) \tag{1.36}$$

and

$$\rho_g(x,y,z,t) = - \varepsilon_s \nabla^2 g_4(x,y,z,t) \tag{1.37}$$

where ε_s is the semiconductor permittivity.

The non-linear current density component in the y direction is therefore given at any point in the semiconductor by

$$J_{ny}(x,y,z,t) = q\mu(y)\rho_f(x,y,z,t)E_{gy}(x,y,z,t)$$

$$+ q\mu(y)\rho_g(x,y,z,t)E_{fy}(x,y,z,t)$$

$$= J_{fg}(x,y,z,t) + J_{gf}(x,y,z,t) \qquad (1.38)$$

The potential across the semiconductor at every point (x,z) is obtained by dividing Eq. (1.160) by the conductivity of the semiconductor (assumed to vary only with y) and integrating along its width in the y direction. This potential, $V_o(x,z,t)$, is given by

$$V_o(x,z,t) = \int_h^d \frac{J_{ny}(x,y,z,t)}{\sigma(y)}\,dy \cdot \qquad (1.39)$$

The total potential at the back ohmic contact of the semiconductor (at y=d) is the average of the potentials at every point (x,z). This potential, $V_1(t)$, is given by

$$V_1(t) = \frac{1}{2aL}\int_o^L \int_{-a}^a V_o(x,z,t)\,dx\,dz \cdot \qquad (1.40)$$

This equation represents the final output of the convolver if a purely resistive load is connected to the back contact of the semiconductor. If an output matching network is utilized, the output must be convolved with the impulse response of this network. Since very little distortion is expected from this output matching network, its transfer function can also be assumed to be slowly varying over the signal bandwidth and therefore this convolution can also be written as a finite number of terms of a moment expansion. It is the output at the back contact of the semiconductor

however, that most clearly characterizes the convolver and the matching network can simply be regarded as another device of a string of device following the convolver.

For a well made convolver only a few terms in sines expansion are required to accurately describe the output. In particular, the fundamental component is given by

$$V_f(t) = \frac{v_o}{2aL} \int_{t-T-t_f}^{t-t_f} f(\tau)g(2(t - \tfrac{1}{2}(T + t_g + t_f)) - \tau)Bl(v_o(t-\tau) - \delta_f)d\tau \tag{1.41}$$

where the substitution $\tau = t - (z+\delta_f)/v_o$ has been made and

$$T = L/v_o \tag{1.42}$$

$$t_f = \delta_f/v_o \tag{1.43}$$

$$t_g = \delta_g/v_o \tag{1.44}$$

and Bl(z) is a function representing the distortion due to different mechanisms discussed earlier.* In general this term will be a constant for a well made convolver.

Other terms arise due to the non-linear interaction of the surface waves with themselves, the average charge density of the semiconductor at every point and applied or internal fields arising due to trapped charges. The resulting current densities are proportional to

$$J_{sf}(x,y,z,t) = q\mu(y)\rho_f(x,y,z,t)E_{fy}(x,y,z,t) \tag{1.45}$$

$$J_{sg}(x,y,z,t) = q\mu(y)\rho_g(x,y,z,t)E_{gy}(x,y,z,t) \tag{1.46}$$

$$J_{fDC}(x,y,z,t) = q\mu(y)n_o(y)E_{fy}(x,y,z,t) \tag{1.47}$$

* For an actual expression for Bl(z) and its derivation see (Arsenault, 1979).

$$J_{gDC}(x,y,z,t) = q\mu(y)n_o(y)E_{gy}(x,y,z,t) \tag{1.48}$$

$$J_{ef}(x,y,z,t) = q\mu(y)\rho_f(x,y,z,t)E(x,y,z) \tag{1.49}$$

$$J_{eg}(x,y,z,t) = q\mu(y)\rho_g(x,y,z,t)E(x,y,z) \tag{1.50}$$

where $n_o(y)$ is the average charge density of the semiconductor and $E(x,y,z)$ is an internal electric field due to outside application or some trapped charge configuration. Note that $\mu(y)$ and $n_o(y)$ may also be functions of x and z, especially when semiconductor edge effects are under consideration. The output potential due to the above-mentioned terms will in general be negligible for a useful convolver.

The foregoing analysis essentially produces a relationship for the non-linear output potential of the convolver in terms of functions that individually describe specific aspects of device behavior. This analysis was based upon treating the input signals to the convolver in terms of their Fourier transforms and treating each component as an independent signal having an infinite duration and a spectific value of magnitude and phase. The output was then obtained by utilizing an expansion that will converge rapidly for small device distortions, which is equivalent to the requirement that the response of the device for two different Fourier components be approximately the same. For a well made device this is essentially the case.

2.2 The Convolver and the Ambiguity Function

Ignoring initial delays and assuming that the entire overlap of f(t) and g(t) occurs beneath the interaction region of the convolver, then its output can be written as

$$\text{convolver output} = K \int_{-\infty}^{\infty} f(t - \tfrac{z}{v}) g(t + \tfrac{z}{v}) dz$$

$$= \frac{K}{v} \int_{-\infty}^{\infty} f(\tau) g(2t - \tau) d\tau \qquad (2.1)$$

where K is simply some constant arising by assuming that the response is independent of frequency. This is valid if the convolver efficiency deviates very little over the passband of the device. Note that no carriers were used for the input signals. In reality, however, the two signals must be carrier modulated and the two carrier frequencies do not have to be the same (degenerate operation) although their bandwidths about these carrier frequencies must pass through the bandpass region of the convolver. In particular, the two input signals will be given by

$$f(t) = f_o(t)\cos\omega_1 t \qquad (2.2)$$

$$g(t) = g_o(t)\cos\omega_2 t \qquad (2.3)$$

These signals can be directly substituted into Eq. (2.1) whereby the output is given by

$$\text{output} = 2 \int_{-\infty}^{\infty} f_o(\tau) g_o(2t-\tau)\cos\omega_1\tau\cos\omega_2(2t-\tau) d\tau$$

$$= \frac{1}{2} e^{j2\omega_2 t} \int_{-\infty}^{\infty} f_o(\tau) g_o(2t-\tau) e^{j(\omega_1-\omega_2)\tau} d\tau + \text{c.c.}$$

$$+ \frac{1}{2} e^{j2\omega_2 t} \int_{-\infty}^{\infty} f_o(\tau) g_o(2t-\tau) e^{-j(\omega_1+\omega_2)\tau} d\tau + \text{c.c.} \qquad (2.4)$$

where all multiplicative constants have been ignored. If ω_1 and ω_2 are large and almost equal, the integrals will be dominated by the variations imposed by their sum and difference, since $f_o(t)$ and $g_o(t)$ are typically slowly varying functions. Since the variations in the second set of integrals, under these conditions, are of much higher frequency than the variations in the first set of integrals, they will essentially integrate to a much smaller value over the entire interaction of $f_o(t)$ and $g_o(t)$. Therefore, only the first set of integrals need be retained. For $g_o(t) = f_o^*(-t)$ Eq. (2.4) becomes

$$\text{output} = \frac{1}{2} e^{j2\omega_2 t} \chi(2t,\phi) + \text{c.c.}$$

$$= R_o(2t,\phi)\cos 2\omega_2 t - X_o(2t,\phi)\sin 2\omega_2 t \qquad (2.5)$$

where

$$\chi(2t,\phi) = \int_{-\infty}^{\infty} f_o(\tau) f_o^*(\tau-2t) e^{-j2\pi\phi\tau}\, d\tau$$

$$= \text{autoambiguity function}$$

$$= R_o(2t,\phi) + jX_o(2t,\phi) \qquad (2.6)$$

$$R_o(2t,\phi) = \int_{-\infty}^{\infty} f_o(\tau) f_o^*(\tau-2t)\cos 2\pi\phi\tau\, d\tau \qquad (2.7)$$

$$X_o(2t,\phi) = -\int_{-\infty}^{\infty} f_o(\tau) f_o^*(\tau-2t)\sin 2\pi\phi\tau\, d\tau \qquad (2.8)$$

$$\phi = (\omega_2-\omega_1)/2\pi \qquad (2.9)$$

and $f_o(t) = f_o^*(t)$ for a real input signal. Eq. (2.6) represents the complex ambiguity function obtained when the signal $f_o(t)\exp(j\omega_1 t)$ is passed through a matched filter having impulse response $f_o^*(-t)\exp(j\omega_2 t)$

where ω_1 is different from ω_2 if the signal has been Doppler shifted. This assumes that a Doppler shift only effects the carrier, which is a good approximation in practice. In actuality a signal reflected from a moving target is expanded or compressed dependent on the velocity and acceleration of the target. This expansion or compression is the cause of the carrier frequency change. For arbitrary target motion the reflected signal for a transmitted signal $f_o(t)$ is of the form $f_o(t-D(t))$, where $D(t)$ is a time dependent delay. Although the time envelope of a radar signal is usually affected by the Doppler shift, it is small in comparison to the change in the output of a matched filter due to a small carrier frequency change. The ambiguity function is determined solely by the transmitted signal and the receiving filter characteristics ($f(t)$ and $g(t)$) and answers questions about resolution, ambiguities, measurement precision, and clutter rejection obtainable using this signal and filter. Eq. (2.5) can also be written as

$$\text{output} = (R_o^2(2t,\phi) + X_o^2(2t,\phi))^{\frac{1}{2}} \cos(2\omega_2 t - \tan^{-1}(X_o(2t,\phi)/R_o(2t,\phi))) \qquad (2.10)$$

This equation shows that the envelope at the output of the convolver is the magnitude of the ambiguity function. The phase of this function is locked up into the phase of the carrier. Envelope detection of this signal for a specific ϕ will give the magnitude of a single slice of this inherently two-dimensional function along its time axis. The convolver forces a time compression factor of two onto this function although the frequency axis is unaffected (i.e. ϕ is directly proportional to the difference $\omega_2-\omega_1$).

For a real time function (i.e. an rf pulse)

$$f_o(t) = f_o^*(t) \tag{2.11}$$

so that

$$\begin{aligned} e^{j2\omega_2 t}\,\chi(2t,\phi) &= e^{j2\omega_2 t}\int_{-\infty}^{\infty} f_o(\tau)f_o(\tau-2t)e^{-j2\pi\phi\tau}\,d\tau \\ &= e^{j2\omega_1 t}\int_{-\infty}^{\infty} f_o(\tau)f_o(\tau-2t)e^{-j2\pi\phi(\tau-2t)}\,d\tau \\ &= e^{j2\omega_1 t}\int_{-\infty}^{\infty} f_o(\tau)f_o(\tau+2t)e^{-j2\pi\phi\tau}\,d\tau \\ &= e^{j2\omega_1 t}\,\chi(-2t,\phi) \end{aligned} \tag{2.12}$$

In general, however,

$$\begin{aligned} f(t) &= f_o(t)\cos(\omega_1 t + \Psi_1(t)) \\ &= p_1(t)\cos\omega_1 t - q_1(t)\sin\omega_1 t \end{aligned} \tag{2.13}$$

Likewise,

$$\begin{aligned} g(t) &= g_o(t)\cos(\omega_2 t + \Psi_2(t)) \\ &= p_2(t)\cos\omega_2 t - q_2(t)\sin\omega_2 t \end{aligned} \tag{2.14}$$

The output of the convolver for these inputs is given by

$$\text{output} = e^{j2\omega_2 t}\int_{-\infty}^{\infty} f_c(\tau)g_c(2t-\tau)e^{-j2\pi\phi\tau}\,d\tau + \text{c.c.} \tag{2.15}$$

where

$$f_c(\tau) = p_1(\tau) + jq_1(\tau) \tag{2.16}$$

$$g_c(\tau) = p_2(\tau) + jq_2(\tau) \tag{2.17}$$

For the matched filter

$$g(t) = f(-t) \tag{2.18}$$

or

$$g_c(t) = f_c^*(-t) \tag{2.19}$$

In this case the output becomes

$$\text{output} = e^{j2\omega_2 t} \int_{-\infty}^{\infty} f_c(\tau) f_c^*(\tau-2t) e^{-j2\pi\phi\tau}\, d\tau + \text{c.c.}$$

$$= e^{j2\omega_2 t}\, \chi(2t,\phi) + \text{c.c.} \tag{2.20}$$

The shape of the ambiguity function for a typical radar signal gives an indication of how well the signal can resolve the distance and velocity of a moving target. Typically the time (or distance) resolution is inversely proportional to the signal bandwidth whereas the Doppler (or velocity) resolution is inversely proportional to the signal duration. The origin of an ambiguity function is always the largest point of the function and the width of this peak along the time axis defines the time resolution and along the frequency axis the frequency or Doppler resolution.

The output of the convolver can also be written in terms of the so-called symmetrical ambiguity function given by

$$\Theta(2t,\phi) = e^{-j2\pi\phi t}\, \chi(2t,\phi) \tag{2.21}$$

so that the output becomes

$$\text{output} = e^{j(\omega_1+\omega_2)t}\, \Theta(2t,\phi) + \text{c.c.}$$

$$= R_1(2t,\phi)\cos((\omega_1+\omega_2)t) - X_1(2t,\phi)\sin((\omega_1+\omega_2)t)$$

$$= (R_1^2(2t,\phi) + X_1^2(2t,\phi))^{\frac{1}{2}} \cos((\omega_1+\omega_2)t$$

$$- \tan^{-1}(X_1(2t,\phi)/R_1(2t,\phi))) \tag{2.22}$$

where

$$\Theta(2t,\phi) = R_1(2t,\phi) + jX_1(2t,\phi)$$

$$= \int_{-\infty}^{\infty} f(\tau)\, f^*(\tau-2t)e^{-j2\pi\phi(\tau+t)}\, d\tau \qquad (2.23)$$

$$R_1(2t,\phi) = \int_{-\infty}^{\infty} f_o(\tau)f_o^*(\tau-2t)\cos(2\pi\phi(\tau+t))d\tau$$

$$= \Theta_e(2t,\phi) + \Theta_o(2t,\phi) \qquad (2.24)$$

$$X_1(2t,\phi) = -\int_{-\infty}^{\infty} f_o(\tau)f_o^*(\tau-2t)\sin(2\pi\phi(\tau+t))d\tau$$

$$= -j\{\Theta_{eo}(2t,\phi) + \Theta_{oe}(2t,\phi)\} \qquad (2.25)$$

(cross-ambiguity functions)

$$f(t) = e(t) + o(t) \qquad (2.26)$$

$$e(t) = (f(t) + f(-t))/2 \qquad (2.27)$$

$$o(t) = (f(t) - f(-t))/2 \qquad (2.28)$$

$$\Theta_e(2t,\phi) = \int_{-\infty}^{\infty} e(\tau)e^*(\tau-2t)e^{-j2\pi\phi(\tau+t)}\, d\tau \qquad (2.29)$$

$$\Theta_o(2t,\phi) = \int_{-\infty}^{\infty} o(\tau)o^*(\tau-2t)e^{-j2\pi\phi(\tau+t)}\, d\tau \qquad (2.30)$$

$$\Theta_{eo}(2t,\phi) = \int_{-\infty}^{\infty} e(\tau)o^*(\tau-2t)e^{-j2\pi\phi(\tau+t)}\, d\tau \qquad (2.31)$$

$$\Theta_{oe}(2t,\phi) = \int_{-\infty}^{\infty} o(\tau)e^*(\tau-2t)e^{-j2\pi\phi(\tau+t)}\, d\tau \qquad (2.32)$$

Note that for 2t=0 (along the frequency axis)

$$\chi(0,\phi) = \int_{-\infty}^{\infty} |f_o(\tau)|^2\, e^{-j2\pi\phi\tau}\, d\tau \qquad (2.33)$$

or the ambiguity function along the frequency axis is the Fourier transform of the squared magnitude of $f_o(t)$. For $\phi=0$

$$\chi(2t,0) = \int_{-\infty}^{\infty} f_o(\tau)f_o^*(\tau-2t)d\tau \qquad (2.34)$$

so that the ambiguity function along the time axis is simply the autocorrelation of $f_o(t)$.

From the above relationships it can be seen that the ambiguity functions obtained using a convolver will have symmetric magnitudes on any line drawn through the origin. Before describing the technique by which three-dimensional displays (time and frequency versus magnitude) of the ambiguity function for a particular radar signal can be obtained using SAW convolvers as the main element, it would be worthwhile to present a few of the major properties of this function and to document the signals and their ambiguity functions that have been utilized in the experimental work.

The time and frequency scaling relationships are given by

$$f(at) \overset{A}{\longleftrightarrow} \frac{1}{|a|}\,\theta_f\left(2at, \frac{\phi}{a}\right) \tag{2.35}$$

$$f(at) \overset{A}{\longleftrightarrow} \frac{1}{|a|}\,\chi_f\left(2at, \frac{\phi}{a}\right) \tag{2.36}$$

$$F(a\omega) \overset{A}{\longleftrightarrow} \frac{1}{|a|}\,\theta_f\left(\frac{2t}{a}, a\phi\right) \tag{2.37}$$

$$F(a\omega) \overset{A}{\longleftrightarrow} \frac{1}{|a|}\,\chi_f\left(\frac{2t}{a}, a\phi\right) \tag{2.38}$$

for

$$f(t) \longleftrightarrow F(\omega) \tag{2.39}$$

and

$$f(t) \text{ or } F(\omega) \overset{A}{\longleftrightarrow} \theta_f(2t,\phi) \text{ or } \chi_f(2t,\phi) \tag{2.40}$$

The ambiguity function of a sum of two functions is given by the sum of the two ambiguity functions and their cross ambiguity functions, namely

$$f(t) \overset{A}{\longleftrightarrow} \theta_f(2t,\phi) \tag{2.41a}$$

$$g(t) \overset{A}{\longleftrightarrow} \Theta_g(2t,\phi) \tag{2.41b}$$

$$f(t) + g(t) \overset{A}{\longleftrightarrow} \Theta_f(2t,\phi) + \Theta_g(2t,\phi) + \Theta_{fg}(2t,\phi) + \Theta_{gf}(2t,\phi) \tag{2.41c}$$

Also

$$f(t)g(t) \overset{A}{\longleftrightarrow} \int_{-\infty}^{\infty} \Theta_f(2t,f)\Theta_g(2t,\phi-f)df \tag{2.42}$$

for the product of the signals and

$$F(\omega)G(\omega) \overset{A}{\longleftrightarrow} 2\int_{-\infty}^{\infty} \Theta_f(2\tau,\phi)\Theta_g(2t-2\tau,\phi)d\tau \tag{2.43}$$

for the convolution of two signals which is equivalent to the product of their transforms. Finally, if a function is given a quadratic phase, then

$$f(t)e^{j\beta t^2} \overset{A}{\longleftrightarrow} \Theta_f(2t,\ \phi + \frac{2\beta}{\pi}\, t) \tag{2.44}$$

or the ambiguity function of f(t) (autoambiguity function) is tilted (the ϕ axis slice remains stationary) or angled with respect to the ϕ axis with slope $2\beta/\pi$. This last property can be demonstrated by comparing the ambiguity function of a square pulse and a finite chirp (see the experimental section). Other properties, of which there are quite a few, can be found in the references (Skolnik, 1970) where the compression factor of two is not used since ideal convolution is assumed.

The autoambiguity function for the rectangular pulse given by ($f(t) = f_o(t)\cos\omega_1 t$)

$$f_o(t) = \frac{1}{\sqrt{a}}\,\text{rect}\,(\frac{t}{a}) = 1/\sqrt{a} \qquad |t| \le \frac{a}{2}$$

$$= 0 \qquad \text{elsewhere} \tag{2.45}$$

is

$$\chi(2t,\phi) = \text{rect}\ (\frac{t}{a}) e^{j2\pi\phi t} (\frac{a - |2t|}{a})\ \frac{\sin\pi\phi(a - |2t|)}{\pi\phi(a - |2t|)} \tag{2.46}$$

where

$$\chi(2t,0) = \mathcal{F}^{-1}\left[|\mathcal{F}(f_o(t))|^2\right] = \mathcal{F}^{-1}\{|F(\omega)|^2\}$$

$$= \text{rect}\ (\frac{t}{a})\ \frac{(a - |2t|)}{a} \tag{2.47}$$

$$\chi(0,\phi) = \mathcal{F}\left[|f_o(t)|^2\right]$$

$$= \frac{\sin\pi\phi a}{\pi\phi a} \tag{2.48}$$

$$\mathcal{F}\left[f_o(t)\right] = \sqrt{a}\ \frac{\sin\frac{a}{2}\omega}{\frac{a}{2}\omega} = F(\omega) \tag{2.49}$$

From Eqs. (2.20) and (2.57), if $\Psi_1(t) = \beta t^2$ or

$$f(t) = f_o(t)\cos(\omega_1 t + \beta t^2) \tag{2.50}$$

then

$$f_c(t) = f_o(t)\cos\beta t^2 + j f_o(t)\sin\beta t^2$$

$$= f_o(t) e^{j\beta t^2} \tag{2.51}$$

and the autoambiguity function for this chirp is given by

$$\chi(2t,\phi) = \text{rect}\ (\frac{t}{a})\ e^{j2\pi\phi t}\ (\frac{a - |2t|}{a})\ e^{j4\beta t^2}$$

$$\frac{\sin\pi(\frac{2\beta t}{\pi} + \phi)(a - |2t|)}{\pi(\frac{2\beta t}{\pi} + \phi)(a - |2t|)} \tag{2.52}$$

where

$$\chi(2t,0) = \text{rect}\ (\frac{t}{a})\ (\frac{a - |2t|}{a})\ \frac{\sin 2\beta t(a - |2t|)}{2\beta t(a - |2t|)}\ e^{j4\beta t^2} \tag{2.53}$$

$$\chi(0,\phi) = \frac{\sin\pi\phi a}{\pi\phi a} \tag{2.54}$$

For this ambiguity function there is a so-called 'knife edge' along the line defined by

$$2\beta t/\pi + \phi = 0 \tag{2.55}$$

Along this line the ambiguity function is given by

$$|\chi(2t,\phi)| = \text{rect}\ (\frac{t}{a})\ (\frac{a - |2t|}{a}) \tag{2.56}$$

The rectangular pulse (linear FM) V-chirp given by

$$f_c(t) = \frac{1}{\sqrt{2}}\left\{\frac{1}{\sqrt{a}}\,\text{rect}\ (\frac{t}{a} + \frac{1}{2})\ e^{-j\beta(t + \frac{a}{2})^2} + \frac{1}{\sqrt{a}}\,\text{rect}\ (\frac{t}{a} - \frac{1}{2})\ e^{j\beta(t - \frac{a}{2})^2}\right\} \tag{2.57}$$

has an autoambiguity function given by

$$\chi(2t,\phi) = \frac{e^{j2\pi\phi t}}{2}\left\{e^{j\pi\phi a}\ \Theta(-2t,\phi) + e^{-j\pi\phi a}\ \Theta(2t,\phi) + \Theta_c(2t,\phi) + \Theta_c^*(-2t,-\phi)\right\} \tag{2.58}$$

where

$$\Theta(2t,\phi) = e^{-j2\pi\phi t}\ \chi_o(2t,\phi) \tag{2.59}$$

$$\chi_o(2t,\phi) = \text{Eq. (2.65)}$$

$$\theta_c(2t,\phi) = \frac{1}{2a}\sqrt{\frac{\pi}{\beta}}\,\mathrm{rect}\left(\frac{t}{a} - \frac{1}{2}\right) e^{-j\beta\frac{(a-2t)^2}{2}}$$

$$e^{j\frac{(\pi\phi)^2}{2\beta}}\left[Z^*(X_1) - Z^*(X_2)\right] \tag{2.60}$$

$$Z(X) = \int_0^X e^{j\pi y^2/2}\,dy \tag{2.61}$$

$$\left.\begin{aligned} X_1 &= 2t\sqrt{\beta/\pi} + \phi\sqrt{\pi/\beta} \\ X_2 &= -2t\sqrt{\beta/\pi} + \phi\sqrt{\pi/\beta} \end{aligned}\right\} \quad 0 \le 2t \le a \tag{2.62}$$

$$\left.\begin{aligned} X_1 &= (2a - 2t)\sqrt{\beta/\pi} + \phi\sqrt{\pi/\beta} \\ X_2 &= (2t - 2a)\sqrt{\beta/\pi} + \phi\sqrt{\pi/\beta} \end{aligned}\right\} \quad a \le 2t \le 2a \tag{2.63}$$

The study of the ambiguity function is a subject in itself and nothing further will be said about it except for the analysis of the technique utilized to generate these functions in the laboratory three dimensionally (appearance wise) on an oscilloscope using SAW convolvers.

Generation of an ambiguity function for a particular signal (so that the frequency-time function can be displayed versus magnitude) simply requires tracing the output of a filter matched to the signal at successively higher points on an oscilloscope for every frequency shift of the signal carrier. For the general function given by Eq. (2.13), the signal applied to one of the convolver inputs would be

$$\text{input 1} = f_o(-t)\cos(\omega_1 t - \Psi_1(-t))$$

$$= p_1(-t)\cos\omega_1 t + q_1(-t)\sin\omega_1 t \tag{2.64}$$

This input signal represents the impulse response of the required match

filter and after application of this signal to the SAW convolver the device output is essentially a compressed version of what would have been obtained from the matched filter where for this situation the input signal is applied to the input not utilized by the reference signal of Eq. (2.64). Although once Eq. (2.64) is applied to one of the convolver inputs, the impulse response of the convolver with respect to the other input is a compressed version of Eq. (2.64), this is only true over a finite length of time and during this time the effective impulse response has a finite initial delay that is not constant but a linear function of the time of application of the impulse (see Section 2.5) used to generate the impulse response. Essentially this is related to the factor of two compression which evolves due to the fact that the device impulse response, which can be represented by either one of the convolver's two input signals, propagates within the device in the same manner that the device input, represented by the remaining input, also propagates.

To generate the ambiguity function of the signal given by Eq. (2.13), this signal's carrier frequency must be varied linearly from one scope trace to the next. Furthermore, each trace must be displayed a predetermined distance above the last. Both these requirements can be met by utilizing a slowly varying ramp. This ramp is summed to the output of the convolver thereby displaying every trace above the last. It is also applied to a voltage controlled oscillator whose output is mixed with the signal. By choosing the initial carrier frequency of the signal (before mixing) properly so that after mixing with the 'slow chirp' the sum and difference spectrums and any strong harmonics do not interfere with one another, the sum term of the mixing process can be filtered from

the rest and made to vary about the non-Doppler shifted frequency ω_1. Usually the natural bandpass characteristics of the convolver input transducers is sufficient for this filtering process. 'Slow' is defined in such a manner such that the variation of the frequency of the 'slow chirp' is small over the time period of a single correlation. The frequency varying signal is given by (input 2)

$$\text{input 2} = f_o(t)\cos((\omega_3+\omega(t))t + \Psi_1(t)) \tag{2.65}$$

and the continuous series of slow ramps can be written as

$$v(t) = \sum_n \left\{ \left[U(t-nT_{SR}) - U(t-(n+1)T_{SR}) \right] \left[\frac{2\omega_D}{\gamma T_{SR}} (t-nT_{SR}) - \frac{\omega_D}{\gamma} \right] \right\} \tag{2.66}$$

where $\omega(t)$ is the output of the VCO given by

$$\omega(t) = \gamma v(t) + \omega_o \tag{2.67}$$

$$\omega_o = \omega_1 - \omega_3 \tag{2.68}$$

so that

$$\omega(t) = \omega_1 - \omega_3 \text{ for } v(t) = 0$$

$$\omega_D = \gamma(v(t))_{max} = \gamma v((n+1)T_{SR}) \tag{2.69}$$

In these equations ω_D represents the maximum plus or minus frequency deviation about $\omega_o = \omega_1 - \omega_3$, γ is the change in output frequency for a change in input voltage or the slope of the VCO and T_{SR} is the periodicity or time duration of every 'slow ramp'. If the oscilloscope is set up so that the trace for $v(t) = -(v(t))_{max} = v(nT_{SR}) = -\omega_D/\gamma$ is displayed at the bottom of the screen and the trace for $v(t) = (v(t))_{max} = v((n+1)T_{SR}) = \omega_D/\gamma$ is displayed at the top of the screen by displaying

the convolver output plus v(t), then with ω_o given by Eq. (2.68) and the output correlations triggered so that they are centered on the screen, the very center of the display will be the origin of the ambiguity function and the top and bottom of the display will represent the $\phi = \omega_D/2\pi$ and $\phi = -\omega_D/2\pi$ slices, respectively, of the ambiguity function.

With the maximum finite duration of the correlation given by T and the period between successive correlations given by T_s, it is important that

$$T <<< T_{SR} \tag{2.70}$$

so that the variation of the carrier over a single correlation given by

$$\omega_\epsilon = \frac{2\omega_D}{T_{SR}} T \text{ rad/sec} \tag{2.71}$$

is small enough to be ignored. Also

$$T_s << T_{SR} \tag{2.72}$$

so that there are enough traces on the oscilloscope so as to give the output an appearance of continuity. The number of scans per frame will be given by T_{SR}/T_s. T_{SR} should, however, be small enough so that flickering of the output display is not observed. This usually requires T_{SR} to be less than about $1/60^{th}$ of a second. The change in carrier frequency between scans will be

$$\omega_s = \frac{2\omega_D}{T_{SR}} T_s \text{ rad/sec} \tag{2.73}$$

This is equal to ω_ϵ if $T = T_s$ which is much too high a repetition rate since there will be cross correlation between preceeding and succeeding inputs and therefore is never used. Usually T can be made much smaller

than T_s (or T_s made much larger than T since T is usually set by the convolver interaction time) with still enough traces to give the appearance of a continuous display. In some cases, however, where there may be ambiguity functions having extremely fast Doppler variations (i.e. the autoambiguity of high TB chirps and V-chirps), it may be desirable to make T_s as close as possible to T in order to obtain a continuous looking display. In such cases it may be necessary to 'home into' the rapidly varying portion of the ambiguity function by decreasing the slope of the slow ramp. This has the effect of expanding the ambiguity function (along the frequency axis) since the oscilloscope display must be expanded after this procedure to again fill up the entire screen with the same number of traces which doesn't change by a change in ramp slope. If the ramp is summed to the convolver output by applying these two signals to the two channels of the oscilloscope and utilizing the scopes sum channel A to channel B feature, then the ambiguity function is expanded along the frequency axis by changing the magnitude display of the ramp channel, it is expanded along the time scale by changing the time per division setting and its magnitude is adjusted by changing the magnitude display of the convolver output channel. The number of scans per Doppler frequency shift can only be changed by changing the slope of the ramp or the correlation repetition frequency (assuming the ramp duration is kept constant to about $1/60^{th}$ of a second). Of course the display can be expanded so that part of the function is off screen; however, this is only a waste and in this case the spacing between scans will increase. By utilizing this technique the scope need only be triggered for every correlation since every frame is automatically reset by the slow ramp.

Because of this, even though the ambiguity function itself will always remain stationary, the individual scans will tend to roll across the screen. When the scan density is high enough this roll presents no problem; however, for low scan line densities it may be desirable to trigger the slow ramp generator by every N^{th} correlation trigger where $N = T_{SR}/T_s$ is the total number of scan lines per frame. A technique such as this would lock the individual scans in place on the screen. An actual system with experimental outputs is described in the experimental section of this report.

2.3 Signal Processing with the Memory Correlator

The essential mechanism in a SAW convolver is a second order output voltage that can essentially be visualized and modeled as a mechanism that squares the total sum of all the electric fields present beneath the interaction region of the device (defined by the slice of semiconducting material) and integrates the result over the length of this region. This is valid since the resulting non-linearity is due to the interaction of the time and spatially varying fields with the time and spatially varying carrier densities of any signal that may be present. This interaction between fields and carriers produces time and spatial variating current densities that are linearly proportional to voltages which become averaged out over the surface of the semiconductor. This second order interaction is small, being derived from the interaction of electric fields propagating with surface waves, where the electrical energy is negligible with respect to the mechanical energy of the wave, and charge carriers in the semiconductor where the charge carrier variation is so small for practical power densities that it is usually treated as a perturbation of the semiconductor carrier density. Even though the result of this interaction is fairly small, the output is usually obtained for timelimited signals whose time duration can be designed small enough so that the input signal is removed before the start of the interaction within the convolver and no interference is obtained between the output and radiation from the input. Furthermore, the convolution obtained through the interaction of two contrapropagating surface waves produces a convolution output on a carrier having

a frequency that is the sum of the two input carrier frequencies. In this case the output can easily be isolated from input radiation by filtering.

In the most general situation, however, there are three mechanisms for introducing electric fields within the convolver interaction region. The electric fields can be introduced by propagating surface waves that carry these fields into this region. This is the usual technique whereby two contrapropagating signals produce an output signal that is a time compressed version of the convolution of the two signals. Another way of introducing fields is by storing a spatially varying charge pattern along the semiconductor. This is the basic mechanism utilized in the storage correlator whereby charges are stored in surface states or within diodes diffused into the semiconductor surface adjacent to the piezoelectric delay line surface. More will be said about the mechanisms utilized to perform this charge storage later. The last means of introducing a field is by applying a time varying potential to the back contact of the semiconductor which behaves as the integrating ohmic contact on the surface facing away from the delay line. When a potential is applied to this contact an essentially uniform field is introduced into the interaction region that is independent of space so long as the semiconductor, the delay line and the spacing between the two is uniform. This spatially uniform field can be varied temporally, whereas the spatially varying field set up by the stored charge is necessarily time independent and the propagating waves have fields that are both spatially and temporally changing. These three forms of electric field cover the possible combinations of time and space variation and induce charge densities that also follow these variations.

If the distances between the convolver inputs and the interaction region are ignored, the signal $f(t - z/v)$ is inputted at the $z = 0$ end of the convolver, the signal $g(t + z/v - D/v)$ is inputted at the $z = D$ end, $t(t)$ is applied to the semiconductor back contact and $s(z/v)$ is stored as a charge patterm in the semiconductor, the second harmonic output voltage from the back contact of the semiconductor for these signals, during the time when both of the propagating signals are beneath the semiconductor, is proportional to

$$\text{output} = \int_{-\infty}^{\infty} (f(t - z/v) + g(t + z/v - D/v) + s(z/v) + t(t))^2 \, dz \quad (3.1)$$

The fact that the two propagating signals are timelimited and completely beneath the semiconductor allows the limits of this integration to extend to plus and minus infinity without error during this time period only. During any other time the limits must be set to 0 and D in place of $-\infty$ and ∞ respectively. Eq. (3.1) can be divided by 2v (twice the acoustic velocity) and rewritten as

$$\text{output} = K_1 t^2(t) + K_2 t(t) + K_3 + C_1(t - D/2v) + C_2(t) + C_3(t - D/v)$$

where

$$K_1 = D/2v = \frac{1}{2v} \int_0^D dz \quad (3.3)$$

$$K_2 = \int_{-\infty}^{\infty} (f(\tau) + g(\tau - D/v) + s(\tau))d\tau \quad (3.4)$$

$$K_3 = \frac{1}{2} \int_{-\infty}^{\infty} (f^2(\tau) + g^2(\tau - D/v) + s^2(\tau))d\tau \quad (3.5)$$

are constants during this time period,

$$C_1(t) = \int_{-\infty}^{\infty} f(\tau)g(2t - \tau)d\tau \quad (3.6)$$

is the time compressed convolution of f(t) and g(t),

$$C_2(t) = \int_{-\infty}^{\infty} f(\tau)s(t - \tau)d\tau \tag{3.7}$$

is the convolution of f(t) and s(t) and

$$C_3(t) = \int_{-\infty}^{\infty} g(\tau)s(\tau - t)d\tau \tag{3.8}$$

is the correlation of g(t) and s(t). To be more specific, if f(t) exist from t = 0 to t = t_f and g(t) exist from t = 0 to t = t_g where $t_f > t_g$, then the period of time over which these equations are accurate is given by

$$t_f \leq t \leq D/v \tag{3.9}$$

Over all time

$$K_2 = \frac{1}{v}\int_0^D \left(f(t - \frac{z}{v}) + g(t + \frac{z}{v} - \frac{D}{v}) + s(\frac{z}{v})\right)dz$$

$$= K_2(t) = \int_{t-D/v}^{t} (f(\tau) + g(\tau))d\tau + \int_0^{D/v} s(\tau)d\tau \tag{3.10}$$

Eq. (3.10) can be rewritten as

$$K_2(t) = \int_{-\infty}^{\infty} \{f(\tau) + g(\tau)\}\{U(\tau - (t - D/v)) - U(\tau - t)\}d\tau$$

$$+ \int_0^{D/v} s(\tau)d\tau$$

$$= (f(t) + g(t)) * (U(t) - U(t - T)) + T\bar{s}(t) \tag{3.11}$$

so that this function is simply the convolution of f(t) and g(t) with the assumed uniform interaction region of the convolver representative of a square pulse plus T times the average value of s(t) where

$$T \triangleq D/v = \text{the interaction time} \tag{3.12}$$

and

$$\bar{s}(t) \triangleq \frac{1}{T}\int_0^T s(\tau)d\tau = \text{a const.} \tag{3.13}$$

Since s(z/v) is space limited between z = 0 and z = D, it has been written as a time function existing from t = 0 to t = T in these integrals (since z/v has units of time).

Similarly, Eq. (3.5) can be rewritten as

$$K_3(t) = \frac{1}{2}\left(f^2(t) + g^2(t)\right) * \left(U(t) - U(t - T)\right) + \frac{T}{2}\left(\hat{s}(t)\right)^2 \tag{3.14}$$

where

$$\hat{s}(t) \triangleq \frac{1}{T}\left\{\int_0^T s^2(\tau)d\tau\right\}^{\frac{1}{2}} = \text{a const.} \tag{3.15}$$

so that this function is half the convolution of the squares of f(t) and g(t) with the interaction region plus T/2 times the square of the RMS value of s(t).

These equations assume uniformity of the air gap between the semiconductor and the delay line along the direction of propagation z. If there is some variation in this gap, the signals f(t - z/v) and g(t + z/v - D/v) will be affected in the same way since they are both surface waves. If the gap variation d(z/v) is small, the fields due to these two waves can be modified by including a linear $1 - a_1 d(z/v)$ factor before these terms in the output equation, where a_1 is some positive constant and a positive d(z/v) represents a wider gap. The time varying function t(t) sets up a time varying potential across the back contact of the semiconductor. The field due to this potential is smaller inside the semiconductor at points with wider gaps so that for small variations this function can be modified by a linear $1 - a_2 d(z/v)$ factor where a_2 is some

positive constant different from a_1. Once a charge pattern has been stored along the semiconductor, the fields produced inside the semiconductor are also weakly dependent on the gap. The function $s(z/v)$ will be considered as the charge distribution along the semiconductor and therefore is independent of gap. As will be seen, when this charge pattern is stored through the interaction of some functions whose interaction is dependent on gap, then the stored signal $s(z/v)$ will represent a distorted version of a signal that has been distorted due to gap variations. Also, once stored this distorted signal will interact with other signals whose fields will also vary with gap. For small variations a linear $1 - a_3 d(z/v)$ factor for $s(z/v)$ can be used. The output becomes

$$\text{output} = \int_0^D \{n_1(z/v)(f(t - z/v) + g(t + z/v - D/v)) \\ n_2(z/v)t(t) + n_3(z/v)s(z/v)\}^2 \, dz \tag{3.16}$$

where

$$n_1(z/v) \approx 1 - a_1 d(z/v) \tag{3.17}$$

$$n_2(z/v) \approx 1 - a_2 d(z/v) \tag{3.18}$$

and $$n_3(z/v) \approx 1 - a_3 d(z/v) \tag{3.19}$$

for small gap variations. This can be seen if the variation of the fields of the surface wave with gap is written approximately as a pure exponential $\exp(-Bd(z/v))$ where B is a constant given by 2π divided by the wavelength of the surface wave carrier and the bandwidth of the modulation is assumed to be small (so that this approximation is valid). In this case, for small variations

$$e^{-Bd(z/v)} \simeq 1 - Bd(z/v) \qquad (3.\;)$$

so that $a_1 = B$. If ε_s and ε_p are the dielectric constants of the semiconductor and piezoelectric, respectively, and d_s, $d_g + d(z/v)$ and d_p are the thicknesses of the semiconductor, gap and piezoelectric, respectively, then the field inside the semiconductor due to a potential t(t) is given by

$$\begin{aligned} E(z,t) &= t(t)/(d_g + d(z/v) + d_s/\varepsilon_s + d_p/\varepsilon_p) \\ &= a_2 t(t)/(1 + a_2 d(z/v)) \\ &\simeq a_2 t(t)(1 - a_2 d(z/v)) \end{aligned} \qquad (3.\;)$$

for small $d(z/v)$ and $a_2 = (d_g + d_s/\varepsilon_s + d_p/\varepsilon_p)^{-1}$. In these equations anything beyond first order in $d(z/v)$ has been ignored. Constant factors are always assumed to be absorbed into the functions. Finally, the electric field within the semiconductor due to the charge pattern $s(z/v)$ is proportional to (for $s(z/v)$ being negative charge)

$$\begin{aligned} E(z/v) &= -s(z/v)\frac{\varepsilon_p d(z/v) + \varepsilon_p d_g + d_p}{\varepsilon_o\{\varepsilon_p d_s + \varepsilon_s\varepsilon_p(d(z/v) + d_g) + \varepsilon_s d_p\}} \\ &\simeq s(z/v)(1 - a_3 d(z/v)) \end{aligned} \qquad (3.\;)$$

from continuous normal displacement, zero potential and small $d(z/v)$ and $a_3 = \varepsilon_s\varepsilon_p/(\varepsilon_p d_s + \varepsilon_s d_p + \varepsilon_s\varepsilon_p d_g) - \varepsilon_p/(d_p + \varepsilon_p d_g)$ where ε_o is the permittivity of free space. Since in general $a_1 \neq a_2 \neq a_3$ a single function cannot be used in equation (3.16) to handle the gap variation with z. For small gap variations the three different forms of signal behave approximately linearly with gap, however, with different linear slopes

Transverse non-uniformities along the width of the slice of semiconductor are essentially averaged out at every point z along the propagation path or equivalently these uniformities contribute to the uniformity defined at every point z so that for parallel propagating wavefronts the transverse variations can be absorbed by the longitudinal variation function. The gap variation will be ignored for the remaining portion of this discussion so that

$$n_1(z/v) = n_2(z/v) = n_3(z/v) = 1 \tag{3.23}$$

will be assumed and would actually be one of the goals in the proper design of a convolver. Minor gap variations can be handled by including the above linear factors, but large variations require the more precise factors for which the linear ones are only approximations.

By including carriers on all these signals the traveling waves become

$$f(t - z/v) = f_o(t - z/v)\cos(\omega_1 t - k_1 z) \tag{3.24}$$

$$g(t + z/v - D/v) = g_o(t + z/v - D/v)\cos(\omega_2 t + k_2 z - k_2 D) \tag{3.25}$$

where

$$k_1 = \omega_1/v \tag{3.26}$$

and

$$k_2 = \omega_2/v \tag{3.27}$$

The time dependent and space dependent terms also become

$$t(t) = t_o(t)\cos(\omega_3 t) \tag{3.28}$$

and

$$s(z/v) = s_o(z/v)\cos(k_4 z) \tag{3.29}$$

where

$$k_4 = \omega_4/v \tag{3.30}$$

Note that since $s(z/v)$ is always stationary and finite, the integrals given by Eqs. (3.7) and (3.8) can always be written with limits of plus and minus infinity without loss of generality. Infinite limits cannot, however, be used in Eq. (3.6) unless the overlap of the two signals is totally beneath the semiconductor or equivalently within the interaction region. By choosing the time durations of $f(t)$ and $g(t)$ (the functions of time applied to the convolver transducers) properly, this can always be the case. Even if part of the overlap of the two surface waves extends outside the interaction region at a certain time and the output is therefore due to truncated versions of these signals at this point in time, any output obtained when the overlap is totally beneath the semiconductor is valid and can be gated from the invalid output where it must then be kept in mind that only part of the valid output convolution is being displayed. During this valid time period the integrals can be written using infinite limits. Note, however, that even though the output may represent over a period of time an invalid portion of the convolution, the output is nonetheless real and can be represented by a convolution integral having the time varying limits given by Eq. (3.6).

Although Eqs. (3.6), (3.7) and (3.8) can have infinite limits over all time (if $f(t)$ and $g(t)$ are properly time limited), the integrals in Eq . (3.10) cannot have infinite limits except over finite periods of time. Over the time periods when $f(t - z/v)$ and $g(t + z/v - D/v)$ have individually passed completely into the interaction

region beneath the semiconductor, their respective integrals can be written using infinite limits and are therefore constants. While these signals are entering and leaving this area, however, the integrals are functions of time. This is obvious from the forms given in Eqs. (3.11) and (3.14).

Substituting Eqs. (3.24) and 3.25) into Eq. (3.6) gives (assuming infinite limits can be used)

$$C_1(t) = \int_{-\infty}^{\infty} f_o(\tau)g_o(2t - \tau)\cos(\omega_1\tau)\cos(\omega_2(2t - \tau)d\tau$$

$$\approx \frac{1}{2} A_R(2t,\phi)\cos(2\omega_2 t) - \frac{1}{2} A_I(2t,\phi)\sin(2\omega_2 t) \qquad (3.31)$$

where

$$A(2t,\phi) = \int_{-\infty}^{\infty} f_o(\tau)g_o(2t - \tau)e^{-j2\pi\phi\tau}\, d\tau$$

$$= A_R(2t,\phi) + jA_I(2t,\phi) \qquad (3.32)$$

is the cross ambiguity function of f(t) and g(t) (see section 2.2 concerning the ambiguity function) which becomes the $\chi(2t,\phi)$ function in section 2.2 if $g(t) = f^*(-t)$ and also

$$A_R(2t,\phi) = \int_{-\infty}^{\infty} f_o(\tau)g_o(2t-\tau)\cos(2\pi\phi\tau)d\tau \qquad (3.33)$$

and

$$A_I(2t,\phi) = -\int_{-\infty}^{\infty} f_o(\tau)g_o(2t-\tau)\sin(2\pi\phi\tau)d\tau \qquad (3.34)$$

are the real and imaginary parts of $A(2t,\phi)$ where $\phi = (\omega_2-\omega_1)/2\pi$. The second set of integrals in Eq. (3.31) will be very much smaller than the first for ω_1 and ω_2 large and approximately equal, which represents the usual case. For $\omega_1 = \omega_2$ (the degenerate case) this output becomes

$$C_1(t) = \frac{1}{2}\cos(2\omega_2 t)\int_{-\infty}^{\infty} f_o(\tau)g_o(2t-\tau)d\tau \qquad (3.35)$$

which is simply the time compressed convolution of the signal modulations $f_o(t)$ and $g_o(t)$ with a $\cos(2\omega_2 t)$ carrier.

Substituting Eqs. (3.24) and (3.29) in Eq. (3.7) results in

$$C_2(t) = \int_{-\infty}^{\infty} f_o(\tau)s_o(t-\tau)\cos(\omega_1\tau)\cos(\omega_4(t-\tau))d\tau$$

$$\approx \frac{1}{2} A_{R1}(t,\phi_1)\cos\omega_4 t - \frac{1}{2} A_{I1}(t,\phi_1)\sin\omega_4 t \qquad (3.36)$$

where

$$A_1(t,\phi_1) = \int_{-\infty}^{\infty} f_o(\tau)s_o(t-\tau)e^{-j2\pi\phi_1\tau}\, d\tau$$

$$= A_{R1}(t,\phi_1) + jA_{I1}(t,\phi_1) \qquad (3.37)$$

is the cross-ambiguity function of f(t) and s(t)

$$A_{R1}(t,\phi_1) = \int_{-\infty}^{\infty} f_o(\tau)s_o(t-\tau)\cos(2\pi\phi_1\tau)d\tau \qquad (3.38)$$

$$A_{I1}(t,\phi_1) = -\int_{-\infty}^{\infty} f_o(\tau)s_o(t-\tau)\sin(2\pi\phi_1\tau)d\tau \qquad (3.39)$$

and

$$\phi_1 = (\omega_4-\omega_1)/2\pi \qquad (3.40)$$

In these equations the limits have been automatically set to plus and minus infinity since s(t) is necessarily finite and equal in length to, at most, T seconds. For the degenerate case, $\omega_1 = \omega_4$, so that

$$C_2(t) = \frac{1}{2}\cos(\omega_4 t)\int_{-\infty}^{\infty} f_o(\tau)s_o(t-\tau)d\tau \qquad (3.41)$$

is the convolution of $f_o(t)$ and $s_o(t)$ with a carrier of frequency ω_4.

Finally, substitution of Eqs. (3.25) and (3.29) into Eq. (3.8) results in an output given by

$$C_3(t) = \int_{-\infty}^{\infty} g_o(\tau)s_o(\tau-t)\cos(\omega_2\tau)\cos(\omega_4(\tau-t))d\tau$$

$$\approx \frac{1}{2} A_{R2}(-t,\phi_2)\cos\omega_4 t - \frac{1}{2} A_{I2}(-t,\phi_2)\sin\omega_4 t \qquad (3.42)$$

where

$$A_2(-t,\phi_2) = \int_{-\infty}^{\infty} g_o(\tau)s_o(\tau-t)e^{-j2\pi\phi_2\tau}\,d\tau$$

$$= A_{R2}(-t,\phi_2) + jA_{I2}(-t,\phi_2) \tag{3.43}$$

is the cross-ambiuity function of g(t) and s(-t)

$$A_{R2}(-t,\phi_2) = \int_{-\infty}^{\infty} g_o(\tau)s_o(\tau-t)\cos(2\pi\phi_2\tau)d\tau \tag{3.44}$$

$$A_{I2}(-t,\phi_2) = -\int_{-\infty}^{\infty} g_o(\tau)s_o(\tau-t)\sin(2\pi\phi_2\tau)d\tau \tag{3.45}$$

and

$$\phi_2 = (\omega_4-\omega_2)/2\pi \tag{3.46}$$

Infinite limits are again being used due to the time limitation of s(t). For the degenerate case, $\omega_2 = \omega_4$, so that

$$C_3(t) = \frac{1}{2}\cos\omega_4 t \int_{-\infty}^{\infty} g_o(\tau)s_o(\tau-t)d\tau \tag{3.47}$$

is the convolution of $g_o(t)$ and $s_o(-t)$ or the correlation of $g_o(t)$ and $s_o(t)$ with a carrier of frequency ω_4.

Note that for all the outputs at the semiconductor back contact, it is the zero (or almost zero) spatial frequency components of the non-linear mixing between signals that is of importance. In general, however, the potential across the semiconductor at every point z is given by

$$\text{potential} \propto f^2(t-z/v) + g^2(t+z/v-D/v) + s^2(z/v) + t^2(t)$$
$$+ 2f(t-z/v)g(t+z/v-D/v) + 2f(t-z/v)s(z/v)$$
$$+ 2f(t-z/v)t(t) + 2g(t+z/v-D/v)s(z/v) + 2g(t+z/v-D/v)t(t)$$
$$+ 2s(z/v)t(t) + \text{first order terms} \tag{3.48}$$

Using Eqs. (3.24) thru (3.30), the individual components of this potential are given by

$$f^2(t-z/v) = \frac{1}{2} f_o^2(t-z/v) + \frac{1}{2} f_o^2(t-z/v)\cos(2\omega_1 t-2k_1 z) \tag{3.49}$$

$$g^2(t+z/v-D/v) = \frac{1}{2} g_o^2(t+z/v-D/v) + \frac{1}{2} g_o^2(t+z/v-D/v)\cos(2\omega_2 t+2k_2 z-2k_2 D) \tag{3.50}$$

$$s^2(z/v) = \frac{1}{2} s_o^2(z/v) + \frac{1}{2} s_o^2(z/v)\cos(2k_4 z) \tag{3.51}$$

$$t^2(t) = \frac{1}{2} t_o^2(t) + \frac{1}{2} t_o^2(t)\cos(2\omega_3 t) \tag{3.52}$$

$$f(t-z/v)g(t+z/v-D/v) = \frac{1}{2} f_o(t-z/v)g_o(t+z/v-D/v)\cos((\omega_1+\omega_2)t - (k_1-k_2)z - 2k_2 D) + \frac{1}{2} f_o(t-z/v)g_o(t+z/v-D/v)\cos((\omega_1-\omega_2)t - (k_1+k_2)z - 2k_2 D) \tag{3.53}$$

$$f(t-z/v)s(z/v) = \frac{1}{2} f_o(t-z/v)s_o(z/v)\cos(\omega_1 t - (k_1-k_4)z) + \frac{1}{2} f_o(t-z/v)s_o(z/v)\cos(\omega_1 t - (k_1+k_4)z) \tag{3.54}$$

$$f(t-z/v)t(t) = \frac{1}{2} f_o(t-z/v)t_o(t)\cos((\omega_1+\omega_3)t - k_1 z) + \frac{1}{2} f_o(t-z/v)t_o(t)\cos((\omega_1-\omega_3)t - k_1 z) \tag{3.55}$$

$$g(t+z/v-D/v)s(z/v) =$$

$$\frac{1}{2} g_o(t+z/v-D/v)s_o(z/v)\cos(\omega_2 t + (k_2+k_4)z - 2k_2D)$$

$$+ \frac{1}{2} g_o(t+z/v-D/v)s_o(z/v)\cos(\omega_2 t + (k_2-k_4)z - 2k_2D) \qquad (3.56)$$

$$g(t+z/v-D/v)t(t) =$$

$$\frac{1}{2} g_o(t+z/v-D/v)t_o(t)\cos((\omega_2+\omega_3)t + k_2 z - k_2 D)$$

$$+ \frac{1}{2} g_o(t+z/v-D/v)t_o(t)\cos((\omega_2-\omega_3)t + k_2 z - k_2 D) \qquad (3.57)$$

and

$$s(z/v)t(t) = \frac{1}{2} s_o(z/v)t_o(t)\cos(\omega_3 t+k_4 z)$$

$$+ \frac{1}{2} s_o(z/v)t_o(t)\cos(\omega_3 t-k_4 z) \qquad (3.58)$$

The first order terms are those given by Eqs. (3.24), (3.25), (3.28) and (3.29). These terms produce outputs by interacting with the DC or average carrier density of the semiconductor and are therefore much larger than the non-linear terms. The function t(t) produces an output directly since it is applied directly to the output contact. In the equations derived previously for the output, it is only those terms in Eqs. (3.49) to (3.53) with small or zero spatial variations that contribute appreciably. Fast spatial variations are integrated by the back contact of the semiconductor to produce negligible outputs since this contact takes the average of the total distributed potential.

During the time when f(t-z/v) and g(t+z/v-D/v) are beneath the semiconductor, the first terms in Eqs. (3.49) and (3.50) produce constant outputs. These terms contribute to the $K_3(t)$ output and as seen in

Eq. (3.14) they are effectively convolved with a square pulse representative of the assumed perfectly uniform interaction region. The second terms in Eqs. (3.49) and (3.50), however, are traveling potential waves having twice the spatial frequencies of their acoustic counterparts so that no appreciable output is produced at the output contact due to these terms. The first order terms due to and proportional to f(t-z/v) and g(t+z/v-D/v) are traveling potential waves of spatial frequencies k_1 and k_2, respectively. The output average of these signals will also be small.

The signal s(z/v) is stationary within the semiconductor. Therefore, both terms in Eq. (3.51) will produce a constant output although the first term will dominate since it has a zero spatial frequency. This term is part of the $K_3(t)$ output. Note that the first order component of this signal, proportional to s(z/v), will produce a negligible output if k_4 is large.

The signal t(t) produces a direct output since it is applied directly to the semiconductor back contact from which the convolver output is derived. Being only dependent on time, the non-linear terms in Eq. (3.52) are outputted as they are with a proportionality constant given by K_1 as given by Eq. (3.3). These terms arise due to the interaction of the fields set up by t(t) and the carrier density modulation produced by these fields. The semiconductor, behaving as a non-linear medium, produces, in this case, the second harmonic of the first order signal t(t).

Eq. (3.53) represents the product of the two contrapropagating surface waves. Note that for the degenerate case, when $\omega_1 = \omega_2$ and $k_1 = k_2$, one of the terms has a zero spatial frequency component whereas the other term has no temporal frequency component. When averaged out or integrated

by the output contact, the term without a spatially varying carrier will dominate the two and produce an output proportional to the convolution of $f_o(t)$ and $g_o(t)$ ($C_1(t)$ Eq. (3.6)) compressed by a factor of two and with a carrier of frequency $2\omega_1 = 2\omega_2$. The other term, having a carrier with only a spatial frequency component, averages out to a small value by the output contact. Note, however, that if this term was to be integrated, by some mechanism, at every point z along the semiconductor, in time, then the resultant spatial distribution of potential, charge or field would be proportional to

$$SD \propto \cos(2k_1(z-D)) \int_{-\infty}^{\infty} f_o(t-z/v)g_o(t+z/v-D/v)dt$$

$$= \frac{1}{v} \cos(2k_1(z-D)) \int_{-\infty}^{\infty} f_o(z'/v)g_o(2z/v+z'/v-D/v)dz' \qquad (3.\ \ )$$

or the correlation of $f_o(t)$ and $g_o(t)$ compressed by a factor of two (due to the contrapropagation of f(t) and g(t)) and with a carrier of spatial frequency $2k_1 = 2k_2$. This is an important realization. It says that by employing some type of non-linear medium, such as a slice of semiconductor, to produce the non-linear current density and potential and also possessing some mechanism for storage of charge at each point proportional to the time average of the non-linear potential seen at these points, then the resultant charge distribution will be proportional to a spatial representation of the correlation of the envelopes of the two surface waves with a carrier at twice their spatial frequencies, assumed to be the same. This represents one of the possible storage techniques. In this case storage is affected by the interaction of two surface waves. The signal is stored spatially as a charge distribution. This charge distribution represents an imbalance

in the otherwise uniform and neutral charge distribution of the semiconductor and therefore an internal field proportional to this distribution is set up with which successive surface waves (and plate fields t(t)) can interact. Semiconductor surface states and high density pre-biased diodes are examples of semiconductor storage mechanisms. In the case of the diodes, if their response times are fast enough, a current will flow in response to the potential set up by the product of the two signals. Over the time period of the interaction the current flow in each diode will deposit, on one side of their junctions, an amount of charge proportional to the average potential seen at that point. The diodes are arranged as a high density matrix over the surface of the semiconductor facing the piezoelectric delay line. When the interaction between the two surface waves is over, the high reverse resistance to flow of the diodes prevents the charges from neutralizing the charge imbalance in the diode by recrossing the junction. In low leakage diodes this neutralization can take milliseconds for diodes of the Schottky barrier type and seconds for p-n diffused diodes. Schottky barriers, however, can respond in nanoseconds, a thousand times faster than p-n diodes. The imbalance in charge at each diode sets up a field that can interact with other signals. In this discussion such fields are represented by the function s(z/v). Any signal varying too quickly in time, such as those given by Eqs. (3.49), (3.50) and (3.52) for large ω_3 and the first term of Eq. (3.53), used to obtain the temporal convolution of $f_o(t)$ and $g_o(t)$ (in contrast to the spatial correlation of these signals), cannot produce a noticeable amount of charge storage in the diodes since their averages at every point in the semiconductor over their durations are extremely small. Semiconductor surface states

represent another storage mechanism where, in this case, the charge is stored, in response to the non-linear potential, in atomic states at the surface of the semiconductor. The storage and response times for these states are functions of their statistical properties.

If the interaction region is non-uniform, the stored charge distribution will be a distorted representation of the correlation of $f_o(t)$ and $g_o(t)$. Due to the device non-uniformity, any future interactions with the charge distribution will produce outputs that are doubly distorted. For small distortions, approximate factors, such as given by Eqs. (3.17) to (3.19), can be utilized. In any case, the interaction between two contra-propagating surface waves produces a component capable of producing the spatial distribution $s(z/v)$ which, in this case, is a representation of the correlation of the envelopes of the two waves having some distortion if the interaction region is non-uniform. Furthermore, if one of the surface waves is an impulse, the stored charge distribution is a spatial representation of the compressed envelope of the other surface wave with a $2k_1$ or $2k_2$ carrier spatial frequency. Likewise, the output from the semiconductor contact is a time compressed version of this envelope with a $2\omega_1$ or $2\omega_2$ carrier frequency. If one input is a continuous tone and the other an impulse, the output convolution is proportional to the non-uniformity of the interaction region (time compressed) and the stored charge would also be proportional to this non-uniformity. In one case, the output occurs concurrently with the interaction, is a time function and has a carrier frequency of twice the tone frequency. In the other case, a charge distribution is stored (until it is intentionally erased, modified or it decays to zero) with a spatial carrier frequency of twice

the spatial frequency of the continuous-tone-surface wave. Since the stored signal is given by the function $s(z/v)$, the mechanisms for reading this information are linked to the interactions of $s(z/v)$ with $f(t-z/v)$, $g(t+z/v-D/v)$ and $t(t)$ as seen in Eqs. (3.54), (3.56) and (3.58) to be discussed shortly.

Eqs. (3.55) and (3.57) show another technique for storing signals as stationary charge distributions along the semiconductor. First, however, it should be mentioned that these signals, being traveling potential waves, would typically produce little output at the output contact since their spatial averages would be small irrespective of the values of ω_1, ω_2 and ω_3. Note, however, that if $\omega_1 = \omega_3$ or $\omega_2 = \omega_3$ there are terms in the expansion of these products without temporal carrier frequencies. In these cases, if the semiconductor possesses a storage mechanism, an appreciable signal could be stored. More precisely, the stored spatial charge distributions would be of the form

$$SF \propto \cos(k_1 z) \int_{-\infty}^{\infty} f_o(t-z/v)t_o(t)dt$$

$$= \frac{1}{v} \cos(k_1 z) \int_{-\infty}^{\infty} f_o(z'/v)t_o(z/v+z'/v)dz' \qquad (3.60)$$

$$SG \propto \cos(k_2(z-D)) \int_{-\infty}^{\infty} g_o(t+z/v-D/v)t_o(t)dt$$

$$= \frac{1}{v} \cos(k_2(z-D)) \int_{-\infty}^{\infty} g_o(z'/v)t_o(z'/v-z/v+D/v)dz' \qquad (3.61)$$

where both distributions are correlations with the time function envelope $t_o(t)$; however, the correlation process in Eq. (3.60) (and likewise Eq. (3.59)) is a spatially reversed correlation relative to the positive z direction. In both cases the stored signals are not spatially compressed, whereas the

correlation stored by the correlation process of Eq. (3.[illegible]) is. The spatial carrier frequencies of the stored signals are given by the spatial frequencies of the respective surface waves. Note that if $t_o(t)$ is an ideal impulse, both terms in Eqs. (3.55) and (3.[illegible]) contribute to the stored signal. Since ideal impulses cannot be realized and such signals would tend to waste too much energy on unneeded portions of the frequency spectrum, a good approximation would be a pulsed rf having whatever number of cycles at the frequency ω_1 or ω_2 is suitable to affect storage. In this case the 'impulse' energy is localized about the signal bandwidth and it can be made long enough in duration so as to give the storage mechanism time to respond yet small enough so that the correlation of the desired signal to be stored with this finite width 'impulse' does not appreciably smooth out the signal. Too many rf cycles would tend to restrict the bandwidth of the impulse and distort the bandwidth of a wide band signal being stored. This is the equivalent operation in the frequency domain of smoothing in the time domain. Too few cycles may be insufficient in terms of time to affect storage. It must be remembered also that although the signal is stored as a function of space, any function that modifies its frequency spectrum will modify its time representation since the idea will be to recall such a function or interact it with some other time function in which case it is treated and actually becomes a time function. If the distorted signal is recalled as it is, its time representation will be distorted in the same manner as the spatial representation so that time and space for the stored signal go hand in hand.

If $k_1 = k_4$ and $k_2 = k_4$, it can be seen in Eqs. (3.[illegible]) and (3.[illegible]) that there will be terms without spatial carriers. These terms can produce

an appreciable output, whereas the remaining terms are of too high a spatial frequency to produce other than a negligible output. Also note that these additional terms are traveling potential waves so that they vary too fast in time to affect storage. The outputs from the convolver due to the terms without spatial frequency carriers are given by Eqs. (3.41) and (3.47) as the convolution of $s_o(t)$ with $f_o(t)$ and the correlation of $s_o(t)$ with $g_o(t)$ with carriers given by the respective carriers of the surface waves $f(t-z/v)$ and $g(t+z/v-D/v)$. This represents one technique for interacting with the stored signal. Moreover, if $f(t)$ is an 'impulse' with a finite number of ω_1 rf cycles, the output of the convolver is proportional to $s(t)$ where $t = z/v$ (where v is the average acoustic velocity beneath the semiconductor). When $g(t)$ is an 'impulse' composed of a finite number of ω_2 rf cycles, the output is proportional to $s(-t)$. In either case, this assumes that the spatial frequency of the stored carrier is the same as the spatial frequency of the surface wave performing the reading operation. When the surface wave is an 'impulse', it is effectively scanning the information stored along the semiconductor and the convolver output is a smoothed time version of this information, since this reading 'impulse' is also of finite width. It must be stressed that any correlation or convolution between two signals, whether they are both surface waves or only one of the two signals is a surface wave, is only valid for the period in time when the surface waves are totally beneath the semiconductor. At any other time the output convolution or correlation is due to only part of the signal represented by the surface wave or waves. The situation is different, however, for spatially stored convolutions and correlations. In this case, every point along the semiconductor 'sees' the entire interaction

between the two signals whether or not they are both surface waves. The only problem is only D/v seconds of this interaction between the two signals can be stored and the portion stored is dependent on the timing between the two signals. In other words, although the correlation and convolution of two T second long square pulses is a triangle with a 2T second long base only D/v of this triangle will be seen. If T = D/v then for the correlation between t(t) and one of the surface waves only half the triangle will be stored. Note, however, that the entire triangle is stored if the two pulses are the two contrapropagating surface waves since the correlation stored by this interaction is compressed by a factor of two. From this discussion it can be seen that extremely long signals can be correlated in a convolver having a small interaction length D or time D/v by utilizing the correlation-storage mechanism, however, the correlation recovered by reading this stored signal can only be a D/v second wide portion of the extremely long correlation of the two signals. This is the basis for the so-called 'integrating correlator'.(Ralston, et.al., 1977)

There is very little output obtained at the semiconductor (spatially-integrating) back contact for both terms in Eq. (3.[illegible]). For large ω_3 there is also very little effect, if any, on storage. However, this term is far from useless. As a matter of fact it represents an alternate technique by which the stored signal can be read. If t(t) is an impulse, the potential function $s_o(z/v)\cos k_4 z$ is impressed onto the surface of the piezoelectric delay line. The resulting fields then produce, in a manner identical to the behavior of an interdigital transducer, propagating surface waves of the form $s_o(t \pm z/v)\cos(\omega_4 t \pm k_4 z)$ where $\omega_4 = k_4 v$. This process can be visualized as the impulsing of an interdigital transducer that has been weighted by the stored function. Surface waves identical

to the impulse response of the transducer would propagate in both the positive and negative z direction for this case. Therefore, the signal stored along the semiconductor can be recovered by 'impulsing' the semiconductor ($t(t) = \delta(t)$) and sensing the signal or its time reversed version at one or the other of the convolver input transducers since such transducers are efficient receivers as well as transmitters. This reading process is non-destructive so long as the impressed fields are not strong enough and of the proper polarity to discharge the storage mechanism in the semiconductor. In the case of diodes, this requires not forcing them into forward bias. In a sense the internal fields set up by the stored charge modify the otherwise uniform field impressed onto the delay line by $t(t)$ in a manner identical to the spatial distribution of this charge. This spatially varying field impressed momentarily onto the delay line is enough to initiate surface wave propagation at this spatial periodicity. The large DC field impressed onto the line by $t(t)$ cannot, however, produce a wave with this periodicity.

Since the output of a convolver having a stored internal charge distribution is the convolution or correlation of its input signal with the stored signal then, in a sense, this device is a programmable-impulse-response filter. Moreover, by properly storing a signal, the convolver becomes a matched filter for the signal, if it is applied to the input that results in correlation with the stored version of the signal. The signal to noise ratio of a signal can furthermore be improved if it is repetitive and is successively stored, without pre-erasure, in the device. In this case the random noise variations are integrated out. A device utilizing this mechanism is called a coherent integrator.

Before concluding this discussion it is worthwhile to note that higher order interactions are also possible. All the interactions alluded to here are of second order in that the fields are effectively summed and then squared. Third order interactions involving a summation followed by a cubic operation are also possible, but they can be expected to be quite small since the second order interactions themselves are small. However, third order interactions have been investigated since they possess the potential for allowing the signals to be stored with spatial variations different from the input signals to the device, thereby suppressing spurious signals related directly to these inputs. The inherent small size of the resultant outputs, however, may ultimately limit the usefulness of such operations. A feel for the process by which such an interaction occurs can be obtained by looking at the interaction of $t(t) = \cos((\omega_1-\omega_2)t)$ with the second term in Eq. (3.53). In this case a first order term is directly interacting with a second order term resulting in a stored spatial charge distribution with spatial frequency $k_1 + k_2$. Not only can the two input signals have different spatial periodicities, but the stored pattern is stored with a higher spatial periodicity than either input signal. Spurious signals stored at the periodicity of either input signal will not be recovered at the same frequency as the stored desired signal and therefore will not interfere with it. The time signal $t(t)$ of frequency $\omega_1-\omega_2$ and uniform amplitude is usually called the pumping signal in this three-signal interaction.

2.4 The Chirp Transformation Using Chirp Filters

The chirp transformation is a process by which quadratic phase signals and devices are utilized to produce the Fourier transform of a signal. In simplified terms, the Fourier transform of the signal, f(t), given by

$$F(\omega) = \int_{-\infty}^{\infty} f(\tau)e^{-j\omega\tau}\, d\tau \tag{4.1}$$

can be written as

$$\begin{aligned} F(2\beta t) &= e^{-j\beta t^2} \int_{-\infty}^{\infty} f(\tau)e^{-j\beta\tau^2}\, e^{j\beta(t-\tau)^2}\, d\tau \\ &= e^{-j\beta t^2}\left(f(t)e^{-j\beta t^2} * e^{j\beta t^2}\right) \\ &= \int_{-\infty}^{\infty} f(\tau)e^{-j2\beta t\tau}\, d\tau \end{aligned} \tag{4.2}$$

where $\omega = 2\beta t$ is the real-time to frequency correspondence of the transform. This equation shows that the Fourier transform of f(t) can be obtained by multiplying this signal by a unit-amplitude-quadratic-phase-complex exponential, $\exp(-j\beta t^2)$, convolving this with another such exponential, $\exp(j\beta t^2)$, having opposite phase variation to the first and then multiplying the result of the convolution by an exponential, $\exp(-j\beta t^2)$, that is identical to the first. This is known as the MCM or Multiply-Convolve-Multipy chirp transformation scheme.

Utilizing the relationship

$$\int_{-\infty}^{\infty} e^{\mp j\beta\tau^2} e^{-j2\beta t\tau}\, d\tau = \sqrt{\frac{\pi}{\beta}}\, e^{\pm j\frac{\pi}{4}}\, e^{\mp j\beta(t+\tau)^2} \tag{4.3}$$

the Fourier transform can also be written as

$$F(2\beta t) = \sqrt{\frac{\beta}{\pi}}\, e^{-j\frac{\pi}{4}} \int_{-\infty}^{\infty} e^{-j\beta t_o^2} \int_{-\infty}^{\infty} f(\tau) e^{j\beta(t_o-\tau)^2}\, d\tau\, e^{j\beta(t-t_o)^2}\, dt_o$$

$$= \sqrt{\frac{\beta}{\pi}}\, e^{-j\frac{\pi}{4}} \left((e^{-j\beta t^2} (f(t) * e^{j\beta t^2})) * e^{j\beta t^2} \right)$$

$$= \int_{-\infty}^{\infty} f(\tau) e^{-j2\beta t\tau}\, d\tau \qquad (4.4)$$

This equation shows that the Fourier transform of f(t) can be obtained by convolving this signal with $\exp(j\beta t^2)$, multiplying by $\exp(-j\beta t^2)$ and then convolving again with $\exp(j\beta t^2)$. This is known as the CMC or Convolve-Multiply-Convolve chirp transformation scheme and is also considered as the dual of the MCM scheme.

The backbone of a practical realization of either of these schemes is the chirp filter. Ideally this device possesses a finite duration impulse response that is perfectly flat over its duration with a zero, first and second order phase variation. Actual devices, of course, are only approximations to this type of device. (Variations from ideally flat amplitude and quadratic phase are treated in Arsenault 1970.) Large time-bandwidth product surface-acoustic-wave (SAW) chirp filters are typically very good approximations to the ideal chirp filter. An ideal chirp filter can have one of two forms of impulse response. These impulse responses are of the form

$$IR_1 = K_1 \left| U(t-t_1) - U(t-t_1-T_1) \right| \cos(\omega_1(t-t_1) - \beta(t-t_1)^2 + \phi_1) \qquad (4.5)$$

and

$$IR_2 = K_2 \left| U(t-t_2) - U(t-t_2-T_2) \right| \cos(\omega_2(t-t_2) + \beta(t-t_2)^2 + \phi_2) \qquad (4.6)$$

In these equations K_1 and K_2 are constant amplitudes and ϕ_1 and ϕ_2 are constant phases. The impulse response given by Eq. (4.5) begins after a t_1 second time delay at an instantaneous frequency of ω_1 radians/sec and

with a phase of ϕ_1 radians. The instantaneous frequency of this response decreases at a rate of 2β radians/sec^2 so that -2β is considered as the slope of the chirp device, which is negative in this case. T_1 is the duration of IR_1. The impulse response, IR_2, given by Eq. (4.6) behaves similarly except that its instantaneous frequency increases at a rate of 2β radians/sec^2 and therefore possesses a positive slope. This T_2 second wide impulse response has an instantaneous frequency of ω_2 radians/sec and phase of ϕ_2 radians after a time delay of t_2 seconds. Equation (4.5) will be considered as the impulse response of a 'down-chirp filter' and Eq. (4.6) will be considered as an 'up-chirp filter' impulse response.

Parseval's theorem

$$\int_{-\infty}^{\infty} |f(t)|^2 \, dt = \frac{1}{2\pi} \int_{-\infty}^{\infty} |F(\omega)|^2 \, d\omega \tag{4.7}$$

is useful for finding the constants K_1 and K_2. In particular, if a chirp filter transfer function can be approximated as flat over a finite $2\pi B$ radian/sec wide passband (which is an accurate approximation for large time-bandwidth product devices) and, if the loss over this passband is given by L, then for an ideal impulse, $\delta(t)$, applied to the input of this device where

$$\delta(t) \longleftrightarrow 1 \tag{4.8}$$

the total spectral energy at the device output is given by

$$\begin{aligned} E_{OUT1} &= \frac{1}{2\pi R} \int_{-\infty}^{\infty} |F(\omega)|^2 \, d\omega \\ &= \frac{1}{2\pi R} \int_{-\infty}^{\infty} |L(U(\omega-\omega_c+\pi B) - U(\omega-\omega_c-\pi B) \\ &\quad + U(\omega+\omega_c+\pi B) - U(\omega+\omega_c-\pi B))|^2 \, d\omega \\ &= 2BL^2/R \text{ joules} \end{aligned} \tag{4.9}$$

where R is the resistance of the output network. If the resulting impulse response is V volts peak (vpp/2) and T seconds wide, then the energy imparted to an R ohm load by this response is given by

$$E_{OUT2} = \frac{1}{2} V^2 T/R \text{ joules} \tag{4.10}$$

Equating equations (4.9) and (4.10) gives

$$V = 2L(B/T)^{\frac{1}{2}} = 2L(\beta/\pi)^{\frac{1}{2}} \tag{4.11}$$

where $\beta = \pi B/T$ is half the slope of the chirp filter. Since V is the peak to peak voltage of the output impulse response, then

$$K_1 = 2L_1(\beta/\pi)^{\frac{1}{2}} \tag{4.12}$$

and

$$K_2 = 2L_2(\beta/\pi)^{\frac{1}{2}} \tag{4.13}$$

where L_1 and L_2 are the respective losses for the down and up chirp filters given by the ratio of the output to input peak voltage for a continuous single frequency input. For SAW chirp filters that have impulse responses varying by many megahertz over tens of microseconds, β is on the order of 10^{12} so that these constants are very large. By not including K_1 and K_2, therefore, the device outputs would seem negligibly small for these devices. L_1 and L_2, for SAW devices, are on the order of .1 to .03 or equivalently 20 to 30 dB of signal attenuation is evidenced (i.e. for SAW RAC's).

In order to obtain the Fourier transform of a signal, f(t), using the MCM technique, this signal must be multiplied by a chirp. ('Chirp' is the general term used to signify a signal having quadratic phase.) A straightforward technique for generating the so-called

pre-multiplying chirp is to impulse a chirp device, thereby utilizing its impulse response. After the chirp is obtained in this manner, it can be mixed with constant frequency rf's and filtered so as to change the sign of its slope or even the range of instantaneous frequencies over which it varies. For instance, by mixing Eq. (4.5) with $\cos(\omega_3(t-t_1))$ the modified chirp

$$IR_3 = K_1\left|U(t-t_1) - U(t-t_1-T_1)\right|\cos((\omega_3-\omega_1)(t-t_1) + \beta(t-t_1)^2 - \phi_1) \quad (4.14)$$

is obtained as the difference term of the mixing process. For $\omega_3 > \omega_1$ the sign of the slope has been changed and the instantaneous frequency at $t=t_1$ is now $\omega_3-\omega_1$ instead of ω_1, as it previously was. Whenever the sign of the chirp slope is changed the chirp is said to have been 'spectrally-inverted'. Modified device impulse responses of this type can also be used for the post-multiplication in an MCM chirp transform system and the single multiplication in a CMC system. Whenever devices having only one particular slope are available, spectral inversion is a powerful technique for obtaining slopes of opposite polarity, as is required for the pre and post-multipliers of an MCM system.

The input to a chirp transformation system can either be at baseband or on a carrier. The two cases, however, must be treated differently. The baseband signal can be pre-multiplied by a chirp that is derived by merely impulsing a device (that is identical to the device through which the signal is to be passed) and then simply 'spectrally inverting' this response by utilizing a mixing rf at twice the chirp center frequency. (This effectively time-inverts the device impulse response.) Essentially, the pre-multiplied baseband signal is, in this

way, mixed up to the bandpass region of the device through which it must pass. Mixing carrier modulated signals in this same way, however, would result in signals that fall outside the bandpass of the device, for large carrier frequencies. These signals must be mixed with chirps that have been properly tailored and, therefore, shifted in frequency so that, upon pre-multiplication, the combined signal passes through the passband of the chirp filter. As a matter of fact, if the carrier frequency of the input signal is chosen properly, then the required 'spectral inversion' of the chirp impulse response can be made to occur automatically when mixed with this signal. If, however, the carrier is too small, the sum and difference terms, resulting from the pre-multiplication, will be both of proper slope and fall within the bandpass of the convolving chirp filter. In this case, it may be necessary to display both the positive and negative spectrums of the signal. Whenever a carrier modulated signal is pre-multiplied by a chirp, two terms result from this process. If the carrier is large enough (i.e. greater than the sum of the device and signal bandwidths), then the output transform can be centered about the transform of one of these terms and little interference will occur from the other. When centered about one of the terms, then the transform represents the Fourier transform of the baseband information (i.e. the modulation envelope). If the carrier is small enough, so that both transforms can be displayed, then this represents the Fourier transform of the carrier modulated signal. Clearly, since Fourier theory shows that either positive or negative spectrums contain all the information in the baseband signal, then, if no overlap or negligible overlap occurs between the two, retaining only one is essentially all that is required for later recovery (by Fourier

inversion) of the baseband signal. Although, at viewing time, it may not seem too important what portion of the transform is being looked at, when inverse transforms are to be taken it is important that the transform be properly displayed for proper reconstruction of the signal (see 'Spectrum Modifications', section 2.6).

In general, let the input signal, over the time interval $0 \leq t \leq T_s$, be given by

$$f(t) = a(t)\cos\omega_o t - b(t)\sin\omega_o t$$

$$= \hat{f}(t)\cos(\omega_o t + \phi(t)) \tag{4.15}$$

where

$$a(t) = \hat{f}(t)\cos\phi(t) \tag{4.16}$$

and

$$b(t) = \hat{f}(t)\sin\phi(t) \tag{4.17}$$

After pre-multiplication (and LPF) this signal is given by

$$f(t)\cos(\omega_1 t - \beta t^2 + \phi_1)$$

$$= a(t)\cos(\omega_s t + \beta t^2 - \phi_1) + b(t)\sin(\omega_s t + \beta t^2 - \phi_1) \tag{4.18}$$

where $\omega_s = \omega_o - \omega_1$. Here it was assumed that a chirp filter with impulse response given by Eq. (4.5) was impulsed at $t = -t_1$ and this response used as the modulation. Since none of the input signal is to be lost, then $T_s < T_1$. This signal will now be convolved with Eq. (4.5), the result of which is equivalent to the output obtained by passing Eq. (4.18) through a device having impulse response given by Eq. (4.5). (The amplitude factors (K_1 and K_2) are being ignored in this derivation.) The output of

the chirp filter, over the time interval $t_1 + T_s \leq t \leq t_1 + T_1$, is proportional to

$$\text{output} = \int_{-\infty}^{\infty} f(\tau)\cos(\omega_1\tau - \beta\tau^2 + \phi_1)\cos(\omega_1(t-\tau-t_1) - \beta(t-\tau-t_1)^2 + \phi_1)d\tau$$

$$= \frac{1}{4} e^{-j(\omega_1(t-t_1) - \beta(t-t_1)^2)} \int_{-\infty}^{\infty} a(\tau)e^{-j(2\beta(t-t_1) - \omega_1 + \omega_s)\tau} d\tau + c.c.$$

$$+ \frac{1}{4} e^{-j(\omega_1(t-t_1) - \beta(t-t_1)^2 - 2\phi_1)} \int_{-\infty}^{\infty} a(\tau)e^{j2\beta\tau^2} e^{-j(2\beta(t-t_1) - \omega_1 - \omega_s)\tau} d\tau + c.c$$

$$+ j\frac{1}{4} e^{-j(\omega_1(t-t_1) - \beta(t-t_1)^2)} \int_{-\infty}^{\infty} b(\tau)e^{-j(2\beta(t-t_1) - \omega_1 + \omega_s)\tau} d\tau + c.c.$$

$$+ j\frac{1}{4} e^{-j(\omega_1(t-t_1) - \beta(t-t_1)^2 - 2\phi_1)} \int_{-\infty}^{\infty} b(\tau)e^{j2\beta\tau^2} e^{-j(2\beta(t-t_1) - \omega_1 - \omega_s)\tau} d\tau + c.c. \qquad (4.19)$$

The first and third set of integrals can be written as

$$FT = \frac{1}{2}(R_a(\omega) - X_b(\omega))\cos(\omega_1(t-t_1) - \beta(t-t_1)^2)$$

$$+ \frac{1}{2}(R_b(\omega) + X_a(\omega))\sin(\omega_1(t-t_1) - \beta(t-t_1)^2) \qquad (4.20)$$

where

$$\omega = 2\beta(t-t_1) - \omega_1 + \omega_s \qquad (4.21)$$

$$R_a(\omega) \quad \int a(\tau)\cos\omega\tau d\tau \qquad (4.22)$$

$$X_a(\omega) = -\int_{-\infty}^{\infty} a(\tau)\sin\omega\tau d\tau \qquad (4.23)$$

$$R_b(\omega) = \int_{-\infty}^{\infty} b(\tau)\cos\omega\tau d\tau \qquad (4.24)$$

$$X_b(\omega) = -\int_{-\infty}^{\infty} b(\tau)\sin\omega\tau d\tau \qquad (4.25)$$

This portion of the output is the real and imaginary components of the Fourier transform of the input on in-phase and quadrature chirp carriers, The transform is of a signal existing from t=0 to $t=T_s$. If it be desired that the transform be of an advanced version, $f(t+t_o)$, of the signal, then the output can be rewritten as

$$FT = \frac{1}{2}\left|\hat{R}_a(\omega) - \hat{X}_b(\omega)\right|\cos(\omega_1(t-t_1) - \beta(t-t_1)^2 + \omega t_o)$$

$$+ \frac{1}{2}\left|\hat{R}_b(\omega) + \hat{X}_a(\omega)\right|\sin(\omega_1(t-t_1) - \beta(t-t_1)^2 + \omega t_o) \qquad (4.26)$$

where

$$\hat{R}_a(\omega) = \int_{-\infty}^{\infty} a(\tau+t_o)\cos\omega\tau d\tau \qquad (4.27)$$

$$\hat{X}_a(\omega) = -\int_{-\infty}^{\infty} a(\tau+t_o)\sin\omega\tau d\tau \qquad (4.28)$$

$$\hat{R}_b(\omega) = \int_{-\infty}^{\infty} b(\tau+t_o)\cos\omega\tau d\tau \qquad (4.29)$$

$$\hat{X}_b(\omega) = -\int_{-\infty}^{\infty} b(\tau+t_o)\sin\omega\tau d\tau \qquad (4.30)$$

Eqs. (4.20) and (4.26) show that the time location of the signal to be transformed can be decided after the chirp convolution by utilizing the prescribed chirp needed to demodulate these real and imaginary Fourier components. In other words, if $\cos(\omega_o(t-t_1) - \beta(t-t_1)^2 + \omega t_o)$ is mixed with Eq. (4.26), the output difference term is

$$\hat{FT} = \frac{1}{2}\left|\hat{R}_a(\omega) - \hat{X}_b(\omega)\right|\cos(\omega_s t)$$

$$- \frac{1}{2}\left|\hat{R}_b(\omega) + \hat{X}_a(\omega)\right|\sin\omega_s t \qquad (4.31)$$

and the Fourier components of the delayed signal are obtained on quadrature carriers. Quadrature carriers can be used, with low pass filters (LPF s), separate the components.

The Fourier components given by Eqs. (4.20) and (4.26) are valid only over the time interval $t_1 + T_s \leq t \leq t_1 + T_1$. It is only during this time that the finite duration signal is totally overlapped by the finite duration impulse response of the chirp device in the convolution integral defining the output of the device. Only during this overlapping time period can the limits of integration in Eq. (4.19) be set to plus and minus infinity. All other times represent invalid portions of the Fourier transform and typically would be time gated from the valid portions. From this it can be seen that the valid portion of the Fourier transform is T_1-T_s seconds wide. If an inverse transformation is to be performed then, unless the entire Fourier transform is centered within this region, the signal obtained is a filtered or distorted version of the input. To center the Fourier transform it is necessary that at the center of the valid region $t_c = t_1 + \frac{1}{2}(T_s+T_1)$

$$\omega\Big|_{t=t_c} = 2\beta(t_c-t_1) - \omega_1 + \omega_s = 0 \tag{4.32}$$

or

$$\omega_s = \omega_1 - \beta(T_s+T_1) \tag{4.33}$$

If this be the case, then the Fourier components from $-\beta(T_1-T_s)$ to $\beta(T_1-T_s)$ radians/second are displayed from t_1+T_s to t_1+T_1 seconds of real time. The time-to-frequency correspondence of a centered transform is therefore given by

$$\omega = 2\beta(t - t_1 - \tfrac{1}{2}(T_s + T_1)) \tag{4.34}$$

The time-to-frequency correspondence of the 2nd and 4th integrals in Eq. (4.19) is given by

$$\omega = 2\beta(t - t_1 + \frac{1}{2}(T_s+T_1)) - 2\omega_1 \tag{4.35}$$

when the 1st and 3rd integrals representing the Fourier transform of f(t) are centered. These other integrals are similar to the 1st and 3rd except that they represent the transform of $f(t)\exp(j2\beta t^2)$. The center of this transform is at

$$t_{c2} = \frac{\omega_1}{\beta} + t_1 - \frac{1}{2}(T_s+T_1) \tag{4.36}$$

which is $\omega_1/\beta - T_s - T_1$ seconds away from the center of the valid time interval. Only for small ω_1 or when $\omega_1 \simeq \beta(T_s+T_1)$ will this other transform greatly interfere. Since $f(t)\exp(j2\beta t^2)$ is a finite duration signal there will always be some portion of its transform in the output valid time interval, however, this will be negligible if ω_1 is much greater than $\beta(T_s+T_1)$. Note that, as discussed in Appendix B on long transformations, it is not necessary to display the transform centered about $\omega=0$, especially if viewing the transform is of prime concern and no Fourier inversion is to be performed. In this case, utilizing judicious filtering, an extremely wide bandwidth signal can have any $2\beta(t_1-T_s)$ rad/sec portion of its spectrum viewed by setting the time-to-frequency correspondence given by Eq. (4.21) equal to the center frequency of the desired portionof the spectrum and solving for the required ω_s with $t=t_c$. The T_s second wide signal may have such a wide bandwidth that filtering may be required to eliminate undesirable cross products. Although Appendix C describes a technique whereby the transform of very long signals can be taken, in many cases it may be just as satisfactory to transform a continuous signal into a contiguous stream of T_1-T_s second wide transforms.

In this case, each transform is the Fourier transform of a T_s second wide segment of the continuous signal each of which is assumed to exist around the time origin. (In fact by utilizing the proper post-multiplying chirps, the individual transforms will be those for time-centered segments of the continuous signal.) To properly transform a continuous signal, however, it must be broken up into at least two alternating streams (see Part III). If $T_1-T_s = T_s$ or $T_s = T_1/2$, then the output transforms will be valid for a time period equal to the width of the input signals. If the two alternating streams are fed into two individual identical chirp transform systems whose chirp filter inherent delays (t_1) are also $T_1/2$ seconds, then the same chirp streams used to modulate the input streams can be used to demodulate the output transform streams. Set up in this way the invalid portions of the output will not interfere with the valid portions and can be gated out. The two transform streams can then be summed together.

The output Fourier transform given by Eq. (4.20) can be rewritten as

$$FT = \frac{1}{2}\left((R_a(\omega) - X_b(\omega))^2 + (R_b(\omega) + X_a(\omega))^2\right)^{\frac{1}{2}}$$

$$\cos(\omega_1(t-t_1) - \beta(t-t_1)^2 + \tan^{-1}((R_b(\omega) + X_a(\omega))/(R_a(\omega) - X_b(\omega))) \tag{4.37}$$

This equation shows that the output is essentially a chirp with an additional phase variation given by the phase component of the Fourier transform and a magnitude given by the magnitude of the Fourier transform. Before post-multiply, the output of the chirp transform system, as seen on an oscilloscope, appears to be the carrier modulated magnitude of the

Fourier transform. The signal given by Eq. (4.15) represents the complex signal $a(t) + jb(t)$ and the output transform given by Eqs. (4.20) and (4.37) represents $(R_a(\omega) - X_b(\omega)) + j(R_b(\omega) + X_a(\omega))$ or $((R_a(\omega) - X_b(\omega))^2 + (R_b(\omega) + X_a(\omega))^2)^{1/2} \exp(j\tan^{-1}((R_b(\omega) + X_a(\omega))/(R_a(\omega) - X_b(\omega))))$. If $f(t)$ is complex then the Fourier transform can be asymmetric about $\omega=0$. If $f(t)$ is real (i.e $b(t) = 0$) then its Fourier transform must have a symmetric real and antisymmetric imaginary component about $\omega=0$. Furthermore, its magnitude must be symmetric about $\omega=0$ and its phase must be antisymmetric. If ϕ is a constant, then $f(t)$ represents the complex signal $\hat{f}(t)\cos\phi + j\hat{f}(t)\sin\phi$. The magnitude of the Fourier transform of this signal is always symmetric, although its real and imaginary components will not, in general, possess symmetry about $\omega=0$. With $\phi=0$ the input is pure real with an even real Fourier component and an odd imaginary component. With $\phi = \pi/2$ the signal is pure imaginary with an odd real Fourier component and an even imaginary component. The magnitude of the Fourier transform looses its even symmetry when ϕ is a function of time. If improperly phased pre and post-multiplying chirps are used in a chirp transform system, a real signal is treated as complex and a complex signal is treated as an altogether different complex signal. When separating the real Fourier component from the imaginary component, part of one of these components is summed into part of the other. As the phase of the output post-multiplying chirp is changed, the real and imaginary Fourier components of the signal can be seen to swap back and forth. The transform components are always valid but they may not be the transform components for the form of the complex signal that may be desired. For the remainder of this discussion the device inherent delays and constant phases will be

ignored to simplify the equations. Furthermore, all chirps and impulse responses will be of the form

$$c(t) = \cos(+) \text{ or } \cos(-) \tag{4.38}$$

where

$$(+) = \omega t + \beta t^2$$

$$(-) = \omega t - \beta t^2$$

and the finite durations will only be implied. The output transforms will be assumed to be accurate over a specified time interval, however, nothing more will be said about this.

The output of a down-chirp filter with impulse response (IR) $\cos(-)$ for an input of $a(t)\cos(+) \pm b(t)\sin(+)$ is given by

$$\text{Output} = \left|R_a(2\beta t) \mp X_b(2\beta t)\right|\cos(-)$$

$$\pm \left|R_b(2\beta t) \pm X_a(2\beta t)\right|\sin(-) \tag{4.39}$$

The down-chirp filter MCM system therefore takes the forward transform of the signal. This will be signified by the following

$$f(t)_+ \longrightarrow (-) \longrightarrow F(\omega)_- \tag{4.40}$$

$$f^*(t)_+ \longrightarrow (-) \longrightarrow F^*(-\omega)_-$$

where the (+) and (-) subscripts refer to up and down-chirp carriers. If Eq. (4.39) is mixed with $\cos 2\omega t$ (spectrally-inverted) the difference term is given by

$$\text{Output} = \left|R_a(2\beta t) \mp X_b(2\beta t)\right|\cos(+)$$

$$\mp \left|R_b(2\beta t) \pm X_a(2\beta t)\right|\sin(+) \tag{4.42}$$

so that this process complex conjugates the Fourier transform as well as changing the chirp slope. This will be signified by the following

$$F(\omega)_{-} \longrightarrow x(2\omega) \longrightarrow F^{*}(\omega)_{+} \tag{4.43}$$

$$F^{*}(-\omega)_{-} \longrightarrow x(2\omega) \longrightarrow F(-\omega)_{+} \tag{4.44}$$

When $a(t)\cos(-) \pm b(t)\sin(-)$ is inputted into an up-chirp filter with impulse response $\cos(+)$ the output is given by

$$\text{Output} = \left|R_a(2\beta t) \pm X_b(2\beta t)\right|\cos(+) \pm \left|R_b(2\beta t) \mp X_a(2\beta t)\right|\sin(+) \tag{4.45}$$

The up-chirp filter MCM system therefore performs a frequency inverted transform, which is equivalent to taking the Fourier transform of a time inverted version of the signal. This will be signified by the following

$$f(t)_{-} \longrightarrow (+) \longrightarrow F(-\omega)_{+} \tag{4.46}$$

$$f^{*}(t)_{-} \longrightarrow (+) \longrightarrow F^{*}(\omega)_{+} \tag{4.47}$$

Multiplying Eq. (4.45) by $\cos 2\omega t$ produces a difference term given by

$$\text{Output} = \left|R_a(2\beta t) \pm X_b(2\beta t)\right|\cos(-) \mp \left|R_b(2\beta t) \mp X_a(2\beta t)\right|\sin(-) \tag{4.48}$$

so that, as before, the transform is complex conjugated and the chirp slope changes sign. This will be signified by the following

$$F(-\omega)_{+} \longrightarrow x(2\omega) \longrightarrow F^{*}(-\omega)_{-} \tag{4.49}$$

$$F^{*}(\omega)_{+} \longrightarrow x(2\omega) \longrightarrow F(\omega)_{-} \tag{4.50}$$

Inverse Fourier transformations will now be taken. An example

will be worked out and then the different possibilities will be listed. Assume the Fourier transform is given by

$$FT = A(t)\cos(-) + B(t)\sin(-) = F(\omega)_{-} \tag{4.51}$$

where

$$A(t) = R_a(2\beta t) - X_b(2\beta t) \tag{4.52}$$

and

$$B(t) = R_b(2\beta t) + X_a(2\beta t) \tag{4.53}$$

Since this is a complex signal similar to the input signal $f(t)_{-}$, then the output of an up-chirp filter for this input can be immediately written down by inspection to give

$$\text{Output} = \left| r_A(2\beta t) + x_B(2\beta t) \right| \cos(+) + \left| r_B(2\beta t) - x_A(2\beta t) \right| \sin(+) \tag{4.54}$$

where

$$r_A(2\beta t) = \int_{-\infty}^{\infty} A(\tau)\cos 2\beta t\tau d\tau = \int_{-\infty}^{\infty} R_a(2\beta\tau)\cos 2\beta\tau t d\tau = \frac{a_e(t)}{2\beta} \tag{4.55}$$

$$x_A(2\beta t) = -\int_{-\infty}^{\infty} A(\tau)\sin 2\beta t\tau d\tau = \int_{-\infty}^{\infty} X_b(2\beta\tau)\sin 2\beta\tau t d\tau = \frac{-b_o(t)}{2\beta} \tag{4.56}$$

$$r_B(2\beta t) = \int_{-\infty}^{\infty} B(\tau)\cos 2\beta t\tau d\tau = \int_{-\infty}^{\infty} R_b(2\beta\tau)\cos 2\beta\tau t d\tau = \frac{b_e(t)}{2\beta} \tag{4.57}$$

$$x_B(2\beta t) = -\int_{-\infty}^{\infty} B(\tau)\sin 2\beta t\tau d\tau = -\int_{-\infty}^{\infty} X_a(2\beta\tau)\sin 2\beta\tau t d\tau = \frac{a_o(t)}{2\beta} \tag{4.58}$$

$$a(t) = a_e(t) + a_o(t) \tag{4.59}$$

$$a_e(t) = \frac{1}{2}\left(a(t) + a(-t)\right) = a_e(-t) \tag{4.60}$$

$$a_o(t) = \frac{1}{2}\left(a(t) - a(-t)\right) = -a_o(-t) \tag{4.61}$$

$$b(t) = b_e(t) + b_o(t) \tag{4.62}$$

$$b_e(t) = \frac{1}{2}\left(b(t) + b(-t)\right) = b_e(-t) \tag{4.63}$$

$$b_o(t) = \frac{1}{2}\left(b(t) - b(-t)\right) = -b_o(-t) \tag{4.64}$$

or

$$\text{Output} = \frac{1}{2\beta}\left|a(t)\cos(+) + b(t)\sin(+)\right| \tag{4.65}$$

Since the actual device impulse responses contain a $(\beta)^{1/2}$ factor, then there will be a factor of β after the inverse transformation process that will cancel the β in Eq. (4.65). The β in this equation arose since the $(\beta)^{1/2}$ factor has been ignored up until now, The $1/2\beta$ factor (and all multiplying factors, for that matter) will hereon be left out. Therefore, the output of an up-chirp device for an input of $(R_a(2\beta t) \mp X_b(2\beta t))\cos(-) \pm (R_b(2\beta t) \pm X_a(2\beta t))\sin(-)$ is given by

$$\text{Output} = a(t)\cos(+) \pm b(t)\cos(+) \tag{4.66}$$

The up-chirp filter MCM system takes the Fourier transform of the Fourier transform, which is treated as though it is time inverted, so that the original signal is obtained. This will be signified by the following

$$F(\omega)_- \longrightarrow (+) \longrightarrow f(t)_+ \tag{4.67}$$

$$F^*(-\omega)_- \longrightarrow (+) \longrightarrow f^*(t)_+ \tag{4.68}$$

When $(R_a(2\beta t) \pm X_b(2\beta t))\cos(+) \pm (R_b(2\beta t) \mp X_a(2\beta t))\sin(+)$ is inputted into a down-chirp device the output is given by

$$\text{Output} = a(t)\cos(-) \pm b(t)\sin(-) \tag{4.69}$$

so that the down-chirp filter MCM system takes the Fourier transform of a

Fourier transform that is time inverted and the original signal is obtained. This will be signified by the following

$$F(-\omega)_+ \longrightarrow (-) \longrightarrow f(t)_- \tag{4.70}$$

$$F^*(\omega)_+ \longrightarrow (-) \longrightarrow f^*(t)_- \tag{4.71}$$

The two complete transform systems, not utilizing spectral inversion, are given by

$$f(t)_+ \longrightarrow (-) \longrightarrow F(\omega)_- \longrightarrow (+) \longrightarrow f(t)_+ \tag{4.72}$$

$$f(t)_- \longrightarrow (+) \longrightarrow F(-\omega)_+ \longrightarrow (-) \longrightarrow f(t)_- \tag{4.73}$$

Both of these systems recover the original signal complete with the original chirp modulation, however, opposite slope devices are required. If spectral inversion is used, the two possible complete transform systems are given by

$$f(t)_+ \longrightarrow (-) \longrightarrow F(\omega)_- \longrightarrow x(2\omega) \longrightarrow F^*(\omega)_+ \longrightarrow (-) \longrightarrow f^*(t)_- \tag{4.74}$$

$$f(t)_- \longrightarrow (+) \longrightarrow F(-\omega)_+ \longrightarrow x(2\omega) \longrightarrow F^*(-\omega)_- \longrightarrow (+) \longrightarrow f^*(t)_+ \tag{4.75}$$

Using these, the signal is recovered as a complex conjugated version of the input signal. In this case, however, identical devices can be used.

The above four schemes will always recover the signal or its complex conjugate. Spectral inversion by itself cannot be utilized as a mechanism for causing a system to produce a time inverted version of the input signal at the output. The reason for this is that only the sign of the transform chirp carrier slope must be changed to allow a repeated transform to be taken and therefore the time inverted signal to be obtained.

However, spectral inversion not only changes the sign of this slope, but it also complex conjugates the Fourier transform.

Time inverted versions of the input signal can only be obtained if somehow the transform slope polarity is changed without complex conjugation or vice versa. By mixing the transform with $\cos(2\omega t \pm 2\beta t^2)$ and low pass filtering, the Fourier transforms can be complex conjugated without a change in the chirp carrier slope polarity. This will be signified by the relations

$$F(\omega)_- \longrightarrow x(2\omega,-2\beta) \longrightarrow LPF \longrightarrow F^*(\omega)_- \tag{4.76}$$

$$F(-\omega)_+ \longrightarrow x(2\omega,2\beta) \longrightarrow LPF \longrightarrow F^*(-\omega)_+ \tag{4.77}$$

Adding a spectral inversion step, the transforms are not conjugated but their slopes change polarity. This will be signified by

$$F(\omega)_- \longrightarrow x(2\omega,-2\beta) \longrightarrow LPF \longrightarrow x(2\omega) \longrightarrow F(\omega)_+ \tag{4.78}$$

$$F(-\omega)_+ \longrightarrow x(2\omega,2\beta) \longrightarrow LPF \longrightarrow x(2\omega) \longrightarrow F(-\omega)_- \tag{4.79}$$

From this, the four possible time inversion schemes are given by

$$f(t)_+ \longrightarrow (-) \longrightarrow x(2\omega,-2\beta) \longrightarrow LPF \longrightarrow F^*(\omega)_- \longrightarrow (+) \longrightarrow f^*(-t)_+ \tag{4.80}$$

$$f(t)_- \longrightarrow (+) \longrightarrow x(2\omega,2\beta) \longrightarrow LPF \longrightarrow F^*(-\omega)_+ \longrightarrow (-) \longrightarrow f^*(-t)_- \tag{4.81}$$

$$f(t)_+ \longrightarrow (-) \longrightarrow x(2\omega,-2\beta) \longrightarrow LPF \longrightarrow x(2\omega) \longrightarrow F(\omega)_+ \longrightarrow (-) \longrightarrow f(-t)_- \tag{4.82}$$

$$f(t)_{-} \longrightarrow (+) \longrightarrow x(2\omega, 2\beta) \longrightarrow \text{LPF} \longrightarrow x(2\omega) \dashrightarrow F(-\omega)_{-} \longrightarrow$$

$$(+) \longrightarrow f(-t)_{+} \tag{4.83}$$

The first two schemes use different devices and complex conjugate the time inverted signal. The second two schemes use identical devices and obtain the time inverted signal with oppositely sloped carriers to the input. The double slope chirp can be obtained by passing the impulse response of a device through a doubler. The above schemes represent exact techniques for obtaining time inverted signals assuming the bandwidth is not restricted by time gating out some of the Fourier transform. This inversion is exact because it is based upon the properties of the Fourier transform. Time inversion, however, can also be performed, exactly, using the Fresnel transform. (The Fresnel transform is detailed in Appendix A.) This can be seen in Eq. (A- 30), which will be repeated here giving

$$e^{j2\beta t^2} F_{\beta}(t) \underset{\beta,t,\tau}{\longleftrightarrow} \frac{\pi}{\beta} e^{-j2\beta\tau^2} f(-\tau) \tag{4.84}$$

where

$$F_{\beta}(t) = \int_{-\infty}^{\infty} f(\tau) e^{-j\beta(\tau-t)^2} d\tau \tag{4.85}$$

is the Fresnel transform of f(t). This equation states that by multiplying the Fresnel transform by a double-slope chirp, a Fresnel transform of this signal produces a chirp-modulated-time-inverted signal. For an input signal $f(t)\cos\omega_1 t$, the output of a chirp filter having impulse response $(U(t) - U(t-T))\cos(\omega_o t - \beta t^2)$ is given over all time by

$$\text{Output} = e^{j\omega_o t} \int_{t-T}^{t} f(\tau) e^{j(\omega_1-\omega_o)\tau} e^{-j\beta(t-\tau)^2} d\tau + \text{c.c.}$$

$$\approx e^{j\omega_o t} \int_{-\infty}^{\infty} f(\tau) e^{j(\omega_1-\omega_o)\tau} e^{-j\beta(t-\tau)^2} d\tau + \text{c.c.} \tag{4.86}$$

since $t - T \leq \tau = t - \frac{1}{2\beta}(\omega_o - \omega_1) \leq t$ is a point of stationary phase. Eq. (4.86) shows that the output of the chirp filter is the Fresnel transform of $f(t)\exp(j(\omega_1-\omega_o)t)$ with a carrier of frequency ω_o. Because of the complex conjugate, the output real and imaginary components of the Fresnel transform are in phase quadrature. By utilizing the Fresnel transform instead of the Fourier, it is not necessary to synchronize a pre-multiplying chirp with a post-multiplying chirp since the input modulation for the Fresnel transform is an rf carrier. This is also an exact time inversion process. Note that if the input signal is extremely narrowband with respect to the chirp filter bandwidth, simply multiplying the signal with a double slope chirp and passing this signal through a single device of opposite slope will produce an approximation to that of a time inverted signal. This technique, however, is not exact since it disperses the frequency components of the signal. The extra chirp filters in both the Fourier and the Fresnel transform time inversion techniques are required to pre-disperse the signal frequency components, which are then brought back together by the second chirp filters, thereby preventing signal distortion.

The CMC chirp transform system must obey a different set of criteria for its practical realization. Therefore, a detailed description of a typical system will be given after which the detail will be dispensed with. The input signal to a down-chirp filter with impulse response given by Eq. (4.5) is given by

$$\text{Input} = a(t)\cos\omega_o t + b(t)\sin\omega_o t = f(t) \tag{4.87}$$

where

$$\omega_1 - 2\beta T_1 \leq \omega_o \leq \omega_1 \tag{4.88}$$

to make passage through the device possible. The output from the chirp filter over the time interval $t_1 + T_s \leq t \leq t_1 + T_1$, where the signal exists from $\tau=0$ to $t=T_s$, as before, is given by

$$\text{Output} = \int_{-\infty}^{\infty} (a(\tau)\cos\omega_o\tau + b(\tau)\sin\omega_o\tau)$$

$$\cos(\omega_1(t-\tau-t_1) - \beta(t-\tau-t_1)^2 + \phi_1)\, d\tau \qquad (4.89)$$

This signal is then multiplied by an up-chirp (that may be obtained by spectrally inverting the impulse response of the down-chirp filter) that must exist from $t = t_1+T_s$ to $t = t_1+T_s+T_1$ so as not to loose any of the output represented by Eq. (4.89). The up-chirp, if gated to the valid output interval $t_1 + T_s \leq t \leq t_1 + T_1$ over which the limits of Eq. (4.89) can be set to plus and minus infinity, will automatically gate out the invalid portions of the first chirp filter output, upon multiplication with this signal. The up-chirp will be given by

$$UC = \cos(\omega_2 t + \beta t^2) \qquad (4.90)$$

Before inputting to the second chirp filter, half of the output to this point can be discarded. The output consists of two identical integrals one having a complex rf carrier of the form $\exp(-j((\omega_1+\omega_2+2\beta t_1)t - \omega_1 t_1 - \beta t_1^2 + \phi_1))$ and the other having a complex chirp carrier of the form $\exp(-j((\omega_1-\omega_2+2\beta t_1)t - 2\beta t^2 - \omega_1 t_1 - \beta t_1^2 + \phi_1))$. Using the rf modulated integrals with $\omega_3 - 2\beta T_3 \leq \omega_1 + \omega_2 + 2\beta t_1 \leq \omega_3$, where all the second chirp filter parameters have the number three as a subscript, the input to this second chirp filter is given by

AD-A089 965 RENSSELAER POLYTECHNIC INST TROY NY MICROWAVE ACOUST--ETC F/G 17/2
SIGNAL PROCESSING USING SURFACE ACOUSTIC WAVE DEVICES AND ITS A--ETC(U)
DEC 79 D R ARSENAULT, L B MILSTEIN, P DAS DAAG29-77-G-0205
UNCLASSIFIED RPI-MA-ARO-10 ARO-15004.14-EL NL

2 OF 4
AD A089965

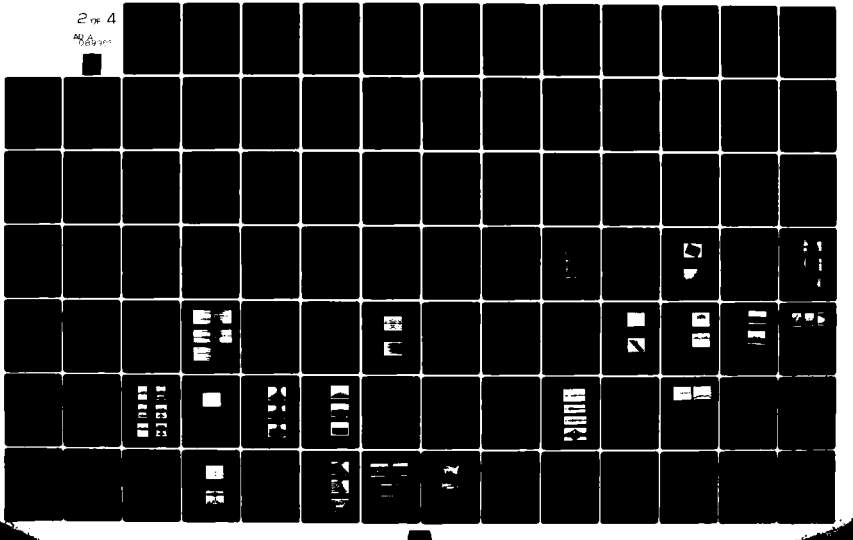

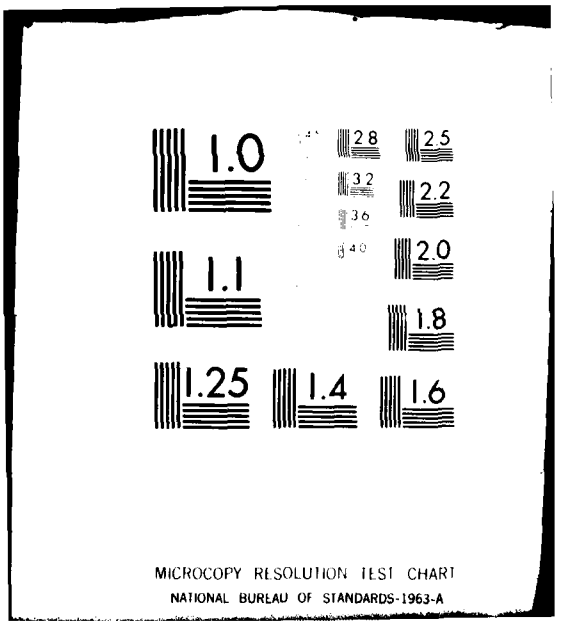
1.0
1.1
1.25
2.8
3.2
3.6
4.0
2.5
2.2
2.0
1.8
1.4
1.6
MICROCOPY RESOLUTION TEST CHART
NATIONAL BUREAU OF STANDARDS-1963-A

$$\text{Input} = \frac{1}{4} e^{-j((\omega_1+\omega_2+2\beta t_1)t-\omega_1 t_1-\beta t_1^2+\phi_1)}$$

$$\int_{-\infty}^{\infty} (a(\tau)\cos\omega_o\tau + b(\tau)\sin\omega_o\tau)e^{j\beta\tau^2} e^{-j(2\beta t-\omega_1-2\beta t_1)\tau}\, d\tau$$

$$+ \text{c.c.} \qquad (4.91)$$

over the interval $t_1 + T_s \leq t \leq t_1 + T_1$. The chirp modulated integrals will not pass through the second chirp filter if $\omega_1 - \omega_2 + 2\beta t_1 < \omega_3 + 2\beta T_3$. The output of this second device is valid over the time interval $t_1 + t_3 + T_1 \leq t \leq t_1 + t_3 + T_s + T_3$. Note that since the input to this device is T_1-T_s seconds wide, then T_1-T_s must be smaller than T_3. As can be expected the output of the second device is valid for a period of time that is the device impulse response duration minus the input signal duration or $T_3 - (T_1-T_s)$ seconds. The output of this device is given by

$$\text{Output} = \frac{1}{8}\sqrt{\frac{\pi}{\beta}}\, e^{j\frac{\pi}{4}} e^{-j\frac{(\omega_3-\omega_2-\omega_1)^2}{4\beta}} e^{-j(\omega_1+\omega_2+2\beta t_1)t}$$

$$e^{-j((\omega_2-\omega_3)t_1 - (\omega_1+\omega_2)t_3-2\beta t_1 t_3+\phi_3)}$$

$$\int_{-\infty}^{\infty} f(\tau)e^{-j(2\beta(t-t_3) + \omega_2-\omega_3)\tau}\, d\tau + \text{c.c.}$$

$$+ \frac{1}{8}\sqrt{\frac{\pi}{\beta}}\, e^{-j\frac{\pi}{4}} e^{j\frac{(\omega_3+\omega_1+\omega_2)^2}{4\beta}} e^{-j(\omega_1+\omega_2+2\beta t_1)t}$$

$$e^{j((2\omega_1+\omega_2+\omega_3)t_1 + (\omega_1+\omega_2)t_3+2\beta t_1 t_3+2\beta t_1^2+\phi_3)}$$

$$\int_{-\infty}^{\infty} f(\tau)e^{j2\beta\tau^2} e^{-j(2\beta(t-t_1-t_3) - 2\omega_1-\omega_2-\omega_3)\tau}\, d\tau \text{ c.c.} \qquad (4.92)$$

Again, as with the MCM technique, there are two transforms. The transform of $f(\tau)\exp(j2\beta\tau^2)$ is not wanted and hopefully does not interfere with the transform of $f(\tau)$. Since $f(\tau)$ is a carrier modulated signal, the Fourier transform of this signal will consist of positive and negative frequency versions of the transform of $a(t) + jb(t)$ (the envelope of the input). For large input carrier frequencies, the positive and negative spectrums do not interfere. In order for one of the spectrums to be centered within the valid window at $t_c = t_1 + t_3 + \frac{1}{2}(T_1+T_3+T_s)$, then the time to frequency correspondence of this transform given by

$$\omega = 2\beta(t-t_3) + \omega_2-\omega_3 \tag{4.93}$$

must satisfy

$$\omega\Big|_{t=t_c} = \omega_o \tag{4.94}$$

or

$$\omega_2 = \omega_3+\omega_o-2\beta(t_1 + \tfrac{1}{2}(T_1+T_3+T_s)) \tag{4.95}$$

With this value of ω_2 the frequency of the Fourier transform at $t = t_1+t_3+T_1$ is $\omega_o-\beta(T_3 - (T_1-T_s))$ radians/sec and at $t = t_1+t_3+T_s+T_3$ is $\omega_o+\beta(T_3 - (T_1-T_s))$ radians/sec, and is therefore centered within this region. With this value of ω_2 the time to frequency correspondence for the Fourier transform of $f(t)\exp(j2\beta t^2)$ is given by

$$\omega = 2\beta(t-t_3) - 2\omega_1-2\omega_3-\omega_o+\beta(T_1+T_3+T_s) \tag{4.96}$$

At $t=t_c$ the frequency at this point is given by

$$\omega_c = 2\beta(T_1+T_3+T_s+t_1) - 2(\omega_1+\omega_3) - \omega_o \tag{4.97}$$

For

$$\omega_1+\omega_3 >> \beta(t_1+T_1+T_3+T_s) \tag{4.98}$$

this transform will not interfere with the desired form and can be ignored.

Since

$$\int_{-\infty}^{\infty} f(\tau)e^{-j\omega\tau}\,d\tau = \frac{1}{2}\Big|A(\omega+\omega_o) + A(\omega-\omega_o) + jB(\omega+\omega_o) - jB(\omega-\omega_o)\Big| \tag{4.99}$$

where

$$A(\omega) = \int_{-\infty}^{\infty} a(\tau)e^{-j\omega\tau}\,d\tau = R_A(\omega) + jX_A(\omega) \tag{4.100}$$

and

$$B(\omega) = \int_{-\infty}^{\infty} b(\tau)e^{-j\omega\tau}\,d\tau = R_B(\omega) + jX_B(\omega) \tag{4.101}$$

then by making the substitution $\omega' = \omega-\omega_o$ and discarding the negative spectrum (since it does not get displayed over the output interval), the output of the CMC chirp transform system over the time interval $t_1+t_3+T_1 \le t \le t_1+t_3+T_s+T_3$ is given by

$$\text{Output} = \frac{1}{16}\sqrt{\frac{\pi}{\beta}}\,e^{-j((\omega_1+\omega_2+2\beta t_1)t+\Phi)}\Big|A(\omega') - jB(\omega')\Big| + \text{c.c.} \tag{4.102}$$

where

$$\omega' = 2\beta(t - t_1 - t_3 - \tfrac{1}{2}(T_1+T_3+T_s)) \tag{4.103}$$

and

$$\Phi = \frac{1}{4\beta}(\omega_3-\omega_2-\omega_1)^2 + (\omega_2-\omega_3)t_1 - (\omega_1+\omega_2)t_3 - 2\beta t_1 t_3 + \phi_3 - \pi/4 \tag{4.104}$$

or

$$\text{Output} = \frac{1}{8}\sqrt{\frac{\pi}{\beta}}\Big|(R_A(\omega) + X_B(\omega))\cos((\omega_1+\omega_2+2\beta t_1)t+\Phi) - (R_B(\omega) - X_A(\omega))\sin((\omega_1+\omega_2+2\beta t_1)t+\Phi)\Big| \tag{4.105}$$

Eq. (4.105) is the complex conjugated and frequency inverted transform of the input signal. Note that the factor $\sqrt{\pi/\beta}$ after every transformation will result in a $1/\beta^2$ term after an inverse transformation. Since, however, there will be four chirp filters, in such a system, the $(\beta)^{1/2}$ factor used for each impulse response will cancel this term.

If the CMC transform is centered about $-\omega_o$, then

$$\omega\Big|_{t=t_c} = -\omega_o \tag{4.106}$$

or

$$\omega_2 = \omega_3 - \omega_o - 2\beta(t_1 + \frac{1}{2}(T_1 + T_3 + T_s)) \tag{4.107}$$

so that the time to frequency correspondence becomes

$$\omega = 2\beta(t - t_1 - t_3 - \frac{1}{2}(T_1+T_3+T_s)) - \omega_o \tag{4.108}$$

for the Fourier transform of f(t) and

$$\omega = 2\beta(t-t_3) - 2\omega_3 - 2\omega_1 + \omega_o + \beta(T_1+T_3+T_s) \tag{4.109}$$

for the Fourier transform of $f(t)\exp(j2\beta t^2)$. At $t=t_c$

$$\omega_c = 2\beta(t_1+T_1+T_3+T_s) - 2(\omega_1+\omega_3) + \omega_o \tag{4.110}$$

so that for

$$\omega_1+\omega_3 >> \beta(t_1+T_1+T_3+T_s) + \omega_o \tag{4.111}$$

the two transforms do not interfere. In this case, making the substitution $\omega' = \omega+\omega_o$ the output is given by

$$\text{Output} = \frac{1}{16}\sqrt{\frac{\pi}{\beta}}\, e^{-j((\omega_1+\omega_2+2\beta t_1)t+\Phi)}\left|A(\omega') + jB(\omega')\right| + \text{c.c.} \tag{4.112}$$

where ω' is given by Eq. (4.103). This equation can be rewritten as

$$\text{Output} = \frac{1}{\delta}\sqrt{\frac{\pi}{\beta}}\left|(R_A(\omega') - X_B(\omega'))\cos((\omega_1+\omega_2+2\beta t_1)t+\Phi)\right.$$

$$\left. + (R_B(\omega') + X_A(\omega'))\sin((\omega_1+\omega_2+2\beta t_1)t+\Phi)\right| \qquad (4.113)$$

which is the Fourier transform of the input signal. As would be expected since

$$A(\omega) + jB(\omega) = (R_A(\omega) - X_B(\omega)) + j(R_B(\omega) + X_A(\omega)) \qquad (4.114)$$

and

$$A(\omega) - jB(\omega) = (R_A(\omega) + X_B(\omega)) - j(R_B(\omega) - X_A(\omega)) \qquad (4.115)$$

the transform obtained using one of the spectrums is the complex conjugated and frequency inverted version of the transform obtained using the other spectrum. In a CMC system, using down-chirp filters, the negative spectrum is required in order to obtain the Fourier transform. Ignoring device delays the output of an up-chirp filter CMC system is given by

$$\text{Output} = \frac{1}{\delta}\sqrt{\frac{\pi}{\beta}}\left|(R_A(\omega) - X_B(\omega))\cos((\omega_1+\omega_2)t+\Phi)\right.$$

$$\left. - (R_B(\omega) + X_A(\omega))\sin((\omega_1+\omega_2)t+\Phi)\right| \qquad (4.116)$$

using the positive frequency spectrum. This output is the complex conjugated Fourier transform of the signal. Using the negative spectrum results in the output

$$\text{Output} = \frac{1}{\delta}\sqrt{\frac{\pi}{\beta}}\left|(R_A(\omega) + X_B(\omega))\cos((\omega_1+\omega_2)t+\Phi)\right.$$

$$\left. + (R_B(\omega) - X_A(\omega))\sin((\omega_1+\omega_2)t+\Phi)\right| \qquad (4.117)$$

which is the frequency inverted transform of the signal. Note the similarity

in these results with respect to those obtained for the MCM technique. In the MCM systems, the transform is frequency inverted when up-chirp filters are used and not inverted if down-chirp filters are used. For CMC systems using their negative spectrums, up-chirp filter systems produce frequency inverted transforms and down-chirp filter inverted systems produce a non-inverted transform. Furthermore, the CMC chirp transform system possesses the additional facility to complex conjugate and time invert its transform by utilizing its positive frequency spectrum. If DP is used to signify a down-chirp filter system utilizing the positive frequency spectrum, DN the same system using the negative spectrum, UP an up-chirp filter system utilizing the positive spectrum and UN this same system using the negative spectrum, then these results can be summarized as follows:

$$f(t) \longrightarrow DP \longrightarrow F^{*}(-\omega) \tag{4.118}$$

$$f(t) \longrightarrow DN \longrightarrow F(\omega) \tag{4.119}$$

$$f(t) \longrightarrow UP \longrightarrow F^{*}(\omega) \tag{4.120}$$

$$f(t) \longrightarrow UN \longrightarrow F(-\omega) \tag{4.121}$$

Since no chirp slope changes are required, these systems are simply cascaded to realize transform inversions. The schemes that will produce a signal that is not time inverted are given by

$$f(t) \longrightarrow UP \longrightarrow DN \longrightarrow f^{*}(t) \tag{4.122}$$

$$f(t) \longrightarrow UN \longrightarrow DN \longrightarrow f(t) \tag{4.123}$$

$$f(t) \longrightarrow UP \longrightarrow UP \longrightarrow f(t) \tag{4.124}$$

$$f(t) \longrightarrow UN \longrightarrow UP \longrightarrow f^{*}(t) \tag{4.125}$$

$$f(t) \longrightarrow DN \longrightarrow DP \longrightarrow f^{*}(t) \tag{4.126}$$

$$f(t) \longrightarrow DP \longrightarrow UN \longrightarrow f^{*}(t) \tag{4.127}$$

$$f(t) \longrightarrow DN \longrightarrow UN \longrightarrow f(t) \tag{4.128}$$

$$f(t) \longrightarrow DP \longrightarrow DP \longrightarrow f(t) \tag{4.129}$$

where the relationships

$$F^{*}(-t) \longleftrightarrow 2\pi\, f^{*}(-\omega) \tag{4.130}$$

$$F^{*}(t) \longleftrightarrow 2\pi\, f^{*}(\omega) \tag{4.131}$$

$$F(-t) \longleftrightarrow 2\pi\, f(\omega) \tag{4.132}$$

have been utilized. Similarly, the time inversion schemes are given by

$$f(t) \longrightarrow DP \longrightarrow DN \longrightarrow f^{*}(-t) \tag{4.133}$$

$$f(t) \longrightarrow DP \longrightarrow UP \longrightarrow f(-t) \tag{4.134}$$

$$f(t) \longrightarrow DN \longrightarrow DN \longrightarrow f(-t) \tag{4.135}$$

$$f(t) \longrightarrow DN \longrightarrow UP \longrightarrow f^{*}(-t) \tag{4.136}$$

$$f(t) \longrightarrow UP \longrightarrow DP \longrightarrow f(-t) \tag{4.137}$$

$$f(t) \longrightarrow UP \longrightarrow UN \longrightarrow f^{*}(-t) \tag{4.138}$$

$$f(t) \longrightarrow UN \longrightarrow DP \longrightarrow f^{*}(-t) \tag{4.139}$$

$$f(t) \longrightarrow UN \longrightarrow UN \longrightarrow f(-t) \tag{4.140}$$

Of course, if the rf carriers on the Fourier transforms are not of the proper frequency for the following system, they must be adjusted before inputting the transform into this other system.

The CMC chirp transform systems require twice as many devices than are required in MCM systems. For cascaded system configurations,

this can represent quite an appreciable loss in system dynamic range. Although MCM systems typically require twice as many mixing operations than is required in CMC systems, a mixing operation can usually be eliminated between cascaded systems. CMC systems do not have the ability to perform properly after the elimination of a chirp filter between stages. CMC systems, however, will not suffer from the many cross products that arise in MCM systems due to their many necessary mixing steps. Compromises may be made, therefore, when cascaded systems are required, by utilizing both structures in one configuration. Note that the final mixing stage can be eliminated in an MCM system and the Fourier transform on a chirp carrier is obtained. Elimination of the final device in a CMC system results in an output of the form of Eq. (4.91), which is a chirp modulated Fresnel transform of the input. Filtering can be performed before the final MCM mixing stage but not before the final CMC chirp filter.

Fourier transformation properties will now be examined in relation to their realizations utilizing these chirp transformation systems. Time inversion has already been covered in some detail. It was seen that the Fresnel transform as well as the Fourier transform can be used to realize this function. (Since the chirp filter has been shown to behave as a Fresnel transformer, this transform may some day prove to be indispensable in the analysis of chirp filter systems. It is for this purpose that Appendix A, concerned with Fresnel analysis, was included in this report. An attempt was made to derive as many relationships as possible, thereby improving the probability of developing some form of signal processing theory based upon this transform.)

Using the Fourier relationship

$$f(t-t_o) \longleftrightarrow F(\omega)e^{-j\omega t_o} \tag{4.141}$$

a variable time delay system can be set up. Since the output transform of a chirp transform system is of the form

$$\text{Output} = e^{j\alpha(t)}\, F(\omega) + e^{-j\alpha(t)}\, F^*(\omega) \tag{4.142}$$

where $\alpha(t)$ is some function of time, then rewritting this as

$$\text{Output} = e^{j(\alpha(t)+\omega t_o)}\; e^{-j\omega t_o}\, F(\omega) + e^{-j(\alpha(t)+\omega t_o)}\; e^{j\omega t_o}\, F^*(\omega) \tag{4.143}$$

the Fourier transform of the delayed function can be obtained if a signal with phase $\alpha(t)+\omega t_o$ is used to demodulate this output. The variable ω represents the time to frequency relationship of the transform. After this demodulation, a signal delayed by t_o seconds is obtained if the transform is inputted into another chirp system set up to perform the inverse Fourier transformation. The converse will occur for signals with high frequency carriers. Since the chirp system will be tuned to either the positive or negative spectrum of this signal, when the carrier is changed the Fourier transform of the signal envelope is shifted. This follows from the Fourier relationships

$$f(t)e^{j\omega_o t} \longleftrightarrow F(\omega-\omega_o) \tag{4.144}$$

$$f(t)\cos\omega_o t \longleftrightarrow \frac{1}{2}\{F(\omega+\omega_o) + F(\omega-\omega_o)\} \tag{4.145}$$

and

$$f(t)\sin\omega_o t \longleftrightarrow \frac{j}{2}\{F(\omega+\omega_o) - F(\omega-\omega_o)\} \tag{4.146}$$

Note, however, that time delay can also be implemented using the

Fresnel transform. When a carrier modulated signal is inputted into a chirp filter, the output is in the form of a Fresnel transform (see Eq. (4.86)). Since this transform itself is carrier modulated, its carrier frequency can be controlled by a mixing process. When the transform is inputted into a chirp filter having opposite slope to the first, the output is the inverse Fresnel transform or the original signal delayed. However, the delay of this signal will be dependent on the carrier frequency of the Fresnel transform. The group delay, in this case, is a linear function of frequency. This can be seen using the Fresnel relationship

$$\mathcal{F}_{\beta,\tau}\{f(t)e^{j\omega_2 t}\} = e^{-j((\omega_1-\omega_2)t - \frac{(\omega_1-\omega_2)^2}{4\beta})}$$

$$\mathcal{F}_{\beta,\tau + (\omega_1-\omega_2)/2\beta}\{f(t)e^{j\omega_1 t}\} \qquad (4.147)$$

Except for a phase factor, the Fresnel transform of two signals having different carrier frequencies are delayed from one another by a delay that is linearly proportional to the difference in these frequencies (i.e. the delay = $(\omega_2-\omega_1)/2\beta$ in Eq. (4.147)). Signal expansion and compression can be performed using the Fourier relationship

$$f(at) \longleftrightarrow \frac{1}{|a|} F(\frac{\omega}{a}) \qquad (4.148)$$

If the Fourier transform of a function, f(t), is obtained using a chirp transform system with chirp filters of slope β_1, then the time to frequency correspondence of this transform is proportional to β_1. If the same signal is transformed by a chirp system having β_2 slopes, then the time to frequency correspondence of this transform is proportional to β_2. Ignoring delay then

$$\omega_1 = 2\beta_1 t \tag{4.149}$$

and

$$\omega_2 = 2\beta_2 t \tag{4.150}$$

so that

$$\omega_1 = \frac{\beta_1}{\beta_2}\ \omega_2 \tag{4.151}$$

With

$$F_1(\omega_1) = \int_{-\infty}^{\infty} f(t)e^{-j\omega_1 t}\ dt \tag{4.152}$$

and

$$F_2(\omega_2) = \int_{-\infty}^{\infty} f(t)e^{-j\omega_2 t}\ dt \tag{4.153}$$

then

$$F_1(\omega_1) = F_2(\frac{\beta_1}{\beta_2}\ \omega_2) \tag{4.154}$$

If $F_1(\omega_1)$ is Fourier inverted using a system set up for $F_2(\omega_2)$, the output of this system will be proportional to $f(\frac{\beta_2}{\beta_1}\ t)$, since

$$F_2(\frac{\beta_1}{\beta_2}\ \omega_2) \longleftrightarrow \frac{\beta_2}{\beta_1}\ f(\frac{\beta_2}{\beta_1}\ t) \tag{4.155}$$

This scale change for $\beta_1 \neq \beta_2$ involves the use of chirp filters having different slopes. The carrier of the Fourier transform must be mixed with a chirp that has a slope that is the sum (or difference) of the two device slopes before the inversion can be performed. Again, this process can also be performed in the Fresnel domain and, as usual, this eliminates the need for pre-multiplying chirps and the need for synchronization that is necessary for the proper performance of a Fourier transform. The main disadvantage in using the Fresnel transform is that spectral modification techniques cannot be used since the Fresnel transform is not a frequency

spectrum representation of the signal. This transform represents the signal as an infinite sum of delayed chirps and maps the magnitude and phase of the chirps (all having the same slope, β, which represents another degree of freedom for this transform) as a function of their delay. (A signal, such as a radar return composed of a sum of delayed chirps, will have a Fresnel transform that is composed of impulses.) When a single chirp is modulated by a signal, the Fresnel transform of this combination (for the proper slope β) is a chirp modulated version of the Fourier transform of the signal. This is a special case (see the Fourier/Fresnel relationship in Appendix A). Since

$$\mathcal{F}_{\beta_1}\left[f(t)\right] = e^{-j\beta_1 t^2}\mathcal{F}^{-1}\left[f(t)e^{-j\beta_1 t^2}\right]\Big|_{\omega=2\beta t} \tag{4.156}$$

then for $\beta_1 = a\beta_2$ this becomes

$$\mathcal{F}_{a\beta_2}\left[f(t)\right] = e^{-ja\beta_2 t^2}\mathcal{F}^{-1}\left[f(t)e^{-ja\beta_1 t^2}\right]\Big|_{\omega=2a\beta_2 t} \tag{4.157}$$

If this is mixed with a chirp of slope $\beta_2(a-1)$ and the inverse Fresnel transform with respect to β_2 is taken then

$$\mathcal{F}^{-1}_{\beta_2}\left[e^{j\beta_2(a-1)t^2}\mathcal{F}_{a\beta_2}\left[f(t)\right]\right] = f(t/a) \tag{4.158}$$

Using the Fourier relationship

$$\int_{-\infty}^{\infty} f_1(\tau)f_2(t-\tau)d\tau \longleftrightarrow F_1(\omega)F_2(\omega) \tag{4.159}$$

where

$$F_1(\omega) = \int_{-\infty}^{\infty} f_1(t)e^{-j\omega t}\, dt \tag{4.160}$$

and

$$F_2(\omega) = \int_{-\infty}^{\infty} f_2(t)e^{-j\omega t}\, dt \tag{4.161}$$

the convolution of two functions can be obtained by taking the inverse transform of the product of their transforms. In particular, if a real signal is to be correlated with itself, then

$$f_2(t) = f_1(-t) \longleftrightarrow F_1^{*}(\omega) \tag{4.162}$$

so that

$$\int_{-\infty}^{\infty} f_1(\tau)f_1(\tau-t)d\tau \longleftrightarrow F_1(\omega)F_1^{*}(\omega) \tag{4.163}$$

Since

$$F_1(\omega) = R_1(\omega) + jX_1(\omega) \tag{4.164}$$

then

$$F_1(\omega)F_1^{*}(\omega) = R_1^{2}(\omega) + X_1^{2}(\omega) \tag{4.165}$$

The output of a chirp transform system for the input $f_1(t)$ is given by

$$\text{Output} = R_1(2\beta t)\cos\alpha(t) + X_1(2\beta t)\sin\alpha(t) \tag{4.166}$$

where $\alpha(t)$ is some function of time (a chirp or an rf). Performing the product with this signal gives

$$F_1(2\beta t)F_1^{*}(2\beta t) = \frac{1}{2}\left(R_1^{2}(2\beta t) - X_1^{2}(2\beta t)\right) + \left(R_1^{2}(2\beta t) + X_1^{2}(2\beta t)\right)\cos(2\alpha(t)) \tag{4.167}$$

where the desired form of the transform is modulated by $cos(2\alpha(t))$ and can be filtered from the baseband terms. The Fourier transform need not be complex conjugated by a special step. For instance, if one transform is given by Eq. (4.166) and the other by

$$F_2(2\beta t) = R_1(2\beta t)\cos(\gamma(t)) + X_1(2\beta t)\sin(\gamma(t)) \tag{4.168}$$

where $\gamma(t)$ is a time function different from $\alpha(t)$, then their product is given by

$$\begin{aligned} F_1(2\beta t)F_2(2\beta t) = \frac{1}{2}\ & R_1^2(2\beta t)\cos(\alpha(t) - \gamma(t)) \\ & + X_1^2(2\beta t)\sin(\alpha(t) - \gamma(t)) \\ & + R_1^2(2\beta t)\cos(\alpha(t) + \gamma(t)) \\ & - X_1^2(2\beta t)\cos(\alpha(t) + \gamma(t)) \\ & + 2R_1(2\beta t)X_1(2\beta t)\sin(\alpha(t) + \gamma(t)) \end{aligned} \tag{4.169}$$

Since

$$(R_1+jX_1)(R_1+jX_1) = R_1^2 - X_1^2 + j2R_1X_1 \tag{4.170}$$

is the Fourier transform of the autoconvolution of $f_1(t)$, Eq. (4.169) shows that by choosing $\alpha(t)$ and $\gamma(t)$ properly, the Fourier transforms of the autocorrelation and autoconvolution can be filtered from one another and used to obtain either of these time functions. The correlation and convolution of two different functions can be obtained in the same way. Note that in order to display the entire valid convolution or correlation of two functions using this technique, the valid time interval after the transform inversion of the product of the two transforms must be of duration equal to the combined duration of the two signals.

If a signal has passed through a linear system, then its Fourier transform is multiplied by the transfer function of the system. The system may actually distort the signal beyond recognition. If, however, the Fourier transform of this distorted signal is obtained and the system transfer function is also available (i.e. by taking the Fourier transform of the system impulse response), then the original signal transform can be theoretically recovered by dividing the distorted signal transform by the system transfer function. The original signal is then obtained by taking theinverse transform of this. This is classified as a 'deconvolution' process. In reality, points at which the system transfer function is zero would blow up if divided into the distorted transform so that only an approximation to this process can typically be realized in actual practice. Also, if major portions of the original signal have been altogether eliminated by the system, then an exact recovery of the original transform is impossible. The product of two different transforms is given by

$$\begin{aligned}\text{Output} = {} & R_1(2\beta t)R_2(2\beta t) - X_1(2\beta t)X_2(2\beta t)\cos(\alpha(t)) \\ & + (R_1(2\beta t)X_2(2\beta t) + X_1(2\beta t)R_2(2\beta t))\sin\alpha(t) \\ & + R_1(2\beta t)R_2(2\beta t) - X_1(2\beta t)X_2(2\beta t)\end{aligned} \tag{4.171}$$

If this product is multiplied by

$$\begin{aligned}M(t) = {} & \frac{R_1(2\beta t)}{(R_1^2(2\beta t) + X_1^2(2\beta t))}\cos(\alpha(t)) \\ & - \frac{X_1(2\beta t)}{(R_1^2(2\beta t) + X_1^2(2\beta t))}\sin(\alpha(t))\end{aligned} \tag{4.172}$$

the transform $R_2(2\beta t) + jX_2(2\beta t)$ is recovered by a high pass filter.

A similar technique is utilized in a 'pre-whitening system'. In this case a continuous signal is transformed in segments. Before the signal is transformed, however, it is delayed long enough so that an estimate can be made of the signal. The signal is subtracted off leaving, ideally, only the noise. (Typically, the signal is a binary code and a matched filter is used to estimate it.) This noise is transformed, the transform is squared and a reciprocal is taken. Then a convolution with a window is performed so as to make this a better approximation of the inverse power spectral density of the noise. This transform is then used to multiply the combined signal and noise spectrum or inverse transformed and convolved with the input signal. The result is that the noise has been optimized for the matched filter by utilizing estimates of the noise power spectral density.

2.5 The Saw Convolver and the Chirp Transform

A chirp filter is typically a single input, single output device. It is usually designed symmetrically so that it behaves identically whether either port is used as input or output. If designed using surface acoustic wave (SAW) technology, its chirp impulse response can be straightforwardly tailored to have a slope of many megahertz, a center frequency into the hundreds of megahertz, time durations up to hundreds of microseconds and initial delays that can be anywhere from a few microseconds to also hundreds of microseconds if this be desired. Utilizing the dispersive properties of the medium, the dispersive properties of specially designed transducers or selective reflections along the surface of the SAW delay line losses in the ballpark of 20 dB can be typically obtained, for devices having time bandwidth products in the hundreds, or 30 dB, for devices having time bandwidth products in the thousands. Once designed and fabricated, the impulse response of the chirp filter, ignoring slight changes in its parameters with age and changing environment, can be depended upon to be the same irrespective of when a signal is applied. In other words, the impulse response of the chirp filter can be assumed to be time invariant and will produce the same response for the same signal irrespective of its application time. Therefore, if its impulse response is known to be, $h(t)$, then the output of the device for an input $f(t)$ can be expected to be given by

$$g(t) = K \int_{-\infty}^{\infty} f(\tau)h(t-\tau)d\tau \qquad (5.1)$$

This makes the analysis of a system utilizing these devices a straight forward (yet not necessarily trivial) task. The section describing the

chirp transform assumed that chirp filters were to be used as the main components. All the analysis there is based upon a device having a somewhat idealized impulse response, given typically by Eq. (4.6) for an 'up chirp' device, and responding as would be expected according to Eq. (5.1).

Besides depending upon a device, such as a SAW chirp filter to perform the necessary chirp convolution (based upon the usual convolutionary response of a linear time invariant device between its impulse response and an input signal), the convolution can be performed using a convolver. The output of a convolver, as the name implies, is expectedly the convolution of its two input signals. To function as a chirp filter, one of its inputs is simply made to be a linear FM or 'chirp'. The convolver need not be a physical device, such as something you'd be able to grasp that has two visible input ports and an output port, but it could be an algorithm in a digital computer. Representative of a physical device would be a CCD convolver set up to perform discrete convolution. However, the subject of this section is neither of these. This section is intended to stress the characteristics of the separated-medium surface-acoustic-wave (SAW) convolver when it is to be utilized in a chirp transform system. Other sections briefly describe other uses for this device along with some discussion on a modifed version possessing storage capability. As a means for comparison, the chirp transform utilizing SAW devices is compared with the current baseband techniques utilized in CCD structures in Arsenault 1979 where the FFT algorithm is also discussed. In this section only the basic criteria necessary in the utilization of a convolver in a chirp system will be

presented where the single stage MCM chirp transform system will be utilized as an example. More complicated system configurations can be analyzed on the basis of this information and that supplied in the section emphasizing the chirp transform and chirp filters.

The SAW convolver is a device that can be grasped having two visible input ports and a single output port. Intuitively, one would not expect to be able to input a signal into one input port, now, and an hour later obtain the convolution at the output port for this signal with some other signal applied to the second input. To do this the device would require a storage mechanism, however, the storage convolver is a topic of another section. The convolver to be characterized in this section has no memory. (Memory convolvers at the present time have too weak an interaction to be useful in a complicated transform type of arrangement in place of the non-memory convolver.) The point to be made here is that the timing of the two signals, to be used as input signal and effective device impulse response, is critical in order to utilize the maximum amount of interaction time that the device can supply without loosing part of the desired output.

A detailed description of the convolver structure and performance is given in another section but for this discussion all that need be understood is the basic mechanism underlying its ability to convolve two signals. All timing criteria will be derived from this. The SAW convolver consist of a crystal medium on whose surface so called Rayleigh waves are caused to propagate. These surface waves penetrate on the order of one surface-wave wavelength (on the order of microns to hundreds of microns) into the crystal and are generated onto the surface by interdigital

transducers that have been metallically deposited on the surface at both of the crystal's extremeties. The surface waves generated by the two transducers propagate toward one another with velocity v (2v with respect to one another). Since the crystal is piezoelectric the surface waves carry with them an electric field (although the majority of the surface wave energy is contained in the mechanical fields). If the two contra-propagating waves are allowed to overlap beneath a slice of semiconductor that is within a few thousand angstroms of the surface, the electric fields interact non-linearly with the charge carriers in the semiconductor producing a non-linear current density. The semiconductor tends to average out this effect which is equivalent to an integration over the length of the overlap of the two signals. The detailed mathematics are left for another section, however, the output of interest is of the form

$$c(t) = \int_{-\infty}^{\infty} f(\tau)g(2t-\tau)d\tau \qquad (5.2)$$

The limits of integration in this equation can be set to plus and minus infinity so long as the overlapping region of the two signals is forced to remain beneath the semiconductor entirely. Here, $f(t)$ and $g(t)$ are the two assumed input signals and the magnitude of this integral has been set to unity for simplification although the actual magnitude is a function of convolver efficiency. It should be stated that, being a second order effect that is typically analyzed as though it were simply a perturbation of the charge carrier density of the semiconductor and the surface wave energy, this convolution output is necessarily small, typically being on the order of 40 to 60 dB below the input levels. Note also from Eq. (5.2) that the convolution output is compressed by

a factor of two. This is inherent in the fact that both signals are propagating with velocity v.

The interdigital transducers in conjunction with their matching networks behave as bandpass filters whose center frequencies are dictated by the surface wave wavelength corresponding to two times the center-to-center transducer finger spacings. Therefore, the input signals must always be modulated upon carriers whose frequencies fall within this band being anywhere from a few to hundreds of megahertz. When both f(t) and g(t) are given carriers of frequency ω in Eq. (5.2) the difference terms integrate to zero leaving

$$c(t) = \cos 2\omega t \int_{-\infty}^{\infty} f(\tau)g(2t-\tau)d\tau \qquad (5.3)$$

where it can be seen that the output carrier is twice the input carrier due to the compression factor. When these input signals are chirps or modulated onto chirps their bandwidths must again fall within the bandpass of the input transducers. (SAW chirp filter bandwidths are also typically set by the input transducers or at least the maximum chirp dispersion cannot be made greater than this.)

Since the SAW convolver possesses an input/output relation of the form of Eq. (5.2), relative to one of the inputs the device has a time varying impulse response. If it is assumed that $g(t) = h(t)$ is the effective impulse response of the device, then an impulse applied at $t=t_1$ will result in the impulse response $h(2t-t_1)$ and an impulse applied at $t=t_2$ will obtain $h(2t-t_2)$ as a response. If the device was time invariant the application of these two impulses spaced t_2-t_1 seconds apart ($t_2 > t_1$) should result in two identical responses spaced t_2-t_1 seconds apart.

Since, however, the responses actually emerge $(t_2-t_1)/2$ seconds apart the device is not time invariant. Moreover the output of the convolver can only be a delayed version of h(2t) so long as h(t), as a modulated surface wave, fits totally beneath the semiconductor and, even if this be the case, the impulse is given a finite slot of time in which to be applied, otherwise a truncated version of this signal, or no signal at all, is obtained.

From this information some basic criteria can be developed to insure that, when obeyed, the SAW convolver can effectively be utilized not only as a convolver but as the main element in a chirp transform system. To this end, we can develop a basic model for the device in terms of time delays and an interaction time. First of all it will be assumed that either signal requires a time t_D after its time of application to its input port, in order to just reach the edge of the interaction region, defined as the region beneath the semiconductor, nearest its port. Then, the last assumption is that the interaction region requires a single point on a signal to travel for T seconds in order to propagate the entire length of this region. In other words, an impulse applied to an input at time t_1 will propagate on the crystal surface as an impulse surface wave for a 'dead time' of t_D seconds reaching the closest edge of the interaction region at time $t_1 + t_D$. It will then propagate until it reaches the farthest end of this region at time $t_1 + t_D + T$. It will continue to propagate on the free surface of the crystal for another 'dead time' t_D until it reaches the other transducer at time $t_1 + 2t_D + T$. Being a delay line, the impulse could now be detected by this transducer in the equivalent manner in which it was generated, although when used

as a convolver this output would generally be ignored. A large portion of the impulse also passes beneath the transducer and is absorb by an acoustic absorber at the end of the crystal.

Now, since a Fourier transformation is desired, we know that one of the signals is required to be a chirp and the other the desired signal to be transformed modulated by a chirp having opposite slope to the first. This, we will assume, is to be a chirp transform system utilizing the MCM configuration. Since the equations have been written up in detail in the section on chirp transformation for the 'down-chirp' filter, let us assume, for comparison, that the convolver also takes on the appearance of a 'down-chirp' filter. To this end, the following chirp signal is applied to one of the convolver inputs at t=0

$$r(t) = [U(t) - U(t-T_r)]\cos(\omega_r t - \beta t^2) \tag{5.4}$$

where T_r is the overall length of the chirp and

$$\frac{d}{dt}(\omega_r t - \beta t^2)\Big|_{t=0} = \omega_r - 2\beta t\Big|_{t=0} = \omega_r \tag{5.5}$$

is the instantaneous starting frequency of the 'down chirp' at t=0. The phase of this chirp at t=0 was arbitrarily set to zero.

The chirp modulated input signal will be given by

$$s(t) = f(t-t_s)[U(t-t_s) - U(t-t_s-T_s)]\cos(\omega_s(t-t_s) + \beta(t-t_s)^2) \tag{5.6}$$

where a delay t_s has been included in anticipation that just such a delay may be required as a method of optimizing the valid output duration of the Fourier transform. The signal duration is assumed to be of length T_s

which has been strictly imposed in Eq. (5.6). Here the chirp modulation is that of an 'up chirp' as required for transformation and its instantaneous starting frequency at the start of the signal $t=t_s$ is ω_s. The phase at $t=t_s$ is again set to zero.

Since, in the convolution between these two signals, the output Fourier transform cannot be valid unless the signal given by Eq. (5.6) is totally overlapped by the signal given by Eq. (5.4), in order that the limits of integration be set to infinity, the first criterion is obviously given by

$$T_s < T_r \tag{5.7}$$

Furthermore, the maximum length of time during which this condition can occur is half the difference between these two durations since both signals are propagating toward one another. Therefore, the maximum duration of the valid portion of the Fourier transform is given by

$$T_{FMAX} = (T_r - T_s)/2 \tag{5.8}$$

To maximize the duration of the valid output, the time at which the signal given by Eq. (5.6) just makes it totally beneath the semiconductor, $t = t_s + t_D + T_s$, should be the same time at which the front edge of the chirp given by Eq. (5.4) just reaches the farthest edge of the semiconductor from its input or the edge closest to the signal input. In this way the signal becomes totally overlapped by the chirp and the interaction region at the same time. If the total overlap of the signal and chirp occurred somewhere else beneath the interaction region, then part of this interaction time has been wasted. If it occurs too early, then the output is not entirely correct until the signal enters the interaction region

entirely, since only a portion of the overlap will be integrated. The point in time at which the chirp reaches the farthest end of the interaction region is $t = t_D + T$ seconds. Therefore, by setting these two times equal to one another the delay required on the input signal to insure maximum interaction is given by

$$t_s = T - T_s \tag{5.9}$$

Due to the finite size of the interaction region, there must necessarily be restrictions on the size of the signal. Assuming that while totally beneath the semiconductor the signal is also totally overlapped by the chirp, the maximum time that the output can be expected to be accurate is the time required for the signal to propagate the length of the semiconductor without ever leaving the confines of the interaction region defined by this semiconductor. This time is given by

$$T_M = T - T_s \tag{5.10}$$

Since it doesn't make sense to try and obtain a valid region that is of duration longer than that defined by Eq. (5.10), which is physically impossible, then the maximum chirp length, T_{rmax}, that is of any use is given by equating Eqs. (5.8) and (5.10) and solving for T_r. This gives

$$T_r \geq 2T - T_s = T_{rmax} \tag{5.11}$$

which states in conjunction with Eqs. (5.9) and (5.10) that an impulse applied at $t_s = T$ will produce a valid output convolution beginning at time $t = t_s + t_D = T + t_D$ and lasting until time $t = t_s + t_D + T = 2T + t_D$ assuming that the other input signal, applied at t=0, is at least 2T seconds long. This is the maximum convolution time obtainable assuming that

the signal, to be Fourier transformed, is totally overlapped by both the chirp and the interaction region, which is a requirement for accurate transformation. An impulse is the limiting size of the input signal that produces the maximum length accurate Fourier transform of duration T or half the duration of the 2T seconds long input chirp (due to the factor-of-two compression). The longest duration that the signal, to be transformed, can have is T seconds. Having this length or greater produces no output that is valid. The chirp need not be limited in duration to the time given by Eq. (5.11), although any excess over this time will be wasted. Any length less than that given by Eq. (5.11) is less than optimum. By meeting the criteria defined by Eqs. (5.9) to (5.11), the output Fourier transform can be assumed accurate over the interval

$$t_s + t_D + T_s \leq t \leq t_s + t_D + T \tag{5.12}$$

Over this interval the output of the convolver for inputs given by Eqs. (5.4) and (5.6) is proportional to

$$c(t + t_D + \frac{T}{2}) = \int_{-\infty}^{\infty} f(\tau - t_s)\cos(\omega_s(\tau - t_s) + \beta(\tau - t_s)^2)$$

$$\cos(\omega_r(2t - \tau) - \beta(2t - \tau)^2)\, d\tau \tag{5.13}$$

where the duration T_s of $f(t)$ is to be assumed. The advance to $t_D + \frac{T}{2}$ included in Eq. (5.13) is the amount of time required for two signals to meet in the device if both are applied at the same time. Eq. (5.2) assumes they meet immediately. Incorporating this advance into the equation and expanding gives

$$c(t) = e^{-j((2\omega_r + 4\beta t_s)(t - t_D - \frac{T}{2}) - 4\beta(t - t_D - \frac{T}{2})^2 - \omega_r t_s - \beta t_s^2)}$$

$$\int_{-\infty}^{\infty} f(\tau) e^{-j(4\beta t - 2\beta t_s - 4\beta t_D - 2\beta T + \omega_s - \omega_r)\tau} \, d\tau + c.c.$$

$$+ e^{-j(2\omega_r + 4\beta t_s)(t - t_D - \frac{T}{2}) - 4\beta(t - t_D - \frac{T}{2})^2 - \omega_r t_s - \beta t_s^2)}$$

$$\int_{-\infty}^{\infty} f(\tau) e^{j2\beta\tau^2} e^{-j(4\beta t - 2\beta t_s - 4\beta t_D - 2\beta T - \omega_s - \omega_r)\tau} \, d\tau + c.c. \tag{5.14}$$

The delay of the function t_s was absorbed into the exponentials by utilizing the relation

$$f(t-t_s) \longleftrightarrow e^{-j\omega t_s} F(\omega) \tag{5.15}$$

since both of the above sets of integrals are Fourier transforms. The first set of integrals is the Fourier transform of $f(t)$ with a time to frequency correspondence given by

$$\omega = \omega_s - \omega_r + 4\beta[t - t_D - \frac{1}{2}(t_s+T)] \tag{5.16}$$

The second set of integrals is the Fourier transform of $f(t)\exp(j2\beta t^2)$ with a time to frequency correspondence given by

$$\omega = 4\beta[t - t_D - \frac{1}{2}(t_s+T)] - \omega_s - \omega_r \tag{5.17}$$

The center of the Fourier transform of $f(t)$ is given by

$$t_{c1} = \frac{\omega_r - \omega_s}{4\beta} + t_D + \frac{1}{2}(t_s+T) \tag{5.18}$$

whereas the center of the Fourier transform of $f(t)\exp[j2\beta t^2]$ is given by

$$t_{c1} = \frac{\omega_r + \omega_s}{4\beta} + t_D + \frac{1}{2}(t_s + T) \tag{5.19}$$

The center of the valid interval given by Eq. (5.12) is given by

$$t_v = t_s + t_D + \frac{1}{2}(T + T_s) \tag{5.20}$$

When Eq. (5.18) is set equal to Eq. (5.20) the following criterion is obtained for centering of the Fourier transform of f(t) within the accurate time interval; namely,

$$\frac{\omega_r - \omega_s}{4\beta} = \frac{1}{2}(t_s + T_s) = T/2 \tag{5.21}$$

where Eq. (5.9) was utilzed assuming the maximum duration output was desired. If the chirp given by Eq. (5.4), being the longest of the two input signals, is designed so that its bandwidth extends over the entire bandwidth B of the convolver, then ω_r is the upper frequency limit and $\omega_r - 2\beta T_r$ is the lower frequency limit. Furthermore, if T_r is set equal to the maximum usable time length given by Eq. (5.11), then

$$2\beta = \frac{2\pi B}{T_r} = \frac{2\pi B}{2T - T_s} \tag{5.22}$$

so that

$$\frac{f_r - f_s}{B} = \left(2 - \frac{T_s}{T}\right)^{-1} \tag{5.23}$$

Since T_s would never be made greater than T (since none of the output would represent the accurate transform if that were to be done), the above ratio is never greater than one. Therefore, by choosing all the parameters so as to optimize the available length of the output transform and to utilize the entire convolver bandwidth, the required value

for ω_s, dictated by Eq. (5.23) where $\omega_s = 2\pi f_s$, will always fall within the bandwidth of the convolver. When $T_s = T$, $\omega_s = \omega_r - 2\beta T_r$ or the lower frequency bound of the convolver and since its width is also T_r seconds wide in this case, its frequency after T_r seconds is ω_r, or the upper bound of the device. In the other extreme, when $T_s = \varepsilon \simeq 0$ then $\omega_s \simeq \omega_r - \beta T_r$ or the center instantaneous frequency of the chirp and, likewise, of the convolver passband.

The Fourier transform of f(t) given by the first set of integrals in Eq. (5.14), when centered in the valid interval given by Eq. (5.12), spans an interval in frequency given by

$$-2\beta(T-T_s) \leq \omega \leq 2\beta(T-T_s) \tag{5.24}$$

If T_s is chosen to be half the interaction region so that the output transform is valid over half the interaction region, then Eq. (5.24) becomes

$$-\beta T \leq \omega \leq \beta T \tag{5.25}$$

where, using Eq. (5.22), βT is one third the total bandwidth of the convolver, so that the Fourier transform spans two thirds of the convolver bandwidth. When $T=T_s$ the transform spans zero bandwidth as is expected since there is no valid output. If $T_s = \varepsilon \simeq 0$ the transform spans $4\beta T$ radians/sec or, using Eq. (5.22), the entire convolver bandwidth. In this case, however, the signal is too small to be of any real use.

From Eq. (5.19) it is seen that, when the Fourier transform of f(t) is centered at $t = 3T/2 + t_D - T_s/2$ or the center of the valid interval, the Fresnel transform, given by the Fourier transform of $f(t)\exp(j2\beta t^2)$ or the second set of integrals in Eq. (5.14), is

centered at

$$t_{c2} = \frac{\omega_s}{2\beta} + t_D + \frac{3T}{2} - \frac{T_s}{2} \tag{5.26}$$

which is $\omega_s/2\beta$ seconds away from the center of the desired transform. This will typically be quite a distance in time away from the valid region so that only negligible high frequency components of this transform will coincide with the desired transform. Therefore, the Fresnel terms can usually be neglected so long as the system is not designed to operate at extremely low frequencies. Neglecting these terms, Eq. (5.14) can be written as

$$c(t) = R(\omega)\cos((2\omega_r + 4\beta t_s)(t - t_D - \tfrac{T}{2}) - 4\beta(t - t_D - \tfrac{T}{2})^2 - \omega_r t_s - \beta t_s^2)$$

$$+ X(\omega)\sin((2\omega_r + 4\beta t_s)(t - t_D - \tfrac{T}{2}) - 4\beta(t - t_D - \tfrac{T}{2})^2$$

$$- \omega_r t_s - \beta t_s^2) \tag{5.27}$$

where ω is given by Eq. (5.16), $t_s = T - T_s$ and

$$F(\omega) = \int_{-\infty}^{\infty} f(\tau)e^{-j\omega\tau}\, d\tau = R(\omega) + jX(\omega) \tag{5.28}$$

The real portion of the Fourier transform, $R(\omega)$, and the imaginary portion, $X(\omega)$, can be isolated by mixing with either the cosine chirp or the sine chirp and low pass filtering. If the criteria developed in this section are adhered to the techniques discussed in the section on the chirp transformation directly apply. Note, however, that the Fourier transform obtained using the convolver is time compressed by a factor of two. Also, the chirp modulation has a higher center frequency and four times the slope of the input chirp. All these characteristics must be

kept in mind for the design of following stages. These stages cannot be identical since every stage causes a compression and $\tilde{a}$ chirp slope quadrupling. An important point to note is that the cascading of an up-chirp transform system with a down-chirp transform system recovers a version of the original signal compressed in time by a factor of four. Although the signal in Eq. (5.28) is assumed to exist from t=0 to $t=T_s$, the transform of this signal centered at zero is obtained by adding an additional $\omega T_s/2$ term into the chirps of Eq. (5.27), where ω is given by Eq. (5.16) (i.e. different chirps are used).

2.6 Spectrum Modifications

General System Specifications:

As discussed in Sect. 2.4 the output of a chirp transformation system for an input of the form

$$\text{input} = f_1(t)\cos\{c(t)\} - f_2(5)\sin\{c(t)\} \tag{6.1}$$

is of the form

$$\text{output} = R(\omega)\cos\{a(t)\} \pm X(\omega)\sin\{a(t)\} \tag{6.2}$$

where ω is given by the time to frequency correspondence for the structure being utilized, $a(t)$ is either a chirp prior to an MCM post-multiply or an rf after this multiply for the MCM system or directly from the last chirp filter of a CMC system. Eq. (6.1) is equivalent to the complex signal

$$f_c(t) = f_1(t) + jf_2(t) \tag{6.3}$$

and Eq. (6.2) is likewise equivalent to

$$F(\omega) = R(\omega) \mp jX(\omega) \tag{6.4}$$

where

$$R(\omega) = R_1(\omega) - X_2(\omega) \tag{6.5}$$

$$X(\omega) = R_2(\omega) + X_1(\omega) \tag{6.6}$$

$$f_c(t) \longleftrightarrow F(\omega) \tag{6.7}$$

$$f_1(t) \longleftrightarrow F_1(\omega) = R_1(\omega) + jX_1(\omega) \tag{6.8}$$

$$f_2(t) \longleftrightarrow F_2(\omega) = R_2(\omega) + jX_2(\omega) \tag{6.9}$$

$$
\begin{aligned}
R_1(\omega) &= R_1(-\omega) \\
R_2(\omega) &= R_2(-\omega) \\
X_1(\omega) &= -X_1(-\omega) \\
X_2(\omega) &= -X_2(-\omega)
\end{aligned}
\tag{6.10}
$$

and the minus sign in Eqs. (6.2) and (6.4), signifying a complex conjugated Fourier transform, results from performing a spectral inversion in the chirp transform system. In Eq. (6.1) c(t) is either an rf so that the signal may enter the first chirp filter of a CMC system or be multiplied by an offset center frequency chirp at the pre-multiplication of an MCM system or it is already a chirp and ready for inputting into the chirp filter of an MCM system. Due to the complex nature of the input signal, the real and imaginary parts of the Fourier transform given by Eqs. (6.5) and (6.6) do not necessarily possess symmetry. The Fourier transformation output of a chirp transform system is only valid over a finite interval of time outside of which it must be gated prior to the following stage. The time duration of this valid time interval is T_F seconds and the input signal is time limited to a duration of $2T_s$ seconds. For every variation of the chirp transform system there is a linear relationship between T_F and T_s. In particular, T_F is given by the difference between the chirp filter impulse response duration and T_s in an MCM system. Knowing the slope of a particular configuration, given by 2β, the frequency span of the T_F seconds wide Fourier transform is $2\beta T_F$ rad/sec. The actual portion of the transform that is displayed within the T_F seconds wide window is a function of chirp modulation frequencies and is contained in the time to frequency correspondence relation ω. Once the Fourier transform of a signal has been

derived mathematically for a particular chirp transformation system, it may be centered about t=0 to simplify the analysis when this signal is inputted into a second stage. When this is done the time to frequency correspondence for this transform becomes $\omega = 2\beta t$.

Finite Signal and Finite Transform Effects:

When the Fourier transformation is performed with the assumption that the signal is centered at zero, then this signal exists over the interval $-T_s \leq t \leq T_s$. The signal being transformed, f(t), may be a $2T_s$ second wide segment of a continuous signal $f_c(t)$. The Fourier transform of the continuous signal, $F_c(\omega)$, can theoretically have a fine structure having infinitesimal proportions since the Fourier transform of an infinite duration signal possesses an infinite resolution. In this case two different frequency, infinite duration, tones produce frequency impulses having zero width. The frequency of the two tones could be made infinitesimally close and yet still be resolved. Since the signal to be chirp transformed must be time limited to $2T_s$ seconds, namely

$$f(t) = \left[U(t) - U(t-2T_s)\right] f_c(t) \tag{6.11}$$

and the chirp transform system performs a Fourier transformation of $f(t+T_s)$ when this signal is applied to it, then over the T_F seconds wide valid time interval the output is given by

$$F(\omega) = F_c(\omega) * \frac{2\sin T_s\omega}{\omega}$$

$$= 2\int_{-\infty}^{\infty} \frac{F_c(\omega_o)\sin T_s(\omega-\omega_o)}{(\omega-\omega_o)}\, d\omega \tag{6.12}$$

where it will always be assumed that the transform of the quadratic phase modulated signal $(f(t+T_s)\exp(j2\beta(t+T_s)^2))$ can be ignored.

Eq. (6.12) shows that the effect of limiting the continuous signal to within a $2T_s$ second wide window is to convolve its transform with a sinx/x function whose main lobe is $2\pi/T_s$ rad/sec wide. By doing this, two things have happened, where the Fourier transform of the continuous signal could have been bandlimited, the transform of the finite segment of this signal is necessarily finite out to infinity since the sinx/x function is an infinite duration continuous function. Also, the convolution of the transform of the continuous function with the sinx/x function has effectively ironed out the fine structure of this transform so that now the resolution in the frequency domain is on the order of $2\pi/T_s$ rad/sec or the width of the main lobe (lobe centered about $\omega=0$) of the sinx/x ($x = T_s(\omega-\omega_o)$) function.

Now, if the Fourier transform is centered within the T_F second wide valid time interval, it has then been bandlimited to the frequency interval $-\beta T_F \leq \omega \leq \beta T_F$ and can be written as

$$F_B(\omega) = \left| U(\omega+\beta T_F) - U(\omega-\beta T_F) \right| F(\omega) \qquad (6.13)$$

where $F(\omega)$ is a transform having infinite duration since the input signal is finite. Since, for further processing through another chirp transform system, the Fourier transform, which in reality is a time domain signal representing a frequency domain one, must be limited in duration, the T_F second duration of the transform in Eq. (6.13) must be designed so that the output of the following stage is accurate over a desirable time interval. This interval will typically be the difference between the

transform width and the chirp device impulse response duration for the second stage of an MCM system. It is not necessary to utilize the entire T_F wide segment of the Fourier transform for the following stage although no more than this can be used.

As discussed in Section 2.4, a down chirp followed by an up-chirp system and vice versa will both produce Fourier transformations. The output of such a system is a filtered version of the input signal since only a finite portion of the infinite duration complex-conjugated Fourier transform can be utilized for the second stage. Other variations of cascaded chirp transformation systems result in filtered versions of either the time inverted input signal, the complex-conjugated input signal or the complex-conjugated and time inverted input signal. If the Fourier transform is centered within its valid T_F second wide interval then the cascaded 'down chirp' system behaves essentially like a low-pass filter having a $2\beta T_F$ double-sided bandwidth and band edge roll offs defined by the switching time slope of the Fourier transform T_F second wide gating function. Any assymmetry in the gating of the Fourier transform will cause what may in actuality be a real input signal to be complex at the output of the cascaded system. In any case the bandlimiting of the Fourier transform results in a signal that possesses an infinite duration although it had been $2T_s$ seconds wide at the input to the cascaded system with zero magnitude outside this time interval. Although of infinite duration only a finite segment of the signal will be valid at the output. Furthermore, by utilizing a technique similar to that used to view long transforms [Arsenault, 1979] the elongated portions of the signal beyond the original $2T_s$ seconds can be displayed. If most of the Fourier transform

is contained within the T_F second wide time interval, then very little is eliminated when it is gated to this time. In this case, the output of the cascaded system will look very much like the input except that a small amount of smoothing will be evident since large time derivatives are suppressed, the gated extremes of the signal will tend to roll off smoothly to plus and minus infinity and a small amount of ripple of period $4\pi/T_F$ will be observable directly attributable to the aforementioned type of sinx/x convolution except this time the signal, not the transform, is being convolved.

Assume that a 'down chirp' cascaded chirp transform system is to be used. The transform is symmetrically gated by a T_F second wide window. In order to recover the original input signal at the output exactly, the entire Fourier transform would have to be utilized. This, of course, as already mentioned, cannot be done. The form of the output for an input f(t) is therefore given by

$$f_\Omega(t) = \frac{1}{2\pi} \int_{-\Omega}^{\Omega} F(\omega) e^{j\omega t} \, d\omega$$

$$= \int_{-\infty}^{\infty} f(\tau) \, \frac{\sin\Omega(t-\tau)}{\pi(t-\tau)} \, d\tau \qquad (6.14)$$

where

$$\Omega = \beta T_F \qquad (6.15)$$

and

$$F(\omega) = \int_{-\infty}^{\infty} f(\tau) e^{-j\omega\tau} \, d\tau \qquad (6.16)$$

$$\int_{-\Omega}^{\Omega} e^{j\omega(t-\tau)} \, d\omega = \frac{2\sin\Omega(t-\tau)}{(t-\tau)} \qquad (6.17)$$

were utilized to obtain the final relation.

Note that

$$\lim_{\Omega \to \infty} f_{\Omega}(t) = \int_{-\infty}^{\infty} f(\tau)\delta(t-\tau)d\tau = f(\tau) \tag{6.18}$$

since

$$\lim_{\Omega \to \infty} \left(\frac{\sin\Omega(t-\tau)}{\pi(t-\tau)}\right) = \delta(t-\tau) \tag{6.19}$$

so that the output of the cascaded chirp transform 'down chirp' system utilizing symmetric transform gating approaches that of the input as $T_F \to \infty$. This, of course, assumes that all non-ideal system behavior can be ignored on the basis of producing no noticeable effect (which may not be true in real practice). If a system could possess chirp devices whose impulse responses can be represented exactly by the idealized equations used in their analysis and the rest of the system functions ideally in such a manner, for instance, that amplifier response is non-distorting and noiseless, that the finite delay through cables is zero and they exhibit no dispersion and that the mixers do not permit carrier leak through or produce harmonics other than the desirable sum and difference terms, to name a few, then the analysis is exact. The effects studied here are inherent even in the most ideal system.

Let's assume that the input signal to a cascaded chirp transform system was originally smooth and continuous prior to the required $2T_g$ seconds wide time gating of this signal. The gating produces a discontinuity to the originally smooth nature of the signal at both extremes of the $2T_g$ seconds wide window. Although no gating pulse can be produced or switch designed so that these discontinuities change at an infinitely fast rate, relative to the frequency content of the signal

the assumption will be made that they do. These discontinuities represent an abrupt change in the signal even if they tend to occur at signal zero crossings, since any real signal will have continuous finite derivatives at such a point whereas the ideal gate imposes a discontinuity in the derivative. The practical gating function will also produce a finite continuous derivative at the zero crossing; however, there will be a much faster change in the derivative (produces larger higher order derivatives) than there would have been in the ungated smooth signal at this point.

The gated smooth function can be written as the sum of two functions. One of these functions is a finite ramp that rises from zero to the function value at both ends of the gated interval and is connected by a straight line between these points. This function typically exhibits very large discontinuities at its extremes under the assumption of an ideal gate. The other function exhibits all the time variation of the original function and goes to zero at the extremes of the window. Since the function was originally assumed to be smooth (slowly time varying), the discontinuities in the derivatives of this second function at the window extremes will be assumed to be a much lower order effect with respect to the ramp discontinuities. Therefore, the input signal can be written as

$$f(t) = \left| U(t) - U(t-2T_s)\, f_c(t) \right|$$

$$= f_s(t) + \left| U(t) - U(t-2T_s) \right| \left| f_c(o) + \alpha t \right| \tag{6.20}$$

where

$$\alpha = \frac{f_c(2T_s) - f_c(o)}{2T_s} \tag{6.21}$$

and $f_s(t)$ is the finite yet smoothly varying portion of the signal.

From Eq. (6.14) the output of the cascaded system for this input is given by

$$f_\Omega(t) = \int_{-\infty}^{\infty} f_s(\tau)\,\frac{\sin\Omega(t-\tau)}{\pi(t-\tau)}\,d\tau$$

$$+ \int_{-\infty}^{\infty} \left| f_c(o) + \alpha\tau \right| \left| U(\tau) - U(\tau-2T_s) \right| \frac{\sin\Omega(t-\tau)}{\pi(t-\tau)}\,d\tau \qquad (6.22)$$

The first integral is very closely given by $f_s(t)$ since this function varies very slowly. The second integral can be broken down into four integrals, namely

$$f_1(t) = f_c(o) \int_o^{\infty} \frac{\sin\Omega(t-\tau)}{\pi(t-\tau)}\,d\tau$$

$$= \frac{1}{2} f_c(o) + \frac{1}{\pi} f_c(o) S_i(\Omega t) \qquad (6.23)$$

where

$$S_i(\Omega t) = \int_o^{\Omega t} \frac{\sin x}{x}\,dx \qquad (6.24)$$

$$f_2(t) = -f_c(o) \int_{2T_s}^{\infty} \frac{\sin\Omega(t-\tau)}{\pi(t-\tau)}\,d\tau$$

$$= -\frac{1}{2} f_c(o) - \frac{1}{\pi} f_c(o) S_i(\Omega(t-2T_s)) \qquad (6.25)$$

$$f_3(t) = \alpha \int_o^{\infty} \tau\,\frac{\sin\Omega(t-\tau)}{\pi(t-\tau)}\,d\tau$$

$$= \alpha t \left| \frac{1}{2} + \frac{1}{\pi} S_i(\Omega t) \right| - \frac{\alpha}{\pi\Omega} \int_{-\infty}^{\Omega t} \sin x\,dx \qquad (6.26)$$

$$f_4(t) = -\alpha \int_{2T_s}^{\infty} \tau \, \frac{\sin\Omega(t-\tau)}{\pi(t-\tau)} \, d\tau$$

$$= -\alpha t \left| \frac{1}{2} + \frac{1}{\pi} S_i(\Omega t - 2\Omega T_s) \right|$$

$$+ \frac{\alpha}{\pi\Omega} \int_{-\infty}^{\Omega t} \sin(x - 2\Omega T_s) \, dx \qquad (6.27)$$

If ΩT_s is some multiple of π, then

$$f_3(t) + f_4(t) = \frac{\alpha t}{\pi} \left| S_i(\Omega t) - S_i(\Omega(t - 2T_s)) \right| \qquad (6.28)$$

since

$$\frac{\alpha}{\pi\Omega} \int_{-\infty}^{\Omega t} (\sin(x - 2\Omega T_s) - \sin x) dx$$

$$= \frac{-2\alpha}{\pi\Omega} \int_{-\infty}^{\Omega t} \sin(\Omega T_s)\cos(x - \Omega T_s) dx = 0 \qquad (6.29)$$

Even if ΩT_s were not some multiple of π, since $\Omega = \beta T_F$ is usually a very large number, the integrals given by Eq. (6.29) will usually be much smaller than those in Eq. (6.28). The 2nd integral of Eq. (6.22) can therefore be written as

$$f_R(t) = \frac{1}{\pi} \left| S_i(\Omega t) - S_i(\Omega t - 2\Omega T_s) \right| \left| f_c(o) + \alpha t \right| \qquad (6.30)$$

Since $f_s(o) = 0$ and $f_R(o) \simeq \frac{f_c(o)}{2}$, then

$$\lim_{\Omega \to \infty} f_\Omega(o) \simeq f_c(o)/2 \qquad (6.31)$$

and since $f_s(2T_s) = 0$ and $f_R(2T_s) \simeq \frac{f_c(o) + 2\alpha T_s}{2}$, then

$$\lim_{\Omega \to \infty} f_\Omega(2T_s) \simeq (f_c(o) + 2\alpha T_s)/2 \qquad (6.32)$$

The total output is therefore given by

$$f_{\Omega}(t) \approx f_s(t) + \frac{1}{\pi}\left|S_i(\Omega t) - S_i(\Omega t - 2\Omega T_s)\right|\left|f_c(o) + \alpha t\right| \qquad (6.33)$$

This equation shows that the bandlimiting of the Fourier transform of f(t) to the interval $-\Omega \leq \omega \leq \Omega$, where $\Omega = \beta T_F$, has effectively only caused ripples to appear before and after both discontinuities of the output of the cascaded system. These ripples at discontinuities in the input signal are a form of behavior typically labeled the Gibb's phenomenon. Increasing $\Omega = \beta T_F$ only changes the time scale of the ripples and not their form. For practical values of Ω the ripples from the two discontinuities essentially do not interact since they become very small over a short segment of the output interval. Interactions would occur, however, between the ripples of close discontinuities that are inherently part of a wideband input signal aside from the imposed gating discontinuities. It is important to note that the ripples obtained at discontinuities for a signal passed through a cascaded chirp transformation system are due to the use of a step-like window to gate the Fourier transform. If this rippling type of behavior at discontinuities cannot be tolerated, a window having smoother transitions toward the extremes of the Fourier transform interval can be utilized so that the rippling is reduced or eliminated at the cost of increased smoothing of the signal and longer rise times at the discontinuities.

Functional Weighting of the Chirp Transform:

The unmodified magnitude of the Fourier transform is given by

$$M_o(\omega) = (R^2(\omega) + X^2(\omega))^{\frac{1}{2}} \qquad (6.34)$$

and the unmodified phase is given by

$$P_o(\omega) = \tan^{-1}(X(\omega)/R(\omega)) \tag{6.35}$$

where ω is a function of time for the output of a chirp transformation system. If only the magnitude is to be modified by a function $A(\omega)$, then the new real and imaginary components of the Fourier transform $R_n(\omega)$ and $X_n(\omega)$ satisfy the relations

$$A(\omega)M_o(\omega) = (R_n^2(\omega) + X_n^2(\omega))^{\frac{1}{2}} = M_n(\omega) \tag{6.36}$$

and

$$P_o(\omega) = \tan^{-1}(X_n(\omega)/R_n(\omega)) \tag{6.37}$$

or $$R_n(\omega) = A(\omega)R(\omega) \tag{6.38}$$

and

$$X_n(\omega) = A(\omega)X(\omega) \tag{6.39}$$

If only the phase is to be modified by a function $B(\omega)$, these components satisfy the relations

$$M_o(\omega) = (R_n^2(\omega) + X_n^2(\omega))^{\frac{1}{2}} \tag{6.40}$$

$$B(\omega)P_o(\omega) = \tan^{-1}(X_n(\omega)/R_n(\omega)) = P_n(\omega) \tag{6.41}$$

or

$$R_n(\omega) = M_o(\omega)/(1 + \tan^2 P_n(\omega))^{\frac{1}{2}} \tag{6.42}$$

and

$$X_n(\omega) = M_o(\omega)\tan P_n(\omega)/(1 + \tan^2 P_n(\omega))^{\frac{1}{2}} \tag{6.43}$$

If both the phase and magnitude are to be modified, then

$$R_n(\omega) = M_n(\omega)/(1 + \tan^2 P_n(\omega))^{\frac{1}{2}} \tag{6.44}$$

and

$$X_n(\omega) = M_n(\omega)\tan P_n(\omega)/(1 + \tan^2 P_n(\omega))^{\frac{1}{2}} \tag{6.45}$$

An Example - The Hilbert Transform:

Assume the input is real, $B(\omega) = 1$ and $A(\omega) = \text{sgn}\omega$ where

$$\begin{aligned} \text{sgn}\omega &= 1 \quad \omega > 0 \\ &= -1 \quad \omega < 0 \\ &= 0 \quad \omega = 0 \end{aligned} \tag{6.46}$$

then

$$R_n(\omega) = R(\omega)\text{sgn}\omega$$

$$X_n(\omega) = X(\omega)\text{sgn}\omega \tag{6.47}$$

$$jf_{ni}(t) = j\hat{f}(t) \longleftrightarrow j\Big(X(\omega)\text{sgn}\omega - jR(\omega)\text{sgn}\omega\Big)$$

$$= F(\omega)\text{sgn}\omega \tag{6.48}$$

or

$$\hat{f}(t) \longleftrightarrow -jF(\omega)\text{sgn}\omega \tag{6.49}$$

since

$$\frac{1}{\pi t} \longleftrightarrow -j\,\text{sgn}\omega \tag{6.50}$$

then the output of the cascaded chirp transform system is

$$f(t) * \frac{1}{\pi t} = \int_{-\infty}^{\infty} \frac{f(\tau)}{\pi(t-\tau)}\, d\tau$$

PART 3

EXPERIMENTAL

3.1 Signal Processing with the SAW Separated-Medium Acoustoelectric Convolver

Convolver Structure and Behavior:

The convolver structure utilized in the experiments can be seen in Figure 3.1. A piezoelectric $LiNbO_3$ delay line crystal was mounted on a ground plane. At both ends, on the top surface of the delay line, are interdigital transducers used to transform the electrical input signals into propagating surface waves on the crystal surface. When signals are applied to both transducers, the generated surface waves propagate toward one another. Waves are also generated that propagate towards the closest edges, but the wax intentionally put on these ends behaves as an excellent acoustic absorber so that little acoustic energy is reflected from these ends. (As a matter of fact, the major troublesome reflection in this device is the'triple-transit echo' obtained when a surface wave reflects once from each of the two transducers. This, however, is usually suppressed by mismatching the transducers.) The transducers utilized for these devices (deposited photolithographically onto the delay line surface) had five finger pairs where each finger was spaced between centers by a half wavelength corresponding to the transducer center frequency. For this number of fingers the bandwidth of the transducer is about twenty percent of its center frequency (i.e. a 20% percentage bandwidth). Since the devices used had center frequencies of 115 Mhz and 230 Mhz, this means that the device bandwidths were about 23 Mhz and 46 Mhz, respectively, about these frequencies. All transducers were matched to 50 Ω, at their center frequencies, by a single inductor. Since the transducers were designed to

be 50 Ω at center frequency, no transforming networks were required. The non-linear interaction between the two surface waves, that is required in order to obtain the convolution, is obtained by placing a slice of semiconductor close enough to the delay line surface so as to be influenced noticeably by the surface wave electric fields. The semiconductor used was 40 Ω-cm n-type silicon. The silicon was highly polished and then sliced to size so as to cover most of the distance between the two transducers, when placed onto the delay line, and to encompass the entire beam width (which is 108 times the acoustic wavelength at center frequency for a 50 Ω transducer). A more or less uniform air gap (adequate for most of the work done here) could be obtained by simply placing the polished side of the silicon in contact with the delay line surface and applying pressure along its length. The 1000 to 2000 angstrom gap is obtained as a result of surface imperfections on the two contacting materials, which prevents a complete and intimate contact along the entire length of the semiconductor. The back side of the silicon was coated with silver conducting paint which played the part of the constant potential or averaging contact that essentially averages out the potential variations over the entire surface of the silicon. Those potential variations that are constant or vary very little over space, such as the potential arising due to the interaction of the charge density modulation due to one surface wave with the electric field of the other contrapropagating wave, will produce large averages and dominate the output potential over the contact defined by the silver conductive paint. The silver paint on the silicon back surface also served as a bond to hold onto the output wire connection. Fine wires were bonded to the pads of the interdigital transducers also by using this

conductive paint. All connections were made through feed throughs through the walls of the milled aluminum container used to house, support and shield the entire convolver structure. The input inductors were housed in separate chambers beneath the device and all connections to the outside world were made through BNC or OSM connectors. The protective milled aluminum container also supported the silicon pressure structure that consisted of foam supported on a plastic slab the same size as the semiconductor. This plastic slab is pressed against the semiconductor (see Figure 3.1) by set screws firmly set within a plastic cover that is bolted to the aluminum casing. Aluminum covers are bolted onto the top and bottom of the finished device so that the entire unit is shielded from outside interference. (Internally, this totally enclosed structure takes on the characteristics of a waveguide.) The convolver gap uniformity is adjusted by selectively changing the pressure exerted by the set screws on the silicon. With an impulse applied to one convolver input and a continuous tone applied to the other, the output convolution will essentially represent a uniformity scan of the device, so that pressure can be dynamically adjusted until this output becomes fairly constant.

Typical separated-medium convolvers are shown in Figures 3.2a and 3.2b. Figures 3.3a, 3.3b and 3.3c show the autoconvolution outputs obtained using such a device when the inputs are both single square waves, double square waves and five pulse square waves, respectively. The single pulses must produce a triangle as they do in the second trace of Figure 3.3a. The third trace in this picture is one of the delayed outputs from the transducer at the opposite end to which it was applied. Note that the two pulses produce three peaks and the five pulses produce nine peaks

Figure 3.1: The Si-on-$LiNbO_3$ SAW separated-medium convolver.

(a) The overall convolver structure. This structure basically consists of a slice of silicon in close proximity (< 2000 Å) to a $LiNbO_3$ piezoelectric delay line. The evanescent surface wave fields produce charge bunching within the silicon. The localized current densities due to the product of the SAW fields and the modulated charge density inside the silicon produces a localized potential through the average conductivity of the silicon. (The charge density modulation due to the SAW merely perturbs the silicon conductivity.) The ohmic contact along the back surface of the silicon integrates over the localized potentials. When two SAW's are launched in counter-propagation, their interaction beneath the silicon produces a stationary product component of potential within the semiconductor that does not possess a spatial carrier variation although it varies in time at twice the frequency of a single surface wave. This component will integrate out to a time varying potential on the silicon back contact that is the convolution of the envelopes of the two SAW's on a carrier having twice their frequencies. The 5.5 pairs of transducer fingers overlap by about 108 times the center frequency wavelength. This structure produces a 20% percentage bandwidth and a 50 Ω match at the center frequency. (The aluminum is typically about 2000 Å thick.) A series inductor is used to tune out the inherent transducer capacitance at bandcenter. Wax damps out the SAW propagating toward the immediate crystal edge.

(b) A cross-sectional view of the composite convolver structure including the silicon pressure support structure. Set screws, in a threaded top plate, press against a plate whose opposite side is covered by a sheet of foam followed by waxed paper. This plate presses against the slice of silicon through the action of the set screws where the localized forces are dispersed somewhat by the foam sheet. The silicon polished front surface is pressed into close proximity (< 2000 Å) to the $LiNbO_3$ polished surface. (Microscopic surface discontinuities prevent a zero gap between the two surfaces from being attained.) The $LiNbO_3$ piezoelectric delay line is mounted upon an aluminum ground plane that is the floor of a cavity within a milled aluminum box.

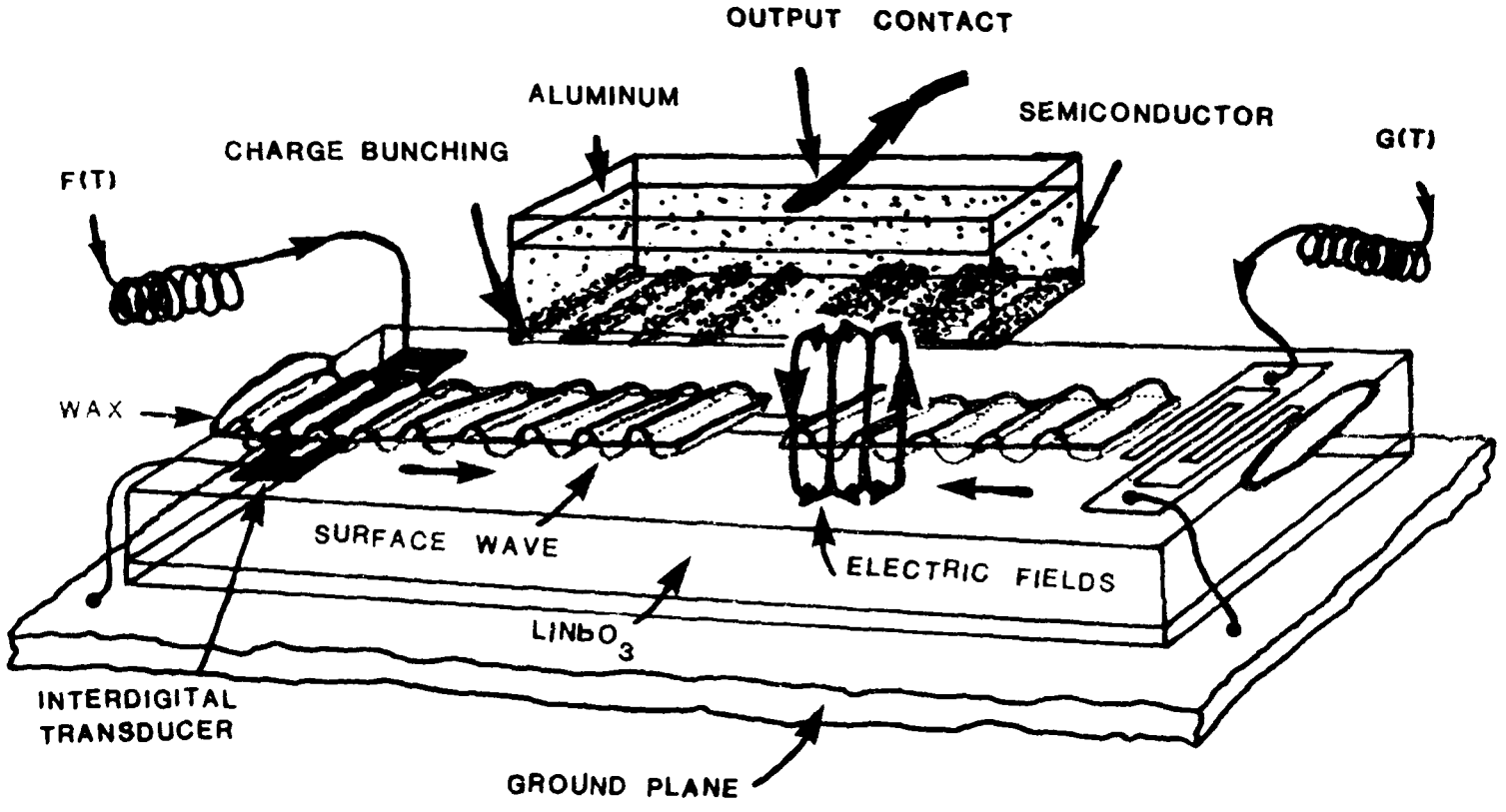
OUTPUT CONTACT
ALUMINUM
SEMICONDUCTOR
CHARGE BUNCHING
F(T)
G(T)
WAX
SURFACE WAVE
ELECTRIC FIELDS
LiNbO3
INTERDIGITAL TRANSDUCER
GROUND PLANE

FIGURE 3.1a

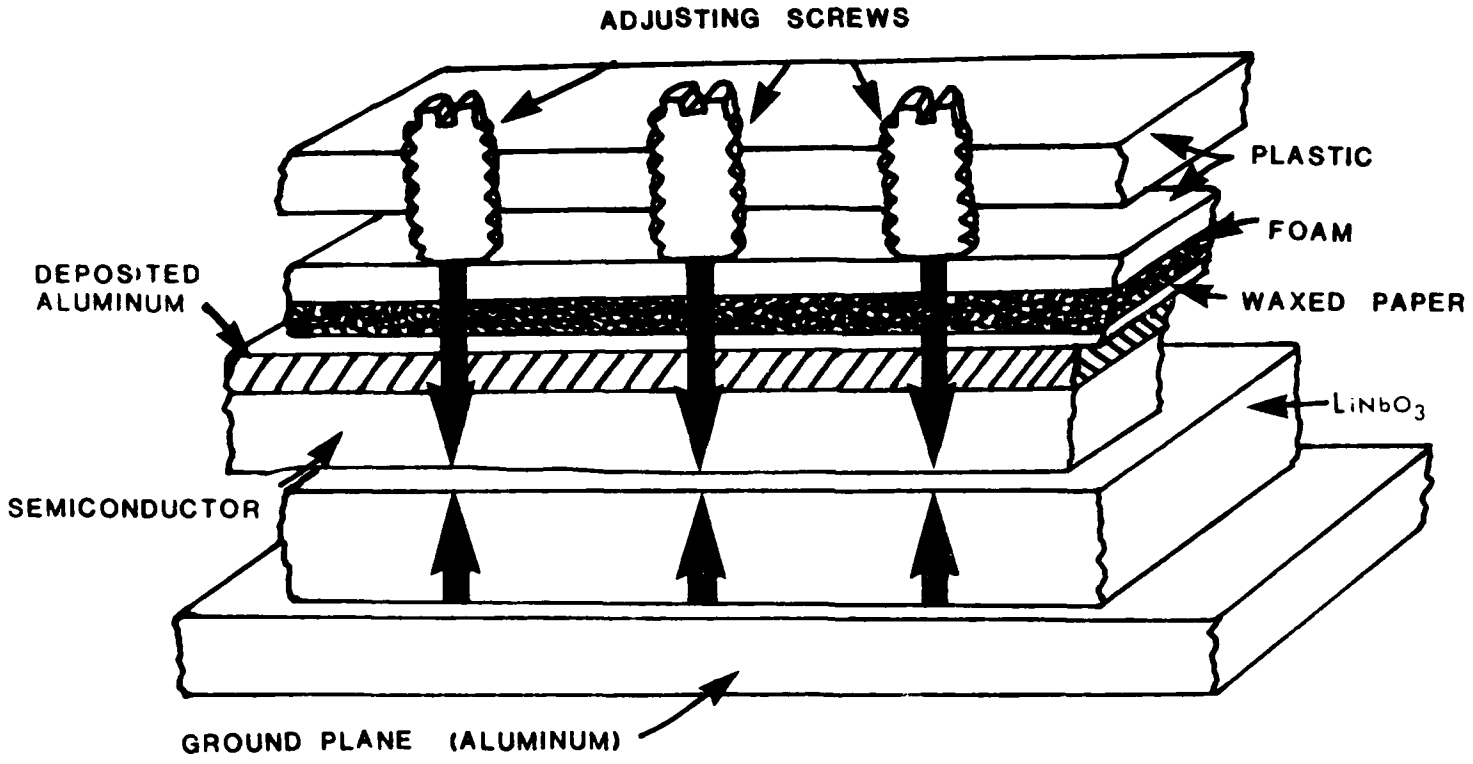
ADJUSTING SCREWS
PLASTIC
FOAM
WAXED PAPER
DEPOSITED ALUMINUM
$LiNbO_3$
SEMICONDUCTOR
GROUND PLANE (ALUMINUM)

FIGURE 3.1b

Figure 3.2: Packaged SAW convolvers.
(a) Small version having OSM input and output connectors.
(b) Larger version (for the longer crystals used in the memory work) having BNC input and output connectors. The interdigital transducer tuning inductors (for tuning out the transducer capacitance at center frequency) are contained in isolated cavities beneath the main crystal cavity all of which are milled into a solid aluminum block and shielded by top and bottom aluminum covers. Both of the devices shown are 110 Mhz center frequency devices having 20% bandwidths. Silicon lengths, and therefore interaction times, varied; however, a typical 3.5 cm-long 40 Ω-cm slice at the YZ-$LiNbO_3$ velocity of 3488 m/sec would produce an interaction time of about 10 μs. Depending on the application, silicon slices as long as 7.5 cm were available from 3 inch diameter silicon samples. The 20% device bandwidths were obtained by utilizing 5-1/2 finger pairs on $LiNbO_3$. Matching of each transducer to 50 Ω for this piezoelectric was obtained by requiring the interdigital finger overlap to be about 108 times the wavelength at the center frequency and using about 2000 Å of aluminum for the transducers at a one-to-one line-to-space ratio. The convolution output was obtained directly from the back surface of the slice of silicon by attaching a fine wire, using conductive silver pain, to this surface. This wire was attached, through a feedthrough, to the output BNC connector.

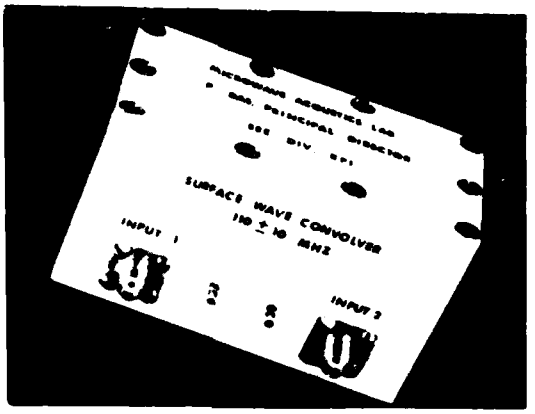

Figure 3.2a

Figure 3.2b

Figure 3.3: Performance characteristics of the SAW convolver.

(a) Trace 1 shows a 10 volts p-p (5 v/div) 11 μs wide (5 μs/div) pulse used as the input to the two input ports of a 110 Mhz convolver. Both pulses (obtained by splitting) have a 110 Mhz carrier. Trace 2 shows the 28 mv p-p output convolution (10 mv/div) of the two input pulses. The 6.5 μs before the start of the convolution is the time required for the two pulses (applied simultaneously) to meet within the device which correponds to half the delay between the two input transducers. Note that, due to the simultaneous propagation of both the square pulses, the triangular convolution is compressed by a factor of two, as are all the convolution outputs obtained in this manner, and is exactly a pulse width wide. This output is 51 dB down from the input corresponding to an efficiency ($F(dBm) = P_{OUT}(dBm) - 2P_{IN}(dBm)$) of about -75 dBm (-27 dBm - 48 dBm). Trace 3 shows the 1 volt p-p delayed output (.5 v/div) of the convolver when it is utilized as a delay line with the silicon in place. This output, obtained from one of the convolver input ports, is 13 μs delayed from the time of application of the pulse to the other input port and has been attenuated by 20 dB. By studying these results it can be seen that the interaction region must be at least 11 μs long so that the 3.8 cm long slice of silicon is situated about a third of a centimeter from either transducer ($3.8 \text{ cm} = 3.488 \times 10^5 \text{ cm/sec} \times 11 \mu s$ & $1/3 \text{ cm} = 3.488 \times 10^5 \text{ cm/sec} \times 1 \mu s$).

(b) Trace 1: A 6.2 μs wide signal (2 μs/div) consisting of two spaced pulses of equal width. Trace 2: The compressed-by-a-factor-of-two convolution of trace 1. The delay of the convolution for this convolver is about 5.8 μs so that the device transducers are spaced about 4 cm apart corresponding to a delay between transducers of 11.6 μs. The silicon must be at least 2.2 cm long to accommodate the entire convolution.

(c) Trace 1: A 9 μs wide signal (2 μs/div) consisting of 5 equally spaced pulses of equal width (1 μs pulse widths and spaces). Trace 2: The compressed output convolution of trace 1. The convolution arises about 7 μs after the signal so that the transducer spacing for this device is about 5 cm. The silicon for this device must be at least 3.14 cm long. The output in trace 2 has been video detected.

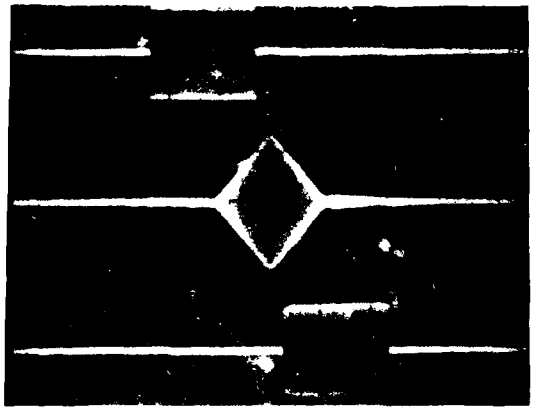

Figure [illegible]34

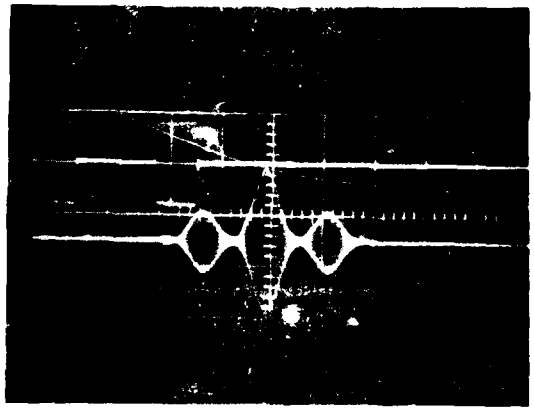

Figure [illegible]35

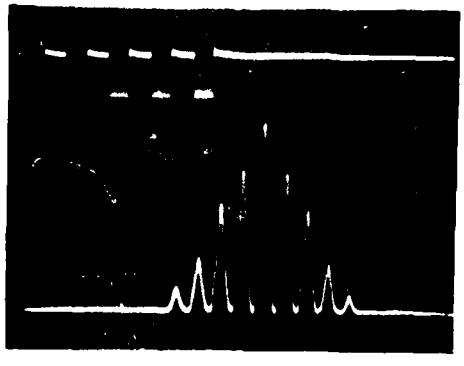

Figure [illegible]36

as they should. In Figure 3.3c the carrier was removed coherently from the output. The output convolution is usually on the order of 50 to 60 dB down from the input level so that a 10 volt peak to peak input pulse produces millivolts of output. The pulses in these figures are a few microseconds wide and the overall interaction time of the devices is 10 to 15 microseconds. Note that the factor of two time compression of the convolution due to contrapropagation of the two waves (only one signal shifts for the usual convolution) is evident in these pictures.

Convolver Fourier Transformation:

A powerful technique utilizing the SAW separated-medium convolver is the performance of a chirp transformation. The technique is described theoretically in Section 2.5. Figure 3.4 shows a block diagram of the system where inverse Fourier transformation is also being performed. As described in Section 2.5, the output transforms are valid only during specific time intervals due to the finiteness of the convolver time-changing impulse response. (The time changing response produces the compression factor.) Due to the output time compression, the Fourier transforms are modulated by chirps having twice the slope and center frequencies of their input signals and therefore must be inputted into a higher frequency convolver to perform the inverse transformation, unless the chirp is mixed to a lower frequency. In any case, after inverse transformation the original signal is recovered compressed by a factor of four.

Figures 3.5a to 3.5f show typical output Fourier transforms for this system.

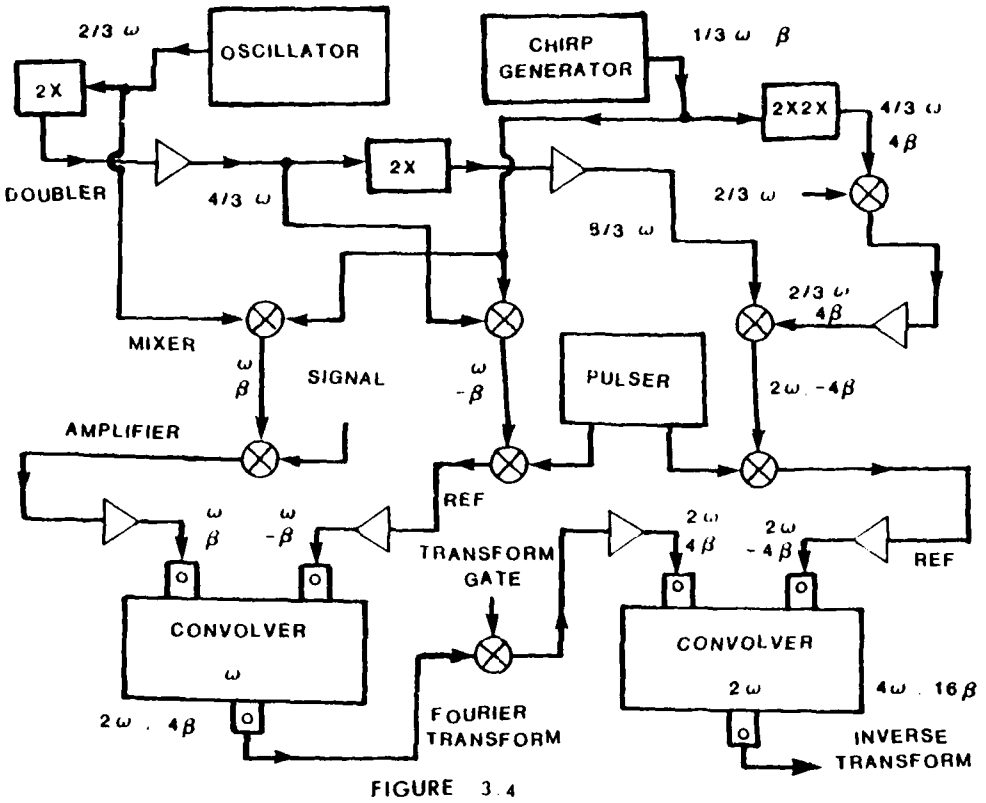

FIGURE 3.4

Figure 3.4: A block diagram showing the utilization of SAW convolvers for Fourier transformation followed by inverse Fourier transformation. There is a factor of two compression after every transformation so that the recovered signal upon inversion is compressed by four relative to the input. Chirps are generated using a ramped VCO, doublers and rf mixing stages. The signals to the 2nd convolver have double the original carrier frequency and four times the chirp slope. The output of this convolver has four times the carrier frequency and sixteen times the original chirp slope.

Figure 3.5: Fourier transformation outputs from the convolver-Fourier-transformation system.

(a) Trace 1: A small input pulse (5 μs/div). Trace 2: The sinx/x Fourier transform of trace 1 (.2 μs/div). This transform was 2 volts p-p (.5 v/div) after amplification.

(b) Trace 1: A positive and negative pulse input signal (5 μs/div). Trace 2: The Fourier transform of trace 1 (.2 μs/div).

(c) Traces 2, 4 and 6: Small positive and negative pulses with varying pulse separations (5 μs/div). Traces 1, 3 and 5: The respective Fourier transforms of traces 2, 4 and 6 (.5 μs/div). Note the increase in frequency for wider pulse spacings.

(d) Traces 2, 4 and 6: A positive and negative, two positive and two negative thin pulses, respectively (5 μs/div). Traces 1, 3 and 5: The respective Fourier transforms of traces 2, 4 and 6 (.5 μs/div). Traces 1 and 2 correspond to the cosine and its transform whereas traces 3 and 4 represent the sine and traces 5 and 6 an inverted cosine. Note the phase changes in the transforms of this figure.

(e) Trace 1: A five pulse input sequence (2 μs/div). Trace 2: The Fourier transform of trace 1 (.2 μs/div). Note that all these Fourier transforms have not been coherently dechirped so that the outputs are the magnitudes of the respective Fourier transforms modulated by chirps whose phase variations from quadratic are the respective phases of the Fourier transforms. The real and imaginary components of these transforms can be obtained by mixing the outputs in this figure with in-phase and quadrature chirps. In this figure, however, all the signals are real and either symmetric or antisymmetric so that the transforms have only real or imaginary components, respectively. (Also, the real and imaginary Fourier components will be symmetric and antisymmetric, respectively.) (See Section 2.5.)

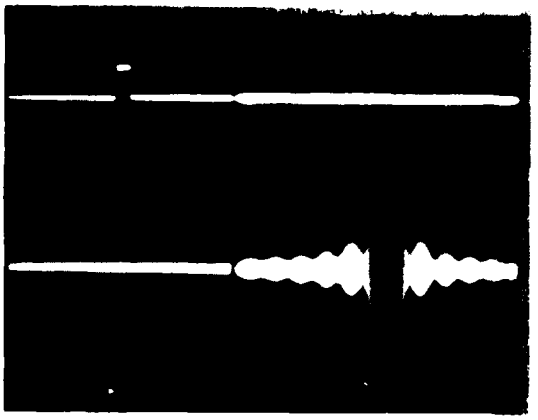

Figure 3.5a

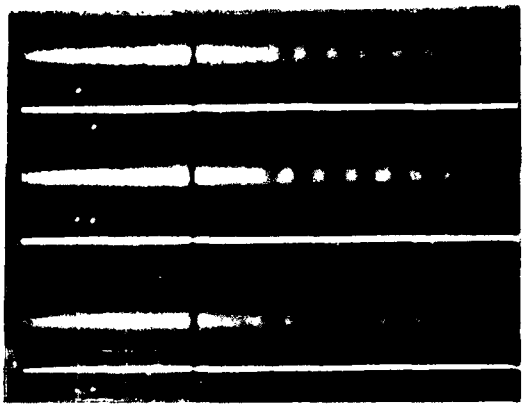

Figure 3.5d

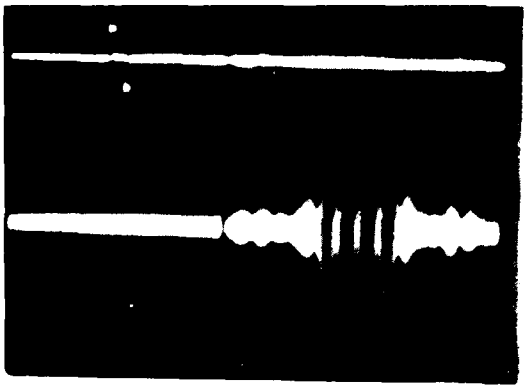

Figure 3.5b

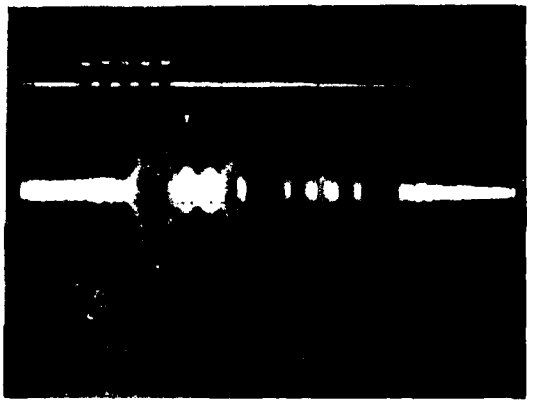

Figure 3.5e

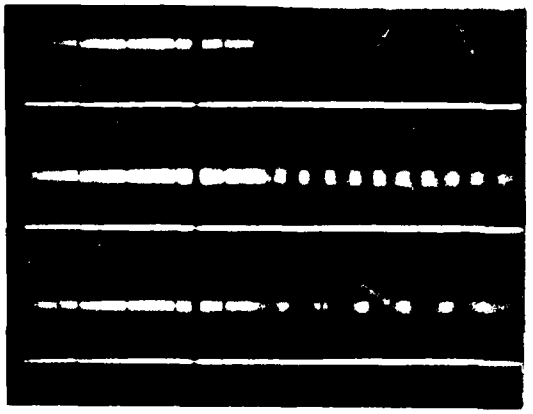

Figure 3.5c

Figure 3.5a shows the Fourier transform of a single 3 μs wide square pulse. All these transforms correspond to about 1 Mhz per division. The exact time to frequency correspondence of the transform is related by twice the slope of the input chirps (i.e. $\omega = 4\beta t$ + a constant where 2β is the chirp slope). Figure 3.5b shows the transform of a positive and a negative pulse. If these pulses are made very thin, the transforms behave as sines and cosines as seen in Figures 3.5c and d. All these Fourier transformations are chirp modulated so that their envelopes are the transform magnitudes and the transform phase is phase modulating the chirp carrier. Phase quadrature chirps could have been used to separate the real Fourier component from the imaginary component (see Section 2.5).

Figures 3.6a and b show some filtering results using this system configuration. In both cases input pulses were added to highly monochromatic 'noise' and the main spectral peaks of this noise were gated out of the combined spectrum. This is most clearly demonstrated in Figure 3.6b where by gating out all but the central portion of the Fourier transform, the orignal signal is essentially recovered.(compressed by a factor of four). The input signal is shown on the same time scale as the output, in this photograph, for comparison. Note that the finite bandwidth of the system has forced the pulses to look like triangles. These outputs have been video detected in a low noise narrowband amplifier.

Ambiguity Function Generation:

As discussed in Section 2.2 the convolver can be used to

Figure 3.6: Filtering by time gating of the Fourier transform in the convolver Fourier transformation system.

(a) Trace 1: Two .8 μs wide pulses (1 μs/div) separated from one another by about 4.5 μs. Trace 2: A 3.3 Mhz sine wave added to the signal given by trace 1. Trace 3: The Fourier transform of trace 2 (.2 μs/div). The central region of this transform is due primarily to the two pulses, whereas the two peaks are due to the 3.3 Mhz signal. Since these peaks are situated at ± 3.3 Mhz in the Fourier domain, then this transform is being displayed on a scale of about .776 Mhz/div. (The frequency scale of the displayed transforms from such a system is dependent on the slope of the VCO generated chirp, which is itself dependent on the controlling ramp slope, so that the time-to-frequency correspondence of the Fourier transforms shown in this figure and Fig. 3.5 may all be different since no effort was made to match one result with another. The situation doesn't arise when chirps are generated utilizing chirp filters (see Section 2.4).) Trace 4: The time gate used to retain only the central portion of the Fourier transform in trace 3. The actual gating is performed by applying both signals to a mixer or preferably an rf switch (i.e. smaller feedthrough due to leakage). Trace 5: The inverse transform (1 μs/div) of the gated Fourier transform. Note that the gating has not only eliminated the rf but has filtered the pulses to the point where they've taken on a triangular appearance. Trace 5 is the factor-of-four compressed version of trace 1 convolved with a sinx/x whose main lobe is about .59 μs wide (i.e. $2(4.4)(.776 \times 10^6))^{-1}$) since the transform gate is 4.4 divisions wide.

(b) Trace 1: Fourier transform (.5 μs/div) of the three pulse signal (2 μs/div) displayed in the upper right quadrant of the display. Trace 2: The inverse transform of trace 1 (.5 μs/div) shown on an expanded scale relative to the three pulse input signal for comparison. Trace 3: The Fourier transform (.5 μs/div) of the three pulse signal with the addition of a monochromatic noise component (≈ 4 Mhz). This combined signal can be seen with a 2 μs/div scale in the bottom right quadrant of the display. Trace 4: The inverse transform (.5 μs/div) of trace 3. Trace 5: A gated version of trace 3 where the dominant portion of the noise spectrum and the high frequency (> 2.4 Mhz) portion of the three pulse signal spectrum have been eliminated. Trace 6: The inverse transform of trace 5. The finite bandwidth (≈ 6 Mhz) of the low-noise narrowband amplifier at the output of the system produced the filtered outputs shown in traces 2 and 4 whereas the transform gating improved the output from that given by trace 4 to that of trace 6.

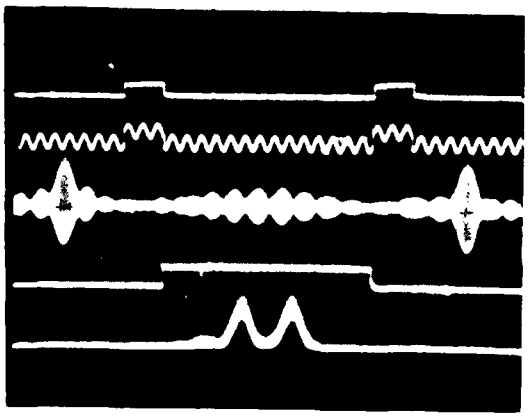

Figure 3.6a

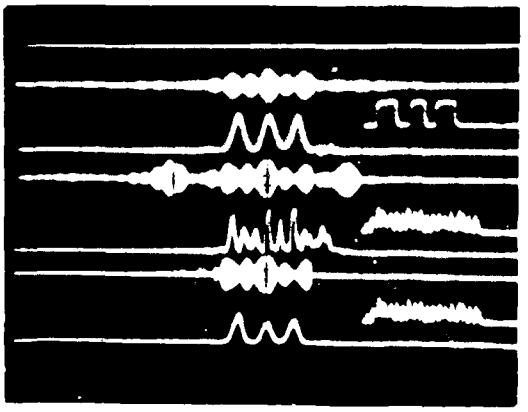

Figure 3.6b

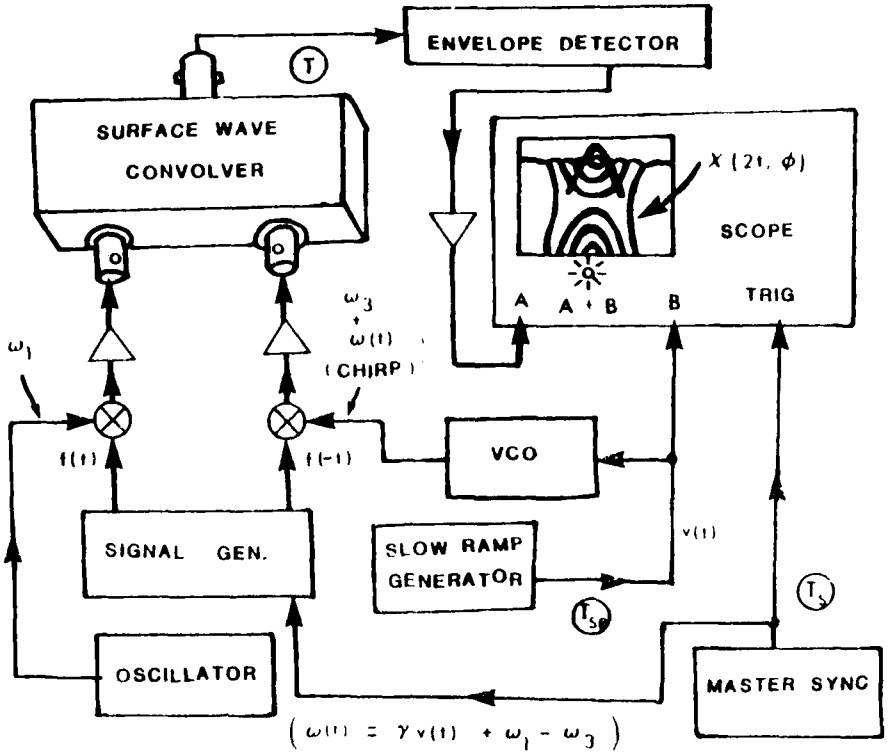

FIGURE 3 7

Figure 3.7: The block diagram of the system used to generate ambiguity functions with three-dimensional formats (i.e. amplitude versus time versus frequency). A 'slow-ramp' is fed to a VCO whose output frequency is used to modify the center frequency of the signal whose ambiguity function is desired. The change in center frequency simulates Doppler shift and the compression of the signal is ignored (since this is usually negligible). The ramp is slow enough so that the frequency is essentially constant over every convolution time interval. The convolver is performed against an unchanging reference version of the signal. The successive convolutions are displayed at increments along the frequency axis by summing them with the slowly varying ramp. A variation of this scheme would be to use a programmable synthesizer that is programmed to jump a specified frequency increment before each scan time of the oscilloscope and to generate a stepwise ramp (using a clocked D/A converter, for instance) as the signal to be summed at the oscilloscope. By such a technique the frequency and oscilloscope display level remain constant over each correlation time. Note that an assymetric signal must be time inverted in order to obtain the autocorrelation by convolving with the reference.

generate delay versus Doppler shift functions otherwise known as ambiguity functions. The essential process is to correlate a signal with a frequency shifted version of itself and to display the correlations one above the other spaced linearly in frequency. The reference version of the signal (whose frequency remains constant) represents the impulse response of a filter matched to the incoming signal. This reference must be a time reversed version of the signal, however, only symmetric signals were used here (except for chirps). To display the ambiguity function for a particular signal, it is applied, properly timed with the reference, to the convolver input after its center frequency has been adjusted in accordance with the slice of the two dimensional (two-variable; frequency vs. time vs. magnitude) ambiguity function that it is to represent. Figure 3.7 shows a block diagram of the technique used to generate this function. A slow ramp is used that produces a chirp (using a VCO) whose frequency remains essentially constant over a single correlation time. The change in frequency from one correlation to the next, however, is not so small and, therefore, every time the signal is applied to the convolver it has a different center frequency (i.e. the carrier has changed). An oscilloscope is triggered to display every correlation in proper time correspondence with one another. By summing the slow ramp to the scope display and adjusting vertical gain and horizontal expansion, the two dimensional ambiguity function is displayed over the entire screen as a three dimensional image. Note, however, that the individual correlations must be envelope detected before display. The rep rate for an entire frame can be (but need not be) synchronized to the correlation trigger. This rep rate is dependent on the time duration of the slow ramp and must be fast

enough to eliminate 'flicker' of the display.

Figures 3.8a and b show slices of the ambiguity function of a square pulse. These photographs were obtained by a multiple exposure technique whereby every correlation is meticulously placed on the oscilloscope before its picture is taken. (The actual form of the ambiguity functions shown here are given in equation form in Section 2.2.) Figures 3.9a and b show the ambiguity functions of square waves for a single and double input pulse, respectively, using the technique described in the previous paragraph. This image has the appearance of a continuous three-dimensional display and can be noted to agree well with the expected form of the function (Skolnik, 1970)(Rihaczek, 1969). Note that the displays are essentially 'see through' versions of the function since no blanking of the correlations is being performed for parts of the signals that appear to fall behind the ambiguity function. Figures 3.10a and b show the ambiguity functions for a linear-FM or chirp and a V-chirp, respectively. Since the shape of the ambiguity function is an indication of the time and frequency resolving capability of the particular form of radar signal used, Figure 3.10a shows that the chirp has a fairly constant resolving capability over the correlation time and Doppler shift interval represented by the 'knife edge' formation. In this case the time and frequency resolution are both good. As seen in Figure 3.9a the square pulse has much better Doppler (frequency) resolution than range (time) resolution. The V-chirp, however, shown in Figure 3.10b is seen to be very selective to a particular time and frequency. Figures 3.11a and b show the chirp and double pulse ambiguity functions on different scales and shifted in position on the display. Figure 3.11c shows the single pulse

Figure 3.8: Multiple exposure square-pulse ambiguity functions obtained using a SAW convolver. (a) Trace 1: The autocorrelation (equivalent to autoconvolution for a symmetric signal) of the square pulse without Doppler shift (i.e. no difference between the signal and reference carriers) (1 μs/div). Trace 2: The autocorrelation when the Doppler frequency shift is equal to the reciprocal of the pulse width or .25 MHz (pulse width = 4 μs). This corresponds to the first null of the sinx/x variation of the ambiguity function along the frequency axis. Traces 3 to 5: The autocorrelation at successive .125 MHz Doppler shift increments corresponding to successive peaks and nulls of the sinx/x response along the frequency axis. Note that all the ambiguity functions are displayed in magnitude only, in all these figures, as is commonly done in practice. The magnitude is obtained by passing the rf modulated convolver outputs into an envelope detector prior to display. Trace 5 corresponds to an overall Doppler shift of .625 MHz from the 110 MHz reference carrier frequency of the 4 μs wide input signal. (b) The autoambiguity function of a 5 μs square pulse (2 μs/div). In this case the first sinx/x null occurs at .2 MHz and each slice in this multiple exposure is spaced 10 KHz from its neighboring slices. The ambiguity function spans about .6 MHz along the Doppler axis.

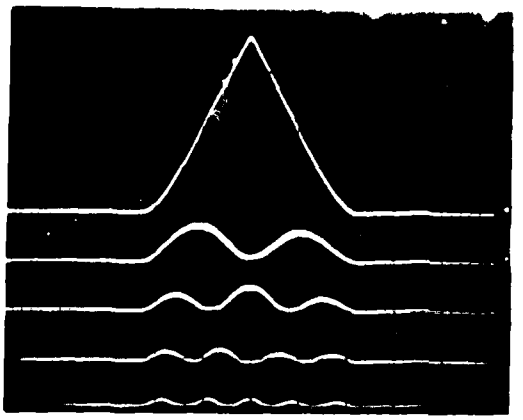

Figure 3.8a

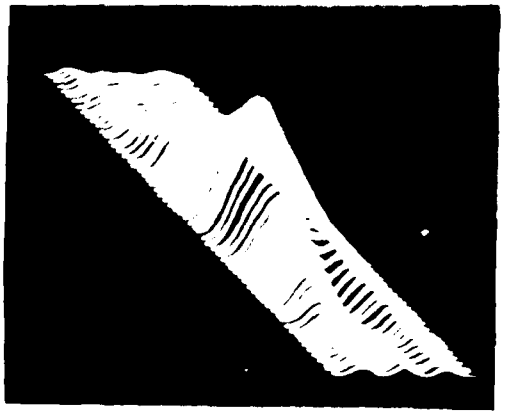

Figure 3.8b

Figure 3.9: Three-dimensional square-pulse ambiguity functions obtained using a SAW convolver (and the system configuration shown in Figure 3.7).

(a) A 5 μs square pulse auto-ambiguity function. This three-dimensional function is being displayed on a frequency scale of approximately .2 Mhz/div along the vertical axis and 1 μs/div along the horizontal axis. The amplitude, a function of the amount of amplification following the convolver, is being displayed at .5 v/div.

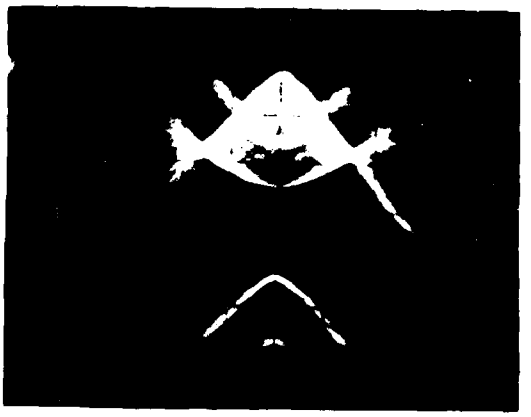

Figure 3.9a

(b) The ambiguity function obtained by convolving a 5 μs square pulse reference with two 5 μs square pulses spaced from one another by 5 μs. By proper timing, two signals whose combined duration equals twice the interaction time of the convolver can be convolved in this device without error. If their combination exceeds twice the device interaction time the convolution output will be in error. (i.e. For a symmetric convolver with interaction time T and input signal durations T_1 and T_2, the maximum value of $T_1 + T_2$ is 2T. Furthermore, if $T_1 + T_2 = 2T$, then the signal having a duration of T_2 seconds (where $T_2 > T_1$) must be applied to its input $(T_2 - T_1)$?? seconds before the T_1-second-duration signal is applied to its input in order to obtain the entire T-second-long convolution without distortion.) The interaction time of this convolver was approximately 10 μs so that the convolution of the 15 μs and 5 μs signals represented the maximum allowable combined signal duration, thereby producing the maximum error-free output duration of 10 μs (1 μs/div). As in (a) the frequency (vertical) axis represents approximately .2 Mhz per division.

Figure 3.9b

Figure 3.10: Three dimensional chirp ambiguity functions.

Figure 3.10a

Figure 3.10b

(a) The autoambiguity function of a 5 μs wide linear FM. Since the frequency scale is approximately 1 Mhz/div and the time scale is 1 μs/div, Eq. 2.55 of Section 2.2 (i.e. the equation of the line along the 'knife-edge' of this ambiguity function) gives a chirp slope of $2\beta = -\pi(3\ \text{Mhz}/5\ \mu\text{s}) \approx -2 \times 10^{12}$. From Eq. 2.56 of that section it is seen that the ambiguity function along this 'knife-edge' describes the triangular (compressed) convolution of the 5 μs envelope of the input chirp. This ambiguity function is thereby similar to the function given in Fig. 3.9a, but angled in the time-frequency plane with a slope given by the chirp slope. Since the input chirp is asymmetric, its time inverse had to be generated in order to produce this ambiguity function using a convolver. (This was accomplished by spectrally inverting the input chirp so that the chirp slopes of the two chirps were exactly matched in magnitude but of opposite polarity.) For a set Doppler shift the output from the convolver is a compressed pulse whose peak position in time is a linear function of the Doppler shift.

(b) The autoambiguity function of a 10 μs wide V-chirp (.5 μs/div). The V-chirp consists of a 5 μs linear increase in frequency followed immediately by a 5 μs linear decrease in frequency. The slope for this chirp was on the order of 3×10^{12} rad/sec^2 in magnitude so that the peak of this ambiguity function is about .5 μs wide or the width of the V-chirp divided by its time-bandwidth product (i.e. TB = (4.8 Mhz) (10 μs) = 48). Note that the width of the correlation peak in (a) along the time axis is approximately .5 μs, since the time-bandwidth product of this 5 μs chirp is about 30. The 'razor-edge' in (a) is therefore about .5 μs wide.

Figure 3.11a

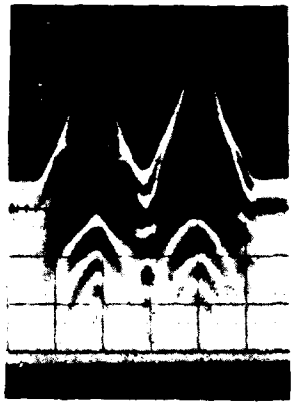

Figure 3.11b

Figure 3.11c

Figure 3.11: Other ambiguity function displays.

(a) The autoambiguity function of a linear-FM having a slope of approximately .12 x 10^{12} rad/sec^2, shown with a time scale of 2 μs/div, a frequency scale of about .2 Mhz/div and displayed utilizing a slow ramp of slope opposite in polarity to that used in Fig. 3.10a so that the 'knife-edge' is angled with slope opposite in polarity to that of Fig. 3.10a.

(b) The same autoambiguity function displayed in Fig. 3.9b except that the time scale has been compressed by a factor of two and the peaks have been shifted upward along the frequency axis by changing the center frequency of the 'slow-chirp' used to produce the Doppler shift. Note that no form of blanking is used in displaying these three-dimensional functions so that they appear transparent in that structures occurring behind taller structures tend to show through.

(c) The autoambiguity function of a 5 μs square pulse (1 μs/div) displayed by modulating the z-axis (intensity) of the oscilloscope display. The frequency scale is about .5 Mhz/div. Deviation from ideal symmetry of this display is a result of non-uniform application of pressure along the slice of silicon inside the SAW convolver thereby obtaining a non-uniform interaction along its length. (i.e. a non-uniform silicon-to-piezoelectric gap width results.)

ambiguity function obtained by z-axis modulation of the oscilloscope display (the intensity of the beam is controlled instead of its position on the screen). Figures 3.12a thru f show the ambiguity function for the square pulse at successive amplitude levels. Note the amplifier saturation in Figures 3.12e and f.

Waveform design can be performed by utilizing the ambiguity function. Figure 3.13 shows two triangular wave functions that are used to drive a VCO. When these functions are gated by five pulses (shown as the second trace) the output of the VCO is five consecutive V-chirps. Note, however, that one function consists of uniform amplitude triangular variations, whereas the other shows decreasing and increasing triangular variation amplitudes. The effect of this slight variation of the amplitude of the VCO controlling function and therefore the slope of the resulting V-chirps on the shape of the resulting ambiguity functions can be seen by comparing Figures 3.14a to c with Figures 3.15a to c. Figure 3.14a shows the compressed ambiguity function (no frequency axis) for the uniform function. Comparing this with Figure 3.15a, it can be seen that the relative peak amplitudes of the ambiguity function have changed. Figures 3.14b and 3.15b show the respective three-dimensional forms of these functions. Figures 3.14c and 3.15c show the respective results when the spacing between pulses has been varied. These results show, in a simplified way, that dynamic signal design is possible.

The Memory Correlator:

The basic structure of the memory correlator is shown in Figure 3.16. Essentially this device is the same as the basic convolver, except that the semiconductor surface facing the delay line contains some

Figure 3.12: Successive three-dimensional 6 μs-square-pulse ambiguity functions obtained by successively increasing the amplitude of the input signal to the convolver (at a constant reference level).
(a) ≃ 11 dBm input level (≃ 2.3 vpp).
(b) ≃ 15.4 dBM input level (≃ 3.7 vpp).
(c) ≃ 18.4 dBm input level (≃ 5.3 vpp).
(d) ≃ 20.5 dBm input level (≃ 6.7 vpp).
(e) ≃ 22.3 dBm input level (≃ 8.3 vpp) with amplifier saturation.
(f) ≃ 24 dBm input level (≃ 10 vpp) with amplifier saturation.
All these functions are displayed on a 1 μs/div time scale, approximately .2 Mhz/div frequency (Doppler) scale and .5 v/div amplitude scale.

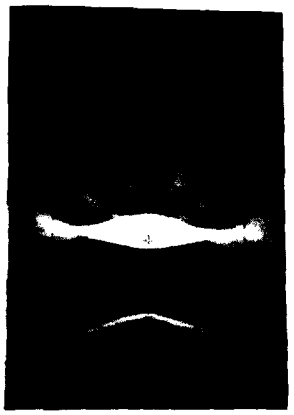

Figure 3.12a

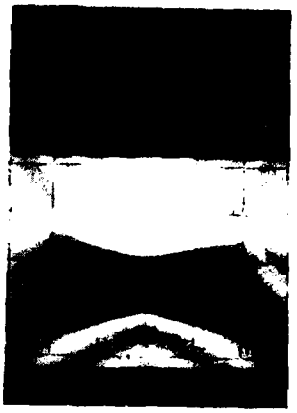

Figure 3.12b

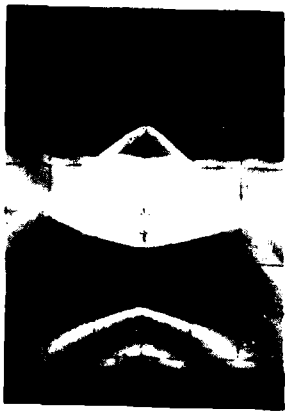

Figure 3.12c

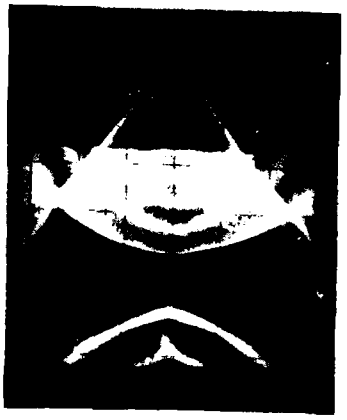

Figure 3.12d

Figure 3.12e

Figure 3.12f

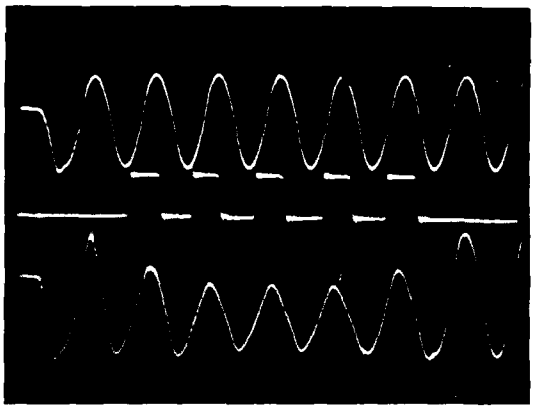

Figure 3.13

Figure 3.13: VCO-control-signal generation for the production of a symmetric series of V-chirps of different slopes (1 μs/div). Trace 1: The triangular wave used to generate V-chirps of constant slope after being gated by trace 2 and applied to the control terminal of a VCO. Trace 2: The gating signal whose pulses define the width of the individual V-chirps. Trace 3: The modified triangular wave that, after being gated by trace 2, is used to generate V-chirps of varying slope by application to a VCO.

Figure 3.14: The autoambiguity function of a series of five constant slope V-chirps (all 1 μs/div).

(a) Shown with a compressed frequency axis (i.e. removal of the slow ramp from the sum port of the oscilloscope).

(b) Three-dimensional ambiguity function.

(c) The ambiguity function obtained by using non-uniform spacings between V-chirps of different widths.

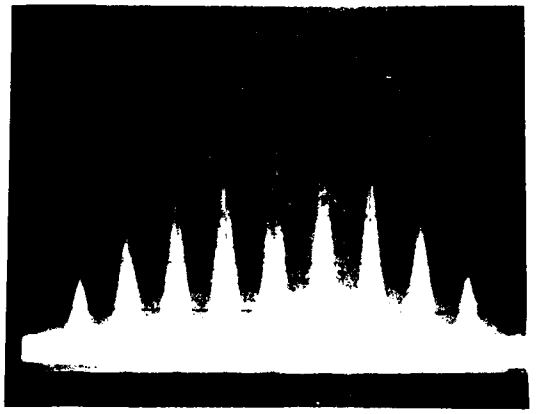

Figure [illegible]

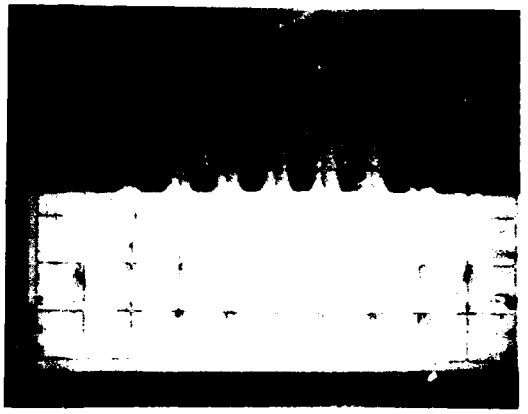

Figure [illegible]

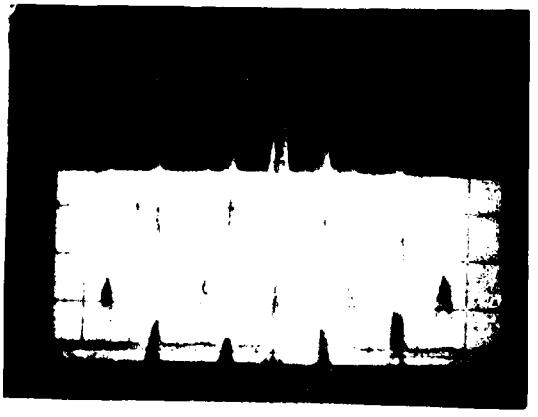

Figure [illegible]

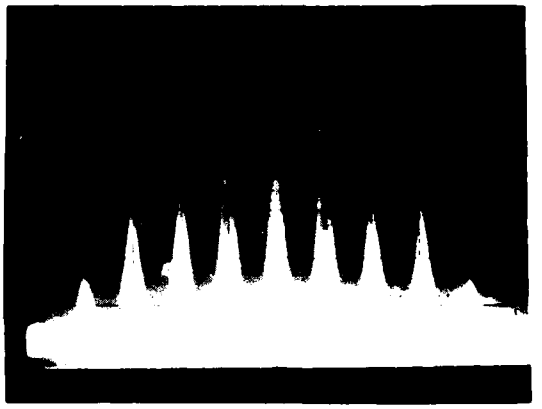

Figure 3.15a

Figure 3.15: The autoambiguity function of a series of five V-chirps with different slopes (all 1 μs/div).

(a) thru (c) are equivalent to (a) thru (c), respectively, of Fig. 3.14 except that the V-chirps have different slopes dictated by the VCO control signal of Fig. 3.13 (trace 3 gated by trace 2).

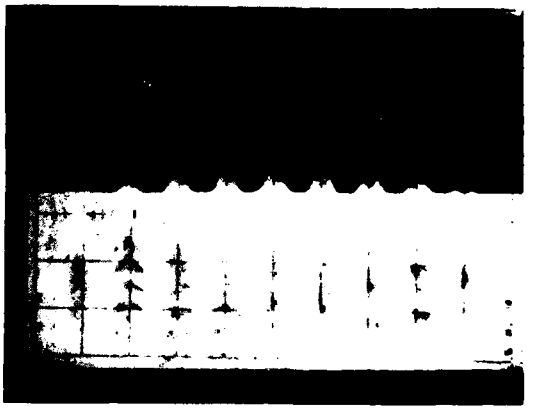

Figure 3.15b

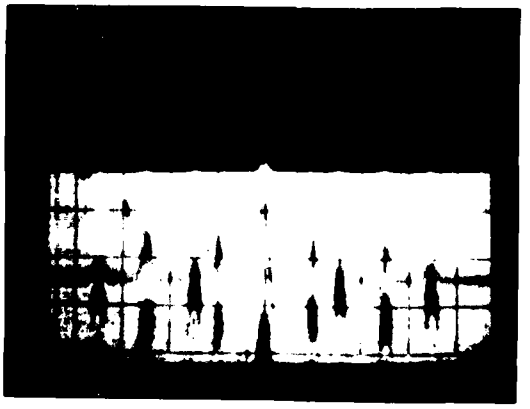

Figure 3.15c

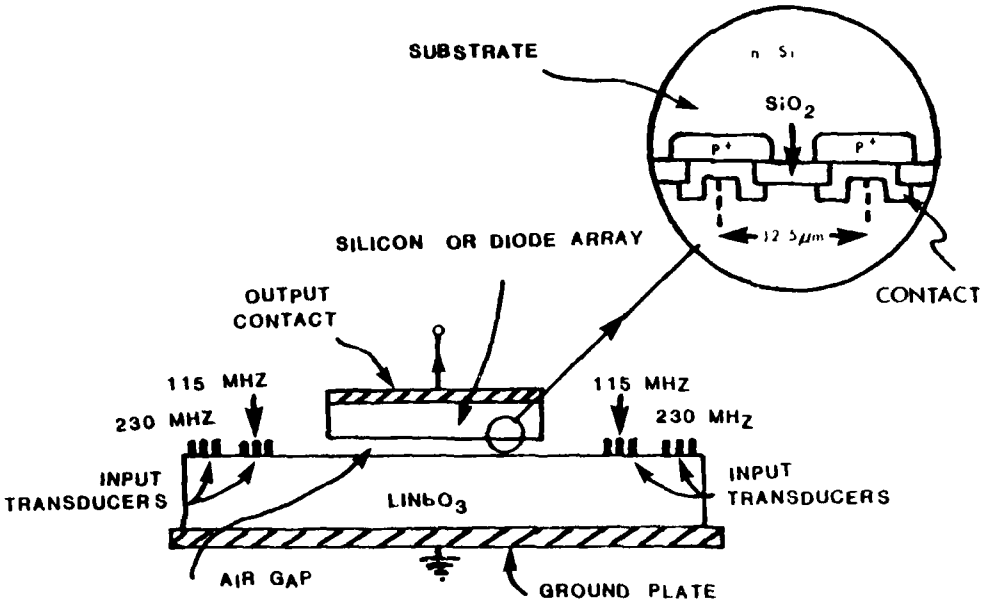

FIGURE 3.16

Figure 3.16: The structure of the SAW memory correlator. The surface of the semiconductor facing the piezoelectric delay line contains a storage mechanism (i.e. diodes or surface states). Two 115 Mhz transducers are used to perform convolution and storage whereas two 230 Mhz transducers are used for recalling the signal stored at a spatial frequency of .066 cycles per micron (i.e. 230 Mhz/3.488 x 10^9 μm/sec). Whereas the output of the convolver at the backplate of the semiconductor for two signals applied to the 115 Mhz transducers is the convolution of these signals, the stored signal is a spatial version of their correlation (see Section 2.3). Depending upon which 230 Mhz transducer a signal is applied to, the output, due to the interaction of this signal with the stored spatial distribution, is either the convolution or the correlation of the two signals.

charge storage mechanism that can be made to react to the surface wave electric fields. Some preliminary work was done using the surface states on the silicon surface. The technique adopted in this work to affect storage consisted of allowing the storage mechanism to integrate the standing wave pattern produced by the interaction of the two contrapropagating surface waves. Since this pattern is stored at half the wavelength of the two signals, the reading surface wave must be inputted at twice the frequency of the two inputs. Therefore, two sets of transducers were required. For this work the fundamental frequency was 115 Mhz and the reading signal was inputted at 230 Mhz. As discussed in Section 2.3 this type of storage process stores the correlation of the two input signals. Depending on which end of the delay line the reading signal is applied, the output signal from the reading process is either the convolution or correlation of this correlation with the reading signal. Figures 3.17a thru d show results of surface state memory. In all these figures a 5 μs-wide pulse is convolved with itself to produce the amplifier saturated triangular convolution seen at the start of (a) thru (c). If the storage mechanism behaves properly, the autocorrelation of the 5 μs pulse is stored along $(3.488 \times 10^5)(5\ \mu s) = 1.744$ cm of the silicon and the 1 μs-wide recall pulse produces a 6 μs-wide convolution with the stored triangular correlation. Figures 3.17a thru c show that, although storage is realized, it does not occur over the entire length of this silicon sample and last for only about 30 μs. Figure 3.17d shows the stored convolution from a better sample. The output is about 80dB below the input.

In order to increase the storage time, p-n diode vidicon arrays were then used in place of the semiconductor. These vidicons were procured from RCA and produced storage times on the order of 10 ms, as seen

Figure 3.17: Surface-state memory.

(a) The triangular convolution of two 5 μs (115 Mhz) square pulses is shown saturated at the start of this trace (5 μs/div). The small pulse toward the middle of the trace is the signal obtained by applying a thin pulse (< 1 μs) to a 230 Mhz transducer, thereby generating a surface wave to scan the stored information along the silicon surface. Since the resultant signal is about half the width that it should have been, this signifies that only part of the silicon surface was being utilized due to some form of non-uniformity. Direct radiative feedthrough of the input square pulses and the recall pulse was quite small when these results were obtained. The distortion seen in the fourth division after the main convolution can be attributed to self-convolution due to reflections at the edges of the slice of silicon. Note that the direct output convolution in division 3 is due to spatial integration at every point in time whereas the stored signal (shown recalled in division 6) is due to temporal integration at every point in space. It is this duality that causes one interaction to produce a convolution while the other produces a correlation. The duality is between time and space and is further exemplified by the fact that the convolution is a time function while the correlation is a spatial function.

(b) The same as (a) except that the scale is 10 μs/div and a very long (≈ 1 ms) recall pulse was used. In this case the stored signal is now essentially scanning the wide recall pulse and it can be seen that its effect decays by a factor of two after about 30 μs beyond the main convolution output.

(c) The same decay phenomenon shown in (b) except that three small consecutive recall pulses have been used.

(d) A recalled triangular convolution scanned by a very thin pulse from a slice of silicon having a more uniform surface state distribution than that used for the results of (a) thru (c). This output is about 30 dB down from the main convolution or 80 dB down from the input signals.

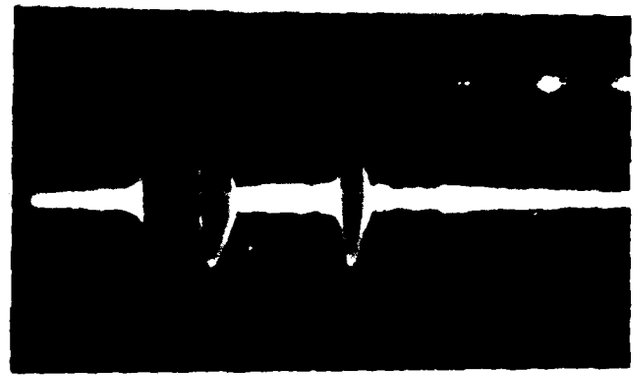

Figure 3.17a

Figure 3.17b

Figure 3.17c

Figure 3.17d

in Figure 3.18a, where every recalled signal is shown spaced 1 ms apart. Figure 3.18b shows the uniformity scans obtained using these vidicons. Due to the back surface etching process that these vidicons always tend to undergo, it was hard to produce a uniform air gap between these devices and the delay line. The 2nd trace in Figure 3.18b shows the uniformity obtained using only a few pressure points at the back surface of the vidicon. The 3rd trace in this figure shows the uniformity obtained by using a double row of higher density pressure points. The last trace was obtained using a triple row of pressure points or 33 pressure points over the vidicon interaction region. The convolver pressure support structure was also modified to facilitate the removal of the vidicons and to eliminate the need for slicing each wafer. The structure used is shown in Figures 3.19a and b. A thin sheet of silver-conductive-paint coated copper was placed between the foam and the vidicon so as to make immediate contact with the vidicon to the outside world without the need for attaching wires for every vidicon tried. Little difference was observed in correlator performance and in diode voltage-current behavior when a gold-chrome ohmic contact was deposited on the back surface of the vidicons. Note in Figure 3.18b that the uniformity of the interaction is improved, by this pressure system, only at the expense of the output amplitude. (The increase in the number of pressure points increased the damping of the surface waves.) It was felt, however, that, for signal processing purposes, uniformity was ultimately more important than output amplitude. It is not suggested that such a scheme be adopted (much better schemes are certainly in use), but that this represented one form of solution to the non-uniformity problem at hand,

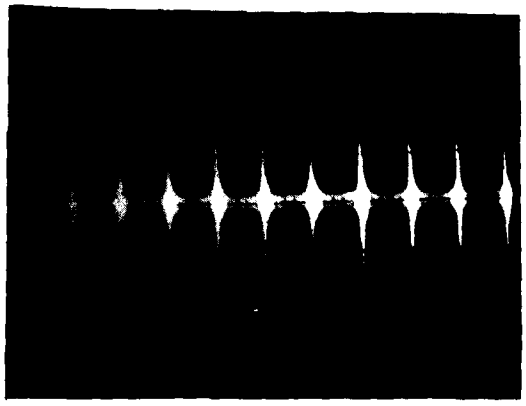

Figure 3.18a

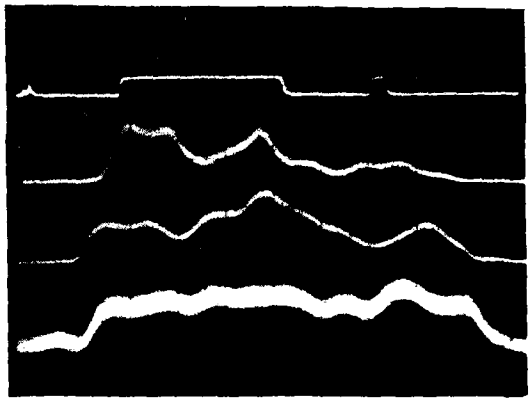

Figure 3.18b

Figure 3.18: PN diode memory correlator performance.
(a) A multiple exposure showing a triangular convolution being recalled at 1 ms intervals for an overall 6 dB decay on the order of 10 ms (1 ms/div).
(b) Uniformity scans obtained by convolving the long and short pulses seen in trace 1 (5 μs/div). Trace 2 is the uniformity resulting when only a single row of 8 pressure points is used to apply pressure over the length of the silicon (1 μs/div). The uniformity improves somewhat in trace 3 where a double row of 8 pressure points or 16 points are used. Trace 4 shows the result of using three rows of eleven or 33 pressure points over the length of the vidicon. Notice that the uniformity is quite good but that damping of the surface waves due to the excessive pressure has decreased the strength of the overall interaction. (This can be seen by comparing the noise levels of the different traces.) These three scans were obtained by dynamically adjusting the pressure at every pressure point (using set screws) in the three different support structures having the above mentioned pressure point densities. These structures were also designed to facilitate the testing of a wide variety of vidicon samples.

Figure 3.19: PN diode SAW memory correlator structure (high pressure point density version).

(a) Three-dimensional view, with cutaways, of the memory correlator (approximately 1.5 times actual size and shown with the vidicon support structure removed from the package). One end of the $LiNbO_3$ crystal is shown, through the cut-out region of the milled aluminum box, to possess three 230 Mhz transducers (closest to the end) and three 115 Mhz transducers. The best of the three of each type of transducer was used. Very little reflections were noticeable from the unused spare transducers. The 230 Mhz transducers had to be placed behind the 115 Mhz transducers since their apertures (108 λ) were smaller for the same impedance value (50 Ω) at midband. The transducers were connected to inductors in cavities beneath the delay line cavity by using feedthroughs. The vidicon support structure, shown above the aluminum box, was designed so that the vidicons need not be diced nor wires bonded onto their back surfaces thereby simplifying the procedure for checking their performance characteristics. This high density pressure structure was constructed by imbedding a high density matrix of set screws into an epoxy mixture. Every set screw applied pressure to a small push rod (shown through pressure structure cutaway) through a plastic guide. These rods pressed at localized points along a silver-conductive-paint-coated copper sheet backed with foam to somewhat disperse this force. The silver coated side of the copper sheet in turn contacted the back of the vidicon which was pressed against the piezoelectric crystal surface. This contact to the vidicon proved to be an excellent electrical contact and a gold-chrome contact on the back surface of the vidicon was shown not to be required. When the vidicon and pressure structure were in place, contact was automatically made between the vidicon back surface contact and the output BNC through the incorporation of a pin (shown through cutaway in box) and socket arrangement. Top and bottom plates could be attached for device shielding purposes.

(b) A two-dimensional cutaway of the memory correlator with the pressure structure and vidicon shown in place. This is a simplified schematic (i.e. only three pressure points of the 33 are shown) and has not been drawn to scale. All the components described in (a) can be seen in this drawing. Note that since there are two sets of transducers, then there are also two sets of tuning inductors and BNC connectors along with the usual output BNC connector. (In (a) one set of BNC connectors is behind the box.)

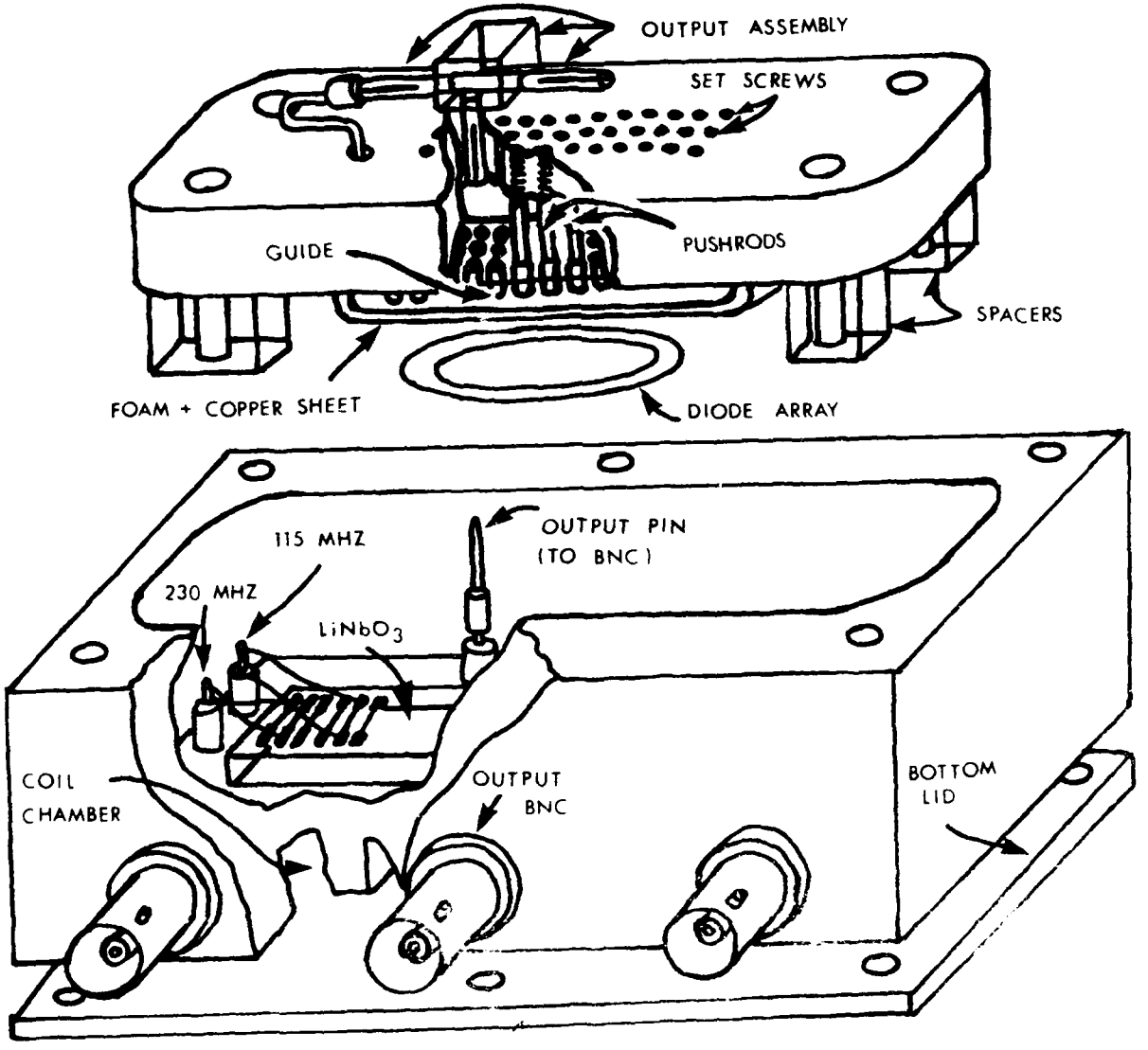
OUTPUT ASSEMBLY
SET SCREWS
PUSHRODS
GUIDE
SPACERS
FOAM + COPPER SHEET
DIODE ARRAY
115 MHZ
230 MHZ
OUTPUT PIN
(TO BNC)
LiNbO3
COIL
CHAMBER
OUTPUT
BNC
BOTTOM
LID

FIGURE 3.19a

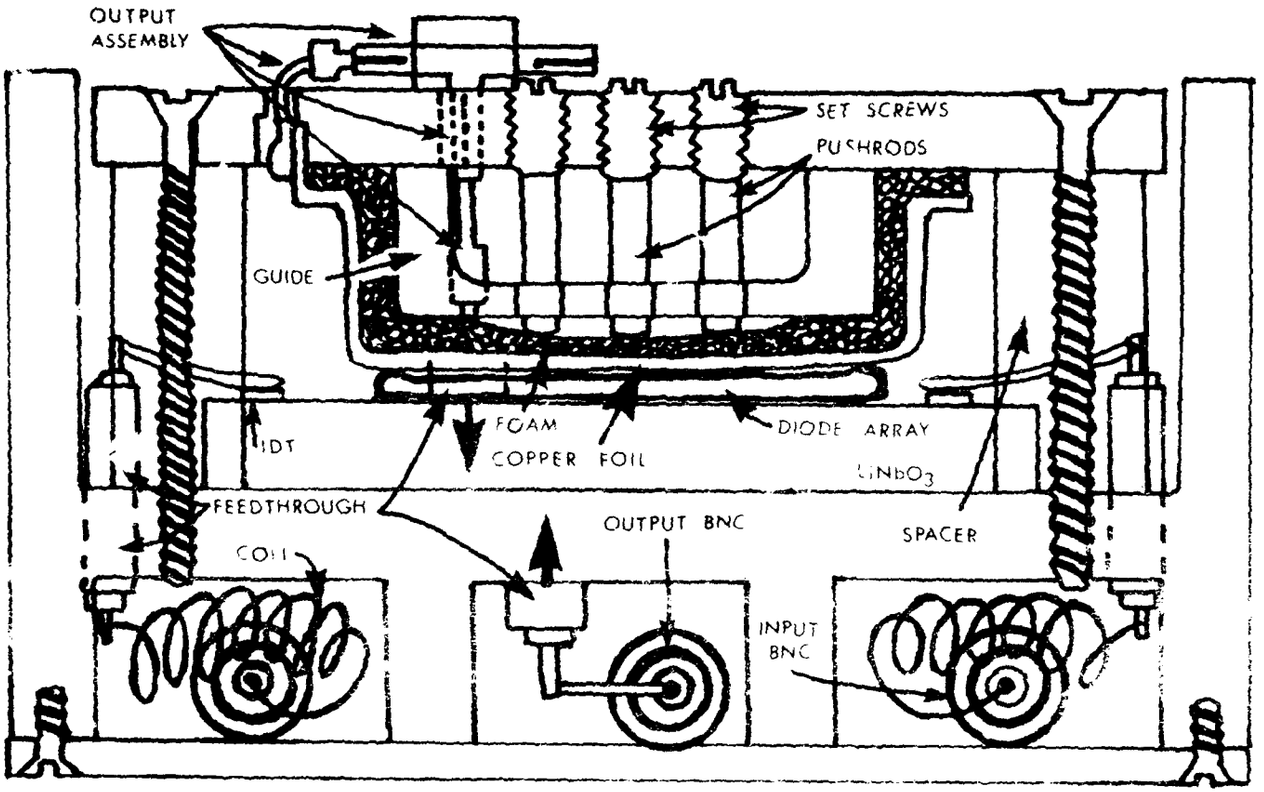
OUTPUT
ASSEMBLY
SET SCREWS
PUSHRODS
GUIDE
IDT
FOAM
COPPER FOIL
DIODE ARRAY
$LiNbO_3$
FEEDTHROUGH
OUTPUT BNC
SPACER
COIL
INPUT
BNC

FIGURE 3.19b

thereby allowing some form of useful signal processing to be performed. The size of the memory output can be inferred by comparing the square pulse convolution output with the memory output in Figure 3.17b for surface state memory. The magnitude of the memory output is related to the strength of interaction between the second order potential set up by the two interacting surface waves and the charge carriers in the diodes or at the surface of the silicon (for surface states).

Figures 3.20a and b show the memory outputs of a vidicon p-n diode convolver for a single square wave autoconvolution and a double square wave autoconvolution. In Figure 3.20a the first trace shows the input convolution performed eighteen times after which the stored correlation (identical to convolution for symmetric signals) is recalled about 400 μs later. Trace two shows the recalled output displayed above an input convolution, where, since the reading pulse is fairly wide, the convolution is seen to be a smoothed version of the actual convolution. The multiple performance of the convolution, prior to reading, was tried to see whether the stored signal would be retained any longer. No difference was noticed from that of a single read in. Figure 3.20b shows the three peaks of a double pulse convolution. Due to the small size of the output signal, the noise level is seen to be quite large.

A single square pulse was then loaded into memory using a scanning impulse. This stored pulse was then correlated by a pulse whose carrier was changed in increments, so that the ambiguity function, with memory, could be generated. In this configuration, the memory correlator behaved as a programmable matched filter. Figues 3.21a and b show a multiple exposure of the ambiguity function obtained in slices.

Figure 3.20: PN diode memory correlator pulse correlations.

(a) Trace 1: Eighteen 3 μs square pulse convolutions are performed (.2 ms/div) after which the stored correlation is recalled by a 1.5 μs pulse about 1.4 ms later. Trace 2: An expanded version (5 μs/div) of the recall pulse and memory signal seen in (a). The convolution or correlation of the 3 μs wide triangular correlation, stored along the silicon, where the 1 μs recall pulse produces an output that appears similar to the correlation due to an impulse recalling signal except that it has a 1 μs round-off of its peak and 1 μs tails (hidden below the noise). The correlation and convolution of the stored signal with the recall signal obtained by using the two 230 Mhz transducers (at opposite ends) produces the same result for symmetric signals. Trace 3: The input convolutions lined up with the memory signal in trace 2 for comparison. These convolutions are on the order of 50 dB below the inputs and the memory signal is about 80 dB below these input signals. The recall signal can be seen in trace 2 due to direct radiative feedthrough from input to output. From this trace it can be seen that this device had approximately 18 μs of delay between its two opposite-end 230 Mhz transducers (≈ 9 μs from pulse center to memory signal center). A slight amount of input pulse radiative feedthrough can be seen in trace 3 which shows that there is about 15 μs of delay between the two 115 Mhz input transducers (≈ 7.5 μs from the pulse center to the convolution peak). No improvement was evident in the magnitude of storage or its retention by the use of multiple convolutions before reading.

(b) Trace 1: Double pulse autoconvolution/autocorrelation obtained by first storing two 1.6 μs pulses spaced .8 μs apart and then correlating with this stored signal by reading with the same type of signal (seen as radiation ahead of the memory signal composed of three triangular pulses). The signal had to be stored using a thin (< 1 μs) pulse and two 3.2 μs pulses separated by 1.6 μs due to the factor of two compression of the stored signal. The reading process does not become compressed, however, so that the output is about 4 μs wide. Trace 2: An envelope detected version of trace 1 (2 μs/div).

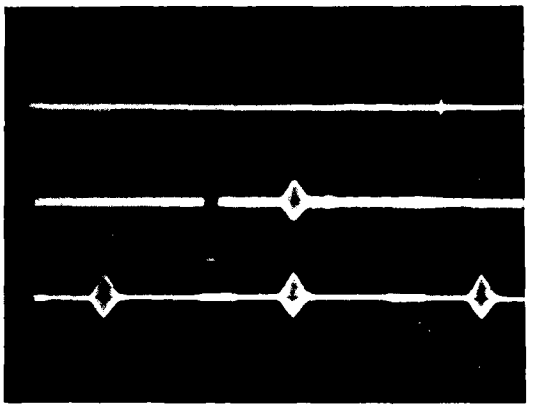

Figure 3.20a

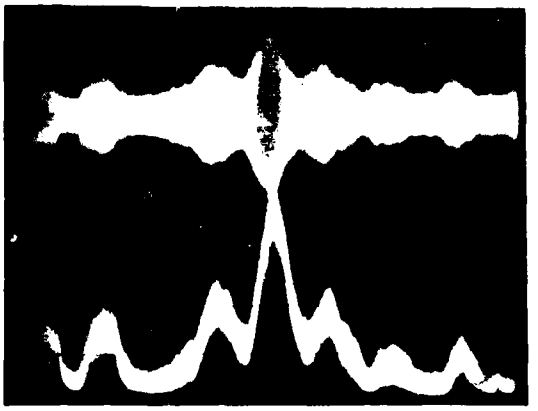

Figure 3.20b

Figure 3.21c is the z-axis modulation technique version of this same ambiguity function. Figues 3.22a, b and c show different views of the three-dimensional images of the ambiguity function obtained utilizing the stored signal as the device impulse response. Although almost buried by the noise, the square pulse ambiguity function can still be seen. The small size of this signal resulted from the trade-off between uniformity and surface wave damping. The form of the ambiguity function is even more undiscernable when the amplitude is increased by releasing some of the pressure on the delay line surface since the uniformity is such a critical factor for proper memory correlation. Figures 3.23a and b are actual photographs of the memory correlator where the top pressure plate structure has been removed and the double set of transducers are visible (along with some unconnected spares that were later removed).

Figure 3.24 was included to show that since the stored signal bandwidth, given by the first plot, is small about its center frequency, then it is not necessary that there be a Nyquist sampling density of diodes to store the signal. In other words, the sampling density need only be high enough to store and recover the signal, not its carrier. As seen by the last trace in Figure 3.24, depending on the sampling density used, there are multitude of replicas of the signal spectrum produced at varying points in frequency that do not overlap and therefore do not interfere with one another. The signals having these spectrums are the same except for their spatial carrier frequencies. Any one of these signals (if their spatial periodicities are not to large) can be recovered by a surface wave matching its spatial carrier freqeuncy. Note, however, that much less energy is possessed by any one frequency band.

Figure 3.21: Square-pulse autoambiguity function utilizing a stored pulse as the reference signal.

(a) A multiple exposure showing the autoambiguity function of a 5 μs square pulse obtained by convolving reference stored along the slice of silicon (in p-n diodes) (2 μs/div).

(b) The same as (a) showing only six of the eleven traces about the central peak.

(c) The ambiguity function displayed by z-axis (intensity) modulation of the oscilloscope display.

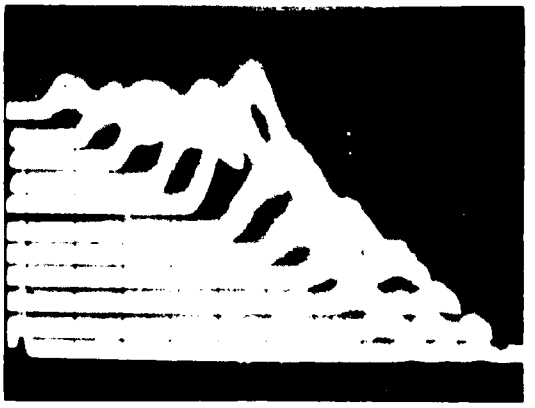

Figure 3.21a

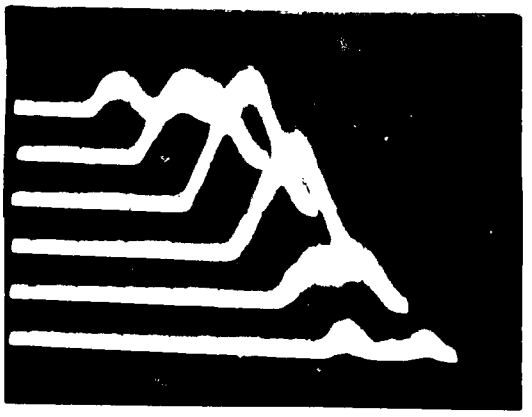

Figure 3.21b

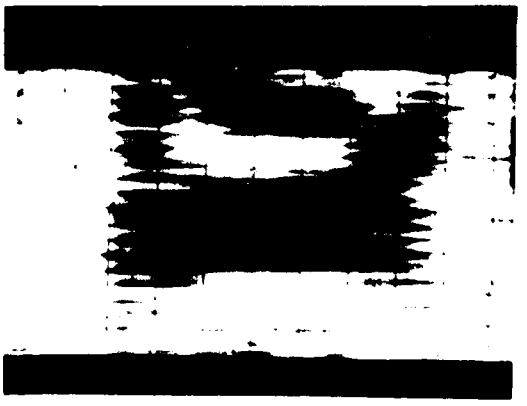

Figure 3.21c

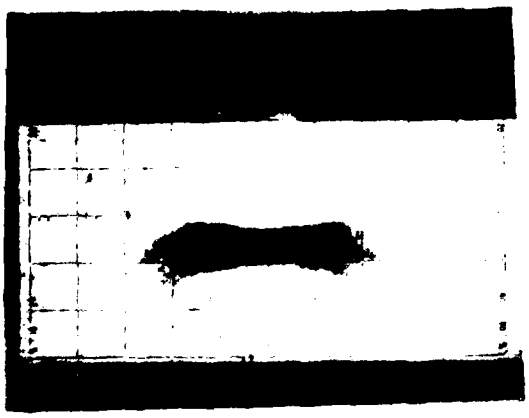

Figure 3.22a

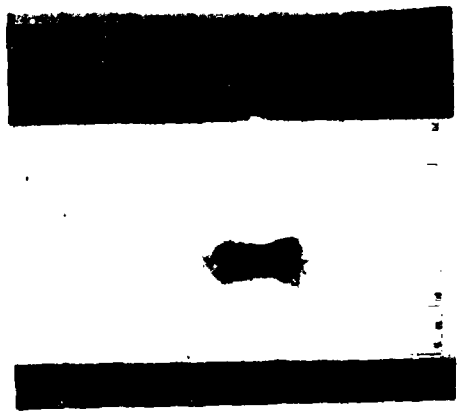

Figure 3.22b

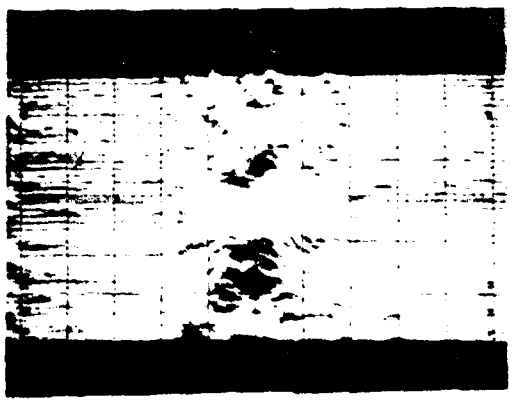

Figure 3.22c

Figure 3.22: Three-dimensional [illegible] utilizing a stored [illegible]
(a) The autoambiguity function [illegible] square pulse using a stored reference ([illegible]). The frequency scale is approximately .4 Mhz/div.
(b) Same as (a) but with a [illegible] scale [illegible] us/div).
(c) Same as (b) but with an expanded frequency scale ([illegible] .2 Mhz/div).

Figure 3.23a

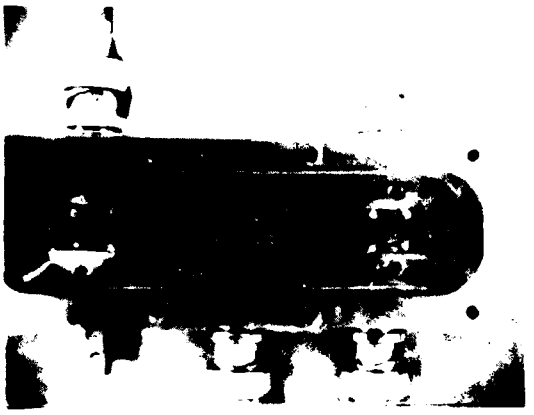

Figure 3.23b

Figure 3.23: Photographs of the memory correlator.
(a) Device with pressure structure removed and displayed so as to view the individual push rods used to apply pressure to the back surface of the vidicon (not shown).
(b) Same device without the pressure structure with all the transducers in plain view. Wires are bonded to the transducers using silver conductive paint. The black area beneath the center of the $LiNbO_3$ crystal is a hole passing through the box to facilitate the illumination of the vidicon with light (to verify storage). The upper BNC's are the 115 Mhz inputs, the bottom left and right BNC's are for the 230 Mhz read signals and the bottom center BNC is the device output.

Figure 3.24: Narrowband sampling. This figure shows the spectrum of the stored signal due to the finite diode density and, therefore, the finite number of signal samples. In the present case each diode is about 10 μm in diameter with a center to center spacing of about 12.5 μm. The bandwidth of the stored signal could be as much as 40 Mhz centered about a center frequency of 230 Mhz and would be stored as such if the storage medium were a continuum. (The input signals possess a bandwidth of, at most, 20 Mhz, however, the stored correlation is compressed in space by a factor of two and will be recalled as a time function compressed by this factor so that its bandwidth is doubled (or 40 Mhz). The 230 Mhz transducers are 5.5 finger pair transducers, as are the 115 Mhz transducers, so that their bandwidths are both 20% or 40 Mhz and 20 Mhz, respectively.) The stored signal is therefore relatively narrowband with respect to the 230 Mhz center frequency. A wavelength on $LiNbO_3$ for 230 Mhz is about 15.2 μm. For the maximum frequency component of the stored signal (i.e. 250 Mhz) this corresponds to a wavelength of about 14 μm. The Nyquist sampling rate requires that there be a sample taken at least once every 7 μm and not once every 12.5 μm as is taken here. However, this sampling rate assumes that the signal bandwidth extends to zero which is not the case. As can be seen in the last plot the sampling at a .4 duty cycle by these diodes produces spectral replicas of the desired spectrum positioned at different points in frequency (representing the same baseband signal on a whole gamut of different carriers), however, there is no overlap between them. What is more, the desired spectrum at 230 Mhz is still available and is the largest, even though it is supposedly not sampled enough. It is therefore available for correlation or convolution with a 230 Mhz carrier modulated signal. The only obvious problem with undersampling a narrowband signal is that more energy is wasted on the unneeded versions of the spectrum centered at other frequencies than for an over sampled signal since in the latter case the sinx/x weighting of the spectrum (due to the finite sample width) would attenuate the other spectrums much more than the desirable spectrum centered about 230 Mhz. (The other spectrums would all fall beyond 230 Mhz.) More energy would have been available if oversampling had been employed for this work, however, this technique has shown that much simpler diode matrices can be utilized by employing undersampling at the expense of a weaker interaction with the stored signal at the desired carrier frequency.

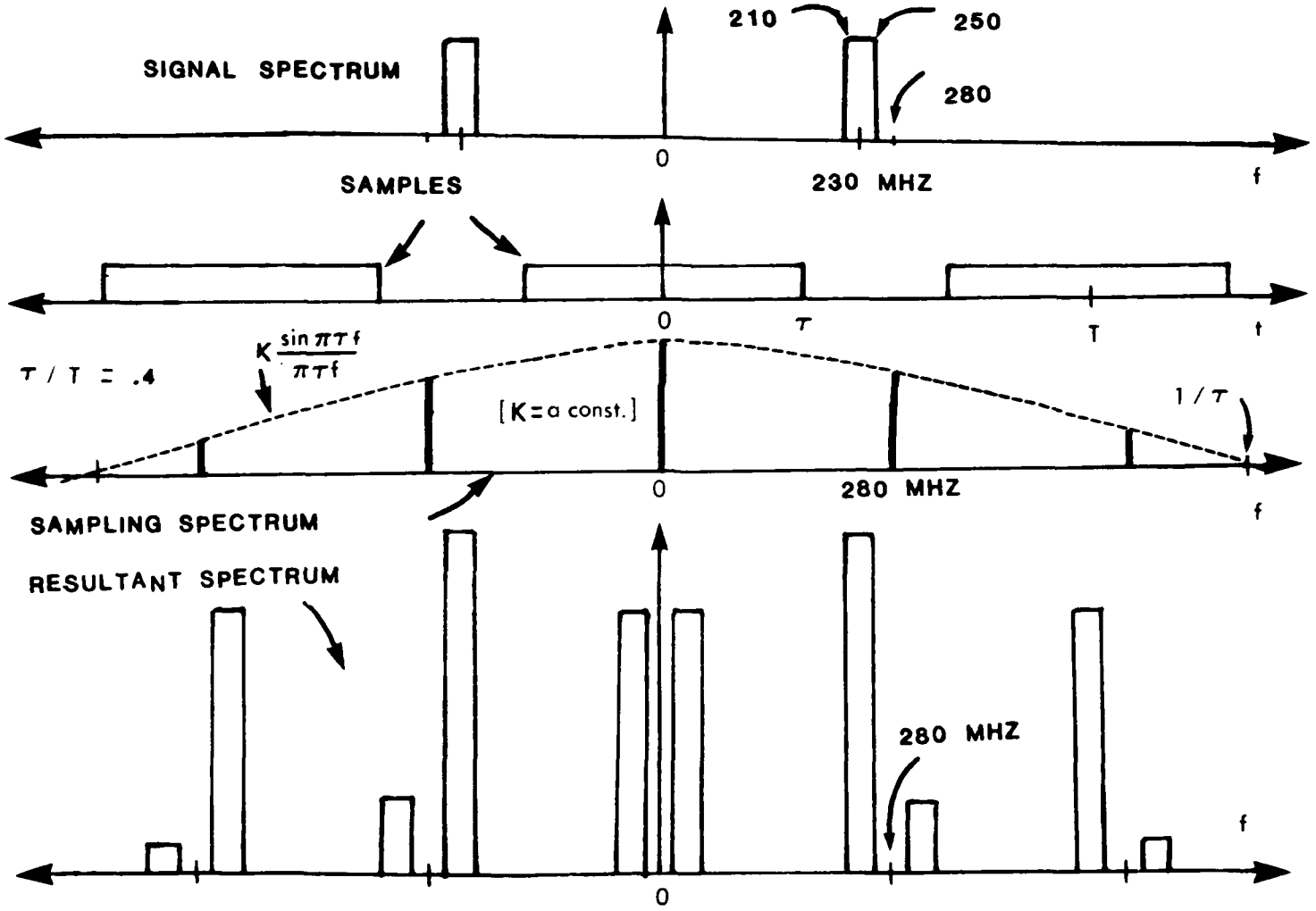
SIGNAL SPECTRUM
210
250
280
0
230 MHZ
f
SAMPLES
0
τ
T
t
τ / T = .4
K sin πτf / πτf
[K = a const.]
1 / τ
0
280 MHZ
f
SAMPLING SPECTRUM
RESULTANT SPECTRUM
280 MHZ
f
0

FIGURE 3.24

3.2 Signal Processing Using Chirp Filters

Chirp Filter Chirp Transformation:

The system depicted in block diagram form in Figure 3.25a was set up to perform the Fourier transformation and inverse transformation processes on an input signal. This process, discussed at length in Section 2.4, was realized using IMCON devices procured from Andersen Laboratory (Martin, 1973 and 1976). These dispersive devices possessed impulse responses with durations on the order of 100 μs and linear frequency dispersions over this duration of about 7 Mhz centered about 15 Mhz. The average loss for these devices was about 20 dB. The chirp transformation scheme utilized (mainly to conserve on the required number of devices) was the MCM structure. From Figure 3.25a it can be seen that this consisted of impulsing one of these devices (all the devices were identical) and then mixing the resulting impulse response with a carrier at twice the device center frequency. This mixing process spectrally inverts the chirp impulse response providing the signal with a chirp carrier that has a slope that is the negative of the chirp device impulse response slope. The output of the first device is a chirp modulated Fourier transform of the signal where the chirp carrier is amplitude modulated by the Fourier transform magnitude and phase modulated by the Fourier transform phase. After spectrally inverting the chirp carrier on the Fourier transform (that may have been modified by mixing with a gate or some other signal) so as to change the chirp slope polarity, this transform is inputted into another chirp filter. The output of this filter, over the valid region defined in Section 2.4, is the complex conjugate of the system input signal. Since only real signals were used

in this work (no quadrature terms), then the original signal was obtained. All the chirp devices used were up-chirp filters.

Figure 3.25b shows the impulse response of one of these chirp filters in the first trace (20 μs/div). The following traces show the resulting output of this device when this impulse is increased successively in width. For very thin pulses the output resembles the sinx/x Fourier transform of the signal (2nd trace). Since the chirp filter behaves more like a Fresnel transformer (see Appendix A) than a Fourier transformer (the 'impulse' is rf modulated), the output doesn't compress any longer when the pulse is made wider than trace 3 (as it would if this was a Fourier transform), but instead, as seen in trace 4, it resembles the input pulse. Distortion on the order of the impulse width exists only at the impulse response extremes which are usually gated out by purposely imposed gating functions or by the finite width of the input signal to be modulated by this chirp. Figures 3.25c and d are the output sin(x)/x Fourier transforms of an input square wave. Figure 3.25d is an expanded version of Figure 3.25c.

Figure 3.26a again shows the transform of a square pulse input shown in the first trace. Figure 3.26b shows the resulting output when all that has been done is that the chirp slope polarity has been reversed. In this case the Fresnel transform of the pulse has been obtained. Figure 3.26c shows the Fourier transform being taken at a high repetition rate using gating to prevent interference between transforms. The transform is the center trace of this figure. The other traces are the

Figure 3.25: Fourier transformation utilizing the chirp transform technique and chirp filters.

(a) This block diagram shows the technique for performing a Fourier transformation, gating this time version of a frequency function and then performing an inverse Fourier transformation. The input signal is modulated onto a chirp that is obtained by spectrally inverting the impulse response of a SAW chirp filter. The modulated signal is passed through another chirp filter whose output is the chirp modulated magnitude of the input signal's Fourier transform. The chirp modulation deviation from quadratic phase is the Fourier transform phase. This transform is gated in time, if filtering is required, and then spectrally inverted prior to inputting into another chirp filter (since all the chirp filters are assumed here to be identical). The output of this last chirp filter is a chirp modulated and filtere (if gating was performed) version of the input signal. In the results to follow, all the chirp filters had impulse responses centered about 15 Mhz with bandwidths of about 7 Mhz and dispersions on the order of 100 μs. These chirp filters were IMCON devices.

(b) Trace 1: The impulse response of an IMCON (20 μs/div). The impulse (shown in the third division) is made to consist of about five cycles of rf at the center frequency of the chirp device (i.e. 15 Mhz in this case) which, in this case, corresponds to a pulse width of about .33 μs. This concentrates most of the impulse energy within the passband of the chirp device. This finite width of the impulse puts only an imperceptable bow onto the impulue response and distorts its extremities over about an impulse in width (see appendices G thru I). The insertion loss for the IMCONs averages about 20 dB. Since the time-bandwidth product of these devices is about 700 (7 Mhz x 100 μs), then the impulse undergoes an additional expansion loss of about 29 dB (i.e. exp. loss = 10 log (TB product)). Therefore, a 20 vpp or 30 dBm impulse produces an impulse response at about a -19 dBm level (i.e. 30 dBm - I.L. - E.L.) or about 71 mvpp. The initial delay of the impluse response from the time of application of the impulse to the point just beyond the rising portion of the response is about 40 μs. Trace 2: The impulse response of the IMCON when the impulse is about 1.5 μs wide. In this case the envelope if the response is approximately a sinx/x having a main lobe half-width given by the reciprocal of the impulse width divided by 7×10^{10} or the device slope divided by 2π (i.e. the device slope $\approx 2\pi$ (7 Mhz/100 μs)). From this the main lobe is seen to be about 20 μs wide. Trace 3: The input to the IMCON is a

pulse on the order of 8 μs in width and the output envelope can no longer be approximated by a sinx/x function. Trace 4: The input pulse to the IMCON has been expanded to about 25 μs. Note that the output of the device seems also to be a pulse on the order of 25 μs in width. In actuality the chirp filter is performing a Fresnel transform on the envelope of the input signal (see Appendix A, Eq. A-85) that appears like a Fourier transform for signals of small duration (i.e. less than the reciprocal of the square root of the device slope). Note the Fresnel ripples on the output pulse of trace 4.

(c) The chirp modulated magnitude of the Fourier transform of a 20 μs square pulse (2 μs/div). This Fourier transform has a time-to-frequency correspondence of about 2 μs for every 140 Khz (i.e. 140 Khz = (2 μs)(7 Mhz/100 μs)). The main lobe of the sinx/x is given by twice the reciprocal of the pulse width in terms of frequency or 100 Khz which translates to about 1.4 μs in time (i.e. 1.4 μs ≃ 100 Khz/$7\text{x}10^{10}$ Hz/sec).

(d) An expanded version of (c) (1 μs/div). Since the signal was only 20 μs wide, the Fourier transforms in (c) and (d) were valid over an 80 μs time interval (i.e. the impulse response duration minus the signal duration). About 110 sinx/x sidelobes can be seen over this time interval.

AD-A089 965 RENSSELAER POLYTECHNIC INST TROY NY MICROWAVE ACOUST--ETC F/G 17/2
SIGNAL PROCESSING USING SURFACE ACOUSTIC WAVE DEVICES AND ITS A--ETC(U)
DEC 79 D R ARSENAULT, L B MILSTEIN, P DAS DAAG29-77-G-0205
UNCLASSIFIED RPI-MA-ARO-10 ARO-15004.14-EL NL

3 OF 4
AD A089965

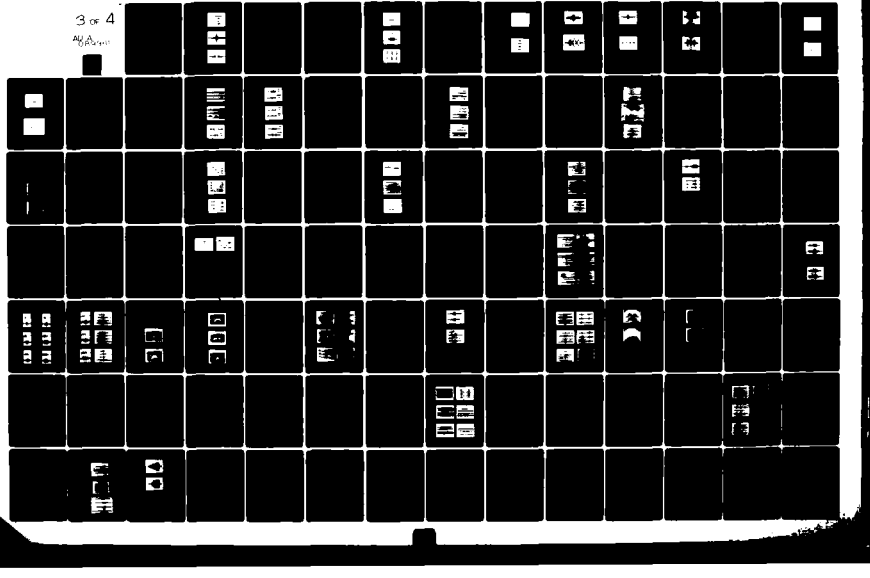

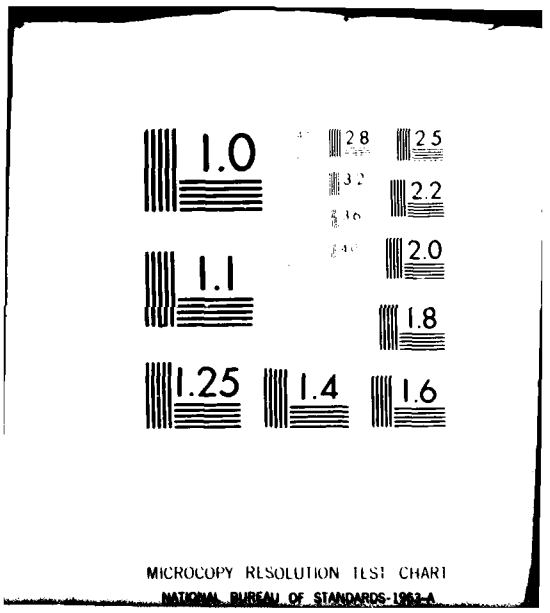
1.0
2.8
2.5
3.2
2.2
3.6
2.0
4.0
1.8
1.1
1.25
1.4
1.6
MICROCOPY RESOLUTION TEST CHART
NATIONAL BUREAU OF STANDARDS-1963-A

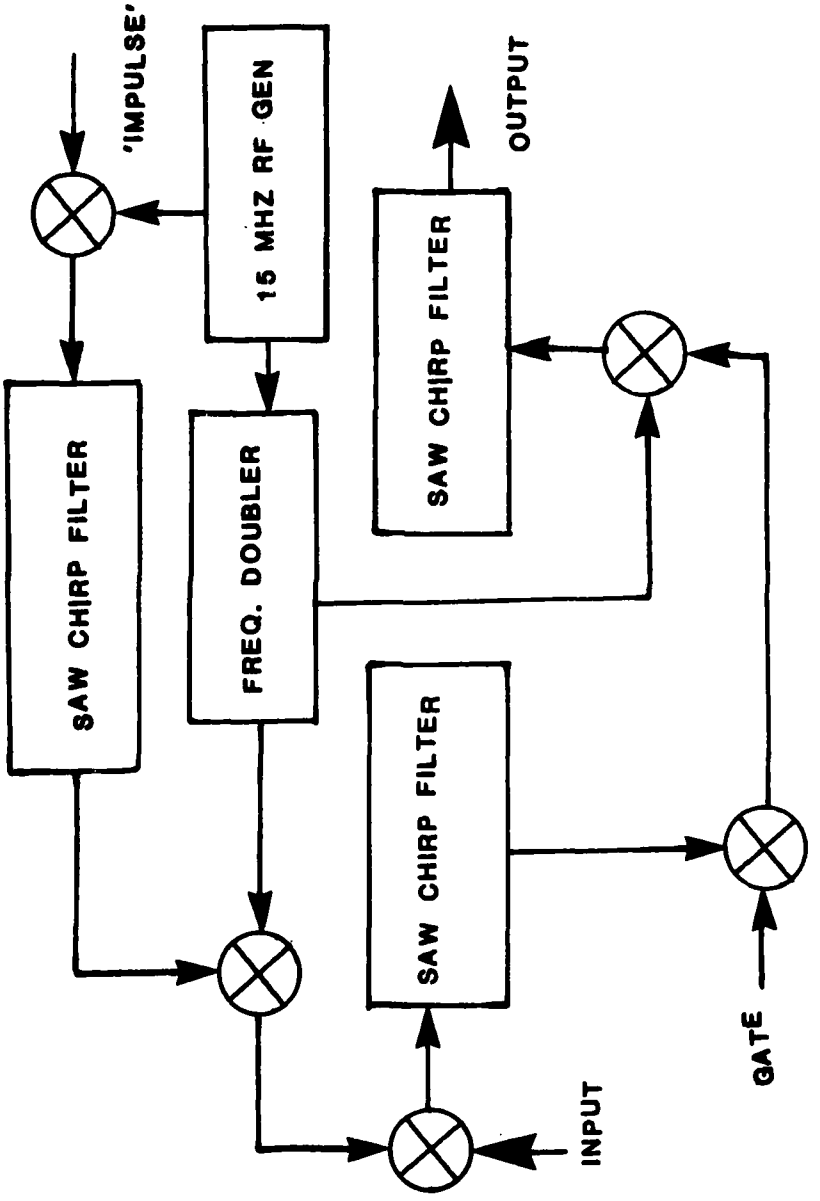
'IMPULSE'
15 MHZ RF GEN
OUTPUT
SAW CHIRP FILTER
SAW CHIRP FILTER
FREQ. DOUBLER
SAW CHIRP FILTER
INPUT
GATE

FIGURE 3.25a

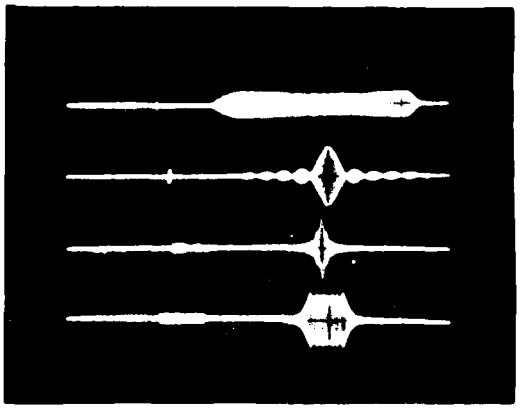

Figure 3.25b

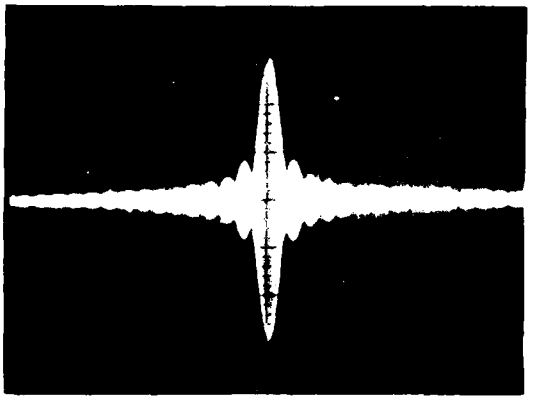

Figure 3.25c

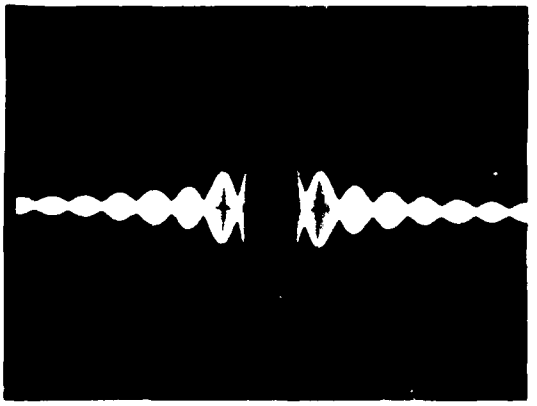

Figure 3.25d

Figure 3.26: Fourier transformation and chirp slope mismatch.
(a) **Trace 1:** A 10 μs square pulse input signal (20 μs/div). **Trace 2:** The chirp modulated magnitude of the Fourier transform of trace 1 (5 μs/div). The chirp modulation of the transform displayed in this manner always possesses the phase of the Fourier transform as a deviation from quadratic. The Fourier transform is shown here centered below the input signal but, in actuality, if the transform is centered within its valid output time interval (approximately 100 μs - 10 μs or 90 μs wide, in this case), the main lobe of the sinx/x will arise about 50 μs after the 10 μs square pulse input. The width of the main lobe in frequency is given by twice the reciprocal of the input pulse width. Dividing this by the chirp slope produces a main lobe width of about 2.9 μs (i.e. $2((10\ \mu s)(7 \times 10^{10}))^{-1}$). Note that the input square pulse must be modulated onto a spectrally-inverted chirp-device impulse response before inputting into a similar device before this transform can be obtained.
(b) The input signal is the same, in this case, as it is in (a) except that the chirp modulation, arising as the impulse response of a chirp device, has not been spectrally inverted before mixing with the baseband square pulse. **Trace 1:** The 10 μs square pulse (20 μs/div). **Trace 2:** The output of a chirp filter (5 μs/div) when the non-spectrally inverted chirp-modulated signal in trace 1 is its input. Since the chirp modulation on the input signal is the same as the chirp device impulse response, correlation between the two chirps is not achieved and the resultant output is a chirp modulated version of a Fresnel transform (see Appendix A) that is valid over the same time interval over which the Fourier transform in (a) is valid. Note, however, that the width of this Fresnel transform does not correspond with the Fresnel transforms of Fig. 3.25b for the same input pulse width (which would look more like a compressed sinx/x as can be extrapolated from this figure). This is due to the fact that a Fresnel transform is a function of two parameters, time and chirp slope (see Appendix A). The Fourier transform is only a function of time in a chirp transformation system which is related linearly to frequency through the chirp slope. Fourier transforms obtained using systems with differing slopes are time scaled versions of one another. The Fresnel transform can be obtained by inputting an rf modulated signal (Fig. 3.25b) or chirp modulated signals of any slope into a chirp device; however, the resultant Fresnel transforms are all different and, therefore, functions of the chirp slope. As a matter of fact, the Fourier transform can be visualized as a special case of this process for which the Fresnel transform when the input modulation and the chirp device slopes are of

opposite polarity and equal magnitude. This is true since the Fresnel transform of a signal is the Fourier transform of the chirp modulated signal where the slope of the chirp, in this case, is the sum of the slopes of the chirp modulation and impulse response of the chirp device.

(c) This figure shows traces consisting of transforms obtained in a continuous transformation system whereby a continuous signal is transformed a piece at a time thereby producing a continuous series of transforms and not the transform of the entire signal (which is impossible to do if the signal was of infinite duration since, if such a technique was available, an infinite amount of time would be required before the transform could be obtained and the signal would have to be cut off somewhere inevitably). The signal, in this case, is a constant DC level and only trace 3 is the Fourier transform stream of this signal consisting of sinx/x's due to the finite 50 μs segments of the chirp modulated DC that can be transformed at each time. The slope of the chirp modulations in all the other traces have been purposely mismatched from the device impulse response slope so that Fresnel transforms have been obtained. The traces above trace 3 have greater chirp modulation slopes and those below have lesser slopes than that required for Fourier transformation (i.e. the negative of the device slope). The technique for performing continuous transformation is covered elsewhere.

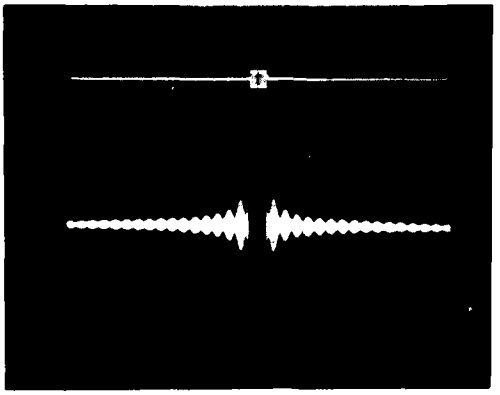

Figure 3.26a

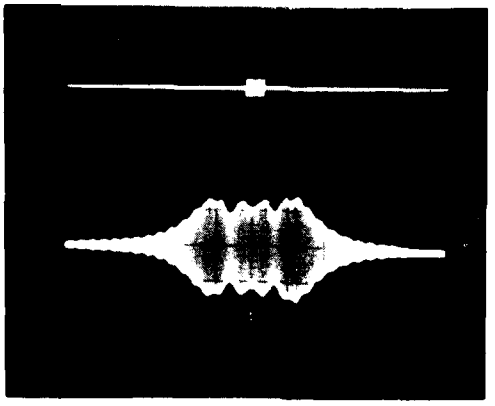

Figure 3.26b

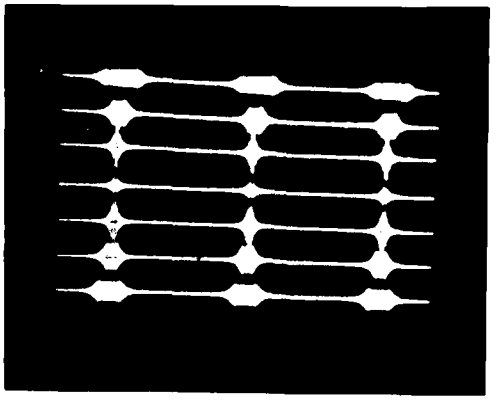

Figure 3.26c

result of making the input chirp modulation slope successively larger (top 3 traces) and smaller (bottom 3 traces) than the chirp device slope.

Figure 3.27a shows the Fourier transform real and imaginary components for the signal (a code) whose Fourier transform components have been calculated using a computer FFT. This photograph was included so that the accuracy with which a chirp transformation can be taken can be assessed. Note that every little variation is essentially reproduced by the chirp transform system. Figure 3.27b shows the Fourier transforms of one, two, three and four pulses in the four traces shown. Figures 3.28, 3.29 and 3.30 show expanded versions of the two, three and four pulse Fourier transforms, respectively. The signals at the top right of the transforms in Figures 3.32c to f are the corresponding input signals for the transform directly below it. Figures 3.33a to c show the Fourier transform of a low frequency ($\simeq$ 3 Mhz) carrier-modulated seven-bit Barker code summed with a sine wave, a square wave and a sawtooth wave, respectively. The top two traces in each figure are the input signal added to a low frequency version of these intentional 'noises' and the transform of this combination. The 3rd trace in each figure is the summation of the carrier modulated code plus the 'noise' having a fundamental frequency of the order of the signal carrier. Note the richness of the harmonics for the square wave and sawtooth wave. The signal transform remains unchanged from transform to transform. The signal sideband at the left of every trace is smaller than the one on the right since it is outside the valid region of Fourier transformation.

Figure 3.27: Chirp system Fourier transformations.

(a) Trace 1: The real component of the Fourier transform of the 13-bit code. This component (2 μs/div) compares extremely well with the computer generated real component.
Trace 2: The imaginary component of the Fourier transform of the 13-bit code. The component (2 μs/div) compares extremely well with the computer generated imaginary component.

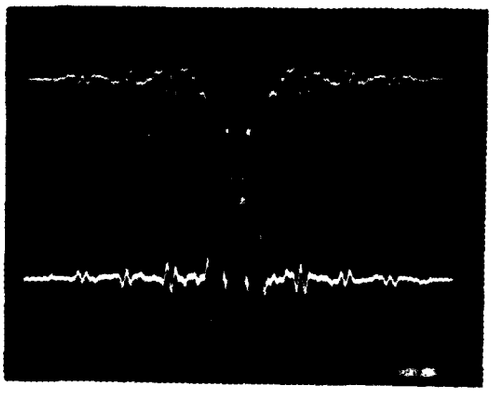

Figure 3.27a

(b) Square pulse chirp-modulated Fourier transforms (Magnitude - transform magnitude and quadratic phase deviation - transform phase) (2 μs/div).
Trace 1: Fourier transform of a single 6 μs pulse.
Trace 2: Fourier transform of two 6 μs pulses separated by 6 μs. Trace 3: Fourier transform of three consecutive 6 μs pulses spaced 6 μs apart.
Traced 4: Fourier transform of four consecutive 6 μs pulses spaced 6 μs apart.
These transforms are all weighted by the magnitude of trace 1 whose main lobe is defined by an individual 6 μs pulse width to be about 4.8 μs wide. The central lobe of each of these transforms (in frequency) is given by twice the reciprocal of the overall signal width which is divided by the chirp slope (x) to obtain their widths in time. Since the signals are 6 μs, 12 μs and 42 μs in width, then these central lobes are 4.8 μs, 1.6 μs, .97 μs and .68 μs wide, respectively, as can be seen in this figure.

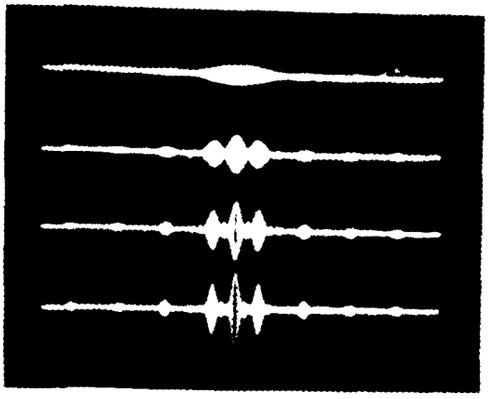

Figure 3.27b

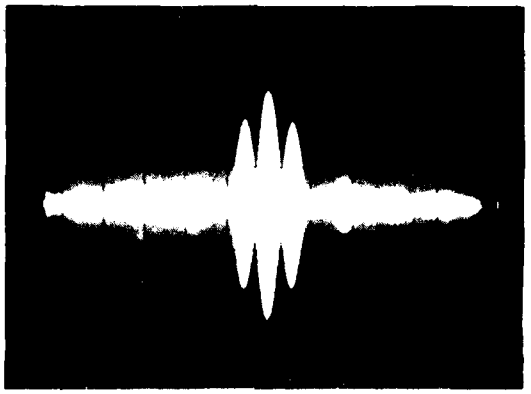

Figure 3.28a

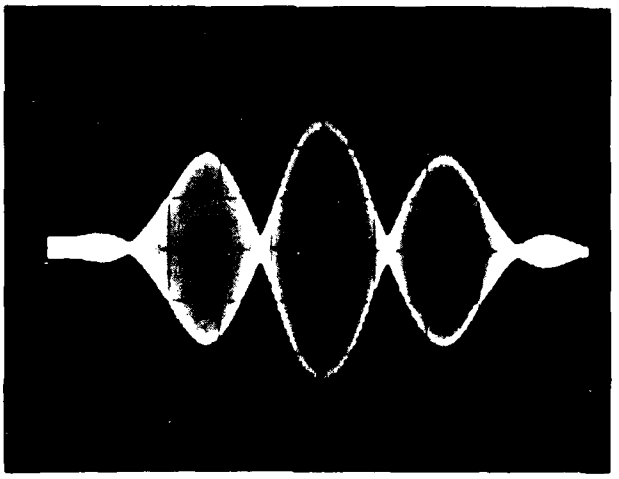

Figure 3.28b

Figure 3.28: The chirp-modulated Fourier transform of two 6 μs wide square pulses separated by 6 μs.
(a) 2 μs/div
(b) .5 μs/div
See Fig. 3.27b, trace 2.

Figure 3.29a

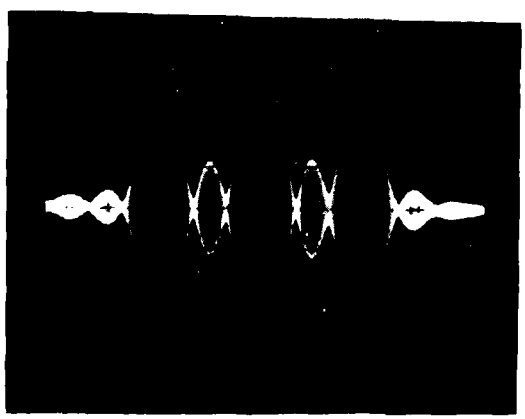

Figure 3.29b

Figure 3.29: The chirp-modulated Fourier transform of three consecutive 6 μs wide square pulses spaced 6 μs apart.
(a) 2 μs/div
(b) .5 μs/div
See Fig. 3.27b, trace 3.

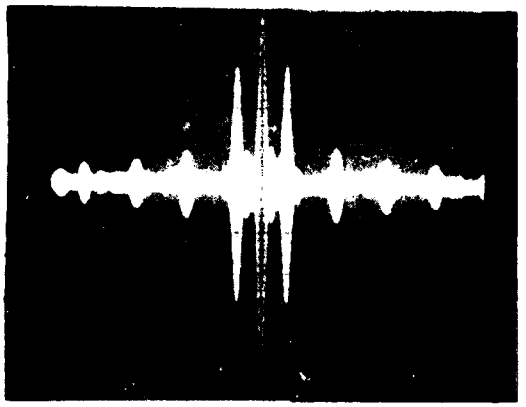

Figure 3.30a

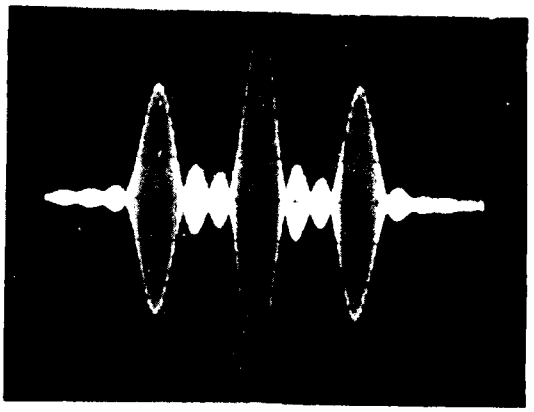

Figure 3.30b

Figure 3.30: The chirp-z[illegible] transform of four consecutive 6 μs wide square pulses spaced 6 μs apart.
(a) 2 μs/div
(b) .5 μs/div
See Fig. [illegible], page [illegible].

Figure 3.31: Chirp transformations of special functions.

(a) Trace 1: A single cycle raised cosine approximately 7 μs wide (10 μs/div). Trace 2: The chirp-modulated Fourier transform of trace 1. The width, in frequency, of the main lobe of this transform is four times the reciprocal of the width of the raised cosine. Dividing by the chirp slope (7×10^{10} Hz/sec, not $2\beta = 2\pi(7 \times 10^{10})$ rad/sec) gives an 8 μs main lobe (10 μs/div).

(b) Trace 1: A 5 μs wide positive pulse and a 5 μs wide negative pulse with no space between the two. Trace 2: The chirp-modulated Fourier transform of trace 1. This transform arises by squaring the transform of Fig. 3.26a and multiplying this by jf or $jt/7x10^{10}$, where $t = 0$ is the center of the main lobe. This is true since the square of the sin/x transform of a square pulse is the transform of the autoconvolution of this square pulse. The signal of trace 1 is the derivative of this convolution so its transform is the convolution's transform ($(\sin x/x)^2$) multiplied by jf (10 μs/div).

(c) Trace 1: A 5 μs wide positive pulse and a 5 μs wide negative pulse spaced a small distance apart. Trace 2: The chirp-modulated Fourier transform of trace 1. This transform is the product of jf and two sinx/x's whose main lobes are slightly larger and smaller, respectively, than the sinx/x of Fig. 3.26a, since the signal of trace 1 is the derivative of the convolution of two pulses whose widths are slightly smaller and larger, respectively, than the pulse in trace 1 of Fig. 3.26g by half the spacing between the pulses in trace 1 of this figure (10 μs/div).

(d) Trace 1: An approximation of a Gaussian pulse (10 μs/div). Trace 2: The chirp-modulated Fourier transform of trace 1 (2 μs/div). Note that the transform looks like the input signal. This is true since the Fourier transform of a Gaussian pulse is also Gaussian in shape.

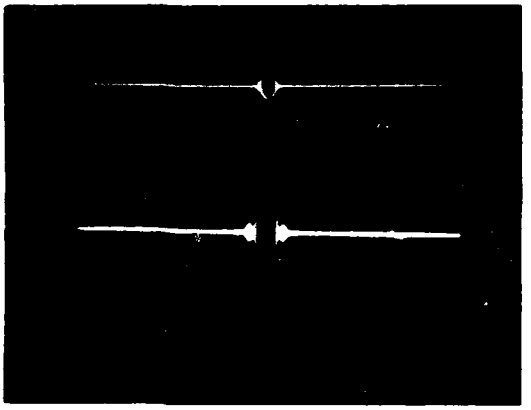

Figure 3.31a

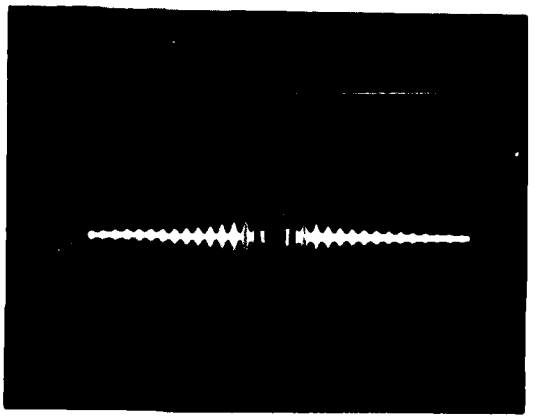

Figure 3.31b

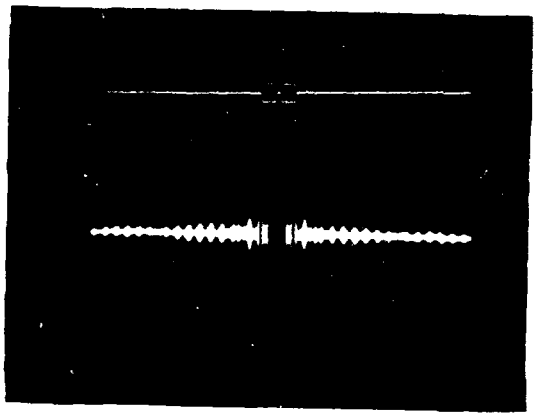

Figure 3.31c

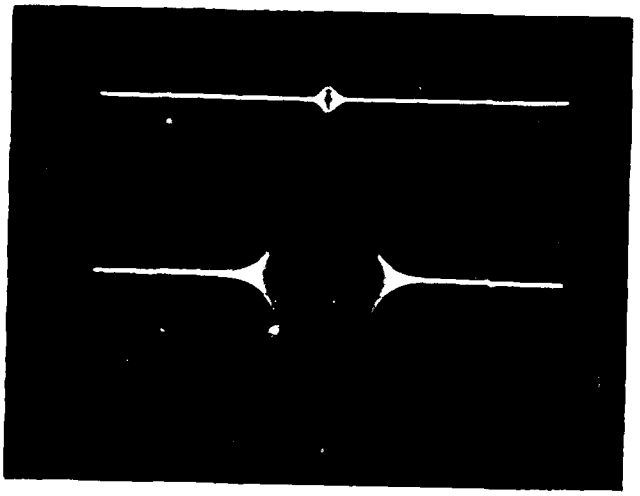

Figure 3.31d

Figure 3.32: Chirp transformations of pulse sequences.

(a) Trace 1: Two .4 μs pulses separated by 7.2 μs (2 μs/div). Trace 2: The chirp-modulated Fourier transform of (a) (2 μs/div). This is a sinx/x moudlated cosine. The width of a single cycle of this cosine is given by the reciprocal of half the spacing between the pulses in trace 1 or about 380 Khz. Dividing by the chirp device slope (in Hz/sec) gives a width of about .4 μs. The width of the main lobe of the sinx/x weighting of this transform is given by twice the reciprocal of a pulse width of about 71 μs. Since the display shows only about one quarter of this main lobe, the cosine varies in height by only about 10% over this portion of the transform. If the two positive pulses were ideally infinitesimally thin in trace 1, the transform would be an unweighted cosine over the valid output time interval. Trace 3: The same as trace 1 except that one of the pulses has been made into a negative pulse (2 μs/div). Trace 4: The same as trace 2 except this time the transform is a sinx/x weighted sine. A cycle width is the same as in trace 2 (2 μs/div). Trace 5: Two negative pulses having the same dimensions as the signal of trace 1 (2 μs/div). Trace 6: The chirp-modulated Fourier transform of trace 5 which, in this case, is a sinx/x weighted cosine of identical appearance to trace 2 but 180° out of phase (i.e. a negative cosine)(2 μs/div).

(b) Trace 1: (Upper left partial trace.) Two 1.5 μs pulses separated by about 8 μs. Whereas pulse spacing to pulse width in (a) was about 18 in this figure, it is only about 5.3 so that the sinx/x weighting over the cosine transform will be more dramatic (10 μs/div). Trace 2: The sinx/x weighted cosine chirp-modulated Fourier transform of trace 1 (2 μs/div). The main lobe of the sinx/x is about 19 μs wide (i.e. $2((1.5\ \mu s)(7 \times 10^{10}))^{-1}$). A single cycle of the cosine is about 3.6 μs wide (i.e. $1/((4\ \mu s)(7 \times 10^{10}))$). The Fourier transform for two impulses spaced $2t_o$ seconds about the time origin would be $\cos(2\pi f t_o)$. Trace 3: (Inset) A negative and positive pulse having the same form as trace 1 (10 μs/div). Trace 4: The chirp-modulated Fourier transform of trace 3. This is the sine version of trace 2 (2 μs/div). Bottom trace: An envelope detected version of trace 4 (5 μs/div). Left bottom inset: Same as the bottom trace except on a 10 μs/div scale. Right bottom inset: Same as trace 4 except on a 10 μs/div scale. Right bottom inset: Same as trace 4 except on a 10 μs/div scale.

(c) Trace 1: (Upper right inset) A 6 μs square pulse (20 μs/div). Trace 2: The chirp-modulated Fourier

transform of trace 1. The main lobe of this transform is about 5 μs wide (i.e. $2((6\ \mu s)(7 \times 10^{10}))^{-1}$) (1 μs/div).
Trace 3: (Lower right inset) A five pulse sequence (20 μs/div).
Trace 4: The chirp-modulated Fourier transform of trace 3 (1 μs/div).

(d) Trace 1: (Upper right inset) A two pulse sequence (20 μs/div).
Trace 2: The chirp-modulated Fourier transform of trace 1 (20 μs/div).
Trace 3: (Lower right inset) A six pulse sequence (20 μs/div).
Trace 4: The chirp-modulated Fourier transform of trace 3 (1 μs/div).
Note the absence of a DC component.

(e) Trace 1: (Upper right inset) A three pulse sequence (20 μs/div).
Trace 2: The chirp-modulated Fourier transform of trace 1 (1 μs/div).
Trace 3: (Lower right inset) A seven pulse sequence (20 μs/div.)
Trace 4: The chirp-modulated Fourier transform of trace 3 (1 μs/div).
Any asymmetry in the transforms is a result of feedthrough through the spectrally inverting mixers. Since all the chirp devices utilized are the same, this feed-through produces a small Fresnel transform that can destroy the symmetry in an otherwise symmetric Fourier transform. The mixer feedthrough can be quite large when mixers are heavily drive.

(f) Trace 1: (Upper right inset) A four pulse sequence (20 μs/div).
Trace 2: The chirp-modulated Fourier transform of trace 1 (1 μs/div).
Note the asymmetry due to Fresnel distortion as discussed in (e). (Some distortion, however, may be attributable to slight mismatches between the impulse responses of the chirp devices used to generate the Fourier transforms.) Trace 3: (Lower right inset) An eight pulse sequence (20 μs/div). Trace 4: The chirp-modulated Fourier transform of trace 3 (1 μs/div). Note that if the 4 negative pulses had been equal in size to the 4 positive pulses in trace 3, then there should not have been a DC component. Essentially, the central lobe of trace 2 should have diminished and split into two lobes smaller than its own sidelobes when the additional opposite-polarity pulses were added to the sequence. Due to an imbalance in the pulse generating circuitry, however, this did not occur and a small sin/x due to the additional DC component was summed with the desired transform.

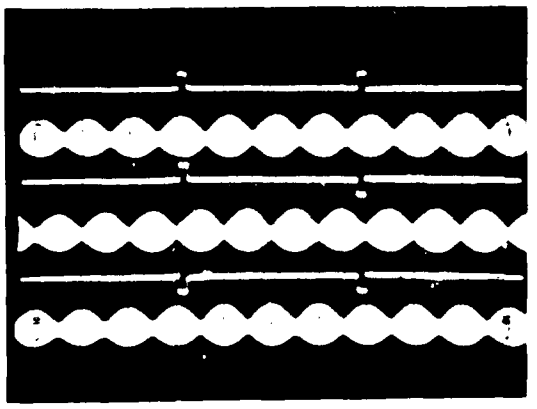

Figure 3.32a

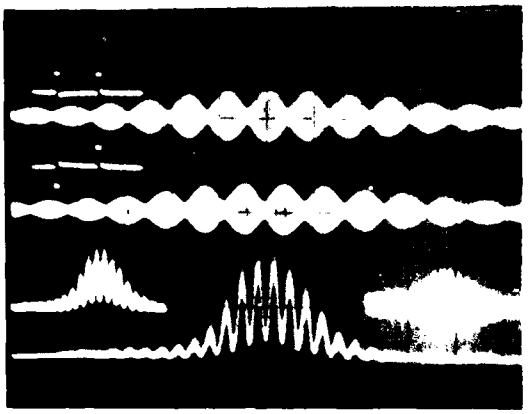

Figure 3.32b

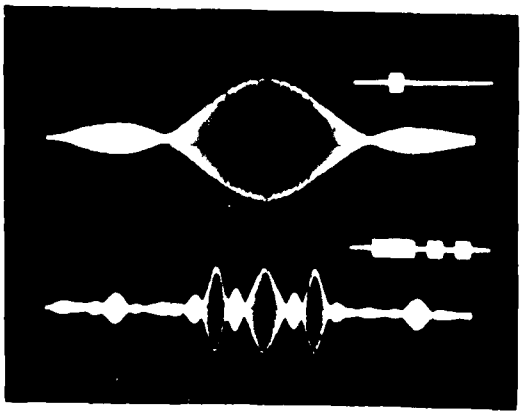

Figure 3.32c

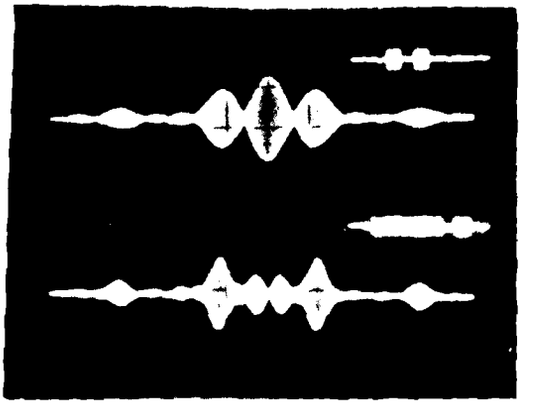

Figure 3.32d

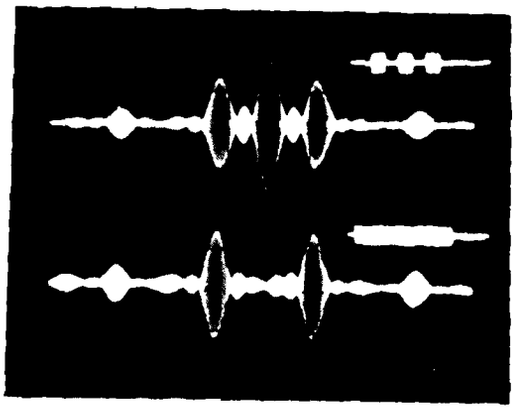

Figure 3.32e

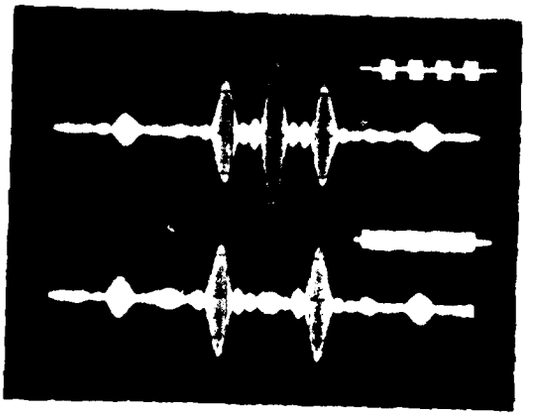

Figure 3.32f

Figure 3.33: Chirp transformations of a carrier-modulated seven-bit Barker code with pure waveform jammers.

(a) Trace 1: The 2.65 Mhz carrier-modulated seven-bit Barker code with a 275 Khz sine-wave jammer at about three times the code carrier peak to peak amplitude (5 μs/div). Trace 2: The chirp-modulated Fourier transform of trace 1 (10 μs/div). The 275 Khz jammer components can be seen to be localized at 275 Khz/$7x10^{10}$ Hz/sec = 3.9 μs on either side of DC. (Third and fifth harmonic components are also visible at 7.8 μs intervals probably resulting from slight input signal saturation.) The positive and negative Barker code spectrums are seen to be situated 2.65 Mhz/$7x10^{10}$ Hz/sec ≃ 38 μs on either side of DC. Since the input signal is about 50 μs in duration, only about 50 μs is available for accurate output Fourier transformation. Therefore only about half of the transform in trace 2 can be accurate. In this figure (and the following two figures) only the right portion of the transforms was tuned by adjusting the center frequency of the input chirp modulation. Thus the difference between the positive and negative Barker code spectrums is due to this selective tuning. Expanded versions of the two spectrums when both have been tuned can be seen in Fig. 3.49a. Trace 3: The same as trace 1 except that the jamming sine-wave frequency has been increased to 3.1 Mhz (5 μs/div). Trace 4: The same as trace 2 except that the jammer sine-wave component at 275 Khz or 3.9 μs has moved to 3.1 Mhz or 3.1 Mhz/$7x10^{10}$ Hz/sec = 44 μs on either side of DC (10 μs/div). Note that (a), (b) and (c) of this figure show explicitly that although the jammers become an integral part of the signal, there is potential for their removal since their energy becomes localized upon Fourier transformation and can be gated from the desired signal transform (usually along with the elimination of negligible portions of the desired transform).

(b) Trace 1: The 2.65 Mhz carrier-modulated seven-bit Barker code with an 85 Khz square-wave jammer (5 μs/div). Trace 2: The chirp-modulated Fourier transform of trace 1 (10 μs/div). The square-wave jammer is rich in harmonic components with a fundamental 85 Khz/$7x10^{10}$ = 1.2 μs on either side of DC. Trace 3: Same as trace 1 except with a square-wave jammer frequency of 3.05 Mhz (5 μs/div). Note that the beat frequency is about 200 Khz or half the difference between the code carrier and fundamental jammer frequencies. Trace 4: The same as trace 2 except that the jammer square-wave fundamental component at 85 Khz or 1.2 μs has moved to 3.05 Mhz or 3.05 Mhz/$7x10^{10}$ Hz/sec = 4.36 μs on either side of DC (10 μs/div). Note that the

square wave transform in trace 2 possesses only odd harmonics.

(c) Trace 1: The 265 Mhz carrier-modulated seven-bit Barker code with 160 Khz saw-tooth wave jammer (5 μs/div). Trace 2: The chirp-modulated Fourier transform of trace 1 (10 μs/div). The fundamental component of the saw-tooth jammer is located 160 Khz or 160 Khz/7×10^{10} Hz/sec = 2.3 μs on either side of DC. Note that the saw-tooth has both even and odd harmonics. Trace 3: The same as trace 1 except with a saw-tooth frequency of 1.15 Mhz (5 μs/div). Trace 4: The same as trace 2 except that the jammer saw-tooth fundamental component at 160 Khz or 2.3 μs has moved to 1.15 Mhz or 1.15 Mhz/7×10^{10} Hz/sec = 16.5 μs on either side of DC (10 μs/div).

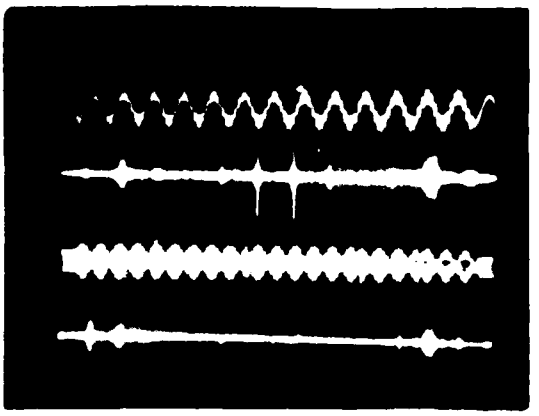

Figure 3.33a

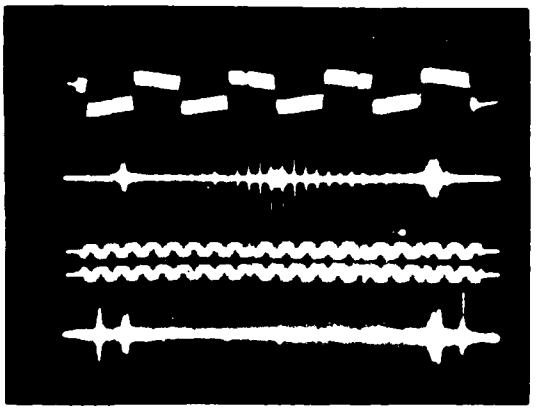

Figure 3.33

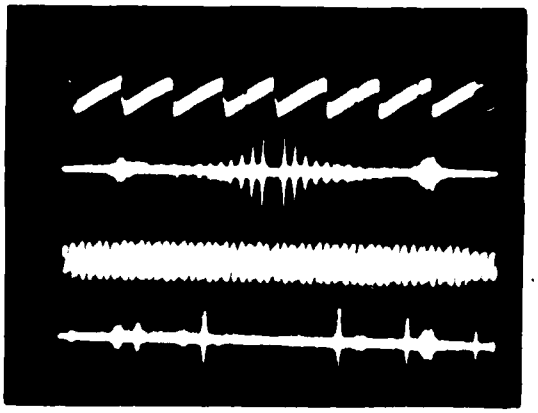

Figure

Mixer carrier feed through can lead to appreciable distortions in the transform domain. Figure 3.34a shows a code and its Fourier transform. Trace 3 is the inverse transform which appears to be a filtered version of the input. As discussed in Section 2.4, however, this signal, being purely real, must have a purely symmetric magnitude spectrum. Figure 3.34b shows the proper spectrum. The distortion in Figure 3.34a was caused by the Fresnel transform of the signal due to leak-through of the original modulating chirp when it was being spectrally inverted. In this way two signals were effectively applied to the convolving chirp filter. These two signals, having opposite slopes, produce a Fourier and a Fresnel transform concurrently. Both transforms, when properly tuned, will inverse transform back to the original signal after spectral inversion and application to the second chirp filter. Therefore, the original signal in Figure 3.34a was recovered although the transform seemed wrong. Figure 3.34c shows a 255 bit P-N code, its Fourier transform and its inverse transform also exhibiting slight transform distortion which is usually dominated by mixer leak-through when the chirp devices in the system are all the same and mixers are driven heavily.

Figure 3.35a shows a signal that was picked up by an acoustic receiver where every pulse represents the reflection of an acoustic impulse

Figure 3.34: Chirp transformation with zero/one codes.

(a) Trace 1: A 13-bit zero/one code (5 μs/div). Trace 2: The chirp-modulated Fourier transform of trace 1 (2 μs/div). This transform is highly asymmetric due to mixer feedthrough producing a Fesnel transform of the code at the same time as the Fourier transform, but of smaller size. The main lobe of this transform is $2((2.1\ \mu s)(7 \times 10^{10}\ Hz/sec))^{-1} = 13.6\ \mu s$ wide since a single code bit is about 2.1 μs wide. Trace 3: The inverse transform of trace 2. In this case the output was optimized so that the inverse Fourier and Fresnel transforms coincided thereby producing a filtered (due to time limiting of the transform) version of the input signal.

(b) Trace 1: (Upper left inset) The same code as in trace 1 of (a) except of different size (5 μs/div) and inputted into a chirp system of slope 10 Mhz/30 μs = 3.33×10^{11} Hz/sec. One bit is .98 μs wide. Trace 2: The chirp-modulated Fourier transform of trace 1 (2 μs/div). The main lobe is $2((.98\ \mu s)(3.33 \times 10^{11}\ Hz/sec))^{-1} = 6.1\ \mu s$ wide since a code bit is .98 s wide. Trace 3: The same as trace 2 except on a .5 μs/div scale.

(c) Trace 1: A 255-bit zero/one pseudo-random code (10 μs/div). A single bit is .12 μs wide. Trace 2: The chirp-modulated Fourier transform of trace 1 (20 μs/div). This output is accurate for over 70 μs (the chirp device impulse response width minus the code width). The main lobe of this transform is about 238 μs wide (i.e. $2(.12\ \mu s)(7 \times 10^{10}\ Hz/sec))^{-1}$) so that only about one-third of the transform is obtained. The DC component of this code is quite prominent. In order to enhance the information that is contained in the main lobe, the component has been saturated down to the level of its nearest sidelobes.

Trace 3: The inverse transform of trace 2 (10 μs/div). Even though only about a third (70 μs) of the main lobe of the Fourier transform (238 μs) was available (the remaining approximately 60 μs of the 130 μs long correlation was gated out). As can be seen in this trace, the code is just about readable. Furthermore, there is enough information in the sidelobes and remaining portion of the central lobe of the sinx/x due to the DC level in the code that the DC level in the inverse transform has not changed very much from its value at the input. The effect of saturating the DC component becomes more prominent as the codes become extremely long, so that the sinx/x due to the DC portion compresses more and more about the DC point of the transform. Such long codes, however, could not be transformed utilizing the same system configuration and devices used to transform the code in trace 1.

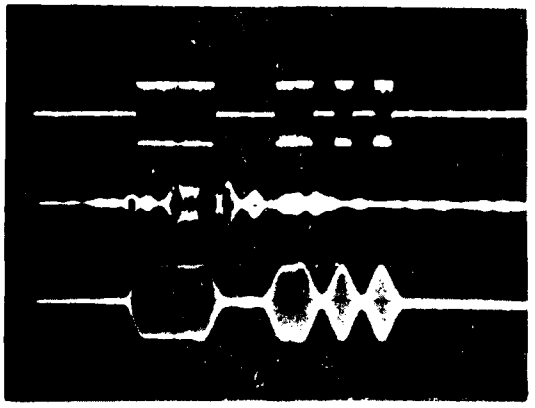

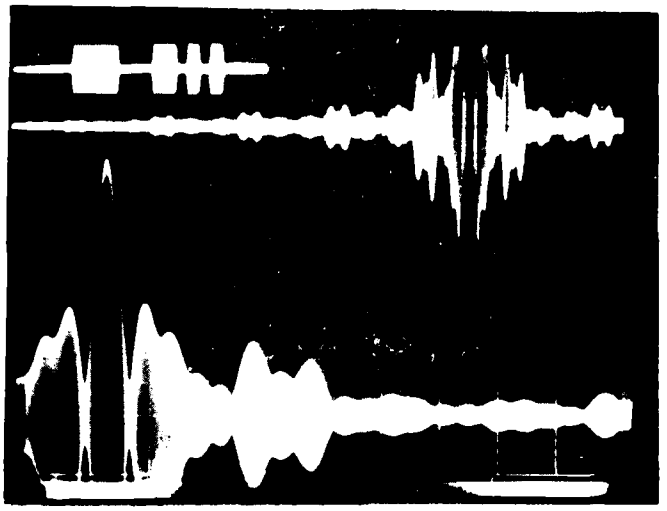

Figure 3.34b

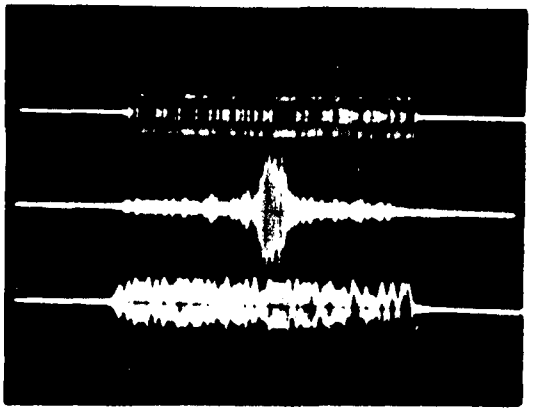

from objects in a water tank. The 2nd trace is the Fourier transform of this signal and the 3rd trace is the inverse transform of this. Note that since the transform of the signal had to be cut off prematurely, the fast pulses end up oscillating a bit when the inverse transform is obtained. Figure 3.35b demonstrates the existence of the Fresnel transform of the signal that always exists at the same time as the Fourier transform, for a chirp transformation system, but at a different location in the frequency spectrum. As the center frequency of the chirp, modulating the input signal, is changed, a different portion of the Fourier transform is seen. However, as the Fourier transform of the signal shifts in one direction, the Fresnel transform of this signal shifts in the other. Every trace in Figure 3.35b represents an approximate 5 Mhz of transform shift toward the left. The central traces have been magnified so that the sidelobe structure is evident. By the 6th trace the Fresnel transform has almost shifted into view within the valid transform time interval. The sidelobe structure in trace 5 is due more to the Fresnel transform, at this point, than the Fourier. Figure 3.35c demonstrates how a wide bandwidth signal transform can be observed. The first trace shows a narrowband version of the signal transform. When the time signal is compressed so that its transform cannot be viewed all at once within the output time interval, the transform can be viewed in slices by varying the center frequency of the input chirp modulation. Traces 2 to 4 each show one third of the transform seen in the first trace obtained by varying this center frequency.

Figure 3.36a demonstrates the delay insensitivity of the Fourier transform. In this figure the input square pulse is delayed by

Figure 3.35: The chirp transform of a pulse-echo return and its inverse along with some chirp system characteristics.

(a) Trace 1: A pulse-echo return from an ultrasonic-nondestructive testing system (2 μs/div). (Unless specified otherwise, the input signal is typically shown to be modulated by the input pre-multiplying chirp.) Trace 2: The chirp-modulated Fourier transform. Since a typical pulse is about .2 μs wide, the main lobe of this transform is about $2((.2\ \mu s) \times (7 \times 10^{10}\ Hz/sec))^{-1} = 143\ \mu s$ wide. Since about 80 μs of the transform is valid, then more than half of the main lobe is being displayed. The portions of the transform more than 40 μs away from DC may look similar to the rest of the transform, but they are the result of transforming a continually decreasing portion of the signal that eventually shrinks to zero about 60 μs away from DC. Trace 3: The inverse transform of trace 2 (2 μs/div). Note that utilizing only about half of the transform main lobe produces oscillations where none previously existed.

(b) The simultaneous existence of a Fresnel transform with the Fourier transform is demonstrated to exist even in a system consisting of ideal components. This Fresnel transform is centered at a different position along the output time axis from the Fourier transform. The distance between the two transforms is linearly dependent upon the chirp device center frequency. At baseband these two transforms coincide. At high device center frequencies the main portion of the Fresnel transform is far away from the Fourier transform and therefore does not appear within the finite valid output time interval when the center of the Fourier transform is within this interval. However, since all input signals are of finite length, there will always be high frequency components of the Fresnel transform within this interval although they may be quite negligible. In this figure all the traces are displayed on a scale of 20 μs/div. The input to the chirp transform system is a 10 s pulse (20 μs/div) seen as an inset in the top left of the figure. In order to demonstrate the existence of the Fresnel transform, the Fourier transform of this square pulse is shifted to the left by changing the center frequency of the input chirp modulation. When the Fourier transform shifts to the left, the Fresnel transform will shift to the right. The two transforms cross outside the valid output time interval and then the Fresnel transform appears. Traces 3 and 4 show expanded portions of the sidelobes of the Fourier transform. Traces 5 and 6, however, are dominated by the sidelobes of the Fresnel transform. The transform to which the sidelobes belong is evident since the sidelobes

decrease with increasing transform shift and then increase as the Fresnel transform begins to dominate. The Fresnel transform appears in the last two traces.

(c) This figure demonstrates the display of a transform of duration longer than the output valid time interval. Trace 1 shows the Fourier transform of four widely and evenly spaced square pulses (20 μs/div). In this case the pulses are about .35 μs wide and spaced about 1.8 μs apart. Traces 2 to 4 show the chirp-modulated Fourier transform of the same signal after it has been compressed by a factor of four. Since the transform of such a signal is four times longer than the transform of trace 1, it must be displayed in slices. This has been done in traces 2 thru 4 where the center frequency of the input modulation is adjusted for the desired portion of the transform to be displayed. Trace 2 shows the central region of the transform (20 μs/div) corresponding to the portion of the transform in trace 1 within the central two divisions. Traces 3 and 4 show the rightmost and leftmost portions of this transform, respectively.

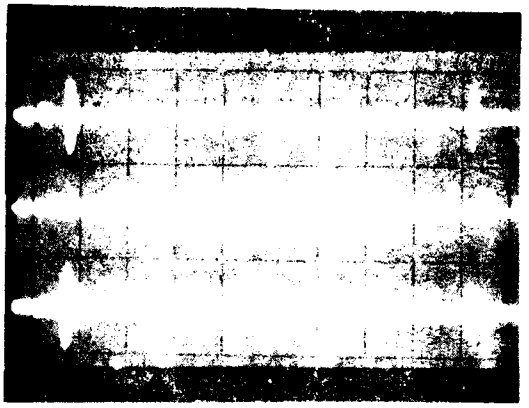

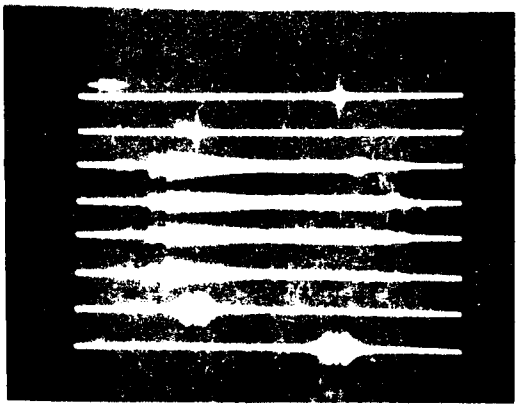

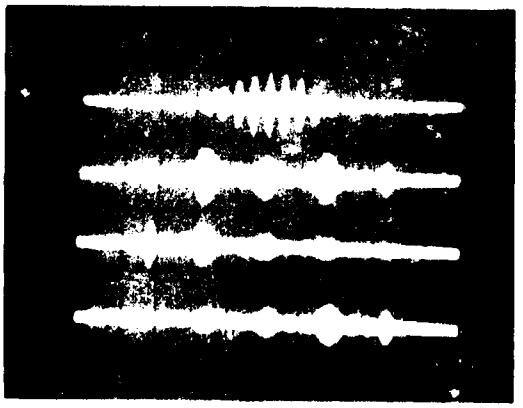

about 10 μs in every other trace, yet the magnitude of the Fourier transform remains stationary and of the same appearance, as it should. Figure 3.36b, on the other hand, demonstrates the converse of Figure 3.36a. In this case a delayed Fourier transform produces a stationary function. The carrier frequency of the signal is changed to affect a specific shift of the Fourier transform. Likewise, the chirp carriers of the Fourier transforms in Figure 3.36a change their center frequencies as the input signal shifts in time. Carrier frequency shifts, in both cases, represent signal or transform phase changes and therefore do not effect magnitude. Figure 3.36c demonstrates the summation of two signals. When the two input signals in traces 1 and 3 are summed, the signal in trace 5 is obtained. Likewise, the summation of their transforms will produce the transform given in the final trace. Figure M-5 corresponds to this situation.

Figures 3.37a, b and c demonstrate how well a chirp transform system can be made to filter a signal by time gating in the Fourier domain. Figure 3.37a shows three small input pulses in the first trace and the same signal after passage through the chirp transform system in the 2nd trace. In the third trace monochromatic noise or jammer has been added to the signal. The detected inverse Fourier transform with the noise is seen in trace 4. Trace 5 is the Fourier transform of the combined signal, where it can be seen that the noise has been localized and seems to dominate the spectrum. However, when the central portion of this transform is all that is inverse transformed, then a low pass filtered version of the signal, without the jammer, is obtained. Figure 3.37b shows this same situation for wider input pulses. Figure 3.37c shows a contrived

Figure 3.36: Chirp transformation results demonstrating some Fourier properties.

(a) Traces 1, 3, 5 and 7: A successively delayed 10 μs wide square pulse (10 μs/div). Traces 2, 4, 6 and 8: The chirp-modulated Fourier transforms of traces 1, 3, 5 and 7, respectively (10 μs/div). These results demonstrate the insensitivity of the magnitude of the Fourier transform to signal delay. Only the phase of each successive transform changes with signal delay change and is seen as a change in the center frequency of the output chirp modulation.

(b) Traces 1, 3, 5 and 7: A 10 μs wide square pulse with successive incremental change of the center frequency of its chirp modulation (10 μs/div). Traces 2, 4, 6 and 8: The chirp modulated Fourier transforms of traces 1, 3, 5 and 7, respectively (10 μs/div). These results demonstrate the converse of (a) in that a delay of the Fourier transform produces nothing more than a change in the signal rf carrier frequency. In (a) the delay of the signal and in (b) the delay of the transfor is 60 μs or more than half the total dispersion of the chirp devices (≈ 100 μs). The center frequencies of the transform in (a) and the signal in (b) change by about 4.2 Mhz over the 60 μs range of delay. The effect of the change in the chirp modulation center frequency of the input signal in (b) on its Fourier transform is the same effect utilized to allow the display of any desired portion of the transform and is demonstrated in Fig. 3.35c. It is a consequence of the Fourier shifting theorem.

(c) This figure demonstrates superposition. Trace 1: Two 5μs positive pulses separated by 5 μs (5 μs/div). Trace 2: The chirp-modulated Fourier transform of trace 1 (5 μs/div). Trace 3: A negative 5 μs pulse and a positive 5 μs pulse separated by 5 μs (5 μs/div). Trace 4: The chirp-modulated Fourier transform of trace 3 (5 μs/div). Trace 5: The sum of traces 1 and 3 (5 μs/div). Trace 6: The sum of traces 2 and 4 (5 μs/div) utilizing two identical chirp systems and the same input chirp modulations. Note that the Fourier transform in trace 6 obtained by summing the transforms in traces 2 and 4 is the expected transforms for a signal given by trace 5 or the sum of traces 1 and 3. If the input time origin is set at the center of the signal of trace 1, then the transform of this signal has only a real component. Likewise, the transform of trace 3 has only an imaginary component. Therefore, since the pulse of trace 4 is offset from the time origin, it will have a real Fourier component given by trace 4 and the magnitude of the transform will be the sinx/x given in trace 6. Note that the two transforms given in traces 2 and 4 possess phase quadrature chirp carriers (having no deviation from quadratic) since one transform is purely real while the other is purely imaginary. The deviation from quadratic of the chirp modulation in trace 6 is given by the inverse tangent of the ratio of trace 4 to trace 2.

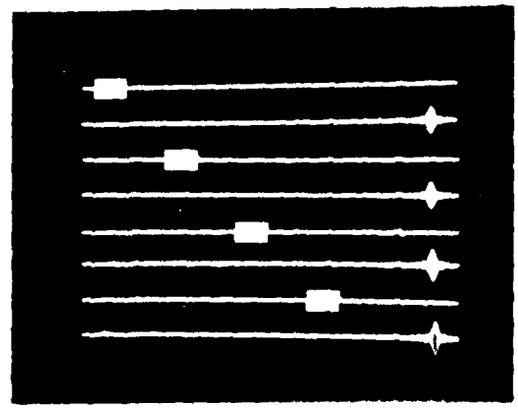

Figure 3.30a

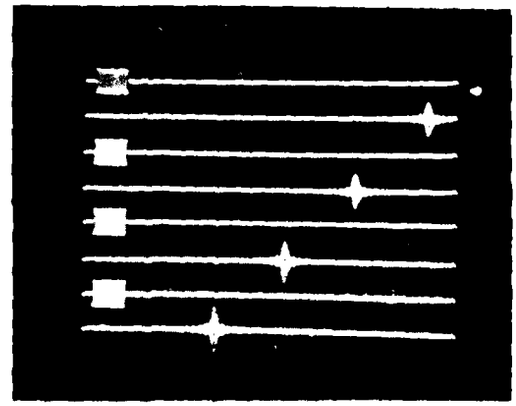

Figure 3.30b

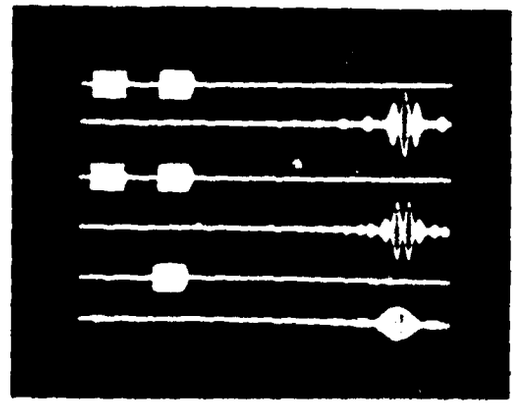

Figure 3.30c

Figure 3.37: Filtering by the time gating of chirp generated Fourier transforms.

(a) Trace 1: Three chirp-modulated input pulses each about 2 μs wide (20 μs/div). Trace 2: The envelope-detected inverse transformation of the chirp-generated transformation of trace 1 (20 μs/div). Trace 3: The same as trace 1 with the addition of a monochromatic (sine wave) 364 Khz jammer (20 μs/div). Trace 4: The envelope-detected inverse transformation of the chirp-generated Fourier transform of trace 3 (20 μs/div). Trace 5: The chirp-modulated Fourier transform of trace 3 (2 μs/div). The $364\ \text{Khz}/7\text{x}10^{10}\ \text{Hz/sec} = 5.2\ \mu\text{s}$ on either side of DC. Trace 6: The time gate used to low pass filter the signal and eliminate the bulk of the jammer (2 μs/div). Trace 7: The envelope-detected inverse transformation of trace 5 gated by trace 6 (20 μs/div). The gating of the Fourier transform has eliminated the jammer almost completely and smoothed out the pulses due to the low pass filtering.

(b) This figure is identical to (a) except that wider pulses of different widths were used as the input.

(c) Trace 1 (consisting of four consecutive insets): Inset 1 is the input signal consisting of two 1 μs pulses (10 μs/div). Inset 2 is the chirp-modulated Fourier transform of inset 1 (20 μs/div). Inset 3 is the chirp-modulated Fourier transform of a 750 Khz square wave gated to 6 cycles (20 μs/div). Inset 4 is the combination of the six cycle square wave and the double pulse (10 μs/div). Trace 2: The chirp-modulated Fourier transform of the signal given by inset 4 of trace 1 (i.e. the six cycle square wave plus the two pulses)(5 μs/div). Trace 3: The envelope-detected inverse transformation of trace 2 (2 μs/div). Note the contrived similarity between the transform and its inverse. Trace 4: A time gate used to pick off only the two large lobes of the Fourier transform in trace 2 (5 μs/div). Trace 5: The transform of trace 2 gated by trace 4 (5 μs/div). Trace 6: The envelope-detected inverse transformation of trace 5 (2 μs/div). Trace 7: A time gate used to pick off only the central nine lobes of the Fourier transform in trace 2 (5 μs/div). Trace 8: The transform of trace 2 gated by trace 7 (5 μs/div). Trace 9: The envelope-detected inverse transformation of trace 8 (2 μs/div). Note that the retention of only the two large transform peaks (with a few sidelobes) produces a signal having twelve peaks, which is a filtered version of the magnitude of the input square wave. Retention of only the nine central lobes of the transform, however, produces a signal (the inverse transform) that is essentially a filtered version of the two input pulses. This form of signal was used to demonstrate the chirp-transformation time-gating filtering technique due to its particular characteristic, whereby the gated portion of

the transform appears to produce a version of the ungated portion upon inverse transformation. Note that only the square wave fundamental component is utilized so that it becomes essentially a sine wave upon inverse transformation. Functions having the above property, whereby the function appears to remain unchanged upon Fourier and inverse transformation, are created by the summation of a real symmetric signal and a baseband version of its transform. This technique was approximated in this figure and is possible due to the symmetry property of Fourier transformation, whereby the performance of two consecutive Fourier transformations recovers a symmetric signal (time-inverted if the signal is asymmetric).

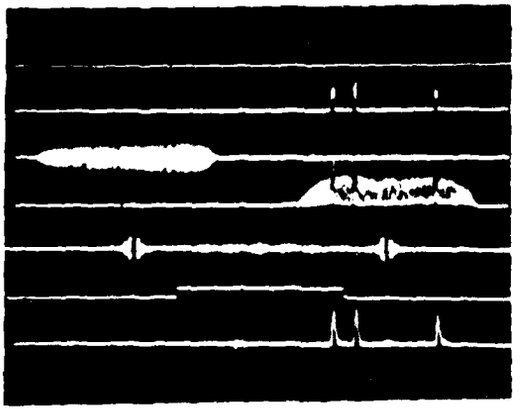

Figure 3.37a

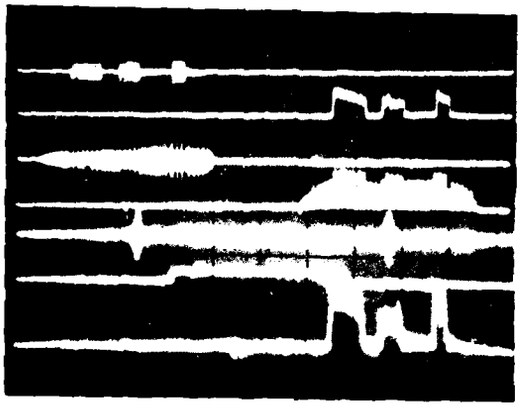

Figure 3.37b

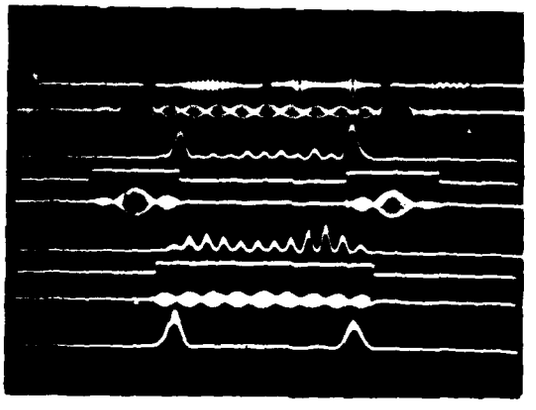

Figure 3.37c

signal that behaves like the center of the unfiltered signal. When the gate in trace 6 is used to only allow the central portion of the transform through, then the resulting signal upon inverse transformation appears to be the end lobes of the original signal. The actual input signal used to generate this transform consisted of two pulses summed with a smaller amplitude six cycle square wave. The two filtering steps, in a sense, separated the two functions.

Figures 3.38a, b and c demonstrate filtering using a realistic reflection return. Figure 3.38a shows the actual signal in the 1st trace, its transform in the 2nd trace and its inverse transform in the 3rd trace. Figure 3.38b shows this same situation where an overwhelming amount of monochromatic noise has been added. Note in the second trace that the noise spikes now dominate the spectrum to the point where the signal spectrum can hardly be seen. Figure 3.38c shows the inverse transform after the noise spikes have been selectively gated from the spectrum. Note that the signal has been greatly improved by the gating process to the point where most of the tiny reflections can now be seen again. (The position of the output with respect to the input is irrelevant in these photographs, since they do not normally coincide due to the chirp system delays. An attempt to keep these signals lined up for these pictures failed for the final trace of Figure 3.38c, which can be seen shifted to the right by one division.) Note in the final trace of Figure 3.38c that a pulse appears at the point defining the start of the noise. This arises since such a discontinuity is rich in harmonics and a small gating pulse cannot be expected to eliminate much of its spectral energy from the Fourier transform.

Figure 3.38: Chirp-transformation filtering of pulse-echo returns by time gating.

(a) Trace 1: A 20 μs long pulse-echo return obtained from an ultrasonic non-destructive testing system (2 μs/div). Trace 2: The chirp-modulated Fourier transform of trace 1 (20 μs/div). This is about half of the main lobe of the transform defined by twice the inverse of the smallest pulse width. The transform is accurate over at least 80 μs and is gated to 80 μs prior to inversion. Trace 3: The inverse transformation of trace 2 (2 μs/div). Oscillations after each pulse are the result of the filtering due to the finite bandwidth of the system corresponding directly to that portion of the transform displayed in trace 2.

(b) This figure is the same as (a) except that a monochromatic noise source was included at the input to the chirp system. The noise is a 1.82 Mhz rf. Trace 1: The pulse-echo reflections plus the 1.82 Mhz rf 'noise'. Note that the echoes have essentially been obliterated (1 μs/div). Trace 2: The chirp-modulated Fourier transform of trace 1 (10 μs/div). The noise peaks dominate the transform and are located 1.82 Mhz/7×10^{10} Hz/sec = 26 μs to either side of DC. Trace 3: The inverse transformation of trace 2.

(c) Gating is utilized in this figure to recover the original signal. Trace 1: The reflections plus the 1.82 Mhz noise (2 μs/div). Trace 2: The chirp-modulated Fourier transform of trace 1 (10 μs/div). Trace 3: A time gate used to eliminate the transform lobes due to the noise source (10 μs/div). Trace 4: The inverse transformation of trace 2 gated by trace 3 (2 μs/div). Note that the original signal is essentially recovered. The trace in this figure has been shifted one division to the right with respect to trace 1. Note also that due to the wide-band nature of the rising edge of the noise the gate was not so effective in eliminating this portion.

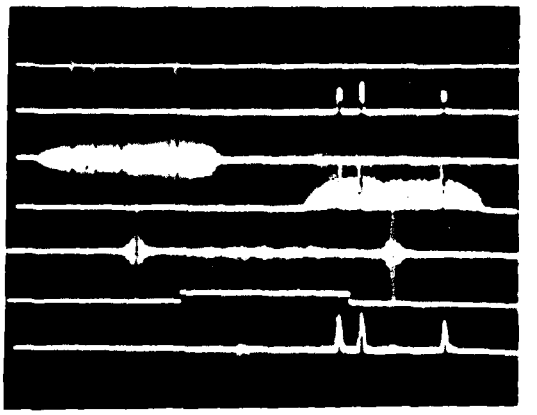

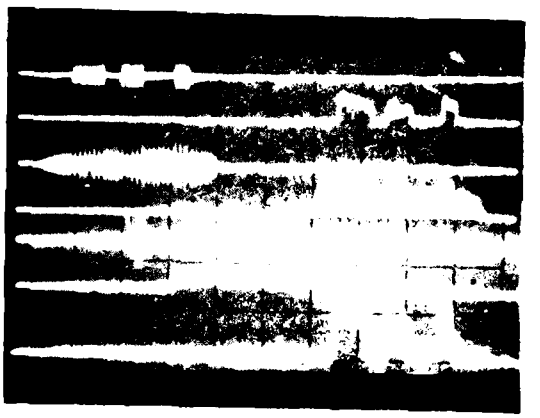

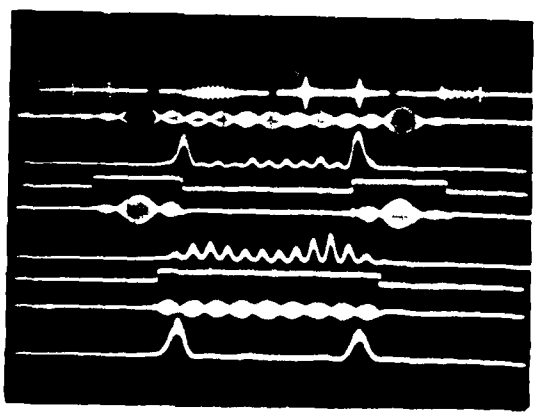

Figures 3.39a and b compare the Fourier transform of a square pulse with the Fresnel transform of the same signal. In Figure 3.39b the pulse is increased in width from the first trace to the last. Note in this figure that the Fresnel transform appears much like the Fourier transform for small pulses (Fourier left, Fresnel right). The Fourier transform continues to compress, however, while the Fresnel transform expands. Fresnel ripples can be seen on the Fresnel transform in Figure 3.39a. (A detailed documentation of the Fresnel transform has been derived and included in Appendix A.) The reason for an interest in the Fresnel transform is two-fold. First of all, the chirp filter possesses an input-output relationship that is essentially a Fresnel transform. Since this is the case, a detailed knowledge of Fresnel analysis could lead to a chirp filter system analysis procedure based upon use of this transform in a manner similar to the way the Fourier transform has become so important in system analysis. Secondly, there are times when the Fresnel implementation of a specific function represents a savings over using a Fourier transform to do the same thing. A lot is said about this in Section 2.4, where it was mentioned that signal time inversion could be performed using either transform. If only the time inversion function is required, then there is no need in obtaining the Fourier transform since none of the special properties of this form of the signal are to be utilized. As discussed in Section 2.4, time inversion essentially involves two repeated Fourier transforms or a second Fresnel transformation after a double chirp multiplication. In this section it was also found that time inversion of a signal using the Fourier transform also required a double chirp mixing process due to

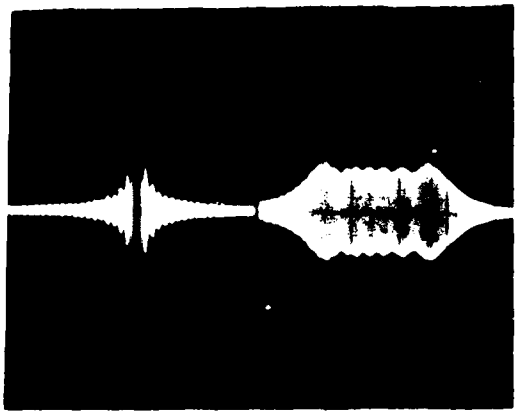

Figure 3.39a

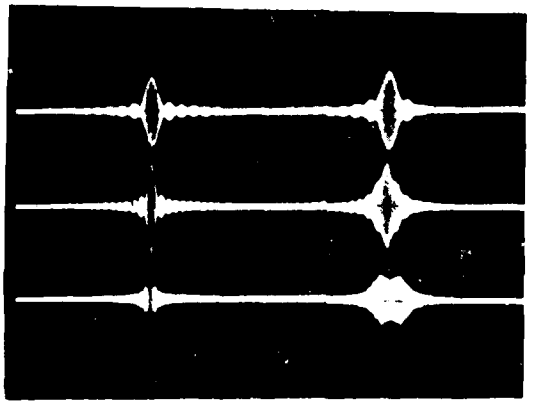

Figure 3.39b

Figure 3.39: The Fresnel transform in comparison to the Fourier transform of the same input signals.
(a) The chirp-modulated Fourier transform (left) and the chirp-modulated Fresnel transform (right) of a 15 μs wide square pulse (10 μs/div).
(b) Trace 1: The Fourier transform (left) and the Fresnel transform (right) of a 3.5 μs square pulse (20 μs/div). Trace 2: Same as trace 1 except that the pulse has been expanded to 6 μs. Trace 3: Same as trace 1 except that the pulse has been expanded to 10 μs. The Fresnel transforms were generated by inputting the square pulses on rf carriers instead of chirps.

the special properties of the spectral inversion process and the inherent difference between a chirp system designed to use an up-chirp device compared to one using a down-chirp device. Since,however, the Fresnel transform scheme does not require a synchronization between multiplying chirps, it is the simplest to implement. Figures 3.40a and b show the two methods for obtaining the Fresnel transform of a signal and its inverse using, in one case, only chirp filters and, in the other, only convolvers, and, in both, only chirps of the same slope. Figures 3.41a and b show the two possible Fresnel time complementation schemes. In one case, all devices are the same and, in the other, an opposite slope device is used saving a mixing and filtering step. Figures 3.42a and b show some actual results utilizing the scheme in Figure 3.41a. Trace 1 of Figure 3.42a is a 255 bit pseudo-random (PN) code. The second trace of this figure is a time inverted portion of the first part of this code obtained by modulating only this portion of the Fresnel transform of the code (since a continuous signal can be continually Fresnel transformed) by the doubly sloped chirp. (The chirp has twice the slope of the chirp filters.) The remaining traces in this figure show the time inversion of successive slices of the signal. Figure 3.42b shows the time inversion of an isolated code in proper time relationship in the first two traces and expanded and re-oriented in the second two traces. Bandwidth limitations produce the rippling effect since the input rise times are very fast.

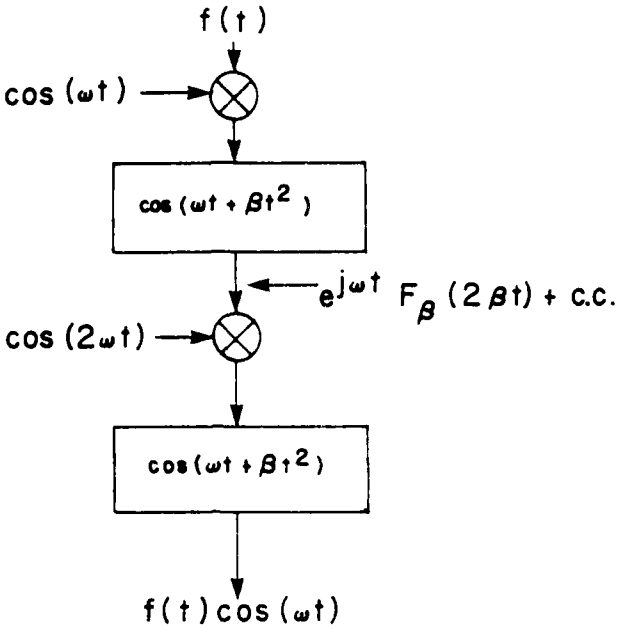

FIGURE 3.40a

Figure 3.40: Fresnel transformation block diagrams.
(a) Fresnel transformation and inversion using chirp filters.

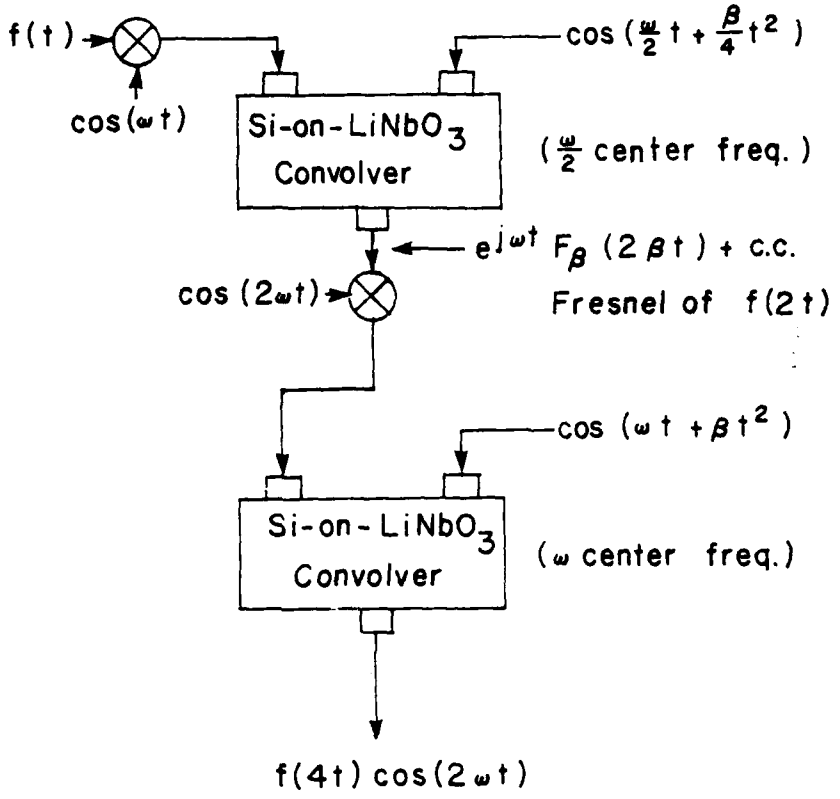

Figure 3.40: Fresnel transormation block diagrams.

(b) Fresnel transformation and inversion using Si-on-$LiNbO_3$ convolvers. In both cases a spectral inversion is required prior to the second device before the inverse Fresnel transformation can be performed since devices having identical slopes are being used. Note that since the output of a convolver is compressed by a factor of two, then a chirp with double the center frequency and four times the slope of the input chirp is required for the second device. Also, the output of the system is compressed by a factor of four.

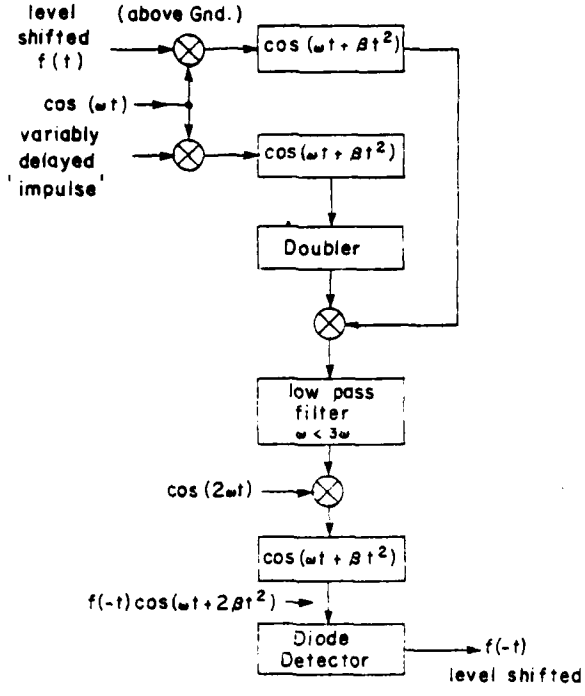

Figure 3.41: Time complementation schemes utilizing Fresnel transformation. (a) Fresnel time complementation (inversion) using identically sloped chirp devices.

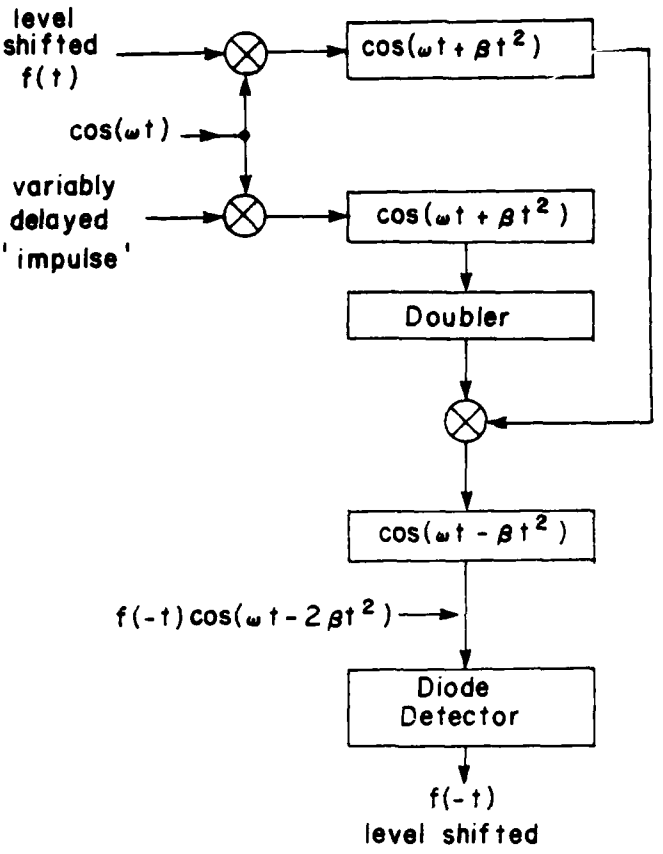

Figure 3.41: Time complementation schemes utilizing Fresnel transformation.

(b) Fresnel time complementation using oppositely sloped chirp devices. This scheme eliminates a filter and a spectral inversion. In any case, the Fresnel transform of the signal must be multiplied by a doubly sloped chirp prior to inverse transformation to obtain a time inverted version of the input signal. Furthermore, since narrowband signals correlate principally with a small portion of the chirp device impulse response centered about the center frequency of the input carrier, then the Fresnel transformation can be performed on a continuous basis with very little distortion resulting from the finite duration of the impulse response. (See Eq. 4.86 of Part III.) Because of this, any portion of the input signal can be selectively time inverted by simply mixing the proper portion of the Fresnel transform (to which there exist a one-to-one correspondence with the input signal) with the doubly sloped chirp that is derived by impulsing a chirp device at the proper time and doubling the resulting impulse response.

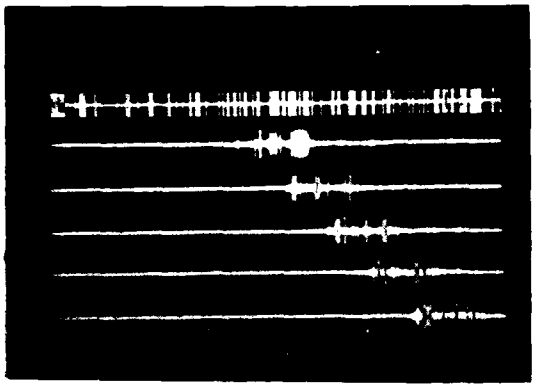

Figure 3.42a

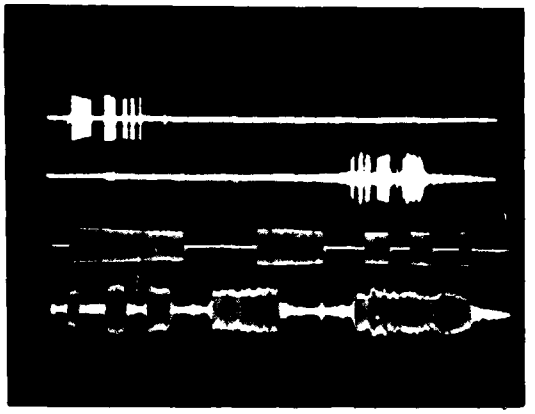

Figure 3.42b

Figure 3.42: Time complementation results utilizing the Fresnel transformation technique.

(a) Trace 1: A repeating 255-bit zero/one pseudo-random code (20 μs/div) modulated onto a 15 Mhz carrier for inputting into the time complementing system. Trace 2: The time complemented version of approximately the first 30 μs of the code in trace 1. Traces 3, 4, 5 and 6: Successive time-complemented portions of the code in trace 1 (20 μs/div). The successive portions were obtained by delaying the impulse to the chirp device used to produce the doubly-sloped chirp.

(b) Trace 1: A zero/one code (20 μs/div). Trace 2: The time complemented version of trace 1 (20 μs/div). Trace 3: An expanded version of trace 1 (4 μs/div (uncalibrated)). Trace 4: An expanded version of trace 2 (≈ 4 μs/div (uncalibrated)). Non-uniformity of the impulse response amplitudes of the chirp devices, phase distortions in these devices, mixer intermods and finite bandwidth restrictions all lead to the type of distortions seen on the time complemented output in trace 4.

3.3 SAW Receivers Utilizing Chirp Transformation

A receiver configuration that takes the Fourier transform of the incoming signal so that spectral modifications can be made (see Section 2.6 on Spectrum Modifications) and then inverse transforms this prior to matched filtering in a SAW convolver, is depicted in Figure 3.43a. All the processes involved in such a receiver have already been demonstrated and very little is to be gained by showing the response of such a receiver. A more versatile receiver can be realized by performing the matched filtering in the Fourier domain. That is, if the signal spectrum were to be multiplied by the spectrum of the impulse response of the matched filter (i.e. its transfer function), then, upon inverse transformation, the desired correlation is obtained. In this way a convolver is not required. The detailed receiver structure is shown in Figure 3.43b. In order to obtain the output correlation of the input signal that is the same as the output from a filter matched to this signal, a time reversed version of the signal is required. In this case, the incoming signal with noise is transformed and its spectrum modified, if it be so desired. The time reversed signal is also transformed and this is mixed (actually a pure multiplier should be used here as will be seen) with the received signal spectrum. The product is then inverse transformed and the correlation obtained. Figures 3.44a thru f demonstrate the behavior of just such a system. In this case a 255 bit PN code was used as the signal and reference. The reference was generated time reversed. These can be seen in traces 1 and 2 of Figure 3.44a. Traces 3 and 4 are their respective transforms, trace 5 is their product and trace 6 is the resulting correlation obtained by inverse transforming

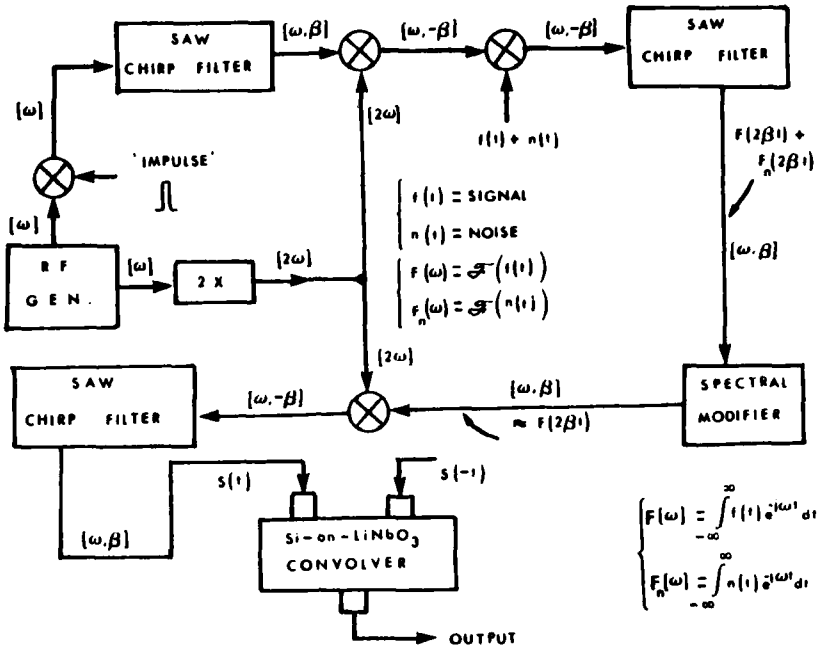

FIGURE 3.43a

Figure 3.43: SAW receivers incorporating chirp transformation.
(a) A SAW receiver utilizing chirp transformation for time-domain filtering and a convolver for matched filtering. The signal and noise are Fourier transformed, weighted and then inverse transformed using chirp devices. The transform weighting can involve simply the removal of a jamming component by gating. After the signal is inverse transformed, it is convolved with its time complemented version (i.e. correlated).

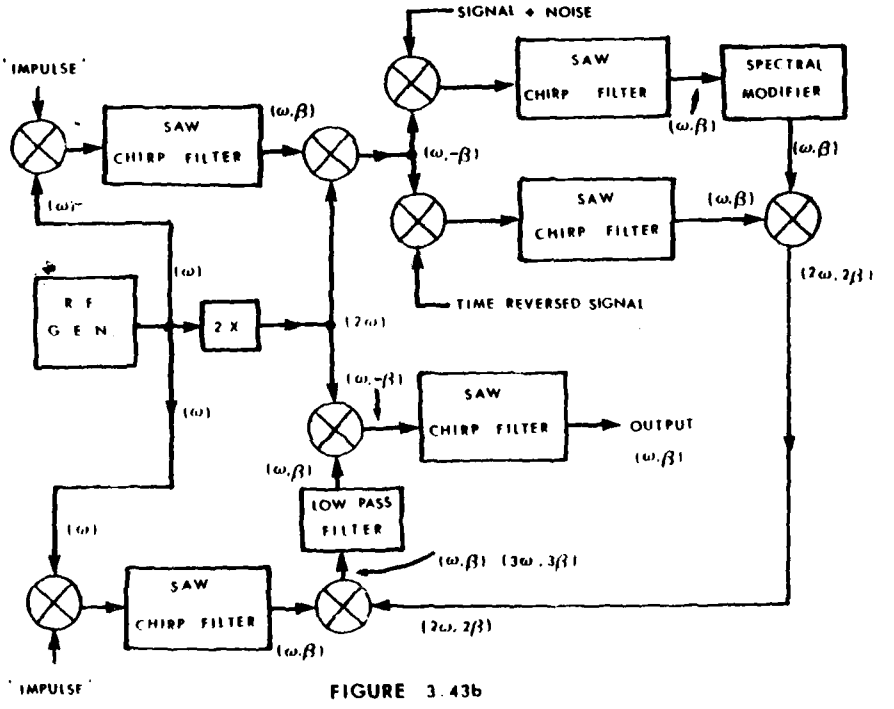

FIGURE 3.43b

Figure 3.43: SAW receivers incorporating chirp transformation.

(b) A SAW receiver whereby correlation is performed in the Fourier domain. The signal (plus noise) and its time complemented version are individually Fourier transformed. The two transforms are multiplied together after the signal transform has undergone weighting. The inverse transformation of this product is the desired correlation. Since the chirp slope is doubled, when the two transforms are multiplied, this product must be mixed with a spectrally-inverted chirp prior to inverse transformation.

the product. Figure 3.45b is the same thing with the last four traces expanded. In these figures all the last four traces were lined up. Figure 3.44c, however, shows the signals with their proper time relationships. The correlation spike is spaced the same distance from the DC transform spikes as they are from the center of the signals. There is an important thing to note here. Since these codes are not plus and minus one as is required for PN correlation (see Appendix M for the corresponding plot), the output correlation spike would normally emerge on a pedestal. However, to the trained eye, trace 5 of Figure 3.44b has undoubtedly been allowed to saturate. This saturation has essentially eliminated most of the DC level in the zero to one input codes so that the output correlation appears as though the codes had been plus and minus one's. The correlation spike is shown expanded in Figure 3.44d. Figures 3.44e and f show results equivalent to Figures 3.44a and c except that one of the codes has been summed to a sawtooth wave. Note that although the spectrum of this signal is now reaping in harmonics, the correlation output has not been overly harmed by the process. Thus the power of the matched filtering process is demonstrated.

Still another improvement can be made. As mentioned in Section 2.4, the reference signal need not be intentional time inverted. If the transform of the same signal as the expected signal to be received by the system is mixed by an rf and the sum term is retained by high pass filtering, then, when this transform is multiplied by the received signal spectrum, there will be a product term representing the product of the signal spectrum and the complex conjugated reference spectrum. This is depicted as a complex conjugation process in Figure 3.45. Figures

Figure 3.44: Performance of a product-of-transforms correlating receiver where the correlation is performed in the Fourier domain by multiplying the signal transform with the transform of its time complement.

(a) Trace 1: A 255-bit zero/one pseudo-random code (5 μs/div). Trace 2: The time complement of trace 1 (5 μs/div). Trace 3: The chirp-modulated Fourier transform of trace 1 (5 μs/div). Trace 4: The chirp-modulated Fourier transform of trace 2 (5 μs/div). Trace 5: The product of traces 3 and 4 (5 μs/div). Trace 6: The chirp-modulated inverse transform of trace 5 or the autocorrelation of trace 1 (5 μs/div). The saturation of the DC spike in trace 5 has essentially produced the autocorrelation of a plus/minus (not zero/one) 255-bit pseudo-random code.

(b) Traces 1 and 2: The same as traces 1 and 2, respectively, of (a). Traces 2 thru 6: The same as traces 2 thru 6, respectively, of (a) except on a .5 μs/div scale.

(c) This figure displays the same signals shown in (a) except that they are being displayed in proper time perspective (20 μs/div all). The transform main lobes in traces 3 and 4 can be seen to arise about 60 μs from the input signal centers. The autocorrelation spike in the last trace arises about 75 μs after these transforms.

(d) The autocorrelation spike (.5 μs/div).

(e) This figure is identical to (a) except that the pseudo-random code in trace 1 of (a) has been corrupted by a 160 Khz saw-tooth signal whose Fourier components can be seen on either side of the main lobe of the signal transform (the fundamental about 2.3 μs to either side of DC). The correlation in trace 6 has changed very little due to this corruption of the signal. Little hint of the existence of the saw-tooth Fourier components can be seen in the product transform of trace 5.

(f) This figure is the same as (e) except that the signals are being displayed in proper time perspective (20 μs/div all). It should be noted that the correlation is undoubtedly heavily distorted since the transform multiplication is being performed using a mixer. This device does not produce a linear multiplication unless one of its inputs is always under saturation. This cannot occur in the performance of the transform product. (See Fig. 3.64.)

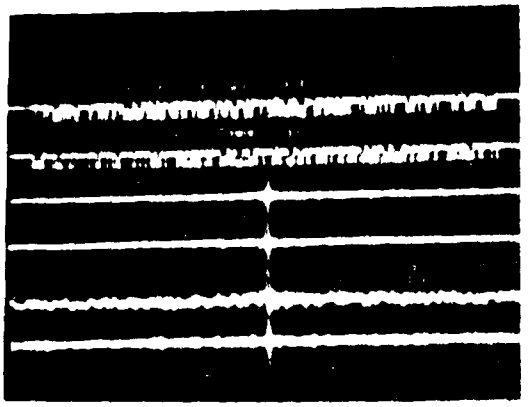

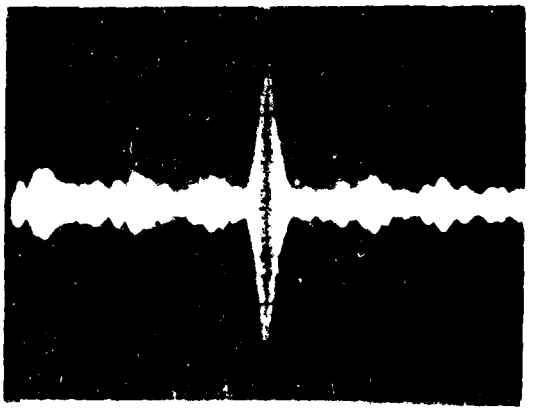

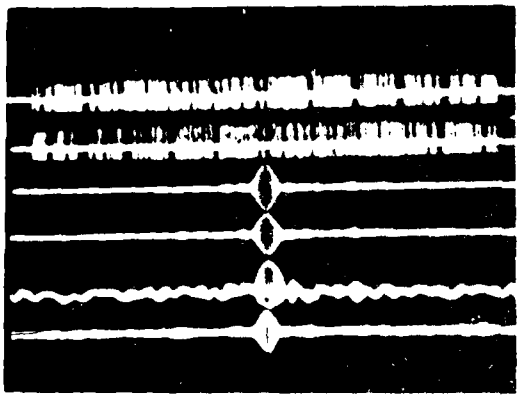

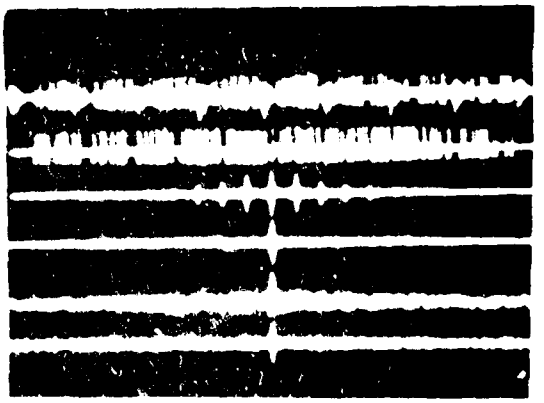

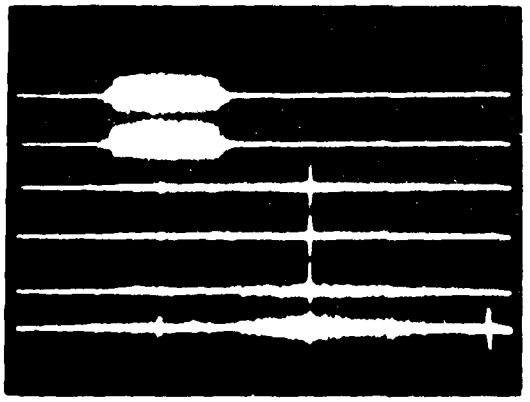

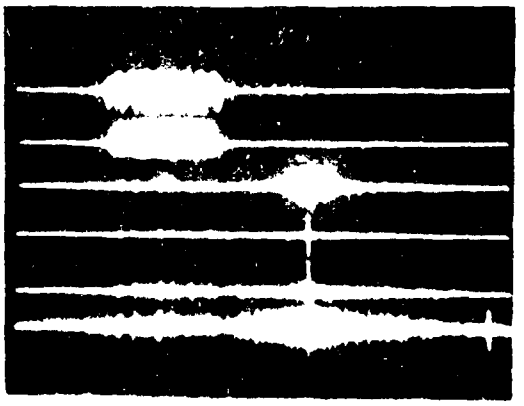

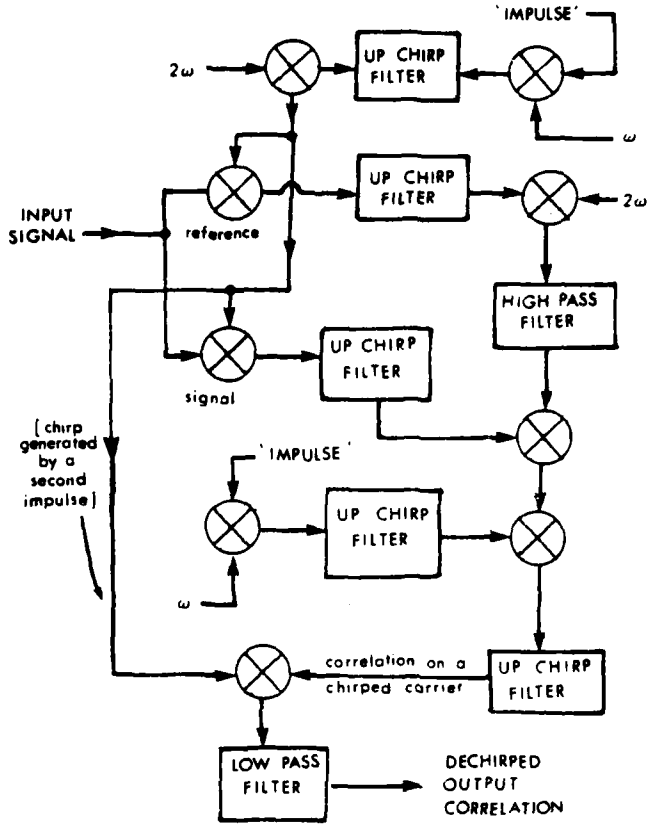

FIGURE 3.45

Figure 3.45: The block diagram of a product-of-transform system utilizing complex conjugation thereby eliminating the need to generate the time complement of the input signal. The same signal expected at the input to the receiver is also used as the reference signal. This signal is Fourier transformed and then mixed with an rf and filtered prior to the multiplication with the received signal's transform. This process effectively complex conjugates the reference signal's transform thereby producing the Fourier transform of a time complemented version of this reference.

3.46a to n demonstrate how well a correlating receiver of this type performs the desired correlation. Figure 3.46a shows an input square pulse and the output triangular correlation obtained. Figure 3.46b shows this same correlation after it has been coherently dechirped since the correlation is obtained on a chirped carrier. Figures 2.36c thru n are correlations of different types of square pulse inputs. Figures 3.47a thru e demonstrate further the correlating ability of the system. Here is a sequence of ambiguity functions obtained for a square pulse using this system. The different figures show the same function on different scales.

Figures 3.48a thru f show the correlations obtained for a seven bit Barker code sequence. Figure 3.48a shows the input Barker code modulated by a low frequency carrier (relative to the chirp filter center frequency) and the output correlation. Figure 3.48b shows the correlation and its envelope obtained by coherently detecting the output using a chirp and low pass filtering. Figure 3.48e shows this on a different scale. Figure 3.48d shows the correlation only partially detected by removing only the quadratic phase variation. Figure 3.48f shows the output detected correlation for a positive bit (where every 7 bit Barker code is a bit of a signal) in the first trace and a negative bit in the second trace. Trace 3 is the output when the bits are allowed to change at a Kilohertz rate. Figure 3.48c shows the correlation when the input is shifted from plus and minus one (first trace) to zero and one (last trace). The upper and lower sidebands of this carrier modulated code are shown in Figure 3.49a where it is seen that this center lobe compares well

Figure 3.46: Autocorrelations obtained using the product-of-transforms correlating receiver. The same uncorrupted signal is used for both the input signal and the reference.

(a) Trace 1: A 16 μs wide square pulse (10 μs/div). The chirp-modulated autocorrelation of trace 1 obtained by passing the product of the signal transform and complex-conjugated reference transform through a chirp filter (< 10 μs/div uncalibrated).

(b) The same as (a) except that the autocorrelation has been coherently dechirped leaving only an rf carrier.

(c) Trace 1: A 5.6 μs square pulse (10 μs/div). Trace 2: The autocorrelation of trace 1 obtained by inverse transformation of a product of transforms as are all the remaining autocorrelations in this figure (10 μs/div).

(d) Trace 1: A 1, -1 pulse train (10 μs/div). Trace 2: The autocorrelation of trace 1 (10 μs/div).

(e) Trace 1: A 1, -1, 1 pulse train (10 μs/div). Trace 2: The autocorrelation of trace 1 (10 μs/div).

(f) Trace 1: A 1, -1, 1, -1 pulse train (10 μs/div). Trace 2: The autocorrelation of trace 1 (10 μs/div).

(g) Trace 1: A 1, -1, 1, -1, 1 pulse train (10 μs/div). Trace 2: The autocorrelation of trace 1 (10 μs/div).

(h) Trace 1: A 1, -1, 1, -1, 1, -1 pulse train (10 μs/div). Trace 2: The autocorrelation of trace 1 (10 μs/div).

(i) Trace 1: A 1, 0, 1 pulse train (10 μs/div). Trace 2: The autocorrelation of trace 1 (10 μs/div).

(j) Trace 1: A 1, 0, 1, 0, 1 pulse train (10 μs/div). Trace 2: The autocorrelation of trace 1 (10 μs/div).

(k) Trace 1: A 1, 0, 1, 0, 1, 0, 1 pulse train (10 μs/div). Trace 2: The autocorrelation of trace 1 (10 μs/div).

(l) Trace 1: A 1, 0, 1, -1, 0, -1 pulse train (10 μs/div). Trace 2: The autocorrelation of trace 1 (10 μs/div). Trace 3: A 1, -1, 0, 0, 1, -1 pulse train (10 μs/div). Trace 4: The autocorrelation of trace 3 (10 μs/div).

(m) Trace 1: A 1, 0, 1, -1, 0, -1, 1 pulse train (10 μs/div). Trace 2: The autocorrelation of trace 1 (10 μs/div). Trace 3: A 1, 0, 1, 0, 1, -1, 1 pulse train (10 μs/div). Trace 4: The autocorrelation of trace 3 (10 μs/div).

(n) Trace 1: A -1, 0, -1, 1, -1 pulse train (10 μs/div). Trace 2: The autocorrelation of trace 1 (10 μs/div). Trace 3: A -1, 0, 0, 1, -1 pulse train (10 μs/div). Trace 4: The autocorrelation of trace 3 (10 μs/div). Note that all thecorrelations are cchip modulated. Furthermore, since the sum of the input signal duration and the correlation cannot exceed about 100 μs, then any correlations due to signals greater than about 33 μs wide are not accurate over their entire durations. For example, the signal in trace 3 of (m) is 40 μs wide so that its correlation should be 80 μs wide. However, due to the finite width (100 μs) of the chirp device impulse responses, the correlation is accurate over only 60 μs.

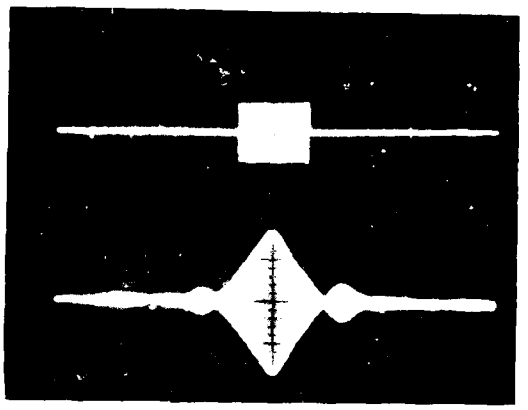

Figure 3.46a

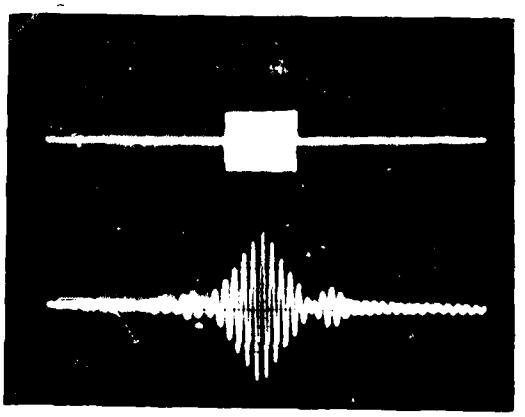

Figure 3.46b

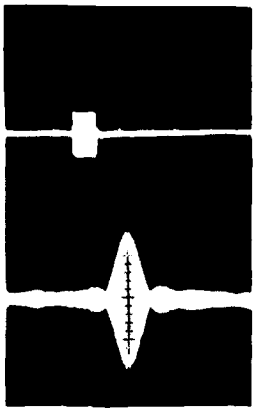

Figure 3.46c

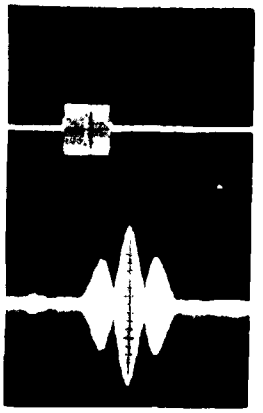

Figure 3.46d

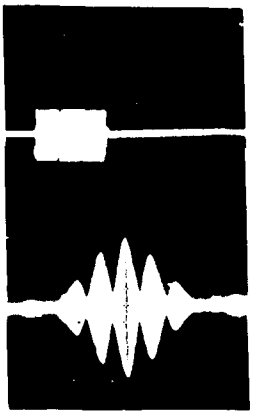

Figure 3.46e

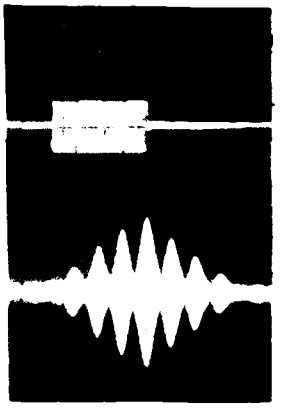

Figure 3.46f

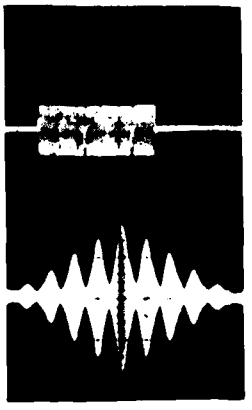

Figure 3.46g

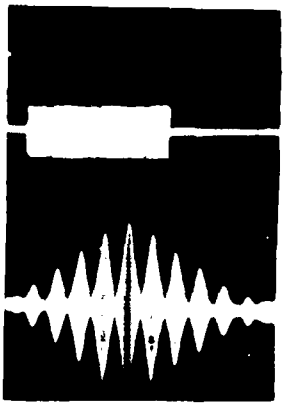

Figure 3.46h

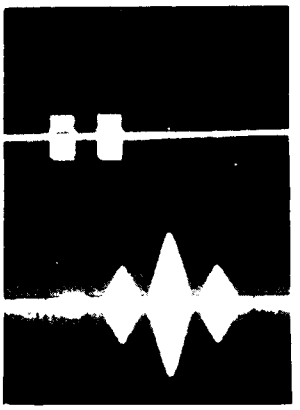

Figure 3.46j

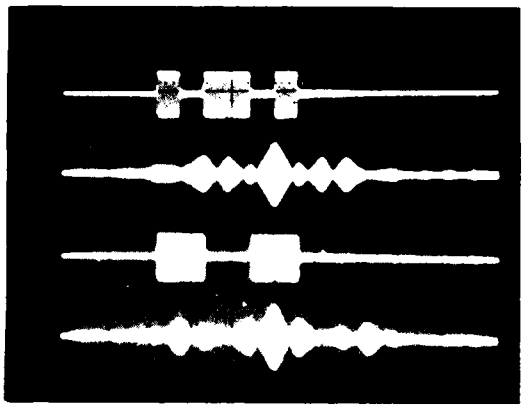

Figure 3.46l

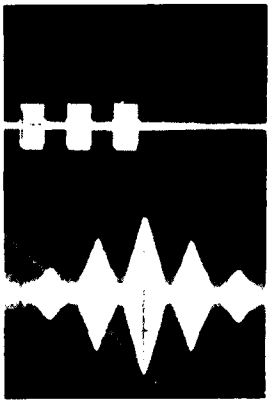

Figure 3.46k

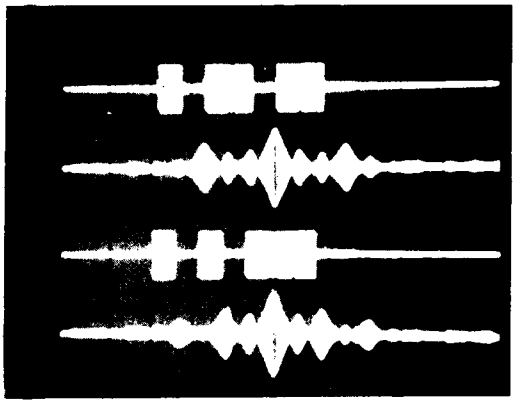

Figure 3.46m

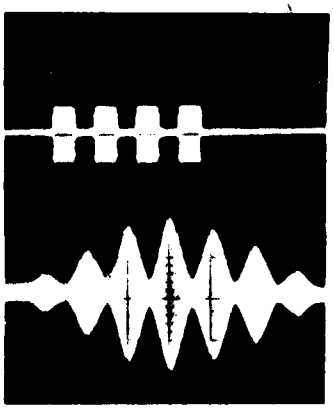

Figure 3.46k

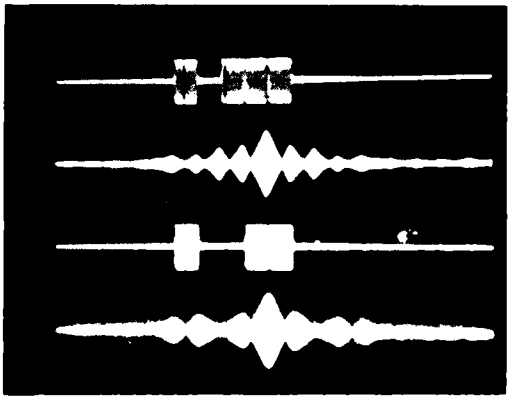

Figure 3.46n

Figure 3.47: Autoambiguity functions obtained using the product-of-transforms correlating receiver.
(a) thru (e) are autoambiguity functions of a 30 μs square pulse shown on different time and frequency scales.
(a) 10 μs/div along the delay axis (horizontal) and about 28 Khz/div along the Doppler axis (vertical).
(b) 10 μs/div along the delay axis and about 37 Khz/div along the Doppler axis.
(c) 10 μs/div along the delay axis and about 61 Khz/div along the Doppler axis.
(d) 10 μs/div along the delay axis and about 100 Khz/div long the Doppler axis.
(e) 20 μs/div along the delay axis and about 37 Khz/div along the Doppler axis. The first null of the sinx/x along the Doppler axis corresponds to a frequency given by the inverse of the pulse width or about 33 Khz.

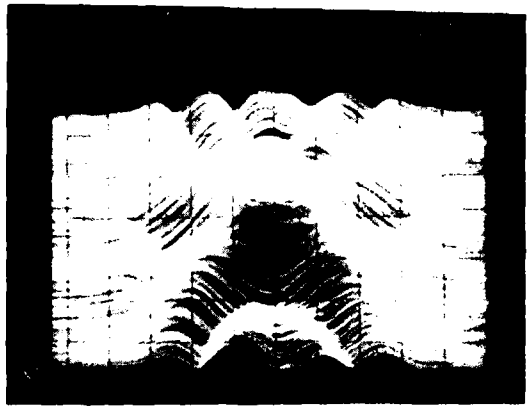

Figure 3.47a

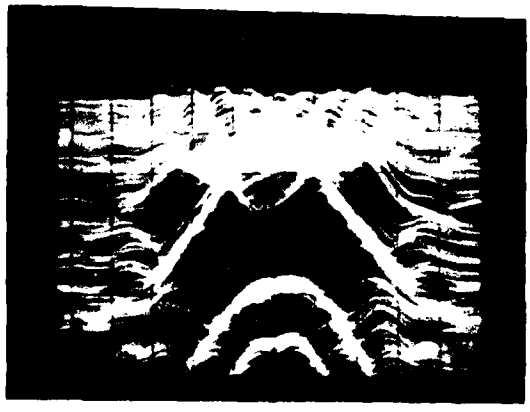

Figure 3.47b

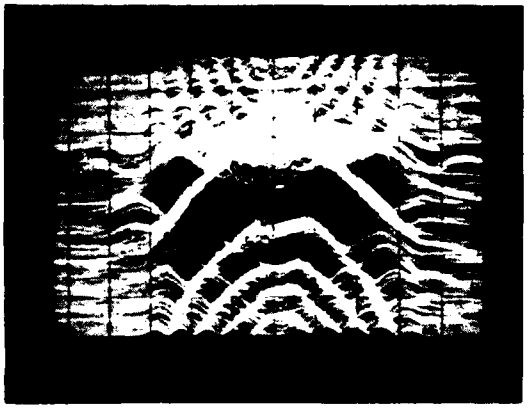

Figure 3.47c

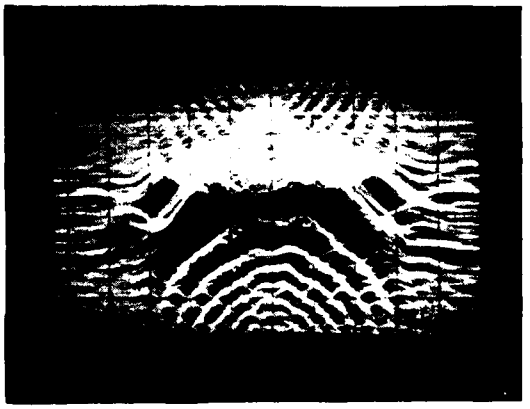

Figure 3.47d

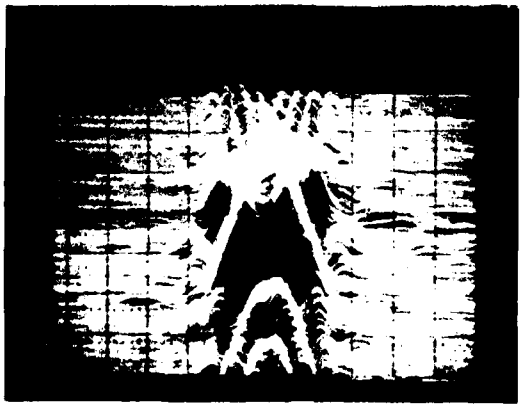

Figure 3.47e

Figure 3.48: Seven-bit Barker code correlations obtained using the product-of-transforms correlating receiver.

(a) Trace 1: (Upper right inset) A 23 μs seven-bit Barker code (5 μs/div). Trace 2: The chirp-modulated autocorrelation of trace 1 (5 μs/div). This correlation is the required 46 μs in duration with a seven-to-one main lobe to sidelobe ratio. The 7-bit Barker code in trace 1 is modulated onto a 2.4 Mhz carrier. Due to this carrier the transform between the positive and negative spectrums spans about 68 μs. Only one of these spectrums, however, is required to obtain the correlation if the code is narrowband enough so that there is little interference between the two.

(b) Trace 1: The chirp-modulated autocorrelation of the 7-bit Barker code (10 μs/div). Trace 2: The coherently dechirped version of trace 1 (10 μs/div). This correlation has been detected down to baseband.

(c) This figure demonstrates the result of level shifting the input code. Trace 1: (Upper left inset) The seven-bit Barker code (50 μs/div). Trace 2: The chirp-modulated Fourier transform of trace 1 (10 μs/div). Trace 3: (Middle left inset) The 7-bit Barker code level shifted so that the positive bits are half the size of the negative bits (50 μs/div). Trace 4: The chirp-modulated Fourier transform of trace 3 (10 μs/div). Trace 5: (Lower left inset) The 7-bit Barker code with no positive bits (50 μs/div) (fully shifted). Trace 6: The chirp-modulated Fourier transform of trace 5 (10 μs/div).

(d) Trace 1: The chirp-modulated autocorrelation of the 7-bit Barker code (5 μs/div). Trace 2: The coherently dechirped version of trace 1 (5 μs/div). The correlation has been detected by a delayed version of the chirp modulation producing a carrier-modulated correlation. The frequency of the carrier is given by the delay between the chirps multiplied by the chirp slope in Hz/sec (7×10^{10} Hz/sec).

(e) The same as (d) except that the correlation has been detected to baseband in the second trace.

(f) Trace 1: The coherently dechirped correlation of a positive 7-bit Barker code (10 μs/div). Trace 2: The coherently dechirped correlation of a negative 7-bit Barker code (10 μs/div). (All the code bits have been inverted or the carrier-modulated bits have been shifted by 180°.) Trace 3: The coherently dechirped correlation of the 7-bit Barker code with the code polarity being continuously changed.

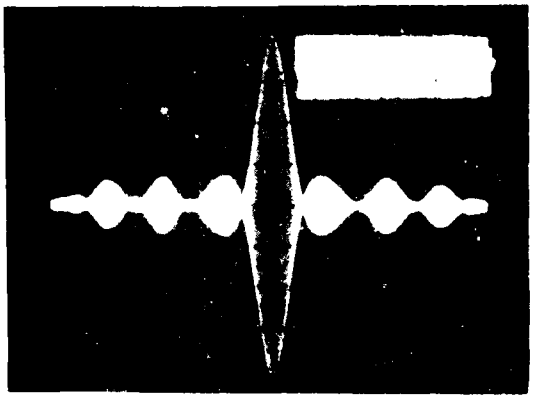

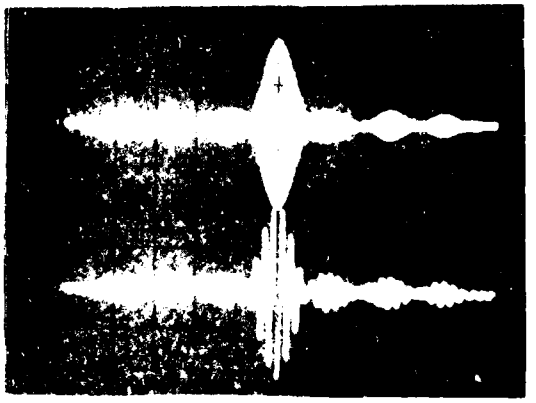

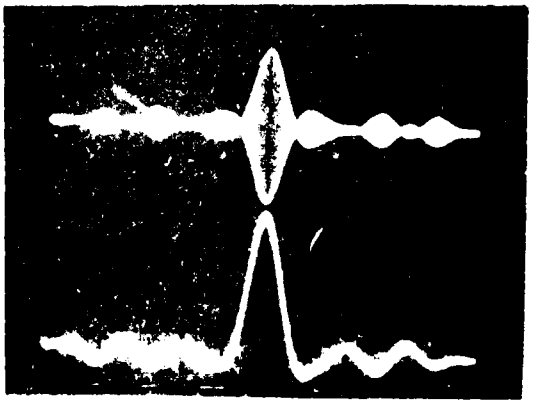

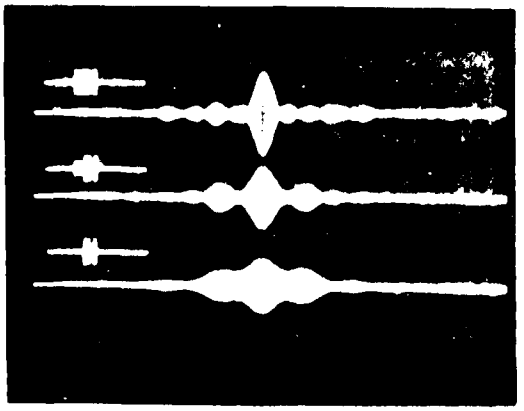

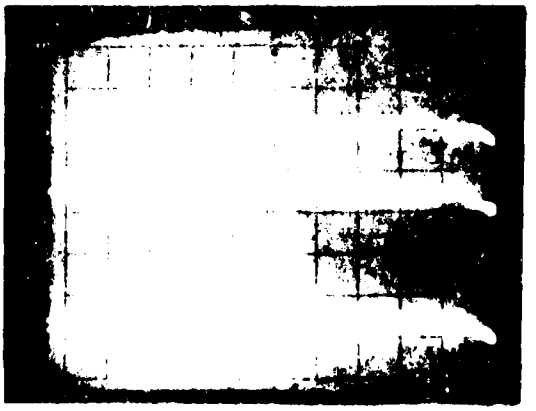

with the computed transform. Figure 3.49b shows the transform of the zero-one code.

Figures 3.50a thru f show the intentional addition of monochromatic noise to the signal resulting in varying degrees of distortion to the output correlation. In all these figures the noise spike is gated from the spectrum and the undistorted correlation is obtained. Figures 3.50d to f show small to large noise levels. In Figure 3.50f the signal was decreased to increase the effect of the noise. Figures 3.50a and b show correlation distortion that is a function of the noise frequency. Figure 3.50c shows spectrum gating and its effect on the detected correlation output.

Probability of error data was obtained using such a product of transforms correlating receiver. At first the required Gaussian noise was obtained by cascading amplifiers. Figure 3.51a shows in the first trace that this wasn't adequate. The signal transform fell near this null in the noise spectrum. When a diode noise circuit was used the spectrum given by the second trace was obtained. Figure 3.51b shows the magnitude non-uniformity of the spectrum analyzer, where constant magnitude tones were used. Figure 3.52a shows the uniformity of the Fourier transform over one-half the spectrum beginning at [illegible]. Each marker was due to a constant magnitude tone. The spacing between markers represents half a megahertz. Figure 3.52b shows the signal spectrum, the

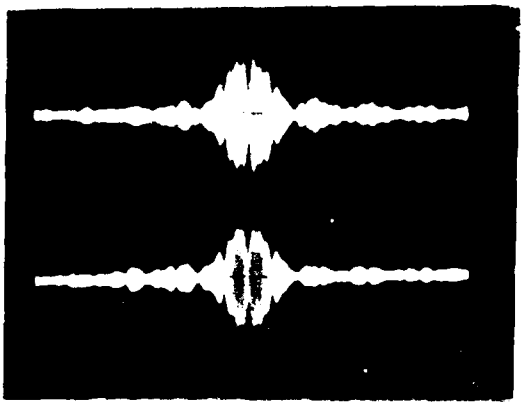

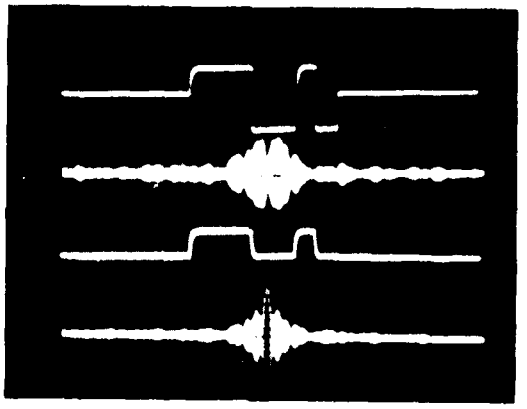

Figure 3.49: The 7-bit [illegible] waveforms.
(a) Trace 1: The chirp-[illegible]ive spectrum of the 7-bit Barker code (2 μs/div). The [illegible] was 50 μs wide and the [illegible] were individually [illegible] time interval. The [illegible] the 7.1 μs width of [illegible] μs)(7x10^10))^-1). Trace 2: The [illegible]ive spectrum of the 7-bit Barker code (2 μs/div).
(b) Trace 1: [illegible] 7-bit Barker code [illegible]. Trace 2: The chirp-[illegible] (2 μs/div). Trace 3: The [illegible] 7-bit Barker code [illegible]. Trace 4: The [illegible] (2 μs/div).

Figure 3.50: Filtering by time gating the Fourier transform and its effect on the output 7-bit Barker code correlation. The Fourier transforms in all these figures and the monochromatic noise can be seen in Fig. 3.33a, traces 3 and 4. Only one of the spectrums is utilized for these results (i.e. the positive spectrum). (a) thru (c) demonstrate the effect on the correlation when the jamming frequency is varied. (d) thru (f) are intended to demonstrate the effect of the jammer for various strengths of the input signal.

(a) Trace 1: The chirp-modulated Fourier transform of the 7-bit Barker code with the fundamental jammer component seen to the right of its main lobe (5 μs/div). Trace 2: The chirp-modulated autocorrelation of the 7-bit Barker code (10 μs/div). (The code duration is 23 μs for all these figures.) Trace 3: The transform of trace 1 gated by trace 4 (5 μs/div). Trace 4: The transform time gate (5 μs/div). Trace 5: The autocorrelation following the time gating of the transform (10 μs/div). Note that the correlation has undoubtedly improved due to the removal of the jammer fundamental component.

(b) This figure is the same as (a) except that the jammer frequency has been increased.

(c) This figure is the same as (a) except for a change in jammer frequency, the gating of the fundamental jammer component along with a parasitic component and the display of the autocorrelation in its envelope detected form. The correlation was poorly tuned in this figure.

(d) Trace 1: (Left) The chirp-modulated 7-bit Barker code Fourier transform positive spectrum (there is a 2.6 Mhz carrier on the code) (5 μs/div). (Right) The chirp-modulated autocorrelation of the code (10 μs/div). Trace 2: The same as trace 1 except with the jammer. Trace 3: The same as trace 2 with the jammer fundamental component gated out.

(e) and (f) are the same as (d) except that the signal is successively decreased in amplitude relative to the jammer and the gating function is displayed. Note the improvement due to gating in each case.

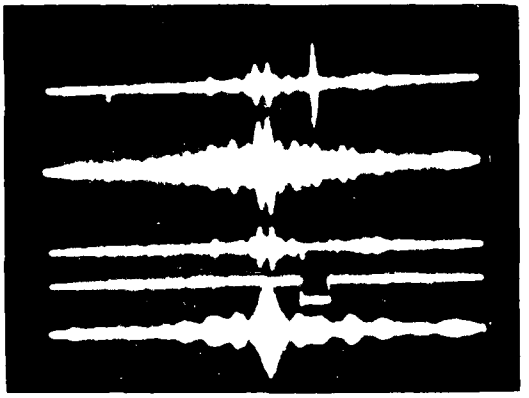

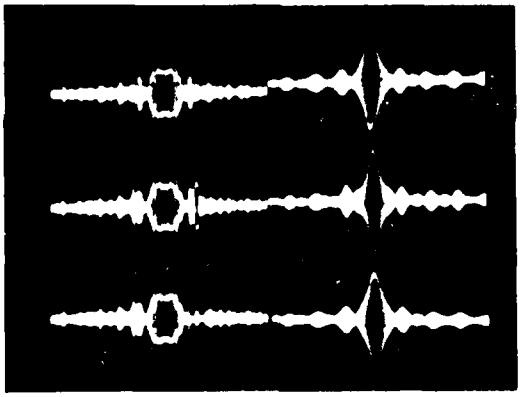

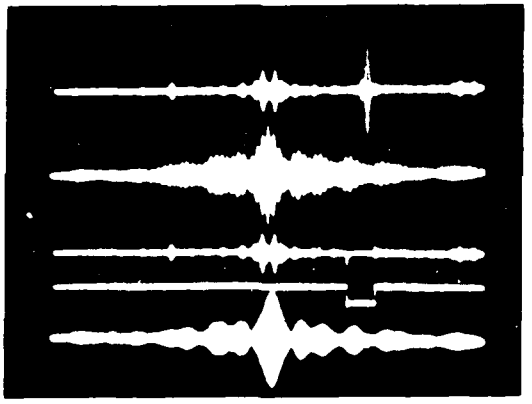

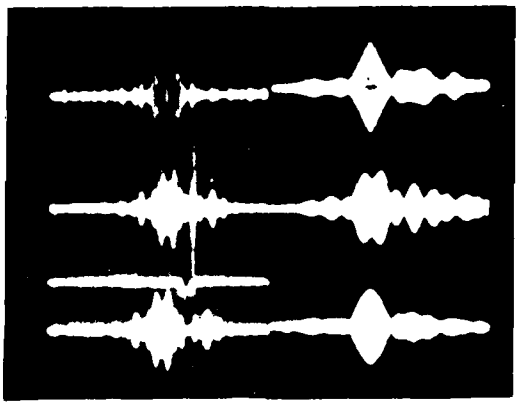

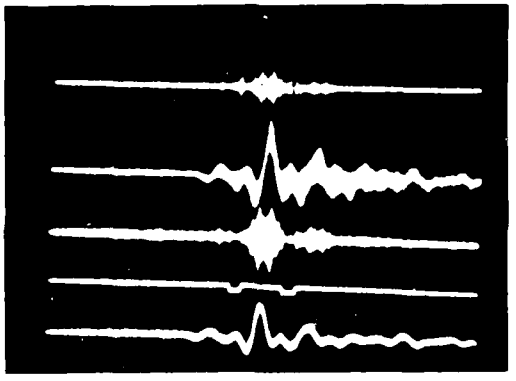

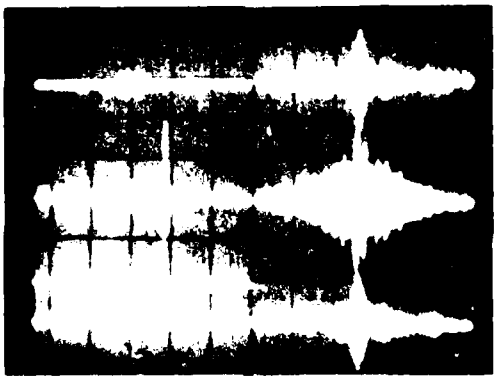

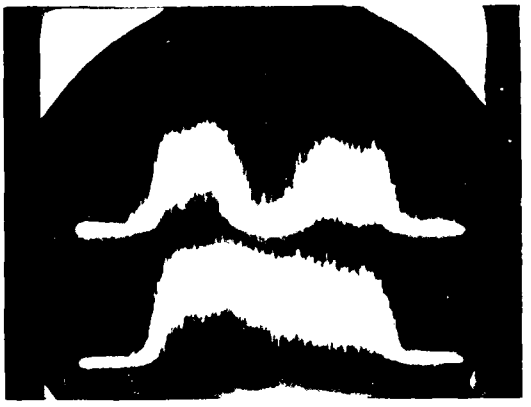

Figure [illegible]

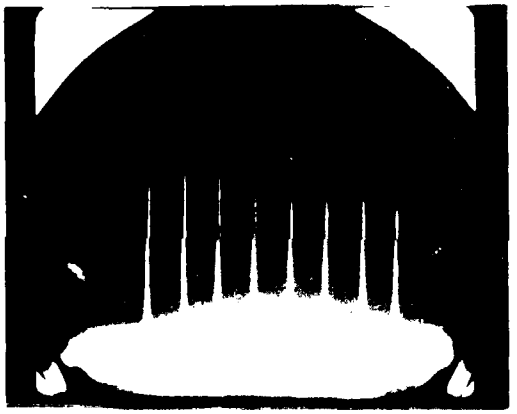

[illegible]

Figure 3.51: The spectrum of the [illegible] of the probability [illegible] correlating receiver.

(a) Trace 1: This was the noise spectrum obtained during the preliminary [illegible] period where the Gaussian noise was [illegible] high gain amplifiers (2 [illegible]). The [illegible]-pass nature of the amplifiers prohibited [illegible] further noise generation applications. [illegible] spectrum coincided with the [illegible] of the noise spectrum.
Trace 2: The noise spectrum obtained when the Gaussian noise was generated [illegible] specifically designed for noise generation [illegible].

(b) Markers [illegible] amplitude [illegible] spectrum [illegible] the spectrum [illegible]. [illegible] the [illegible] [illegible].

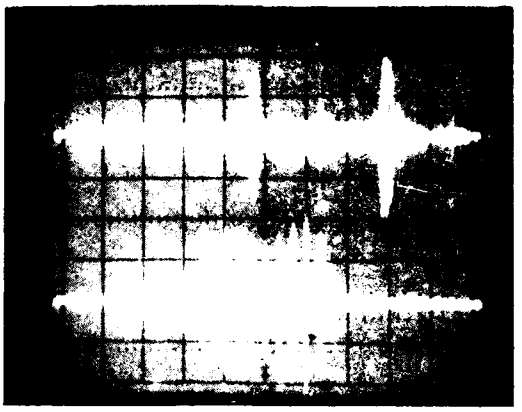

Figure 3.52a

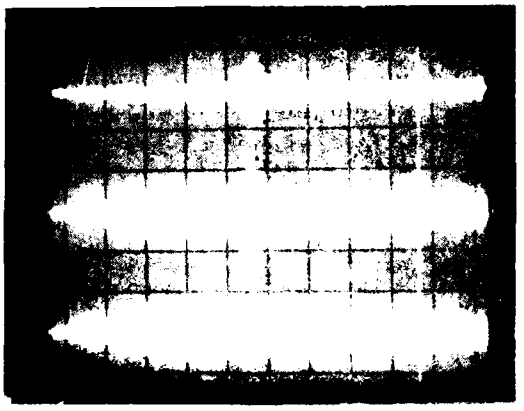

Figure 3.52b

Figure 3.52: The uniformity of the [illegible] and the Barker [illegible] spectrum with the [illegible].

(a) Trace 1: The [illegible] transform of the 7-bit Barker [illegible]. Trace 2: Marker [illegible] to constant [illegible] frequency by [illegible] markers showing [illegible] portion of the [illegible] 7-bit Barker code transform [illegible]. The [illegible] variation over [illegible] falls roughly [illegible] 10 dB down [illegible].

(b) Trace 1: The [illegible] Barker code [illegible]. Trace 2: The [illegible] input. [illegible] Fourier [illegible].

signal and noise spectrum and just the noise spectrum in the three traces. The probability of error data obtained using this correlating receiver, along with level detection and error counting circuitry, is shown in Figure 3.53. Curve A is the theoretical matched filter curve. Curve B is the response of this receiver which tends to stay within a half dB of the ideal curve over a wide range. Curve C was obtained for a jammer to signal level of about 18 dB. (The error rate was a sensitive function of the jammer frequency in this case.) Curve D was obtained by gating the jammer from the Fourier transform.

An attempt was made to obtain similar data for a continuous system. A preliminary continuous Fourier transform system is shown in Figure 3.54. Essentially, a continuous signal is broken up into two alternating streams by mixing with two alternating chirp streams. The individual streams are transformed separately. In this case the transform streams were summed together before being inverse transformed, due to a lack of chirp devices. Although this led to interference between adjacent transforms, it was enough to prove the principle at that time. Figures 3.55a thru f give an indication of the performance of this system. Figure 3.55a shows a continuous data stream followed by the two alternating chirp streams, the two alternating transform streams, the summed transform stream and the inverse transform of this. Figures 3.55b and c show expanded displays of the input and output for this system. Figure 3.55c contains a 13 bit code for every bit of the signal. Figure 3.55d shows the different transforms obtained for different slices of the signal. The output detail can be seen in Figure 3.55e where the code

Figure 3.53: The probability-of-error performance of the product-of-transforms correlating receiver. (a) Curve A is for optimum detection by matched filtering in the presence of white Gaussian noise. Curve B is the performance of the correlating receiver in the absence of jamming. Curve C shows the degradation as a result of a constant jammer level of 16 dB relative to the signal at a signal-to-noise ratio of about 13 dB. Since the noise was held constant and the signal decreased to change the signal-to-noise ratio, then the jammer-to-signal ratio increased as the signal-to-noise ratio decreased. For these curves the code carrier was set at exactly 2 Mhz and the jammer was set at 2.069 Mhz, where the greatest error seemed to occur. The code length was 28 μs, the jammer was a constant tone of 3 vpp and 50 s duration and the noise was kept at a level of .375 URMS. Since the single-sided noise bandwidth was about 6 Mhz, the noise spectral density was $\eta_o = (.375)^2/(50)(6\text{x}10^6) = 4.7\text{x}10^{-10}$ joules/hz and the signal energy per bit E was given by $E = (V_{peak})^2(28\text{x}10^{-6})/100 = (2.8\text{x}10^{-7})(V_{peak})^2$ joules where V_{peak} is the peak voltage of the Barker code and a bit is considered as an entire code. The signal-to-noise ratio was varied by varying V_{peak}. Curve D shows the result of gating out essentially the main lobe of the jammer which was about .6 μs wide. The gating produced an appreciable improvement. Note that curve C was obtained by varying the jammer frequency to produce the greatest amount of error while curve D was obtained by varying the gate position and width to effect the greatest improvement. Since the Barker code polarity was controlled by a 2Khz pseudo-random code that repeated once every few hours, these results were obtained by counting the errors after every count of 1,048,575 which took 8.7 minutes per point. The repetition cycle of 500 μs was chosen to leave plenty of time between individual correlations. Each pseudo-random code bit lasted long enough so that it could be directly compared with the pulse polarity obtained upon threshold detecting the output correlation peak. Any discrepancies between the proper polarity and that obtained from the detection process produced a pulse from the logic circuitry that incremented the count in a counter. Latches were used to pick up the error count after bit counts of powers of two-minus one. The width of the correlation-peak window could be varied. Only during the time period of this window would discrepancies be looked for. The threshold level of the correlation threshold detector could also be varied, however, this was always set to zero (since the output was either plus or minus). (b) Error counting circuitry. The correlation is zero-level detected and its peak value is compared to the input bit used to generate the correlation. An error triggers a counter and the count is regularly latched and displayed. (c) The system used in the error analysis. An extremely long PN code has every bit modulated by a seven-bit Barker code and is correlated by this code in the product-of-transforms correlating receiver.

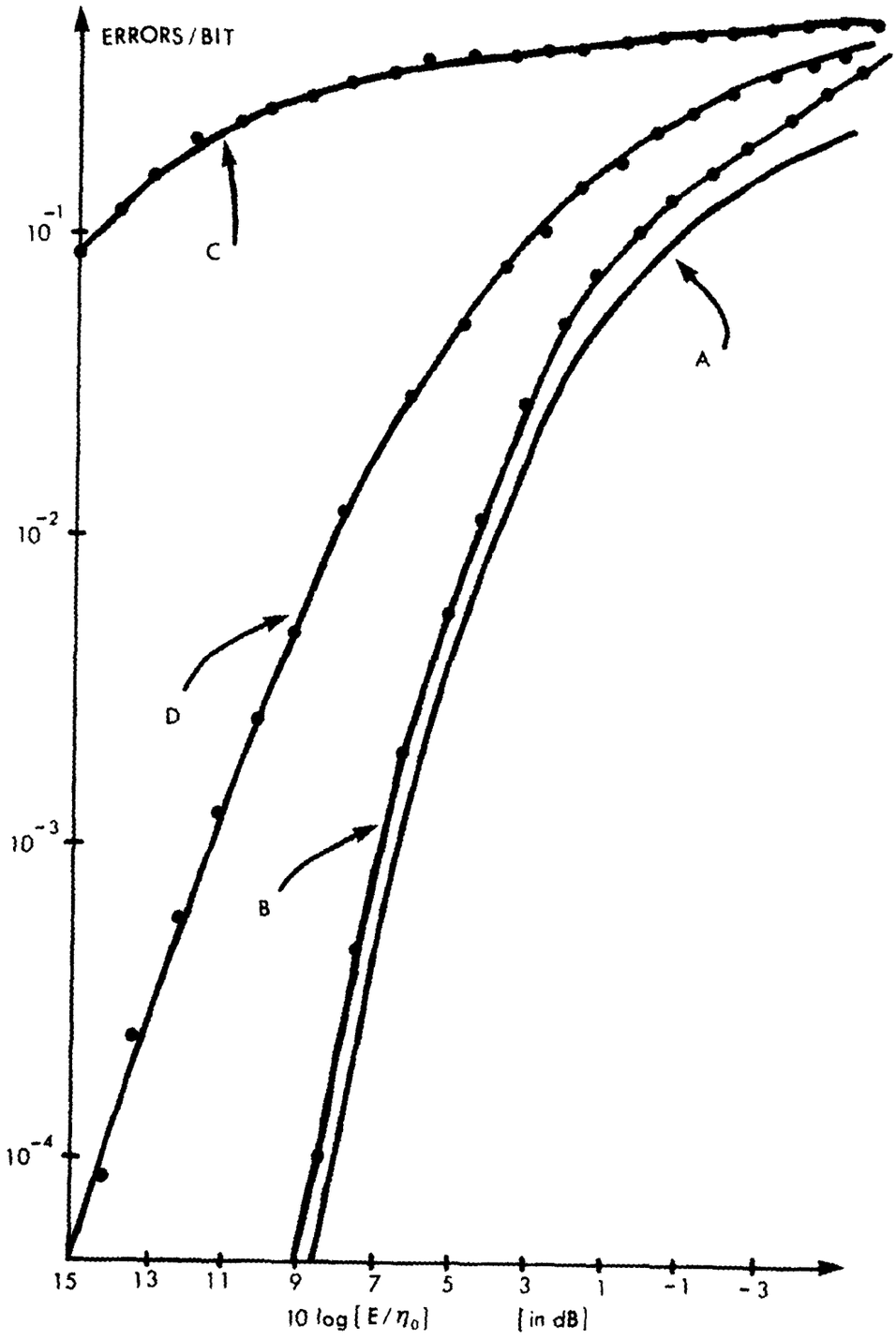
ERRORS / BIT
10^{-1}
10^{-2}
10^{-3}
10^{-4}
C
A
D
B
15
13
11
9
7
5
3
1
-1
-3
10 log [E/η_o] [in dB]

FIGURE 3.53 a

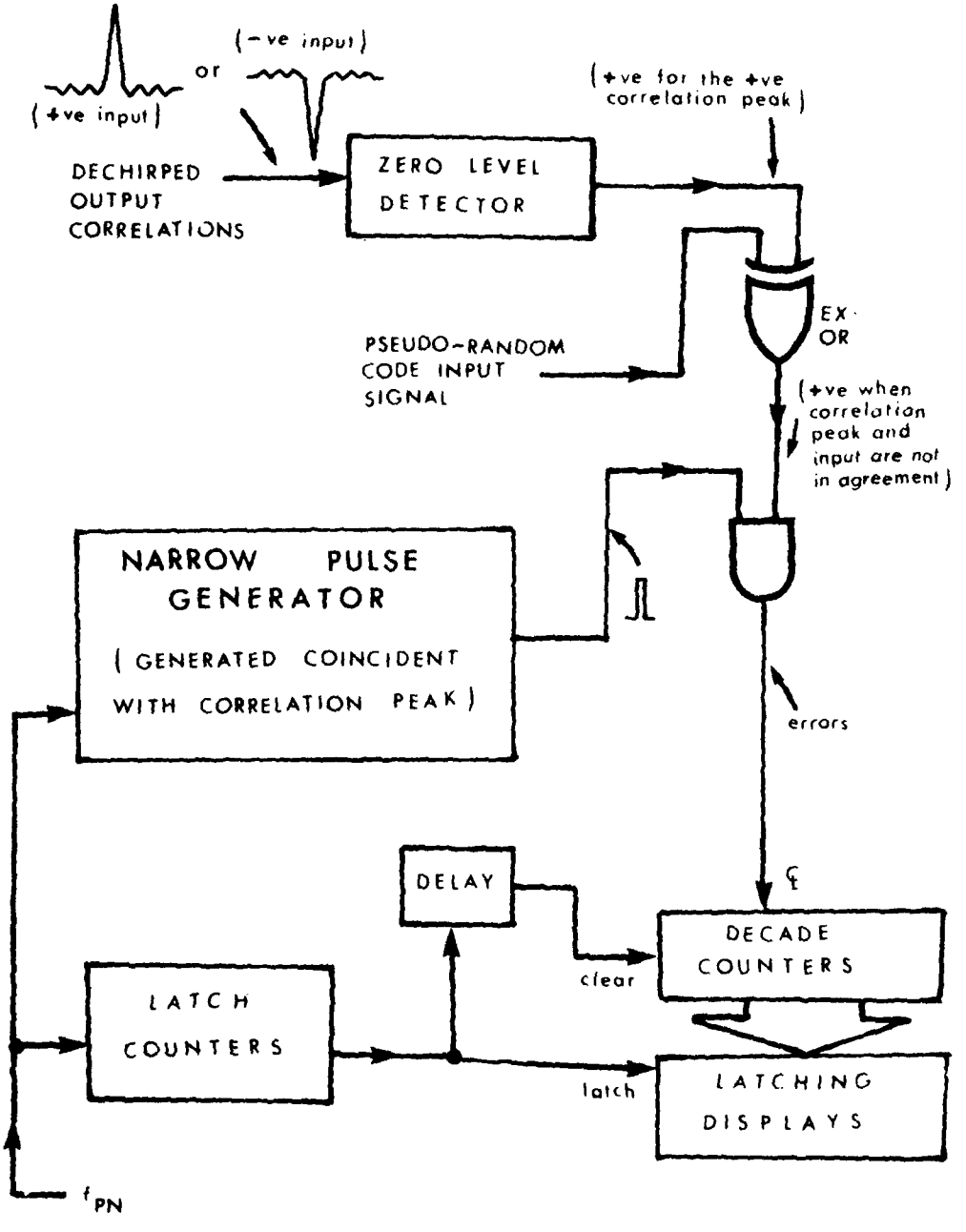
(+ve input)
or
(-ve input)
DECHIRPED OUTPUT CORRELATIONS
ZERO LEVEL DETECTOR
(+ve for the +ve correlation peak)
EX-OR
PSEUDO-RANDOM CODE INPUT SIGNAL
(+ve when correlation peak and input are not in agreement)
NARROW PULSE GENERATOR
(GENERATED COINCIDENT WITH CORRELATION PEAK)
errors
DELAY
DECADE COUNTERS
clear
LATCH COUNTERS
latch
LATCHING DISPLAYS
f_{PN}

FIGURE 3.53b

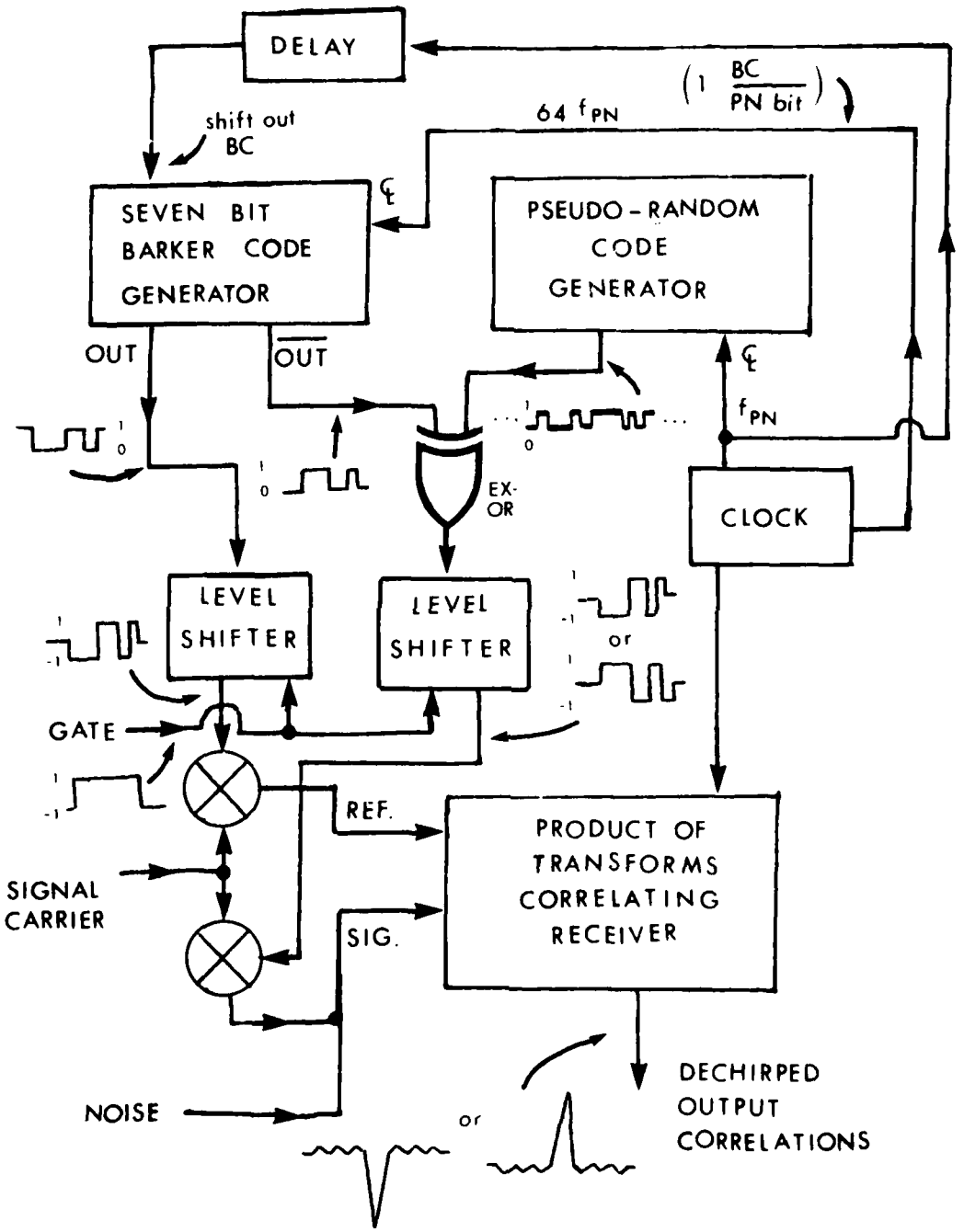
DELAY
shift out BC
64 f_{PN}
$\left(1 \frac{BC}{PN\ bit}\right)$
SEVEN BIT BARKER CODE GENERATOR
PSEUDO-RANDOM CODE GENERATOR
OUT
$\overline{OUT}$
f_{PN}
EX-OR
CLOCK
LEVEL SHIFTER
LEVEL SHIFTER
or
GATE
REF.
PRODUCT OF TRANSFORMS CORRELATING RECEIVER
SIGNAL CARRIER
SIG.
NOISE
or
DECHIRPED OUTPUT CORRELATIONS

FIGURE 3.53c

Figure 3.54: The block diagram of a system used to Fourier transform a continuous signal. Two identical chirp transform systems are used each handling 50% of the continuous signal. The signal is gated back and forth between the two systems by a flip-flop controlled gating process. This arrangement permitted adequate time before and after the signal to eliminate interference from neighboring portions of the signal. The gated time interval was set at anywhere from 50 to 80 μs leaving 20 to 50 μs for the Fourier transform (enough to handle 1.4 to 3.5 Mhz bandwidth signals). The system shown here summed the two transform streams and utilized a single device to inverse transform this continuous transform stream. This technique, however, can only work to an extent even when the transforms are gated thereby leaving appreciable space between one another. In this case, a large portion of the inverse transform will be a version of the original continuous signal, however, there will always be an appreciable amount of distortion over a percentage of this output due to interaction between transforms when convolving with the chirp device impulse response. If less of each transform is retained, the output is distorted over a smaller percentage of time (due to the transform interaction) but it also becomes more filtered due to this gating.

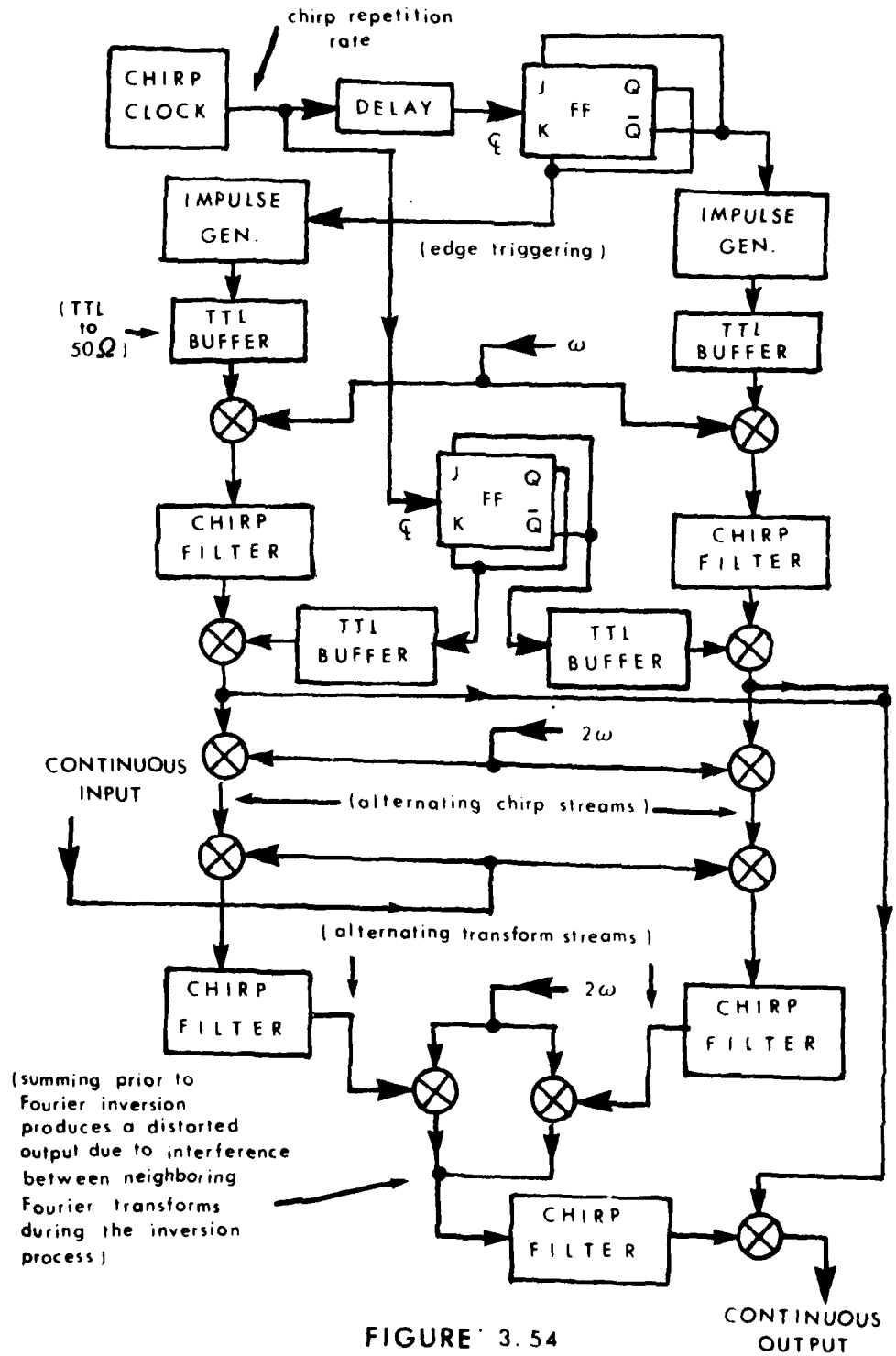
chirp repetition rate
CHIRP CLOCK
DELAY
J
K
FF
Q
$\bar{Q}$
IMPULSE GEN.
(edge triggering)
IMPULSE GEN.
(TTL to 50Ω)
TTL BUFFER
TTL BUFFER
ω
CHIRP FILTER
CHIRP FILTER
TTL BUFFER
TTL BUFFER
2ω
CONTINUOUS INPUT
(alternating chirp streams)
(alternating transform streams)
CHIRP FILTER
2ω
CHIRP FILTER
(summing prior to Fourier inversion produces a distorted output due to interference between neighboring Fourier transforms during the inversion process)
CHIRP FILTER
CONTINUOUS OUTPUT

FIGURE 3.54

for an individual bit can be seen at the output in trace 4. The first four traces of Figure 3.55f show the input signal, the output signal, the summed chirp streams (used for coherent detection of the output) and the transform stream. The last two traces are expanded versions of the input and output.

A continuous product of transforms correlating receiver was then built. Figure 3.56 shows the structure of this system which consists of two independent product of transforms systems. Figure 3.57 shows the timing of signals within this system and Figure 3.58 gives a detailed description of signal flow through the system. Figure 3.59a shows the two alternating input chirp modulation streams, the two alternating transform streams, the two alternating correlation streams and the summed correlation streams. Figure 3.59b shows expanded portions of the transform stream, the input codes and the output correlations. Figure 3.59c shows continuous correlation of a six pulse repetitive signal. Only part of the resulting eleven peak correlation can be seen. Figure 3.59d shows the correlation peaks when the system is mistuned in frequency in the first and third traces. Figure 3.59e shows the result when the chirp stream slopes do not match the chirp filter slopes (traces 1 and 3). Figure 3.59f shows filtering by time gating of the continuous signal transform stream. The transform for every coded bit has an upper and lower sideband due to the carrier that was included to facilitate the addition of noise to this signal in a microwave summer. The signal was decreased in size so that it could be overwhelmed by the noise. The first two traces are the transform stream and the correlation

Figure 3.55: Results using the system of Fig. 3.54.

(a) Trace 1: A baseband pseudo-random code input signal (200 μs/div). Trace 2: Alternating chirp stream ($\phi 1$) (50 μs/div). Trace 3: Alternating chirp stream ($\phi 2$) (50 μs/div). Trace 4: Alternating Fourier transform stream ($\phi 1$) (chirp modulated) (50 μs/div). Trace 5: Alternating Fourier transform stream ($\phi 2$) (chirp modulated) (50 μs/div). Trace 6: The sum of traces 4 and 5 (50 μs/div). Trace 7: The inverse transform of trace 6 (chirp modulated) (200 μs/div). Since the individual 80 μs segments of the input signal were of relatively small bandwidth, the interaction distortion between transforms is hard to see and somewhat integrated out in time by the oscilloscope. This is true since the chirp streams and input code ran asynchronously, although they have been individually locked for this photograph.

(b) Trace 1: The baseband pseudo-random code (200 μs/div). Trace 2: The chirp-modulated output of the system delayed by about 100 s from the input (200 μs/div).

(c) This figure is the same as (b) except that every bit of the pseudo-random code is a 13-bit plus/minus code. This increases the bandwidth of the signal and even with oscilloscope integration the degradation due to enhanced transform interaction can be seen.

(d) These traces show the Fourier transforms seen at consecutive locations along the Fourier transform stream (10 μs/div). Even though the input signal for any one transform was continually changing some synchronism was evident since every Fourier transform appeared to be different from the next.

(e) Trace 1: The coded pseudo-random baseband code (200 s/div). Trace 2: The chirp-modulated output of the system (200 μs/div). Trace 3: Trace 1 expanded to 2 μs/div. Trace 4: Trace 2 expanded to 2 μs/div. Note that the codes for every pseudo-random code bit are clearly seen.

(f) Trace 1: The coded pseudo-random baseband code (200 μs/div). Trace 2: The chirp-modulated output of the continuous transformation and inverse transformation system (200 μs/div). Trace 3: The summation of the two alternating chirp streams (200 μs/div) used for coherent detection of trace 2. Trace 4: The chirp-modulated Fourier transform stream (the summation of the two channels) (200 μs/div). Trace 5: Trace 1 expanded to 10 μs/div. Trace 6: Trace 2 expanded to 10 μs/div where the individual codes of each bit can be discerned.

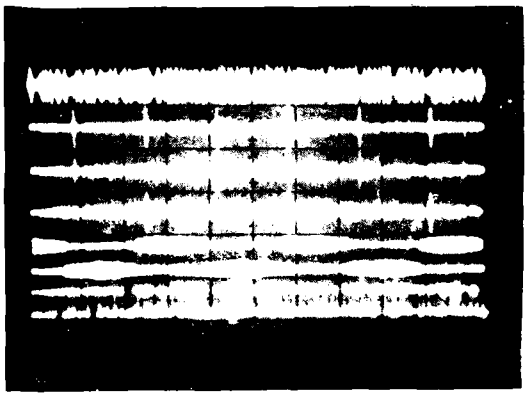

Figure 3.55a

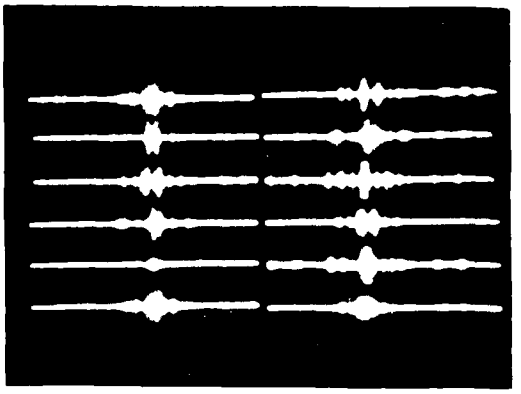

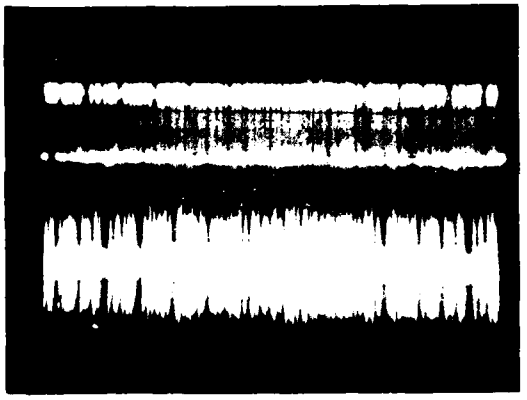

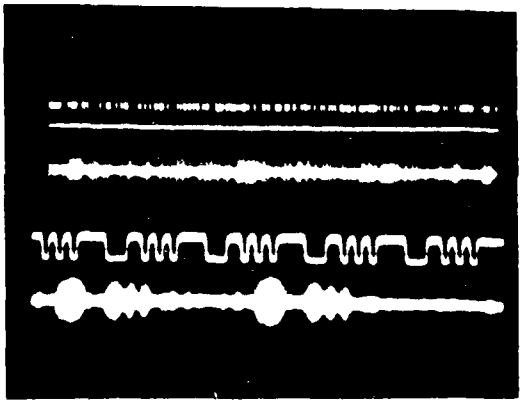

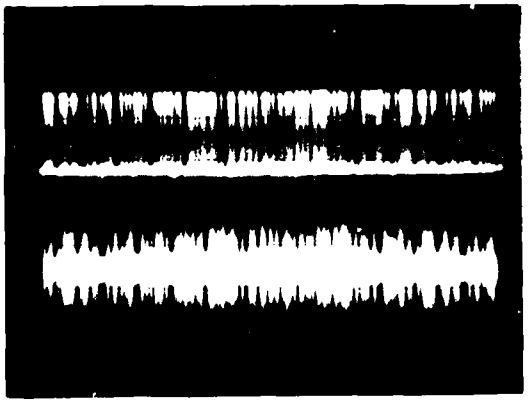

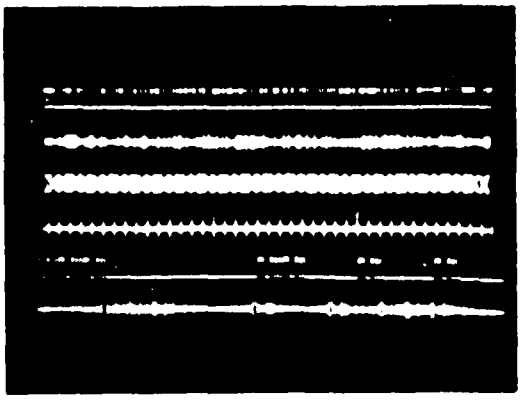

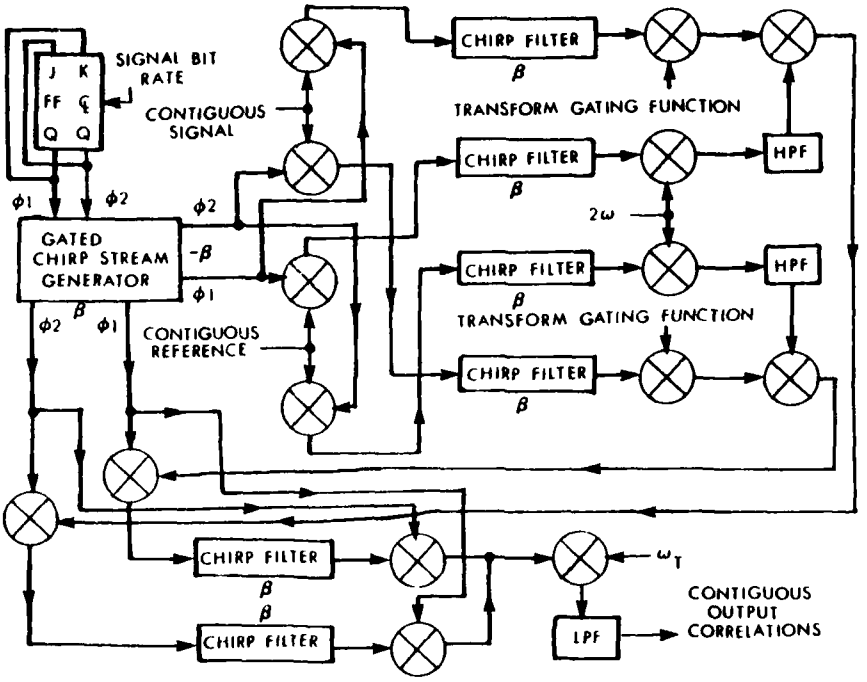

FIGURE 3 56

Figure 3.56: The block diagram of a continuous product-of-transforms correlating receiver. This system produces a continuous stream of output correlations by processing every other coded bit of the input signal in one system and the remaining coded bits in another identical system. By 'ping-ponging' between two systems in this fashion, streams of 50% duty cycle are processed to produce alternating correlation streams which become summed at the system output. Both of the identical halves of the receiver employ complex conjugation thereby eliminating the need for generation of the code time complement. The product transforms from the two halves of the system are separately inverse transformed before summation.

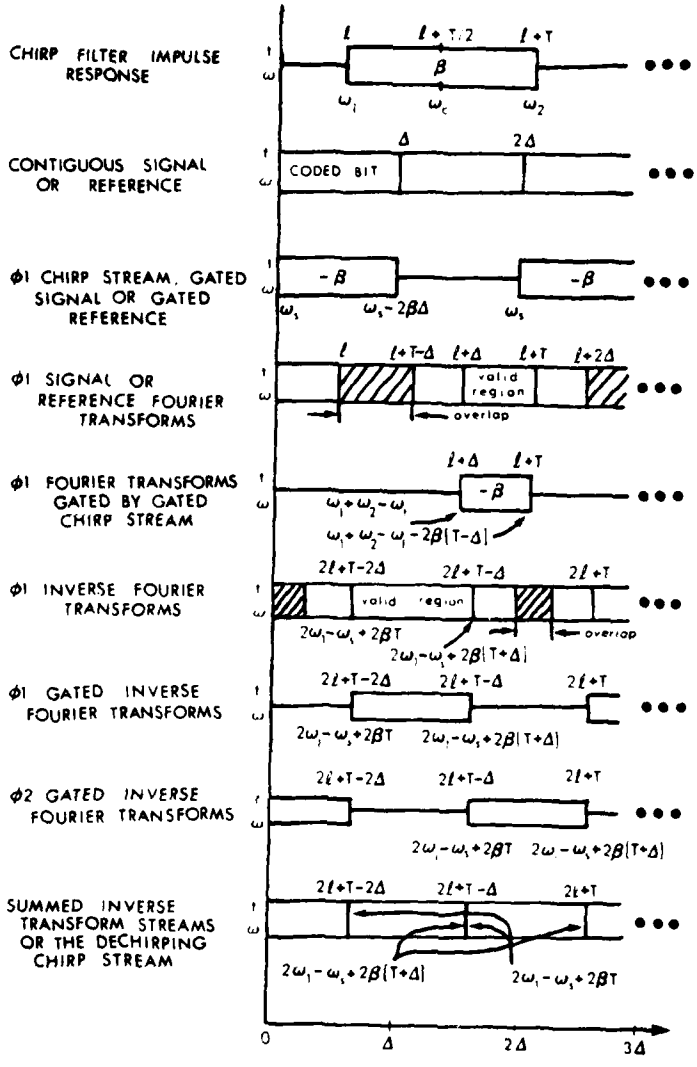

FIGURE 3.57

Figure 3.57: Signal flow through the continuous product-of-transforms correlating receiver. In this figure Δ is the width of a single coded bit, ℓ is a chirp device pedestal of delay, T is the impulse response duration, 2β is the slope (in rad/sec^2) of the chirp devices, ω_1 and ω_2 are the starting and ending frequencies, respectively, of the chirp device impulse responses, ω_c is a chirp device center frequency and ω_s and ω_f are the respective starting and ending frequencies of the chirps when limited to Δ seconds.

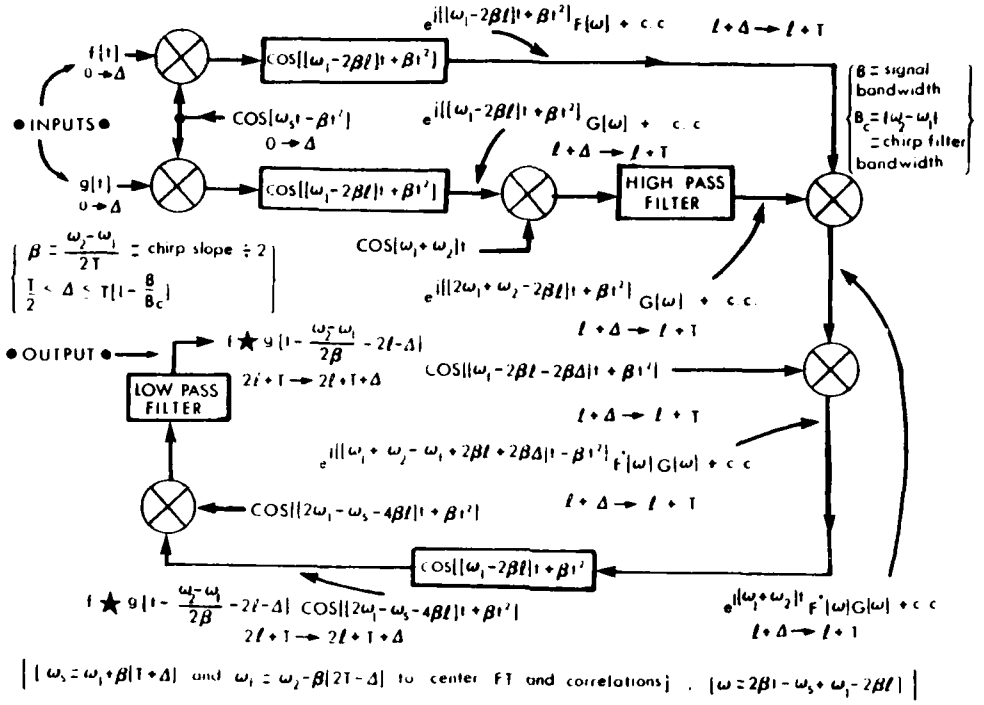

Figure 3.58: A block diagram of one of the two identical correlating halves of the receiver showing somewhat rigorously the flow of information through the system. Below each mathematical representation of the pertinent signal at each point is the time period over which it is valid relative to a coded bit existing from t = 0 to t = Δ. The terminology is the same in this figure as that used in Fig. 3.57. B_c is the bandwidth of the chirp filters. The relationships for the centering of the Fourier transforms and the correlations within their valid regions are also given. When sum or difference terms resulting from a mixing process are ignored, it is because these terms are not important and will be filtered by a purposely placed filter or the chirp devices themselves.

Figure 3.59: Performance characteristics of and results obtained from the continuous product-of-transforms correlation receiver.

(a) Traces 1 and 2: The alternating chirp streams (50 μs/div). (These streams in this work had to be generated using an external VCO since not enough IMCON's were available. This led to difficulties in coherently detecting the output correlations due to VCO instability.) Traces 3 and 4: The chirp-modulated alternating Fourier transform streams (50 μs div). Traces 5 and 6: The chirp-modulated alternating correlation streams (50 μs/div). Trace 7: The sum of traces 5 and 6 (50 μs/div).

(b) Trace 1: The chirp-modulated stream of contiguous transforms (summed for display) (20 μs/div). Trace 2: The baseband input signal consisting of a contiguous train of 13-bit codes (20 μs/div). Trace 3: The chirp-modulated stream of contiguous correlations (20 μs/div).

(c) Trace 1: The baseband input signal consisting of a contiguous train of signals composed of 13 alternating plus/minus pulses (20 μs/div). Trace 2: The chirp-modulated stream of contiguous correlations with trace 1 as the input. Note that since the correlations must be gated to the same duration as the input signals, only half of their duration can be displayed. In this case only 12.5 of the 25 correlation peaks can be viewed. Due to improper system tuning, however, only about 8 peaks can be seen in this figure. Trace 3: Trace 1 expanded to 10 μs/div. Trace 4: Trace 2 expanded to 10 μs/div.

(d) Trace 1: Improperly centered contiguous output correlations (20 μs/div). Trace 2: Properly centered correlations (poorly tuned, however) (20 μs/div). Trace 3: Improperly centered correlations (20 μs/div).

(e) Trace 1: A positive mismatch between the slope of the input chirp modulations and the chirp device slopes and the effect on the output correlation stream (20 μs/div). Trace 2: A good match (20 μs/div). Trace 3: A negative mismatch between slopes (20 μs/div).

(f) Trace 1: The chirp-modulated contiguous stream of Fourier transforms of a 2 Mhz carrier-modulated code (50 μs/div). Trace 2: The autocorrelations (chirp-modulated) of this continuous code stream (50 μs/div). Trace 3: Trace 1 with the addition of wideband noise (50 μs/div). Trace 4: The autocorrelation stream with this noise (50 μs/div). Trace 5: A gating pulse stream used to perform low-pass filtering to eliminate a large portion of the noise energy (50 μs/div). Trace 6: The gated transform stream (50 μs/div). (Trace 3 gated by trace 5.) Trace 7: The correlation stream after gating (50 μs/div) showing low-pass filtered correlation peaks.

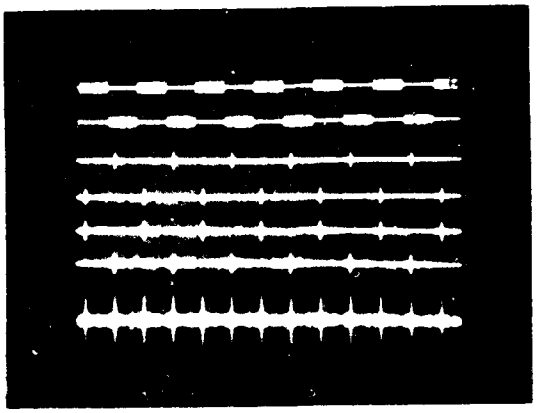

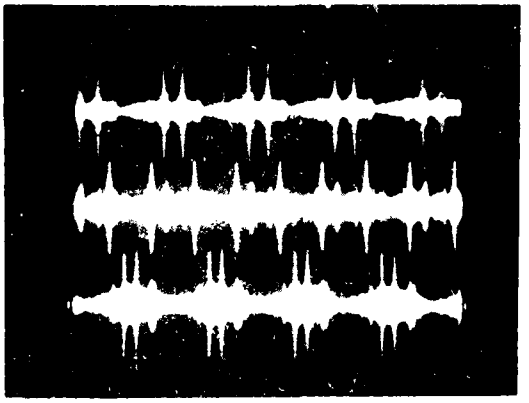

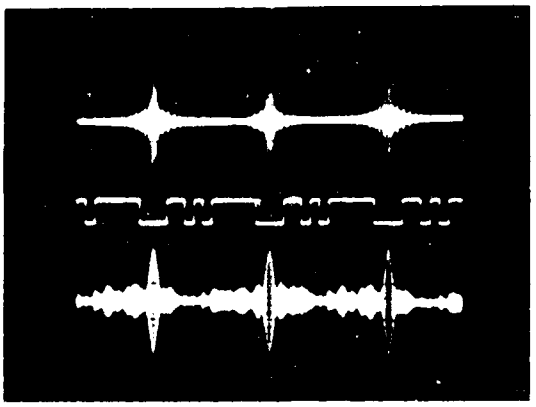

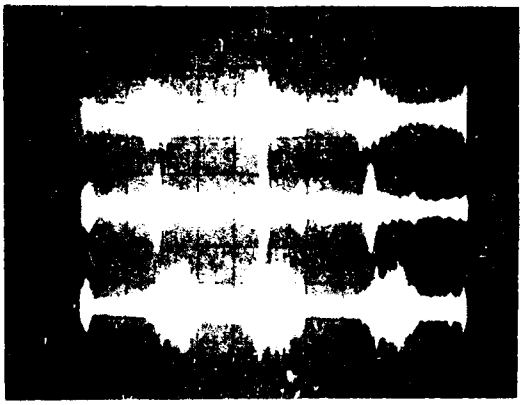

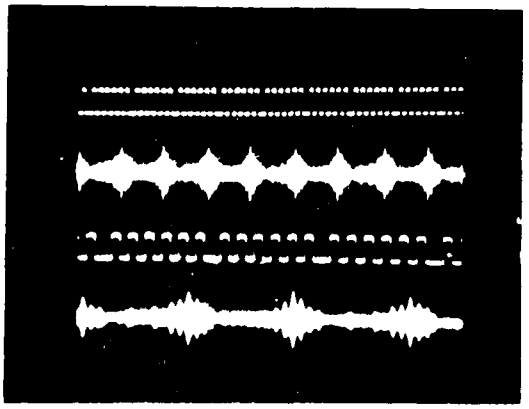

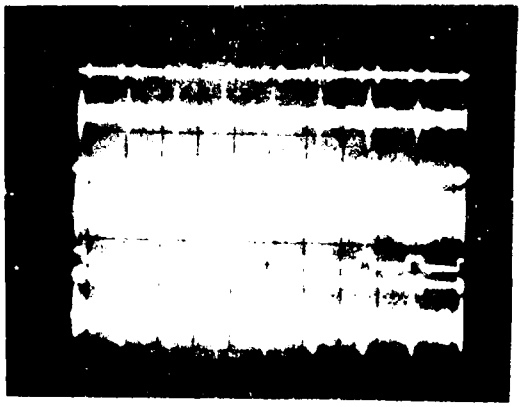

stream. The next two traces are the same except with noise added. Using the gating signal, trace 5, the correlation has been slightly improved as seen in trace 7. Figure 3.60 shows an isolated 7 bit Barker code correlation oscillating between plus and minus one. In the 2nd trace noise has been added, yet only the sidelobes are smeared by the noise. Figure 3.61 shows why this continuous system could not be used for probability of error measurements. What are supposed to be definite positive and negative peaks turn out to be peaks of all sizes. This, as it turns out, was due to the fact that an external chirp generator had to be used (due to the lack of enough chirp filters) that could not be locked to the system rf's.

Figure 3.62 has been included to demonstrate the lack of aliasing in a chirp transform system. These traces are the Fourier transforms of consecutively higher frequency square waves.

Finally, Figures 3.63a and b show the output of a mixer for a ramp at one input and a continuous tone at the other for differing amplitudes of this tone. Note in Figure 3.63a that as the level of the continuous signal begins to fall, the mixing process becomes non-linear and deviates markedly (Figure 3.63b) for very small signal levels. Therefore, except in places where one of the signals can be made to saturate the mixer, multipliers should be used in place of mixers to perform the multiplication between two varying signals. Special high frequency multipliers are required in the microwave area.

Figure 3.60: Trace 1: An isolated 13-bit Barker code correlation fluctuating positive and negative to the polarity of the input bits (20 μs/div). Trace 2: Gaussian noise used to sum to the input Barker code (20 μs/div). Trace 3: . The correlation after the addition of the noise (20 μs/div). Note that the sidelobes are most greatly affected.

Figure 3.61: Trace 1: The chirp-modulated stream of output correlations (50 μs/div). Traces 2 thru 7: The result of coherently dechirping the correlation stream with an unstable VCO chirp generator. In these traces all the correlation peaks were supposed to be positive (50 μs/div).

Figure 3.62: This figure demonstrates the absence of aliasing in a chirp transformation system. If there were aliasing, the harmonics of the Fourier transform (of a square wave) in trace 1 would double back into the viewing region as the square wave frequency was progressively increased in the following traces (2 μs/div).

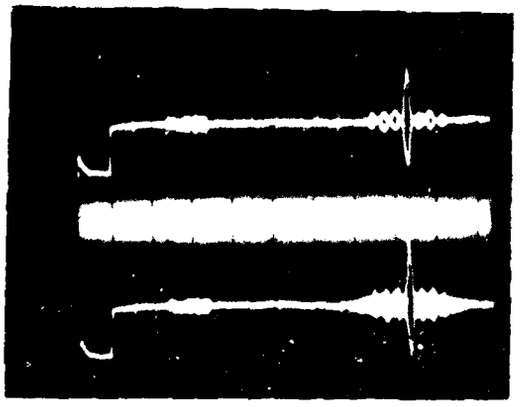

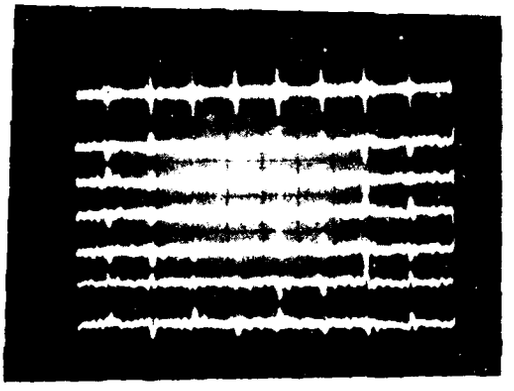

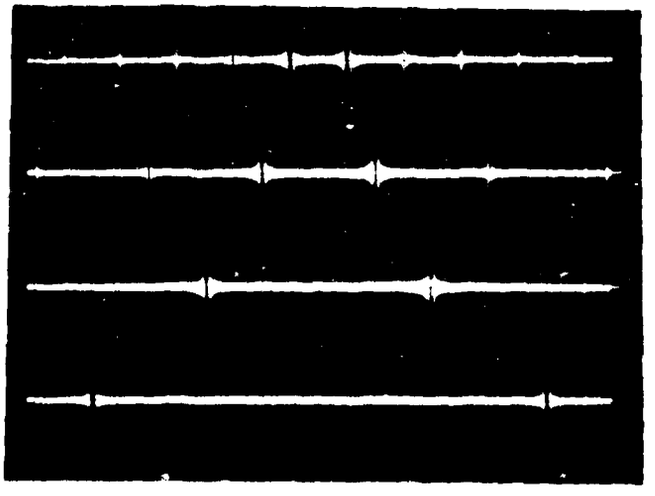

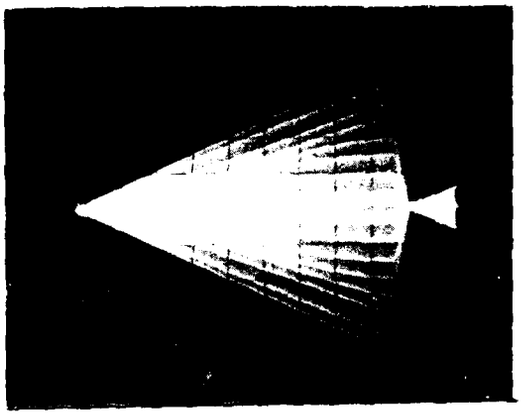

Figure 4.6

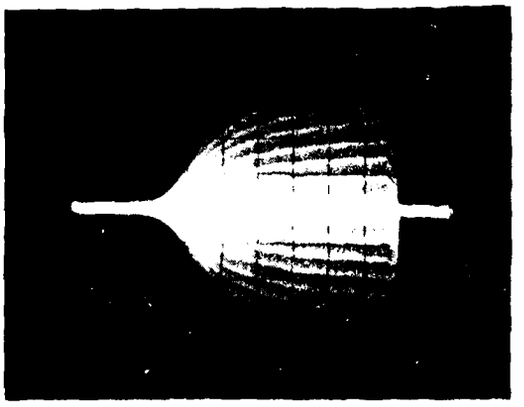

Figure 4.6a

Figure 4.6: **Mixer** non-linearity in the absence of a saturating input.
(a) This figure shows the output of a mixer for a triangular modulated signal applied to one mixer input and an rf at the other. The successive multiple exposures show the result of decreasing the rf power from the saturating level of 7 dBm in downward. The innermost (largest) signals behave fairly linearly when the rf saturates the mixer or is large. After a while, however, the linearity deteriorates, as can be seen by the centrally located outputs which should ideally remain triangular for a triangular input and a [illegible] rf.
(b) This figure is an expanded [illegible] central portion of (a) presented to [illegible] portions of the non-linearity [illegible] small) rf input.

PART IV

DISCUSSION AND CONCLUSIONS

In Section 2.1 an analytic model of the convolver has been developed that essentially follows the flow of information through the device. The analysis decomposes the two input signals into their Fourier components and determines the effect the convolver has upon every component on an individual basis. By such a process the potentials at any point inside the semiconductor due to the two counter propagating surface waves are found to be given by the desired surface waves convolved by distortion functions that are dependent upon the input transducer matching networks, the functional dependence of the fields upon distance above the delay line and upon frequency, the mode structure of the surface waves beneath the semiconductor as a function of space and frequency and the dispersive nature of the wave in terms of both the frequency dependence of velocity and of attenuation. Both the input signals and the distortion terms are real and in general they are signals whose rf carriers can be both amplitude and phase modulated. These signals were decomposed immediately into in-phase and quadrature components and the potentials within the semiconductor were used to obtain an equation for the output potential at the back contract of the semiconductor was obtained where only the second order interaction was of interest. As a result of this analytic approach the potential can be shown to be given by a summation of terms consisting of a dominant component that is essentially the desired convolution with a zero-order-moment related distortion weighting within the convolution integral and

also additional smaller distortion terms that are integrals involving higher order moments and derivatives of both the input signals and the distortion terms.

In Section 2.2 a technique was described for the generation of three-dimensional ambiguity functions utilizing the SAW convolver and based upon the use of a 'slow ramp' and it application to a VCO for the generation of a 'slow chirp' and to the oscilloscope where it is summed to the correlation output of the convolver. The slow ramp must be slow enough to be essentially constant over the time interval of a single correlation and to allow enough correlations to occur over its duration so as to produce a continuous display. The technique was demonstrated to work quite well and in particular it was shown that the functions can be dynamically modified with the potential for wave form optimization.

In Section 2.3 a general formulism was described for the interpretation of convolver operation in the presence of storage. The direct convolver output was shown to be the result of the interaction between the fields accompanying the surface waves, due to stored charge along the semiconductor and applied directly to the semiconductor back contact and the perturbation of the average charge density of the semiconductor due to these fields. The field/charge-density second order interaction was shown to produce a multitude of time dependent terms some of which are constant over a large portion of the interaction time whereas others represent the desired convolution between the two surface waves and convolution or correlation between these waves and the stored charge pattern. This formulism furthermore led to the types of interactions capable of

inducing appreciable charge storage along the semiconductor from which the evolution of the dual nature of storage correlation vs. output convolution becomes evident. Storage and recollection utilizing the potential applied directly to the back semiconductor contact and the convolutionary relationships involving this signal also evolve from this study. Higher order interactions of which there is growing interest are mentioned simply in passing. Some experimental results demonstrating the existence of the storage mechanism utilizing surface states and P-N diodes have been presented. An attempt to produce a simple convolver structure with the inherent capability of producing a uniform interaction while simultaneously allowing quick and easy sample substitution has been described. Results demonstrating the capability of storing a reference signal and later generating an ambiguity function using this reference have also been presented in which case the uniformity of interaction was necessarily an important performance characteristic. Although weak due to excessive damping (in an attempt to obtain uniformity) the presence of the ambiguity function was noted so that the existence of storage and its correlating interaction with surface waves had been verified. During the performance of this short lived investigation and thereafter the technology for convolver related storage has been well developed whereby essentially all the techniques and interactions here described have at some time been verified and utilized in one form or another. At the present time much of the work in this area is related to such devices as the integrating correlator for which a third order (three signal) interaction is employed These higher order interactions are being studied for their potential in producing spurious-free outputs.

In the remaining three sections of Part II of this report chirp transformation has been described in some detail and its capabilities have been demonstrated with respect to time domain spectrum modification and most notably the ability to remove the bulk of a narrowband jammer utilizing nothing more than a time gate. The formulism was developed for both the chirp filter and the convolver implementations. Some analysis was also presented showing the inherent differences between the utilization of up versus down chirp devices and the MCM versus the CMC chirp transformation configurations. This formulism developed the relationships necessary for the proper Fourier transformation of a necessarily finite duration input signal. From this it was shown that the time origin of the input signal is dependent upon the center frequency of the chirp used to coherently dechirp the transform whereas the position of the transform within the calculable output time interval is dependent upon the center frequency of the chirp used to modulate the input signal.

The analysis also formulated the required multiplying factor for a typical device impulse response (in order to produce reasonable results) and it was found to be of the order of magnitude equal to the square root of the chirp slope which, in most cases, is quite large (typically about 10^6). Most of the analysis was performed utilizing input signals having in-phase and quadrature components so that complex-data Fourier transformation was automatically included and the necessary formulism derived. The existence of the Fresnel component concurrently with the desired Fourier component of the output was discussed and the necessary criteria through which this unwanted component can be ignored

were presented. The utilization of the properties of the Fourier transform and the results of modifications to this transform with respect to the inverse transform were also covered and the results of the experimental work verify this discussion.

The experimental results demonstrated conclusively that the Fourier transform can accurately be obtained in real-time and both its real and imaginary components are readily accessible and seem visually to correspond extremely well with the calculated components of the transform when obtained using a well optimized system. It was shown that optimization involves the use of well-matched devices (implying extremely linear chirp slopes of equal magnitude) and offset center frequencies between the expansion chirp device (used to generate the chirp) and the compression chirp device (from which the transform arises) so as to eliminate interference from mixer internods and mixer feedthrough which itself can produce a Fresnel transform arising simultaneously with the Fourier transform at the device output.

The Fresnel transform was shown, in its own right, to possess the capability to perform a useful signal processing function. This transform, fairly completely documented in the appendix, was shown to be applicable for the selective time complementation of a signal. The transform is furthermore shown to be the natural describing relationship between the input and output of a chirp filter from whence its power is derived. Chirp modulated signals also produce Fresnel transforms where the Fourier transform arises only for a special case.

The power behind the Fourier transformation utilizing chirp transformation has been demonstrated by employing the technique in a

variety of correlating receiver structures. Here it was shown that inverse transformations performed on the product of two chirp transformations produced output signals equivalent to the correlation between the two input signals which is a direct application of a well known Fourier property (i.e. the convolution theorm). The correlating ability of such a system was demonstrated using a variety of signals and by the generation of ambiguity functions. The signal processing capability of this system was shown to be quite competitive by the generation of its probability of error curve with and without jammer and with and without time gating of the jammer from the Fourier transform. The ability to dramatically improve signal detection by time gating the jammer, however, sets this receiver apart from other existing correlating receivers.

Overall, this report has demonstrated and analyzed a variety of SAW signal processing techniques all some way or another involved with convolution or Fourier transformation. The techniques were typically built around the use of SAW convolvers and SAW chirp filters. Although most of the convolver analysis has been directed specifically toward the SAW separated-medium convolver the chirp-filter-related information is general enough to apply to any filter capable of producing an approximation to the idealized form of device response assumed in this analytical approach. All the analysis, however, was mainly directed toward surface wave technology and the chirp filters of large time bandwidth product that are evolving in this area.

PART 5

LITERATURE CITED

Arsenault, D. R., "Signal Processing using Surface Acoustic Wave Devices", Ph.D Thesis, RPI, 1979.

Arsenault, D. R. and Das, P., "SAW Fresnel Transform Devices and Their Applications", 1977 Ultrasonics Symp. Proc., (IEEE, New York, 1977), pp. 969-973.

Arsenault, D. R., Das. P. and Milstein, L. B., "Matched Filtering of Continuous Signals by the Product of Transforms Technique Using SAW Chirp Filters", 1978 Ultrasonics Symp. Proc., (IEEE, New York, 1978), pp. 543-548.

Ash, E. A., "Fundamentals of Signal Processing Devices", Acoustic Surface Waves, edited by A. A. Oliner, (Springer-Verlag, New York, 1978), Chapter 4, pp. 97-185.

Atzeni, C., Manes, G. and Masotti, L., "Programmable Signal Processing by Analog Chirp Transformation Using SAW Devices", 1975 Ultrasonics Symp. Proc., (IEEE, New York, 1975), pp. 371-376.

Barr, A., private communication.

Becker, R. A. and Hurlburt, D. H., "Wideband $LiNbO_3$ Elastic Convolver with Parabolic Horns", 1979 Ultrasonics Symp. Proc., (IEEE, New York), to be published.

Bers, A. and Cafarella, J. H., "Surface Wave Correlator/Convolver with Memory", 1974 Ultrasonics Symp. Proc., (IEEE, New York, 1974), p. 778.

Cafarella, J. H., Bers, A. and Burke, B. E., "Surface Mobility on Silicon from Acoustoelectric Current Measurements", 1972 Ultrasonics Symp. Proc., (IEEE, New York, 1972), pp. 181-185.

Cafarella, J. H., Brown, Jr., W. M., Stern, E. and Alusow, J. A., "Acoustoelectric Convolvers for Programmable Matched Filtering in Spread Spectrum Systems", Proc. of the IEEE, vol. 64, p. 756, 1976.

Casasent, D. and Psaltis, D., "New Optical Transforms for Pattern Recognition", Proc. of the IEEE, vol. 65, pp. 77-84, 1977.

Collins, J. H., Grant, P. M. and Darby, B. J., "Application of Surface Acoustic Wave Devices to Spread Spectrum Communications", Wave Electronics, (Elsevier Scientific, Amsterdam, Netherlands, 1976), pp. 311-341.

Cook, C. E. and Bernfield, M., Radar Signals, (Academic Press, New York, 1967).

Das, P., Araghi, M. N. and Wang, W. C., "Ambiguity Function Generator Using Acoustic Surface Wave Convolvers", Proc. of the IEEE, vol. 62, pp. 1714-1716, 1974.

Das, P. and Milstein, L. B., "Space Charge Coupled Acoustic Surface Wave Signal Processor", 1975 Nat. Telecomm. Conf. Rec., vol. II, pp. 1.21-1.23.

Das, P. and Arsenault, D. R., "SAW Space Charge Coupled Signal Processing and Transform Device with Storage", Ext. Abst. Electrochem. Soc., vol. 77-1, p. 112, 1977.

Das, P. and Arsenault, D. R., "Application of SAW Devices in Non-destructive Testing Using Ultrasound", 1977 Ultrasonics Symp. Proc., (IEEE, New York, 1977), pp. 245-252.

Das., P., Arsenault, D. R. and Milstein, L. B., "Adaptive Spread Spectrum Receiver Using SAW Technology", Nat. Telecomm. Conf. Rec., IEEE Publication No. 77 CH 1290-2, pp. 35.7-1 to 35.7-6, 1977.

Das, P., Milstein, L. B. and Arsenault, D. R., "Variable Format Radar Receiver Using a SAW Convolver", IEEE Trans. on Aerospace and Elec. Sys., vol. AES-14, no. 6, pp. 843-852, November 1978.

Defranould, Ph., Gautier, H., Maerfeld, D. and Tournois, P., "P-N Diode Memory Correlator", 1976 Ultrasonics Symp. Proc., (IEEE, New York, 1976), pp. 336-347.

Dolat, V. S. and Williamson, R. C., "A Continuously Variable Delay-Line System", 1976 Ultrasonics Symp. Proc., (IEEE, New York, 1976), pp. 419-423.

Dolat, V. S., Schulz, M. B., Veilleux, L. A., McCully, G. R. and Williamson, R. C., "High-Performance Hybrid SAW Chirp-Fourier-Transform System" 1978 Ultrasonics Symp. Proc., (IEEE, New York, 1972), pp. 527-532.

Gautier, H. and Kino, G. S., "A Detailed Theory of the Acoustic Wave Semiconductor Convolver", IEEE Trans. on Sonics and Ultrasonics, vol. SU-24, no. 1, January 1977, pp. 23-33.

Gerard, H. M., Smith, W. R., Jones, W. E. and Harrington, J. B., "The Design and Applications of Highly Dispersive Acoustic Surface Wave Filters", IEEE Trans. on Sonics and Ultrasonics, vol. SU-20, pp. 94-103, 1973.

Gerard, H. M., "Surface Wave Interdigital Electrode Chirp Filters", Surface Wave Filters, edited by H. Matthews, (John Wiley and Sons, New York, 1977), Chapter 8, pp. 347-380.

Gerard, H. M., Yao, P. J. and Otto, O. W., "Performance of a Programmable Radar Pulse Compression Filter Based on a Chirp Transformation with RAC Filters", 1977 Ultrasonics Symp. Proc., (IEEE, New York, 1977), pp. 947-951.

Hays, R. M., Shreve, W. R. and Bell, D. T., "Surface Wave Transform Adaptable Processor System", 1975 Ultrasonics Symp. Proc., (IEEE, New York, 1975), pp. 363-370.

Hays, R. M. and Hartmann, C. S., "Surface Acoustic Wave Devices for Communications", Proceedings of the IEEE, vol. 64, no. 5, May 1976, pp. 652-671.

Ingebrigtsen, K. and Stern, E., "Holographic Storage of Acoustic Surface Waves with Schottky Diode Arrays", 1975 Ultrasonics Symposium Proceedings, (IEEE, New York, 1975), pp. 212-216.

Jack, M. A., Manes, G. F., Grant, P. M., Atzeni, C., Masotti, L., and Collins, J. H., "Real Time Network Analyzers Based on SAW Chirp Transform Processors", 1976 Ultrasonics Symposium Proceedings, (IEEE, New York, 1976), pp. 376-381.

Kino, G. S. and Matthews, H., "Signal Processing in Acoustic Surface Wave Devices", IEEE Spectrum, August 1971, pp. 22-35.

Kino, G. S., Ludvik, S., Shaw, H. J., Shreve, W. R., White, J. M. and Winslow, D. K., "Signal Processing by Parametric Interactions in Delay-Line Devices", IEEE Transactions on Microwave Theory and Techniques, vol. MTT-21, no. 4, April 1973, pp. 244-254.

Kino, G. S., "Correlation with the Storage Convolver", Applied Physics Letters, vol. 29, no. 9, pp. 527-529, 1976.

Kino, G. S., "Acoustoelectric Interactions in Acoustic Surface Wave Devices", Proceedings of the IEEE, vol. 64, p. 724, 1976.

Luukkala, M. and Kino, G. S., "Convolution and Time Inversion Using Parametric Interactions of Acoustic Surface Waves", Applied Physics Letters, vol. 18, p. 393 (1971).

Maines, J. D., Moule, G. L., Newton, C. O. and Paige, E. G. S., "A Novel SAW Variable Frequency Filter", 1975 Ultrasonics Symposium Proceedings, (IEEE, New York, 1975), pp. 355-358.

Maines, J. D. and Paige, "Surface Acoustic Wave Devices for Signal Processing Applications", Proceedings of the IEEE, vol. 64, no. 5, May 1976, pp. 639-652.

Maines, J., "Surface Wave Devices for Radar Equipment", Surface Wave Filters, Edited by H. Matthews, (John Wiley & Sons, New York, 1977), Chapter 10, pp. 443-476.

Martin, T. A., "The IMCON Pulse Compression Filter and its Applications", IEEE Transactions on Microwave Theory and Techniques, vol. 21, 1973, pp. 186-194.

Martin, T., "Low Sidelobe IMCON Pulse Compression", 1976 Ultrasonics Symposium Proceedings, (IEEE, New York, 1976), pp. 411-414.

Matthews, H., Ed., Surface Wave Filters, (John Wiley & Sons, New York, 1977).

Milstein, L. B., Das, P. K. and Arsenault, D. R., "Narrowband Jammer Suppression in Spread Spectrum System Using SAW Devices", National Telecommunication Conference Record, IEEE Cat. No. 78 CH 1354 COCCB, pp. 4a.5.1 - 4a.5.5, 1978.

Milstein, L. B. and Das, P., "Spread Spectrum Receiver Using Surface Acoustic Wave Technology", IEEE Transactions on Communications, vol. com-25, no. 8, pp. 841-847, August 1977.

Milstein, L. B., Arsenault, D. R. and Das, P., "Transform Domain Processing for Digital Communication Systems Using Surface Acoustic Wave Devices", AGARD Conference Preprint No. 239 on Digital Communications in Avionics, pp. 28-1 to 28-15, 1978.

Nudd, G. R. and Otto, D. W., "Chirp Signal Processing Using Acoustic Surface Wave Filters", 1975 Ultrasonics Symposium Proceedings, (IEEE, New York, 1975), pp. 350-354.

Oliner, A. A., Ed., Acoustic Surface Waves, (Springer-Verlag, New York, 1978).

Otto, O. W., "Real Time Fourier Transform with a Surface Wave Convolver", Electron Letters, vol. 8, pp. 623, 1972.

Otto, O. W., "The Chirp Transform Signal Processor", 1976 Ultrasonics Symposium Proceedings, (IEEE, New York, 1976), pp. 365-370.

Papoulis, A., The Fourier Integral and its Applications, (McGraw-Hill, New York, 1962).

Papoulis, A., Systems and Transforms with Applications in Optics, (McGraw-Hill, New York, 1968).

Papoulis, A., Signal Analysis, (McGraw-Hill, New York, 1977).

Quate, C. F. and Thompson, R. B., "Convolution and Correlation in Real Time with Non-linear Acoustics", Applied Physics Letters, vol. 16, p. 494 (1970).

Ralston, R. W., Hurlburt, D. H., Leonberger, F. J., Cafarella, J. H. and Stern, E., "A New Signal-Processing Device, The Integrating Correlator", 1977 Ultrasonics Sysposium Proceedings, (IEEE, New York, 1977), pp. 623-628.

Reeder, T. M. and Gliden, M., "Convolution and Correlation by Non-linear Interaction in a Diode Coupled Tapped Delay Line", Applied Physics Letters, vol. 22, pp. 8-10 (1973).

Rihaczek, A. W., Principles of High Resolution Radar, (McGraw-Hill, New York, 1969).

Skolnik, M. I., Radar Handbook, (McGraw-Hill, New York, 1970).

Smith, J. M., Stern, E. and Bers, A., "Accumulation Layer Surface Wave Convolver", Electron Letters, vol. 9, pp. 145-146, March 1973.

Sneddon, I. N., The Use of Integral Transforms, (McGraw-Hill, New York, 1972).

Tiemann, J. J., Young, J. D. and Das, P., "Acoustic Surface Wave Filter Using Chirp Transform for NDT", 1976 Ultrasonics Symposium Proceedings, (IEEE, New York, 1976), pp. 382-385.

Turner, C. W., Mason, I. M. and Chambers, J., "Acoustic Convolution Using Non-linear Surface Wave Interactions in a Piezoelectric Semiconductor", Electron Letters, vol. 7, p. 696 (1971).

Unkauf, M. G., "Surface Wave Devices in Spread Spectrum Systems", Surface Wave Filters, Edited by H. Matthews, (John Wiley & Sons, New York, 1977), chapter 10, pp. 443-476.

Wang, W. C. and Das, P., "Surface Wave Convolvers via Space Charge Nonlinearity", 1972 Ultrasonics Symposium Proceedings, (IEEE, New York, 1972), pp. 316-321.

Wang, W. C. and Das, P., "Surface Wave Convolution in Piezoelectric Semiconductors", Proceedings of the IEEE, vol. 60, p. 1109 (1972).

Whitehouse, H. J. and Means, R. W., "Signal Processing Using Charge Coupled Devices and Surface Wave Devices", 1973 Ultrasonics Symposium Proceedings, (IEEE, New York, 1973), p. 572.

Williamson, R. C. and Smith, H. I., "The Use of Surface Elastic Wave Reflection Gratings in Large Time Bandwidth Pulse Compression Filters", IEEE Transactions on Microwave Theory and Techniques, vol. MTT-21, no. 4, pp. 195-205, 1973.

Williamson, R. C., "Reflection Grating Filters", Surface Wave Filters, Edited by H. Matthews, (John Wiley & Sons, New York, 1977), chapter 9, pp. 381-441.

Yamanishi, M. and Kawamura, T., "Acoustic Surface Wave Convolver Using Nonlinear Electron Interactions in Coupled Semiconductor Piezoelectric Systems", 1972 Ultrasonics Symposium Proceedings, (IEEE, New York, 1972), pp. 288-291.

AD-A089 965 RENSSELAER POLYTECHNIC INST TROY NY MICROWAVE ACOUST--ETC F/G 17/2
SIGNAL PROCESSING USING SURFACE ACOUSTIC WAVE DEVICES AND ITS A--ETC(U)
DEC 79 D R ARSENAULT, L B MILSTEIN, P DAS DAAG29-77-G-0205
UNCLASSIFIED RPI-MA-ARO-10 ARO-15004.14-EL NL

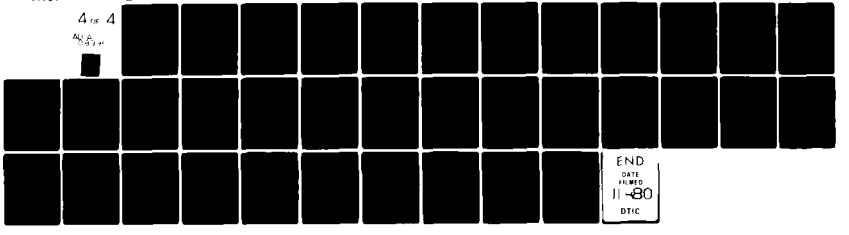

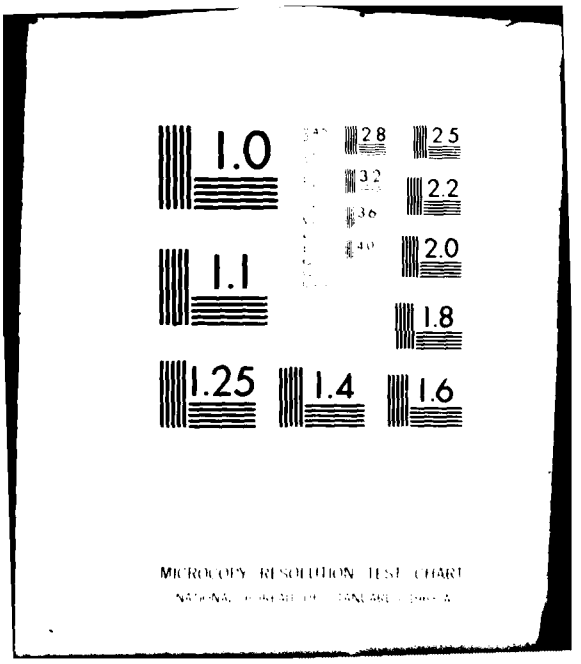
1.0
1.1
1.25
2.8
3.2
3.6
4.0
2.5
2.2
2.0
1.8
1.4
1.6
MICROCOPY RESOLUTION TEST CHART

APPENDIX A

Fresnel Analysis*

Defining Equations (convolutional relationships)

Fresnel Transform:

$$F_\beta(\tau) = \mathcal{F}_{\beta,\tau}[f(t)] = \int_{-\infty}^{\infty} f(t)e^{-j\beta(t-\tau)^2}dt = f(\tau) * e^{-j\beta\tau^2} \qquad \text{(A-1)}$$

Inverse Relationship:

$$f(t) = \mathcal{F}^{-1}_{\beta,t}[F_\beta(\tau)] = \frac{\beta}{\pi}\int_{-\infty}^{\infty} F_\beta(\tau)e^{j\beta(t-\tau)^2}d\tau = \frac{\beta}{\pi}\,(F_\beta(t) * e^{j\beta t^2}) \qquad \text{(A-2)}$$

Proof of Transform:

$$f(t) = \frac{\beta}{\pi}\int_{-\infty}^{\infty}\left[\int_{-\infty}^{\infty} f(t_o)e^{-j\beta(t_o-\tau)^2}dt_o\right]e^{j\beta(t-\tau)^2}dt$$

$$= \frac{\beta}{\pi}\int_{-\infty}^{\infty} f(t_o)e^{j\beta(t^2-t_o^2)}\left[\int_{-\infty}^{\infty} e^{j2\beta(t_o-t)\tau}\,d\tau\right]dt_o$$

$$= \int_{-\infty}^{\infty} f(t_o)e^{j\beta(t^2-t_o^2)}\delta(t_o-t)dt_o = f(t)$$

Expansion of a Periodic Function in Quadratic Orthogonal Terms

$$f(t) = \sum_{n=-\infty}^{\infty} \alpha_{\beta n}e^{j\beta(t-n\tau_o)^2} \qquad \text{(A-3)}$$

where $\tau_o = \pi/\beta T$.

Since

$$\int_{-T/2}^{T/2} e^{j\beta(t-n\tau_o)^2}e^{-j\beta(t-n'\tau_o)^2}dt \qquad \text{(A-4)}$$

$$= T \text{ when } n = n'$$
$$= o \text{ otherwise}$$
$$= T\delta(n-n')$$

---

* For further details see Arsenault (1979).

then

$$\alpha_{\beta n} = \frac{1}{T} \int_{-T/2}^{T/2} f(t) e^{-j\beta(t-n\tau_o)^2} dt \qquad \text{(A-5)}$$

In the limit as T approaches infinity

$$T\alpha_{\beta n} = \int_{-T/2}^{T/2} f(t) e^{-j\beta(t-n\tau_o)^2} dt \xrightarrow[T\to\infty]{} \int_{-\infty}^{\infty} f(t) e^{-j\beta(t-\tau)^2} dt \qquad \text{(A-6a)}$$

$$= F_\beta(\tau)$$

$$f(t) = \frac{\beta}{\pi} \sum_{n=-\infty}^{\infty} T\alpha_{\beta n} e^{j\beta(t-n\tau_o)^2} \tau_o \xrightarrow[T\to\infty]{} \frac{\beta}{\pi} \int_{-\infty}^{\infty} F_\beta(\tau) e^{j\beta(t-\tau)^2} d\tau \qquad \text{(A-6b)}$$

The Fresnel transform of the periodic signal given by equation (A-3) is

$$F_\beta(\tau) = \frac{\pi}{\beta} \sum_{n=-\infty}^{\infty} \alpha_{\beta n} \delta(\tau - n\tau_o) \qquad \text{(A-7)}$$

As can be inferred form these equations, the Fresnel transform of a signal represents a mapping of the magnitudes of infinite duration quadratic phase terms as a function of their delays. A periodic signal can be written as an infinite sum of these terms having magnitudes $\alpha_{\beta n}$ and delays that are multiples of $\tau_o = \pi/\beta T$. The Fresnel transform maps time to delay as a function of the variable β. This β is arbitrary and can be chosen to meet the requirements of the analysis to which the Fresnel transform is employed.

In general

$$F_\beta(\tau) = R_\beta(\tau) + jX_\beta(\tau) = A_\beta(\tau) e^{j\phi_\beta(\tau)} \qquad \text{(A-8)}$$

where

$$A_\beta(\tau) = (R_\beta^2(\tau) + X_\beta^2(\tau))^{\frac{1}{2}} \tag{A-9}$$

and

$$\phi_\beta(\tau) = \tan^{-1}[X_\beta(\tau)/R_\beta(\tau)] \ . \tag{A-10}$$

With $f(t) = f_R(t) + jf_I(t)$ (A-11)

then

$$F_\beta(\tau) = \int_{-\infty}^{\infty} [f_R(t)\cos(\beta(t-\tau)^2) + f_I(t)\sin(\beta(t-\tau)^2)]dt$$

$$- j \int_{-\infty}^{\infty} [f_R(t)\sin(\beta(t-\tau)^2) - f_I(t)\cos(\beta(t-\tau)^2)]dt \tag{A-12}$$

so that

$$R_\beta(\tau) = \int_{-\infty}^{\infty} [f_R(t)\cos(\beta(t-\tau)^2) + f_I(t)\sin(\beta(t-\tau)^2)]dt \tag{A-13}$$

and

$$X_\beta(\tau) = -\int_{-\infty}^{\infty} [f_R(t)\sin(\beta(t-\tau)^2) - f_I(t)\cos(\beta(t-\tau)^2)]dt \ . \tag{A-14}$$

Furthermore

$$f(t) = \frac{\beta}{\pi} \int_{-\infty}^{\infty} [R_\beta(\tau)\cos(\beta(t-\tau)^2) - X_\beta(\tau)\sin(\beta(t-\tau)^2)]d\tau$$

$$+ j \frac{\beta}{\pi} \int_{-\infty}^{\infty} [R_\beta(\tau)\sin(\beta(t-\tau)^2) + X_\beta(\tau)\cos(\beta(t-\tau)^2)]d\tau \tag{A-15}$$

so that

$$f_R(t) = \frac{\beta}{\pi} \int_{-\infty}^{\infty} [R_\beta(\tau)\cos(\beta(t-\tau)^2) - X_\beta(\tau)\sin(\beta(t-\tau)^2)]d\tau \tag{A-16}$$

$$f_I(t) = \frac{\beta}{\pi} \int_{-\infty}^{\infty} [R_\beta(\tau)\sin(\beta(t-\tau)^2) + X_\beta(\tau)\cos(\beta(t-\tau)^2)]d\tau \ . \qquad \text{(A-17)}$$

From these equations it can be seen that with

$$f(t) \underset{\beta,t,\tau}{\longleftrightarrow} F_\beta(\tau) \qquad \text{(A-18)}$$

then

$$f^*(t) \underset{\beta,t,\tau}{\longleftrightarrow} F^*_{-\beta}(\tau) \ . \qquad \text{(A-19)}$$

Some other general relationships are

$$F_\beta(o) = \int_{-\infty}^{\infty} f(t)e^{-j\beta t^2}dt \qquad \text{(A-20)}$$

$$f(o) = \frac{\beta}{\pi} \int_{-\infty}^{\infty} F_\beta(\tau)e^{j\beta\tau^2}d\tau \qquad \text{(A-21)}$$

$$\int_{-\infty}^{\infty} F_\beta(\tau)d\beta = \frac{\pi}{\tau} e^{-j\beta\tau^2}[f(2\tau)+f(o)] \qquad \text{(A-22)}$$

Eq. (A-22) is obtained as follows:

$$\int_{-\infty}^{\infty} F_\beta(\tau)d\beta = \int_{-\infty}^{\infty}\int_{-\infty}^{\infty} f(t)e^{-j\beta(t-\tau)^2}dtd\beta$$

$$= \int_{-\infty}^{\infty} f(t)e^{-j\beta\tau^2}2\pi\delta(-t^2+2t\tau)dt$$

$$= \frac{\pi}{\tau} e^{-j\beta\tau^2} \int_{-\infty}^{\infty} f(t)[\delta(t-2\tau) + \delta(t)]dt$$

$$= \frac{\pi}{\tau} e^{-j\beta\tau^2}[f(2\tau) + f(o)] \ .$$

Here the equation

$$\delta(\alpha(t)) = \sum_n \frac{\delta(t-t_n)}{|\alpha'(t_n)|} \qquad \text{(A-23)}$$

where

$$\alpha(t) = -t^2 + 2t\tau$$

$$\alpha'(t) = -2t + 2\tau$$

$$\left.\begin{aligned} t_1 &= 0 \\ t_2 &= 2\tau \end{aligned}\right\} \text{ zeroes of } \alpha(t)$$

was used so that

$$\delta(-t^2 + 2t\tau) = \frac{\delta(t)}{2\tau} + \frac{\delta(t-2\tau)}{2\tau} \tag{A-24}$$

Energy Conservation

Since

$$f(t)f^*(t) = |f(t)|^2$$

$$= \frac{\beta^2}{\pi^2} \int_{-\infty}^{\infty} \int_{-\infty}^{\infty} F_\beta(\tau) F_\beta^*(\tau') e^{j\beta(\tau^2-\tau'^2)} e^{j2\beta(\tau'-\tau)t} \, d\tau d\tau'$$

then

$$\int_{-\infty}^{\infty} |f(t)|^2 dt = \frac{\beta}{\pi} \int_{-\infty}^{\infty} |F_\beta(\tau)|^2 d\tau \tag{A-25}$$

since

$$\int_{-\infty}^{\infty} e^{j2\beta(\tau'-\tau)t} \, dt = \frac{\pi}{\beta} \delta(\tau'-\tau) \tag{A-26}$$

Therefore, if f(t) represents the voltage across a 1 Ω resistive load, equation (A-25) says that the total energy dissipated in this resistor by f(t) is proportional to the integral of the square of the Fresnel transform over its entire spectrum.

Causal Time Functions (real)

$$f_e(t) = [f(t) + f(-t)]/2 \tag{A-27}$$

Linearity

$$a_1 f_1(t) + \cdots + a_n f_n(t) \underset{\beta,\tau,t}{\longleftrightarrow} a_1 F_{\beta 1}(\tau) + \cdots + a_n F_{\beta n}(\tau) \tag{A-28}$$

Symmetry

$$F_{-\beta}(t) \underset{\beta,\tau,t}{\longleftrightarrow} \frac{\pi}{\beta} f(\tau) \tag{A-29}$$

i.e.

$$f(\tau) = \frac{\beta}{\pi} \int_{-\infty}^{\infty} F_{-\beta}(t) e^{-j\beta(t-\tau)^2} dt$$

Function Inversion

$$f(t) \underset{\beta,t,\tau}{\longleftrightarrow} F_\beta(\tau)$$

$$e^{j2\beta t^2} F_\beta(t) \underset{\beta,t,\tau}{\longleftrightarrow} \frac{\pi}{\beta} e^{-j2\beta\tau^2} f(-\tau) \tag{A-30}$$

Proof:

$$F_\beta(\tau) = e^{-j\beta\tau^2} \left[f(t) e^{-j\beta t^2} \right]\Big|_{\omega=2\beta\tau}$$

$$= e^{-j\beta\tau^2} \int_{-\infty}^{\infty} \left(f(t) e^{-j\beta t^2} \right) e^{j2\beta\tau t} \, dt \tag{A-31}$$

$$\int_{-\infty}^{\infty} e^{j2\beta t^2} F_\beta(t) e^{-j\beta(t-\tau)^2} dt$$

$$= e^{-j\beta\tau^2} \int_{-\infty}^{\infty} \left[\int_{-\infty}^{\infty} \left(f(\lambda) e^{-j\beta\lambda^2} \right) e^{j2\beta\lambda t} \, d\lambda \right] e^{j2\beta t\tau} \, dt$$

$$= e^{-j\beta\tau^2} \frac{2\pi}{2\beta} f(-\tau) e^{-j\beta\tau^2}$$

$$= \frac{\pi}{\beta} e^{-j2\beta\tau^2} f(-\tau)$$

Q.E.

Proof:

$$\int_{-\infty}^{\infty} f(t-t_o)e^{-j\beta(t-\tau)^2}dt \qquad \text{(subst. } \lambda = t-t_o,\ d\lambda = dt\text{)}$$

$$= \int_{-\infty}^{\infty} f(\lambda)e^{-j\beta(\lambda + t_o-\tau)^2}d\lambda$$

$$= \int_{-\infty}^{\infty} f(t)e^{-j\beta(t-(\tau-t_o))^2}dt$$

Q.E.

Time Differentiation

$$\frac{df(t)}{dt} \underset{\beta,t,\tau}{\longleftrightarrow} \frac{dF_\beta(\tau)}{d\tau} \qquad \text{(A-32)}$$

Proof:

$$\frac{df(t)}{dt} = \frac{\beta}{\pi}\int_{-\infty}^{\infty} 2j\beta(t-\tau)F_\beta(\tau)e^{j\beta(t-\tau)^2}d\tau$$

$$= 2j\beta tf(t) - \frac{\beta}{\pi}\int_{-\infty}^{\infty} 2j\beta\tau F_\beta(\tau)e^{j\beta(t-\tau)^2}d\tau$$

$$\frac{dF(\tau)}{d\tau} = \int_{-\infty}^{\infty} 2j\beta(t-\tau)f(t)e^{-j\beta(t-\tau)^2}dt$$

$$= -2j\beta\tau F(\tau) + \int_{-\infty}^{\infty} 2j\beta tf(t)e^{-j\beta(t-\tau)^2}dt$$

$$\frac{df(t)}{dt} = \frac{\beta}{\pi}\int_{-\infty}^{\infty}\frac{dF(\tau)}{d\tau}e^{j\beta(t-\tau)^2}d\tau + 2j\beta tf(t)$$

$$- \frac{\beta}{\pi}\int_{-\infty}^{\infty}\int_{-\infty}^{\infty} 2j\beta t_o f(t_o)e^{-j\beta(t_o-\tau)^2}e^{j\beta(t-\tau)^2}dt_o d\tau$$

$$\int_{-\infty}^{\infty} e^{-j\beta(t_o-\tau)^2}e^{j\beta(t-\tau)^2}d\tau = e^{j\beta(t^2-t_o^2)}\frac{\pi}{\beta}\delta(t_o-t)$$

$$\frac{df(t)}{dt} = \frac{\beta}{\pi}\int_{-\infty}^{\infty}\frac{dF(\tau)}{d\tau}e^{j\beta(t-\tau)^2}d\tau + 2j\beta tf(t) - 2j\beta tf(t)$$

$$= \frac{\beta}{\pi}\int_{-\infty}^{\infty}\frac{dF(\tau)}{d\tau}e^{j\beta(t-\tau)^2}d\tau$$

Q.E.

Time Scaling

$$f(at) \underset{\beta,t,\tau}{\longleftrightarrow} \frac{1}{|a|} F_{\frac{\beta}{a^2}}(a\tau) \qquad \text{(a pos. or neg.)} \qquad \text{(A-33)}$$

Fresnel Transform Conversions

$$\mathcal{F}_{a\beta,b\tau}[f(ct)] = \frac{1}{|c|} \mathcal{F}_{\frac{a}{c^2}\beta,bc\tau}[f(t)] \qquad \text{(c pos. or neg.)} \qquad \text{(A-34)}$$

$$= \frac{1}{\sqrt{a}} \mathcal{F}_{\beta,\sqrt{a}\,b\tau}[f(\frac{c}{\sqrt{a}}t)] \qquad \text{(a pos.)} \qquad \text{(A-35)}$$

$$= \frac{1}{\sqrt{|a|}} \mathcal{F}^{*}_{\beta,\sqrt{|a|}\,b\tau}[f(\frac{c}{\sqrt{|a|}}t)] \qquad \text{(a neg. f(t) real)} \qquad \text{(A-36)}$$

$$= |b| \mathcal{F}_{ab^2\beta,\tau}[f(bct)] \qquad \text{(a pos. or neg.)} \qquad \text{(A-37)}$$

Time Shifting

$$f(t-t_o) \underset{\beta,t,\tau}{\longleftrightarrow} F_\beta(\tau-t_o) \qquad \text{(A-38)}$$

Integration Theorem

$$\int_{-\infty}^{t} f(t_o)dt_o \underset{\beta,t,\tau}{\longleftrightarrow} \int_{-\infty}^{\tau} F_\beta(\tau_o)d\tau_o \qquad \text{(A-39)}$$

Time Convolution

$$f_1(t) \underset{\beta,t,\tau}{\longleftrightarrow} F_\beta(\tau) \quad , \quad f_2(t) \underset{\beta,t,\tau}{\longleftrightarrow} G_\beta(\tau)$$

$$f_1(t) * f_2(t) \underset{\beta,t,\tau}{\longleftrightarrow} f_1(\tau) * G_\beta(\tau) \qquad \text{(A-40)}$$

or

$$f_1(t) * f_2(t) \underset{\beta,t,\tau}{\longleftrightarrow} F_\beta(\tau) * f_2(\tau) \qquad \text{(A-41)}$$

Frequency Convolution

$$f_1(t) \underset{\beta,t,\tau}{\longleftrightarrow} F_\beta(\tau) \quad , \quad f_2(t) \underset{\beta,t,\tau}{\longleftrightarrow} G_\beta(\tau)$$

$$F_\beta(t) * f_2(t) \underset{\beta,t,\tau}{\longleftrightarrow} F_\beta(\tau) * G_\beta(\tau) \tag{A-42}$$

or

$$f_1(t) * G_\beta(t) \underset{\beta,t,\tau}{\longleftrightarrow} F_\beta(\tau) * G_\beta(\tau) \tag{A-43}$$

Fresnel/Fourier Relationships

With

$$F_\beta(\tau) = \int_{-\infty}^{\infty} f(t) e^{-j\beta(t-\tau)^2} dt = \mathcal{F}_{\beta,\tau}[f(t)]$$

and

$$\mathcal{F}^{\circ}_{\omega}[f(t)] = \int_{-\infty}^{\infty} f(t) e^{-j\omega t} \, dt \tag{A-44}$$

then

$$F_\beta(\tau) = e^{-j\beta\tau^2} \mathcal{F}^{\circ}_{-2\beta\tau}[f(t) e^{-j\beta t^2}] \tag{A-45}$$

and

$$\mathcal{F}^{\circ}_{-2\beta\tau}[f(t)] = e^{j\beta\tau^2} \mathcal{F}_{\beta,\tau}[f(t) e^{j\beta t^2}] \tag{A-46}$$

Product of Two Signals

$$f(t)g(t) \underset{\beta,t,\tau}{\longleftrightarrow} \frac{\beta}{\pi} e^{-j\beta\tau^2} [\mathcal{F}_{\beta,\tau}[f(t)] e^{j\beta\tau^2} * \mathcal{F}^{*}_{\beta,-\tau}[g^{*}(t) e^{j\beta t^2}] e^{-j\beta\tau^2}]$$

or

$$f(t)g(t) \underset{\beta,t,\tau}{\longleftrightarrow} \frac{\beta}{\pi} e^{-j\beta\tau^2} [\mathcal{F}_{\beta,\tau}[g(t)] e^{j\beta\tau^2} * \mathcal{F}^{*}_{\beta,-\tau}[f^{*}(t) e^{j\beta t^2}] e^{-j\beta\tau^2}] \tag{A-47}$$

Product of Fresnel Transforms

$$\frac{\beta}{\pi} e^{j\beta t^2} [f(t) e^{-j\beta t^2} * \mathcal{F}^{-1^{*}}_{\beta,t}[G^{*}_{\beta}(\tau) e^{-j\beta\tau^2}] e^{j\beta t^2}] \underset{\beta,t,\tau}{\longleftrightarrow} F_\beta(\tau) G_\beta(\tau) \tag{A-48}$$

or

$$\frac{\beta}{\pi} e^{j\beta t^2} [g(t) e^{-j\beta t^2} * \mathcal{F}^{-1^{*}}_{\beta,t}[F^{*}_{\beta}(\tau) e^{-j\beta\tau^2}] e^{j\beta t^2}] \underset{\beta,t,\tau}{\longleftrightarrow} F_\beta(\tau) G_\beta(\tau)$$

The Equivalent Gibbs Phenomenon For Fresnel Transforms

With $F_\beta(\tau) = \int_{-\infty}^{\infty} f(t_o)e^{-j\beta(t_o-\tau)^2}\, dt_o$

then

$$f_\Omega(t) = \frac{\beta}{\pi}\int_{-\Omega}^{\Omega} F_\beta(\tau)e^{j\beta(t-\tau)^2}\, d\tau$$

$$= \frac{\beta}{\pi}\int_{-\Omega}^{\Omega}\int_{-\infty}^{\infty} f(t_o)e^{-j\beta(t_o-\tau)^2}e^{j\beta(t-\tau)^2}\, dt_o\, d\tau$$

$$= \frac{\beta}{\pi}\int_{-\infty}^{\infty} f(t_o)e^{j\beta(t^2-t_o^2)}\int_{-\Omega}^{\Omega} e^{j2\beta(t_o-t)\tau}\, d\tau\, dt_o$$

$$= \frac{\beta}{\pi}\int_{-\infty}^{\infty} f(t_o)e^{j\beta(t^2-t_o^2)}\frac{\sin(2\beta(t_o-t)\Omega)}{\beta(t_o-t)}\, dt_o$$

$$= \frac{\beta}{\pi}e^{j\beta t^2}\left[f(t)e^{-j\beta t^2} * \frac{\sin 2\beta\Omega t}{\beta t}\right]. \qquad \text{(A-49)}$$

For

$$f(t) = f_c(t) + [f(0^+) - f(0^-)]U(t) \qquad \text{(A-50)}$$

$$f_\Omega(t) = \frac{e^{j\beta t^2}}{\pi} \int_{-\infty}^{\infty} f_c(t_o) e^{-j\beta t_o^2} \frac{\sin(2\beta\Omega(t_o-t))}{(t_o-t)} dt_o$$

$$+ \frac{e^{j\beta t^2}}{\pi} [f(0^+) - f(0^-)] \int_{-\infty}^{\infty} U(t_o) e^{-j\beta t_o^2} \frac{\sin(2\beta\Omega(t_o-t))}{(t_o-t)} dt_o \; . \qquad \text{(A-51)}$$

The discontinuity at t=0 has now been replaced by the correlation of a $\frac{\sin x}{x}$ function with a causal baseband chirp due to the partial elimination of the Fresnel transform prior to inversion. In Fourier transform theory the discontinuity becomes the correlation of a sinx/x function with a unit step. This approaches a constant for t >> 0. Due to the chirp high frequency variation, however, the step discontinuity approaches zero as $t \to \infty$ for finite Ω.

Signal Product (Different Slopes)

In general

$$f(t)g(t) \xleftrightarrow[\beta,t,\tau]{} \frac{\alpha}{\pi} e^{-j\beta\tau^2} \int_{-\infty}^{\infty} F_\alpha(\tau_1) e^{j\alpha\tau_1^2} \int_{-\infty}^{\infty} g(t) e^{-j\gamma t^2}$$

$$e^{j(\alpha+\gamma-\beta)\left(t - \frac{(\alpha\tau_1-\beta\tau)}{\alpha+\gamma-\beta}\right)^2} dt \; e^{-j\frac{(\alpha\tau_1-\beta\tau)^2}{\alpha+\gamma-\beta}} d\tau_1 \qquad \text{(A-52)}$$

or for $\gamma=0$ and $\beta=2\alpha$

$$f(t)g(t) \xleftrightarrow[\beta,t,\tau]{} \frac{\beta}{2\pi} e^{-j\beta\tau^2} \int_{-\infty}^{\infty} F_{\frac{\beta}{2}}(\tau_1) e^{j\frac{\beta}{2}\tau_1^2}$$

$$\int_{-\infty}^{\infty} g(t) e^{-j\frac{\beta}{2}(t-(2\tau-\tau_1))^2} dt \; e^{j\frac{\beta}{2}(2\tau-\tau_1)^2} d\tau_1$$

$$f(t)g(t) \xleftrightarrow[\beta,t,\frac{\tau}{2}]{} \frac{\beta}{2\pi} e^{-j\beta\tau^2} [\mathcal{F}_{\frac{\beta}{2},\tau}[f(t)e^{j\frac{\beta}{2}\tau^2}] * \mathcal{F}_{\frac{\beta}{2},\tau}[g(t)]$$

$$e^{j\frac{\beta}{2}\tau^2}] \qquad \text{(A-53)}$$

Product of Fresnel Transforms (Different Slopes)

In general

$$\frac{\beta}{\gamma} e^{j\beta t^2} \int_{-\infty}^{\infty} f(t_1) e^{-j\alpha t_1^2} \int_{-\infty}^{\infty} G_\gamma(\tau) e^{j\gamma\tau^2} e^{-j(\alpha+\gamma-\beta)\left(\tau - \frac{(\alpha t_1 - \beta\tau)}{\alpha+\gamma-\beta}\right)^2} d\tau$$

$$e^{j \frac{(\alpha t_1 - \beta t)^2}{\alpha+\gamma-\beta}} dt_1 \underset{\beta,t,\tau}{\longleftrightarrow} F_\alpha(\tau) G_\gamma(\tau) \qquad \text{(A-54)}$$

Fresnel Transform Pairs

$$\delta(t) \underset{\beta,t,\tau}{\longleftrightarrow} e^{-j\beta\tau^2} \qquad \text{(A-55)}$$

$$1 \underset{\beta,t,\tau}{\longleftrightarrow} \sqrt{\frac{\pi}{\beta}} e^{-j\frac{\pi}{4}} \qquad \text{(A-56)}$$

or by using Eq. (A-146) and the symmetry property.

$$e^{j\alpha t^2} \underset{\beta,t,\tau}{\longleftrightarrow} \sqrt{\frac{\pi}{|\beta-\alpha|}} e^{-j\frac{|\beta-\alpha|}{\beta-\alpha}\frac{\pi}{4}} e^{j\frac{\alpha\beta}{\beta-\alpha}\tau^2} \quad \text{(for } \alpha \text{ pos. or neg.)} \qquad \text{(A-57)}$$

$$\underset{\beta,t,\tau}{\longleftrightarrow} \frac{\pi}{\beta}\delta(\tau) \qquad \text{for } \alpha = \beta \quad \text{(see Eq. (A-148))}$$

$$\cos\beta t^2 \underset{\beta,t,\tau}{\longleftrightarrow} \frac{\pi}{2\beta}\delta(\tau) + \sqrt{\frac{\pi}{8\beta}} e^{-j\frac{\pi}{4}} e^{-j\frac{\beta}{2}\tau^2} \qquad \text{(A-58)}$$

Likewise

$$\sin\beta t^2 \underset{\beta,t,\tau}{\longleftrightarrow} -j\frac{\pi}{2\beta}\delta(\tau) + j\sqrt{\frac{\pi}{8\beta}} e^{-j\frac{\pi}{4}} e^{-j\frac{\beta}{2}\tau^2} \qquad \text{(A-59)}$$

$$\cos(\beta t^2+\phi) \underset{\beta,t,\tau}{\longleftrightarrow} \frac{\pi}{2\beta} e^{j\phi}\delta(\tau) + \sqrt{\frac{\pi}{8\beta}} e^{-j\phi} e^{-j\frac{\pi}{4}} e^{-j\frac{\beta}{2}\tau^2} \qquad \text{(A-60)}$$

$$e^{\pm j\omega_o t} \underset{\beta,t,\tau}{\longleftrightarrow} \sqrt{\frac{\pi}{\beta}} e^{-j\frac{\pi}{4}} e^{j\frac{\omega_o^2}{4\beta}} e^{\pm j\omega_o\tau} \qquad \text{(A-61)}$$

$$\cos\omega_o t \underset{\beta,t,\tau}{\longleftrightarrow} \sqrt{\frac{\pi}{\beta}}\, e^{-j\frac{\pi}{4}}\, e^{j\frac{\omega_o^2}{4\beta}} \cos\omega_o\tau \tag{A-62}$$

$$\cos\alpha t^2 \underset{\beta,t,\tau}{\longleftrightarrow} \frac{1}{2}\, e^{-j\frac{|\beta-\alpha|}{\beta-\alpha}\frac{\pi}{4}} \left[\sqrt{\frac{\pi}{|\beta-\alpha|}}\, e^{j\frac{\alpha\beta}{\beta-\alpha}\tau^2} + \sqrt{\frac{\pi}{|\beta+\alpha|}}\, e^{-j\frac{\alpha\beta}{\beta+\alpha}\tau^2}\right] \tag{A-63}$$

$$e^{j(\omega_o t + \beta t^2)} \underset{\beta,t,\tau}{\longleftrightarrow} \frac{\pi}{\beta}\, e^{-j\frac{\omega_o^2}{4\beta}}\, \delta(\tau + \frac{\omega_o}{2\beta}) \tag{A-64}$$

$$e^{j(\omega_o t + \alpha t^2)} \underset{\beta,t,\tau}{\longleftrightarrow} e^{-j\beta\tau^2} \sqrt{\frac{\pi}{|\beta-\alpha|}}\, e^{-j\frac{\pi}{4}}\, e^{j\frac{(2\beta\tau + \omega_o)^2}{4(\beta-\alpha)}} \tag{A-65}$$

$$e^{-j(\omega_o t + \alpha t^2)} \underset{\beta,t,\tau}{\longleftrightarrow} e^{-j\beta\tau^2} \sqrt{\frac{\pi}{|\beta+\alpha|}}\, e^{-j\frac{\pi}{4}}\, e^{j\frac{(2\beta\tau - \omega_o)^2}{4(\beta+\alpha)}} \tag{A-66}$$

$$e^{-j(\omega_o t + \beta t^2)} \underset{\beta,t,\tau}{\longleftrightarrow} e^{-j\beta\tau^2} \sqrt{\frac{\pi}{2\beta}}\, e^{-j\frac{\pi}{4}}\, e^{j\frac{(2\beta\tau - \omega_o)^2}{8\beta}} \tag{A-67}$$

$$U(t) \underset{\beta,t,\tau}{\longleftrightarrow} \int_{-\infty}^{\tau} e^{-j\beta x^2} dx \tag{A-68}$$

$$= \sqrt{\frac{\pi}{2\beta}} \left[\frac{e^{-j\frac{\pi}{4}}}{2} + C(\tau\sqrt{\frac{2\beta}{\pi}}) - jS(\tau\sqrt{\frac{2\beta}{\pi}})\right]$$

$$\int_{-\infty}^{t} e^{j\beta t_o^2} dt_o \underset{\beta,t,\tau}{\longleftrightarrow} \frac{\pi}{\beta}\, U(\tau) \tag{A-69}$$

$$te^{-j\beta t^2} \underset{\beta,t,\tau}{\longleftrightarrow} \sqrt{\frac{\pi}{8\beta}}\, e^{-j\frac{\pi}{4}}\, \tau e^{-j\frac{\beta}{2}\tau^2} \tag{A-70}$$

$$\int_{-\infty}^{t} \cos\beta x^2 dx \underset{\beta,t,\tau}{\longleftrightarrow} \frac{\pi}{2\beta}\, U(\tau) + \sqrt{\frac{\pi}{8\beta}}\, e^{-j\frac{\pi}{4}} \int_{-\infty}^{\tau} e^{-j\frac{\beta}{2}\tau_o^2} d\tau_o \tag{A-71}$$

$$\sqrt{\frac{\pi}{8\beta}} + \sqrt{\frac{\pi}{2\beta}}\, C(t\sqrt{\frac{2\beta}{\pi}}) = \int_{-\infty}^{t} \cos\beta x^2 dx$$

$$f(t) = \begin{cases} \text{at } t>0 \\ 0 \ t<0 \end{cases} \underset{\beta,t,\tau}{\longleftrightarrow} \int_{-\infty}^{a\tau} \int_{-\infty}^{\tau_o} e^{-j\beta x^2} dx \, d\tau_o \tag{A-72}$$

$$P_{\frac{T}{2}}(t) = [U(T + \tfrac{T}{2}) - U(t - \tfrac{T}{2})] \underset{\beta,t,\tau}{\longleftrightarrow} \int_{\tau-T}^{\tau+T} e^{-j\beta x^2} dx \tag{A-73}$$

$$= \sqrt{\frac{\pi}{2\beta}} \left[e^{-j\frac{\pi}{4}} + C((\tau+T)\sqrt{\tfrac{2\beta}{\pi}}) + C((\tau-T)\sqrt{\tfrac{2\beta}{\pi}})\right.$$

$$\left. - jS((\tau+T)\sqrt{\tfrac{2\beta}{\pi}}) - jS((\tau-T)\sqrt{\tfrac{2\beta}{\pi}})\right]$$

Proof:

$$\delta(t+t_o) + \delta(t-t_o) \underset{\beta,t,\tau}{\longleftrightarrow} 2e^{-j\beta(\tau^2+t_o^2)}\cos 2\beta t_o\tau \tag{A-74}$$

$$\frac{2\beta}{\pi} e^{j\beta(t^2+\tau_o^2)}\cos 2\beta\tau_o t \underset{\beta,t,\tau}{\longleftrightarrow} \delta(\tau+\tau_o) + \delta(\tau-\tau_o) \tag{A-75}$$

$$\delta(t+t_o) - \delta(t-t_o) \underset{\beta,t,\tau}{\longleftrightarrow} 2je^{-j\beta(\tau^2+t_o^2)}\sin 2\beta t_o\tau \tag{A-76}$$

$$j\frac{2\beta}{\pi} e^{j\beta(t^2+\tau_o^2)}\sin 2\beta\tau_o t \underset{\beta,t,\tau}{\longleftrightarrow} \delta(\tau+\tau_o) - \delta(\tau-\tau_o) \tag{A-77}$$

$$\sqrt{\frac{\pi}{2\beta}} S(t\sqrt{\tfrac{2\beta}{\pi}}) + \sqrt{\frac{\pi}{8\beta}} = \int_{-\infty}^{t} \sin\beta x^2 dx \underset{\beta,t,\tau}{\longleftrightarrow} -j\frac{\pi}{2\beta} U(\tau)$$

$$+ j\sqrt{\frac{\pi}{8\beta}} e^{-j\frac{\pi}{4}} \int_{-\infty}^{\tau} e^{-j\frac{\beta}{2}x^2} dx \tag{A-78}$$

$$\frac{\sin at}{t} e^{j\beta t^2} \underset{\beta,t,\tau}{\longleftrightarrow} \frac{\pi}{\beta} e^{-j\beta\tau^2}[U(\tau + \tfrac{a}{2\beta}) - U(\tau - \tfrac{a}{2\beta})] \tag{A-79}$$

In general

$$f(t)e^{j\beta t^2} \underset{\beta,t,\tau}{\longleftrightarrow} e^{-j\beta\tau^2} \mathcal{F}^{o}_{-2\beta\tau}(f(t)) \tag{A-80}$$

$$= e^{-j\beta\tau^2} \int_{-\infty}^{\infty} f(t)e^{j(2\beta\tau)t} \, dt$$

$$U(t)e^{j\beta t^2} \underset{\beta,t,\tau}{\longleftrightarrow} j\frac{\tau}{\beta}\frac{e^{-j\beta\tau^2}}{\tau} \qquad \text{(A-81)}$$

The Fresnel Transform and the Chirp Filter

The output, g(t), for an input, f(t), of a device having the impulse response given by

$$h(t) = e^{-j\beta t^2} \qquad \text{(A-82)}$$

is

$$g(t) = \int_{-\infty}^{\infty} f(\tau)e^{-j\beta(t-\tau)^2}d\tau \qquad \text{(A-83)}$$

which is exactly the Fresnel transform of f(t).

The impulse response given by Eq. (A-82), however, is not realizable. A realizable form is given by

$$h_r(t) = [U(t) - U(t-T)]\cos(\omega_o t - \beta t^2) \ . \qquad \text{(A-84)}$$

If f(t) exist over the interval $0 \le t \le T_1$ (only) where $T_1 < T$, then over the interval $T_1 \le t \le T$ the output of this device is given by

$$g(t) = \frac{1}{2}e^{j\omega_o t}\int_{-\infty}^{\infty} f(\tau)e^{-j\omega_o\tau}e^{-j\beta(t-\tau)^2}d\tau + c.c.$$

$$= \frac{1}{2}e^{j\omega_o t}\mathcal{F}_{\beta,\tau}[f(\tau)e^{-j\omega_o\tau}] + c.c.$$

$$= \frac{1}{2}e^{j\omega_o t}[R_{\beta,t} + jX_{\beta,t}] + c.c.$$

$$= \frac{1}{2}[R_{\beta,t}[f(\tau)e^{-j\omega_o\tau}]\cos\omega_o\tau - X_{\beta,t}[f(\tau)e^{-j\omega_o\tau}]\sin\omega_o t] \ . \qquad \text{(A-85)}$$

The output of this realizable (yet still somewhat idealized) device is therefore the real and imaginary Fresnel transforms of f(t) in phase quadrature to one another.

With $f(t) = f_o(t)\cos\omega_o t$

then

$$g(t) = \frac{1}{2}\left[R_{\beta,t}[f(\tau)]\cos\omega_o t - X_{\beta,t}[f(\tau)]\sin\omega_o t + R_{\beta,t}[f(\tau)e^{-j2\omega_o\tau}]\right.$$

$$\left.\cos\omega_o t - X_{\beta,t}[f(\tau)e^{-j2\omega_o\tau}]\sin\omega_o t\right] \qquad \text{(A-86)}$$

and with $f(t) = f_o(t)\cos\omega_1 t$

then

$$g(t) = \frac{1}{2}\left[R_{\beta,t}[f(\tau)e^{-j(\omega_o-\omega_1)\tau}]\cos\omega_o t - X_{\beta,t}[f(\tau)e^{-j(\omega_o-\omega_1)\tau}]\sin\omega_o t\right.$$

$$+ R_{\beta,t}[f(\tau)e^{-j(\omega_o+\omega_1)\tau}]\cos\omega_o t - X_{\beta,t}[f(\tau)e^{-j(\omega_o+\omega_1)\tau}]$$

$$\left.\sin\omega_o t\right] \qquad \text{(A-87)}$$

In most cases the sum frequency terms in Eqs. (A-86) and (A-87) will integrate to a much smaller value than the difference terms since they will usually be of a much higher frequency. In this case, only one set of quadrature real and imaginary Fresnel transforms is obtained. If the slope is negated in Eq. (A-84), all the terms modulating sines in Eqs. (A-86) and (A-87) are made positive and the complex exponentials are complex conjugated. Note that since

$$\mathcal{F}_{\beta,t}\{f(t)e^{j\omega_o t}\} = e^{j(\omega_o t + \omega_o^2/4\beta)}\mathcal{F}_{\beta,\ t+\omega_o/2\beta}\{f(t)\} \qquad \text{(A-88)}$$

Eq. A-179 becomes

$$g(t) = \frac{1}{2}\{R^{\{f(t)\}}_{\beta,t-(\omega_o-\omega_1)/2\beta}\cos(\omega_1 t + (\omega_1-\omega_o)^2/4\beta)$$

$$+ X^{\{f(t)\}}_{\beta,t-(\omega_o-\omega_1)/2\beta}\sin(\omega_1 t + (\omega_1-\omega_o)^2/4\beta)\} \qquad \text{(A-89)}$$

or the delayed components of the Fresnel transform of f(t).

APPENDIX B

Other Transforms

Section 2.5 describes the process by which the SAW convolver can be used as the main constituent of a Fourier transform system. Essentially the Fourier transform of a signal is obtained by convolving a signal, that has been pre-multiplied by a chirp of one slope, with a chirp (linear FM) of the opposite slope. The result of this process is the Fourier transform on a chirp carrier. Coherent detection by mixing this convolver output with properly phased chirps results in the isolation of the real and imaginary components of the Fourier transform as baseband signals. Section 2.4 describes the equivalent technique whereby a chirp filter can be used to perform the Fourier transformation. In this case the chirp modulated input signal is automatically convolved by an oppositely sloped chirp since this is exactly the impulse response of a chirp filter. Although the output of the convolver and the chirp filter are both chirp modulated Fourier transforms, the convolver output is compressed by a factor of two since it performs a factor-of-two-compressed convolution.

The question may arise as to whether other transforms can be obtained utilizing convolvers, chirp filters or both. It is the purpose of this section to demonstrate that this is indeed the case. After describing the operations involved in obtaining some readily obtainable transforms, some general criteria will be presented by which tests can be performed on transform kernels to determine whether the transform can be obtained by a convolution process. A variable transformation procedure will then be described that shows how to transform a non-convolutionary transform into a transform that can be obtained by a convolution process. Transforms obtainable using a linear to exponential time transformation will then be

described as well as a technique by which a signal can be exponentially time transformed using a large time-bandwidth-product chirp filter.

The Laplace transform given by

$$L(\alpha,\omega) = \int_0^\infty f(t)e^{-(\alpha+j\omega)t}\,dt$$

$$= \int_0^\infty (f(t)e^{-\alpha t})e^{-j\omega t}\,dt \qquad \text{(B-1)}$$

is a function of the two variables α and ω. As seen in Eq. (B-1), since $f(t)$ is always causal ($f(t) = 0$ for $t < 0$) this transform for any particular value of α is given by the Fourier transform of $f(t)e^{-\alpha t}$. This suggests that the Laplace transform can be displayed for a causal time function by multiplying this function by $e^{-\alpha t}$ and using either the convolver or the chirp filter Fourier-transformation schemes (see sections 2.4 and 2.5) as methods for obtaining the Fourier transform of this combination. The Fourier transform obtained for a particular value of α can be displayed in a raster type of display, alongside but spaced from the transform for the previous value, on an oscilloscope screen. The parameter would be incremented by a constant value between successive scans and all the scans would be displayed evenly spaced. For very high scanning densities the Laplace transform would appear as a continuous three-dimensional function. The exponential function $\exp(-\alpha t)$ could be obtained by electronically switching in smaller values of resistance in a passive RC network. At the time for mixing between $f(t)$ and $\exp(-\alpha t)$ the RC network can be discharged and the exponentially decaying potential across the resistor applied to a mixer to which $f(t)$, already on some carrier, is also applied. For negative values of α the same RC circuit output can be

passed through a reciprocal producing circuit, which is simply a divide-into-one process, and the output from this circuit then applied to the mixer. In either case, the exponentially weighted function is then mixed with a chirp and convolved with a chirp of opposite slope in either a convolver or a chirp filter. The resultant slice of the Laplace transform (along the $j\omega$ axis at α) will be modulated onto a chirp after passage through these devices. Removal of the chirp by diode detection will produce a baseband output that is the square of the magnitude of this transform slice. By coherently detecting using sine and cosine chirps, the real and imaginary components of the Laplace transform can be separated and displayed independently. This technique can be used to pinpoint the poles and zeroes of a passive network by impulsing the network and using the resulting impulse response as the input function for every slice of the Laplace transform that may be required for a clear and continuous display. Since SAW convolvers and chirp filters utilize signals that are measured in microseconds, the longer device impulse responses can be captured into a CCD buffer memory using a slow clock (greater than the required Nyquist sampling rate, however) and then clocked, using a much faster clock, into the chirp transform system after the exponential multiplication. As with the Fourier transform obtained using these finite-impulse-response devices, the Laplace transform output will be valid only over a calculable time interval.

The Stieltjes transform $S(t)$ given by

$$S(t) = \int_0^\infty \frac{f(\tau)d\tau}{\tau+t} = f(-t) * \frac{1}{t} \qquad \text{(B-2)}$$

or

$$S(-t) = f(t) * \frac{1}{-t} \quad \text{for } f(t) = 0 \quad t < 0$$

and the Hilbert transform H(y) given by

$$H(t) = \frac{1}{\pi} \int_{-\infty}^{\infty} \frac{f(\tau)d\tau}{\tau - t} = \frac{1}{\pi} f(t) * \frac{1}{-t} \tag{B-3}$$

are both convolutionary transforms and can therefore be immediately obtained, for a finite duration signal f(t), using a SAW convolver or any other type of convolver for that matter. The Stieltjes transform assumes a causal signal (a device impulse response, for instance) whereas the Hilbert transform does not. Note that except for a factor of $1/\pi$, for causal signals the two transforms are time inverse versions of one another. Whether or not a signal is causal, however, the Hilbert transform of the signal is nevertheless of identical form to the time inverted Stieltjes transform and the Hilbert transform of a non-causal signal is exactly the time inverted Stieltjes transform of a delayed and causal version of the signal. Both transforms can therefore be obtained in an identical fashion where one will be time inverted and the t = 0 reference point for the input signal must be decided upon ahead of time. This flexibility is due to the fact that the transforms are themselves delayed for a delayed input signal.

The Stieltjes transform is obtained when two repeated Laplace transforms are performed on a function, i.e.

$$S(t) = \int_0^{\infty} \int_0^{\infty} f(x)e^{-px}\, dx\, e^{-pt}\, dp \tag{B-4}$$

since

$$\int_0^{\infty} e^{-p(x-y)}\, dp = 1/(x+y) \tag{B-5}$$

The Hilbert transform of a function, when summed with this function, produces a complex signal (which can be carrier modulated producing in-phase and quadrature components) that is purely single-sidebanded. This transform can also be obtained by amplitude inverting the negative portion of the Fourier transform of the signal and then taking an inverse transform of this using a chirp transform system (see section 2.4).

If it is desired to obtain these two transforms directly using a convolver, then the function f(-t) or f(t) must be convolved with 1/t or -1/t in order to obtain S(t) or H(t), respectively. In either case a reciprocal of t function is required and this function 'blows up' at t = 0. A close approximation to this function can be used since the signal, f(t), will typically have negligible frequency components beyond $\omega = \omega_o$ rad/sec. Since

$$-\frac{1}{t} \longleftrightarrow j\pi \operatorname{sgn}\omega = \begin{cases} j\pi & \omega > 0 \\ -j\pi & \omega < 0 \end{cases} \qquad \text{(B-6)}$$

the spectrum of -1/t for the bandlimited signal f(t) can be replaced by

$$g(\omega) = j\pi\left[2U(\omega) - U(\omega-2\omega_o) - U(\omega+2\omega_o)\right] \qquad \text{(B-7)}$$

so that

$$\frac{-2\sin^2\omega_o t}{t} \longleftrightarrow g(\omega) \qquad \text{(B-8)}$$

and the Hilbert transform becomes

$$H(t) = \frac{1}{\pi} f(t) * \frac{2\sin^2\omega_o t}{-t} \qquad \text{(B-9)}$$

Likewise the Stieltjes transform can be approximated by

$$S(t) = f(-t) * \frac{2\sin^2 \omega_o t}{t} \tag{B-10}$$

Two other transforms can be readily obtained since they are mere extensions of the Fourier transform. The Fourier sine and cosine transforms given by

$$F_s(\omega) = \int_o^\infty f(t)\sin\omega t \, dt \tag{B-11}$$

and

$$F_c(\omega) = \int_o^\infty f(t)\cos\omega t \, dt \tag{B-12}$$

are simply the real and imaginary components, respectively, of the complex Fourier transform of the causal function $f(t)$. These components are natural products of a chirp transform system where the origin for the time is controlled by adjusting the form of the post multiplying chirp (see section 2.4). If the signal is not causal in such a system, the resultant real and imaginary Fourier components are the Fourier cosine and sine transforms, respectively, of the even and odd components, respectively, of the signal.

In general, the output of a convolution process can be written as

$$\int_{-\infty}^{\infty} f(\tau)K(t,\tau)d\tau = h(t) \int_{-\infty}^{\infty} f(\tau)g(\tau)\ell(t-\tau)d\tau$$

$$= h(t)\left[f(t)g(t) * \ell(t)\right] \tag{B-13}$$

where

$$K(t,\tau) = g(\tau)h(t)\ell(t-\tau) \tag{B-14}$$

can be the kernel for a transformation. In other words, if a transform kernel can be written in the form of Eq. (B-14), then the transform can be obtained as a result of a convolution. For such a kernel, since

$$\frac{\partial \ell(t-\tau)}{\partial \tau} = -\frac{\partial \ell(t-\tau)}{\partial t} = -\frac{\partial \ell(t-\tau)}{\partial (t-\tau)} \tag{B-15}$$

then

$$L \triangleq \frac{1}{K(t,\tau)}\left[\frac{\partial}{\partial t} K(t,\tau) + \frac{\partial}{\partial \tau} K(t,\tau)\right]$$

$$= \frac{1}{h(t)} \frac{\partial h(t)}{\partial t} + \frac{1}{g(\tau)} \frac{\partial g(\tau)}{\partial \tau} \tag{B-16}$$

and

$$\frac{\partial^2}{\partial t \partial \tau} L = 0 \tag{B-17}$$

Eq. (B-17) is a necessary condition that must be satisfied by a kernel in order that it have a form given by Eq. (B-14). Up to this point, it was found that a kernel having the form of Eq. (B-14) must definitely satisfy Eq. (B-17), but this does not imply that other forms will not satisfy this condition. However, in order for Eq. (B-17) to always be true, then

$$\frac{\partial}{\partial t} K(t,\tau) + \frac{\partial}{\partial \tau} K(t,\tau) = K(t,\tau)\left[\alpha(t) + \beta(t)\right]$$

$$= \frac{\partial K(t,\tau)}{\partial \lambda} \tag{B-18}$$

where

$$t = \lambda + f_1(s) \tag{B-19}$$

and

$$\tau = \lambda + f_2(s) \tag{B-20}$$

Solution of Eq. (B-18) gives

$$K(t,\tau) = \exp\left[\int(\alpha(\lambda+f_1(s)) + \beta(\lambda+f_2(s)))d\lambda + f_3(s)\right]$$

$$= \exp\left[\hat{\alpha}(t) + \hat{\beta}(\tau) + f_3(s)\right]$$

$$= \tilde{\alpha}(t)\tilde{\beta}(\tau)\gamma(t-\tau) \tag{B-21}$$

since

$$t-\tau = f_1(s) - f_2(s) = f_o(s) \tag{B-22}$$

or

$$s = f^{-1}(t-\tau) \tag{B-23}$$

so that

$$\gamma(t-\tau) = \exp\left[f_3(f^{-1}(t-\tau))\right] \tag{B-24}$$

Therefore, Eq. (B-21) states that the form of kernel given by Eq. (B-14) is the only form that will satisfy Eq. (B-17). From this, Eq. (B-17) can be designated as a necessary and sufficient condition that must be satisfied by a kernel of the form of Eq. (B-14). If a kernel fails this test it does not have such a form and if it passes it does.

If a transform kernel has the form of Eq. (B-14), then since

$$\frac{\partial}{\partial t} L = \frac{\partial}{\partial t}\left(\frac{1}{h(t)} \frac{\partial h(t)}{\partial t}\right) = L_t \tag{B-25}$$

and

$$\frac{\partial}{\partial \tau} L = \frac{\partial}{\partial \tau}\left(\frac{1}{g(\tau)} \frac{\partial g(\tau)}{\partial \tau}\right) = L_\tau \tag{B-26}$$

$h(t)$ and $g(\tau)$ are given by

$$h(t) = \exp\left[\int\int L_t dt^2\right] \tag{B-27}$$

and

$$g(\tau) = \exp\left[\int\int L_\tau d\tau^2\right] \tag{B-28}$$

Using the relationship

$$\frac{1}{\ell(t-\tau)} \frac{\partial \ell(t-\tau)}{\partial(t-\tau)} = \frac{1}{g(\tau)} \frac{\partial g(\tau)}{\partial \tau} - \frac{1}{K(t,\tau)} \frac{\partial}{\partial \tau} K(t,\tau) \tag{B-29}$$

and making the substitution $z = t-\tau$ gives

$$\ell(z) = \exp\left[\int\left(\int L_\tau d\tau - \frac{1}{K(z+\tau,\tau)}\frac{\partial}{\partial\tau}K(z+\tau,\tau)\right)dz\right] \tag{B-30}$$

These results can now be applied to some well known transforms. The Mellin transform given by

$$M(\omega) = \int_0^\infty f(t)t^{j\omega-1}\,dt \tag{B-31}$$

has a kernel given by

$$K(t,\omega) = t^{j\omega-1} \tag{B-32}$$

Substitution into Eq. (B-17) gives

$$\frac{\partial^2}{\partial t\partial\omega}L = -j/t^2 \neq 0 \tag{B-33}$$

so that the Mellin transform cannot be written in the form of Eq. (B-13)

The Fourier transform given by

$$F(\omega) = \int_{-\infty}^\infty f(t)e^{-j\omega t}\,dt \tag{B-34}$$

has a kernel given by

$$K(t,\tau) = e^{-j\omega t} \tag{B-35}$$

This kernel does satisfy Eq. (B-17) and using Eqs. (B-27), (B-28) and (B-30)

$$h(t) = \exp\left(-j\frac{t^2}{2}\right) \tag{B-36}$$

$$g(\omega) = \exp\left(-j\frac{\omega^2}{2}\right) \tag{B-37}$$

and

$$\ell(z) = \exp\left(j\frac{z^2}{2}\right) \tag{B-38}$$

so that

$$F(\omega) = e^{-j\frac{\omega^2}{2}}\left[f(t)e^{-j\frac{t^2}{2}} * e^{j\frac{t^2}{2}}\right] \tag{B-39}$$

Since $K(t,\omega)$ can also be written as

$$K(t,\omega) = K(t,2\beta\tau) = e^{-j\beta t^2}\, e^{-j\beta\tau^2}\, e^{j\beta(t-\tau)^2} \tag{B-40}$$

then

$$F(\omega) = e^{-j\beta\tau^2}\left[f(t)e^{-j\beta t^2} * e^{j\beta t^2}\right] \tag{B-41}$$

where $\omega = 2\beta\tau$ and Eq. (B-41) is the complex baseband version of the already familiar chirp transform algorithm.

The Hilbert transform given by Eq. (B-3) has already been shown to be of convolutional form. This transform satisfies the criterion, as it should, and Eqs. (B-27), (B-28) and (B-30) give for this case

$$h(t) = g(\omega) = 1 \tag{B-42}$$

$$\ell(z) = \ell(t-\omega) = (t-\omega)^{-1} \tag{B-43}$$

In actual practice there are few transforms that can be expected to satisfy Eq. (B-14) and therefore become readily obtainable by the performance of a single convolution. However, if variable transformations can be made, an extra degree of freedom is introduced so that the transform kernel may be forced into the proper form. As will be shown, at the convenience of being able to obtain a particular transform by a convolution, the input and output signals must undergo variable transformations to realize the overall transformation process.

It would now be desirable to find the variable transformations

$$t = f_1(\tau) \tag{B-44}$$

and

$$\omega = f_2(\nu) \tag{B-45}$$

that would transform $K(t,\omega)$ into the form

$$K(t,\omega) = K(f_o(\nu-\tau)) \tag{B-46}$$

Since

$$\frac{\partial f_o(\nu-\tau)}{\partial \tau} = \frac{-\partial f_o(\nu-\tau)}{\partial \nu} \tag{B-47}$$

then a kernel will satisfy the relationship

$$\frac{\partial K(t,\omega)}{\partial t}\frac{\partial t}{\partial \tau} + \frac{\partial K(t,\omega)}{\partial \omega}\frac{\partial \omega}{\partial \nu} = K_t t_\tau + K_\omega \omega_\nu = 0 \tag{B-48}$$

From this it can be seen that

$$(Mt_\tau)_t = M_t t_\tau + Mt_{\tau t} = 0 \tag{B-49}$$

where

$$M = K_t/K_\omega \tag{B-50}$$

and the criteria

$$\left(\frac{Mt}{M}\right)_\omega = 0 \tag{B-51}$$

follows directly from this. A kernel must satisfy Eq. (B-51) in order to be a candidate for a transformation of the form of Eq. (B-46). Eq. (B-49) can be solved for τ to give

$$\tau = \int \exp(\int (M_t/M)dt)dt \tag{B-52}$$

From Eq. (B-48) the variable ν is found to be given by

$$\nu = -\int (M)^{-1}\exp(\int (M_t/M)dt)d\omega \tag{B-53}$$

When these equations are used for the kernel of the form

$$K(t,\omega) = G(t\omega) \tag{B-54}$$

Eq. (B-51) is satisfied and the variable transformations are given by

$$\tau = \ell nt \tag{B-55}$$

and

$$\nu = - \ell n\omega \tag{B-56}$$

so that for

$$T(\omega) = \int_{t_1}^{t_2} f(t)G(t\omega)dt \tag{B-57}$$

we obtain

$$T(-\ell n\omega) = \int_{\ell nt_1}^{\ell nt_2} f(e^{\tau})e^{\tau}G(e^{-(\nu-\tau)})d\tau \tag{B-58}$$

This result can now be applied to some typical transforms. The Hankel Transform $H_a(\omega)$ is given by

$$H_a(\omega) = \int_0^{\infty} tf(t)J_v(\omega t)dt \tag{B-59}$$

where $J_v(t)$ is a Bessel function of the first kind and order v. Using Eq. (B-58) this becomes

$$H_a(-\ell n\omega) = \int_{-\infty}^{\infty} f(e^{\tau})e^{2\tau}J_v(e^{-(\nu-\tau)})d\tau$$

$$= f(e^{\nu})e^{2\nu} * J_v(e^{-\nu}) = H_a(\nu) \tag{B-60}$$

In this case the signal f(t) requires an exponential time transformation and the result of the above convolution also requires an exponential transformation before the Hankel transform is obtained. The Fourier sine and cosine transforms given by Eqs. (B-11) and (B-12) can be transformed to give

$$F_s(-\ell n\omega) = \int_{-\infty}^{\infty} f(e^{\tau})e^{\tau}\sin(e^{-(\nu-\tau)})d\tau$$

$$= f(e^{\nu})e^{\nu} * \sin(e^{-\nu}) = F_3(\nu) \tag{B-61}$$

and

$$F_c(-\ell n\omega) = \int_{-\infty}^{\infty} f(e^{\tau})e^{\tau}\cos(e^{-(\nu-\tau)})d\tau$$

$$= f(e^{\nu})e^{\nu} * \cos(e^{-\nu}) = F_c(\nu) \qquad \text{(B-62)}$$

The Y transform given by

$$g(\omega) = \int_0^{\infty} (\omega t)^{\frac{1}{2}} f(t)Y_v(\omega t)dt \qquad \text{(B-63)}$$

where $Y_v(t)$ is a Bessel function of the second kind and order v, and its inverse, the H transform, given by

$$f(t) = \int_0^{\infty} (\omega t)^{\frac{1}{2}} g(\omega)H_v(\omega t)d\omega \qquad \text{(B-64)}$$

where $H_v(t)$ is Struve's function given by

$$H_v(t) = \sum_{r=0}^{\infty} \frac{(-1)^r(\frac{1}{2}t)^{v+2r+1}}{\Gamma(r+\frac{3}{2})\Gamma(r+v+\frac{3}{2})} \quad v > -\frac{3}{2} \qquad \text{(B-65)}$$

can both be transformed using Eq. (B-58) to give

$$g(-\ell n\omega) = \int_{-\infty}^{\infty} f(e^{\tau})e^{\tau}e^{-\frac{1}{2}(\nu-\tau)}Y_v(e^{-(\nu-\tau)})d\tau$$

$$= f(e^{\nu})e^{\nu} * e^{-\frac{1}{2}\nu}Y_v(e^{-\nu}) = g(\nu) \qquad \text{(B-66)}$$

and

$$f(\ell nt) = \int_{-\infty}^{\infty} g(e^{-\nu})e^{-\nu}e^{\frac{1}{2}(\tau-\nu)}H_v(e^{\tau-\nu})d\nu$$

$$= g(e^{-\tau})e^{-\tau} * e^{\frac{1}{2}\tau}H_v(e^{\tau}) \qquad \text{(B-67)}$$

Note that all these transforms can be obtained over a finite time period and for signals of the proper duration using a SAW convolver assuming that

the exponential variable change can be accomplished for both the signal and the output. The functions multiplying the signal and those convolving with it must be electronically generated; however, they never have to be changed. The output using a SAW convolver, it must be remembered, is compressed by a factor of two.

A technique for the exponential time scaling of a signal that utilizes the large time-bandwidth product of SAW chirp filters will be described after the technique for taking the Mellin transform is discussed, since exponential scaling for this process is to be used as an example. The Mellin transform given by Eq. (B-31) can be transformed into

$$M(\omega) = \int_{-\infty}^{\infty} f(e^{\tau})e^{j\omega\tau}\, d\tau = \overline{M}(f(t)) \tag{B-68}$$

by the substitution $t = e^{\tau}$. Note that by exponentially time scaling only the input signal, the Mellin transform can be readily obtained by taking the Fourier transform of this modified signal. A convolver or chirp filter chirp transform system can be used to take the Fourier transform. The Mellin transform is a powerful transform in optical processing since its magnitude is invariant to a scale change in the signal that can occur by variable adjustment of lens positions in an imaging system. In particular the following relationship is obtained:

$$\overline{M}(f(at)) = a^{-j\omega}\, \overline{M}(f(t)) = a^{-j\omega}\, M(\omega) \tag{B-69}$$

The Mellin transform assumes a causal signal. For this discussion it will be assumed that the signal exists over the interval $a \leq t \leq b$ where 'a' can approach but never be zero since an exponential scaling of a signal beginning at time $t = 0$ results in a signal of infinite duratior Using the form of the Mellin transform given by

$$M(\omega) = e^{j\omega \ell na} \int_{-\infty}^{\infty} f(e^{(\tau+\ell na)}) e^{j\omega\tau}\, d\tau \qquad \text{(B-70)}$$

and the identity

$$\overline{M}(f(t^c)) = c^{-1} M(\omega/c) \qquad \text{(B-71)}$$

the following equation is obtained

$$M(\omega/c) = c\, e^{j\frac{\omega}{c}\ell na} \int_{-\infty}^{\infty} f(ae^{c\tau}) e^{j\omega\tau}\, d\tau \qquad \text{(B-72)}$$

Eq. (B-72) states that an expanded version (for $c > 1$) of the Mellin transform can be obtained for the function $f(t)$, existing between $t = a$ and $t = b$, by taking the Fourier transform of the function $f(ae^{c\tau})$, existing from $\tau = 0$ to $\tau = c^{-1}\ell n(b/a)$, and multiplying this result by c and the phase term $\exp j(\omega/c)\ell na$. If $b-a$ is confined to being less than some time T (as it will have to be) and if the exponentially varying version of the signal is to be of duration $T-(b-a)$, then

$$c = \frac{\ell n(b/a)}{T-(b-a)} \qquad \text{(B-73)}$$

This is the value of c that is also derived in the discussion of the exponential scaling technique. Note that for $\ell n(b/a) << 1$ the exponent $c\tau$ is always small so that

$$M(\omega/c) \approx c\, e^{j\omega(\ell na - c^{-1})} \int_{-\infty}^{\infty} f(ac\tau) e^{j\omega\tau}\, d\tau \qquad \text{(B-74)}$$

and the exponential scaling becomes a linear time scaling. For a constant duration signal this occurs when a becomes approximately equal to b.

The exponential scaling technique assumes that the input to a chirp filter having an impulse response given by

$$IR = \cos(\omega_o(t-t_o) + \beta(t-t_o)^2 + \phi_o) \qquad \text{(B-75)}$$

over the time interval $t_o \leq t \leq t_o + T$ is given by

$$\text{INPUT} = f(t+a)\cos\omega(t) \tag{B-76}$$

where $f(t+a)$ exists over the interval $0 \leq t \leq b - a$. The desired output of the chirp filter will be assumed of the form

$$\text{OUTPUT} = A(t)f(ae^{c(t-t_d)}) \tag{B-77}$$

where t_d is some delay. The actual output over the interval $t_o + b - a \leq t \leq t_o + T$ is given by

$$\text{OUTPUT} = \text{Re} \int_{-\infty}^{\infty} f(\tau+a)e^{j\beta\mu(t,\tau)}d\tau \tag{B-78}$$

where

$$\mu(t,\tau) = \pm \frac{\omega(\tau)}{\beta} + \frac{\omega_o}{\beta}(t-\tau-t_o) + (t-\tau-t_o)^2 + \frac{\phi_o}{\beta} \tag{B-79}$$

The chirp filter slope, 2β, is typically very large ($> 10^{12}$) for SAW devices so that the method of stationary phase can be utilized to approximate the output. In particular, at any point in real time t, the function $\mu(t,\tau)$ will be forced to be stationary in τ at

$$\tau_c = a(\exp(c(t-t_d)) - 1) \tag{B-80}$$

If this is to be true then

$$\left.\frac{\partial\mu(t,\tau)}{\partial\tau}\right|_{\tau=\tau_c} = \mu'(t,\tau_c) = 0 \tag{B-81}$$

which, using Eq. (B-79), gives

$$\omega'(\tau_c) = \pm(\omega_o + 2\beta(t-\tau_c-t_o))$$

$$= \pm(\omega_o + 2\beta(c^{-1}\ell n(\tau_c+a) - c^{-1}\ell na + t_d - \tau_c - t_o)) \tag{B-82}$$

The function, $\omega(\tau)$, is therefore given by

$$\omega(\tau) = \pm \omega_o\tau \mp 2\beta\tau(c^{-1}\ell na - t_d + t_o) \mp \beta\tau^2$$

$$\pm 2\beta c^{-1}((\tau+a)\ell n(\tau+a) - \tau) + C \qquad (B-83)$$

where C is some constant. When this function is inserted into Eq. (B-79) and this into Eq. (B-78), one of the resulting integrals will be negligible compared to the other since it will have a much higher frequency variation. Therefore,

$$\omega(\tau) = \omega_o\tau - 2\beta\tau(c^{-1}\ell na - t_d + t_o) - \beta\tau^2$$

$$+ 2\beta c^{-1}((\tau+a)\ell n(\tau+a) - \tau) + C \qquad (B-84)$$

and

$$\mu(t,\tau) = 2c^{-1}(\tau+a)\ell n(\tau+a) - 2(c^{-1}(\ell na+1) - t_d + t)$$

$$+ (t-t_o)(t - t_o + \omega_o/\beta) + C/\beta \qquad (B-85)$$

The derivative of this function is given by

$$\mu'(t,\tau) = 2c^{-1}\ell n(\tau+a) - 2(c^{-1}\ell na - t_d + t) \qquad (B-86)$$

which equals zero for $\tau = \tau_c$, as it should.

For very large β, the functions $\mu(t,\tau)$ and $f(\tau+a)$, where $f(\tau+a)$ is assumed to vary more slowly that $\mu(t,\tau)$, can be expanded about the point τ_c, of stationary phase, as follows:

$$\mu(t,\tau) \approx \mu(\tau_c) + \frac{1}{2}\mu''(\tau_c)(\tau-\tau_c)^2 \qquad (B-87)$$

and

$$f(\tau+a) \approx f(\tau_c+a) = f(ae^{c(\tau-t_d)}) \qquad (B-88)$$

so that the output becomes

$$\text{OUTPUT} = \text{Re}\sqrt{\frac{2\pi}{\beta\mu''(t,\tau_c)}}\; e^{j(\beta\mu(t,\tau_c)+\frac{\pi}{4})}\; f(\tau_c+a) \tag{B-89}$$

Using the equations

$$\mu(t,\tau_c) = t^2 + (\omega_o/\beta - 2t_o + 2a)t - 2ac^{-1}\, e^{c(t-t_d)}$$

$$+ t_o^{\,2} - \omega_o t_o/\beta + 2ac^{-1}\ell na$$

$$- 2at_d - 2ac^{-1} + \phi_o/\beta + C/\beta \tag{B-90}$$

$$\mu''(t,\tau) = 2/(c(\tau+a))^{-1} \tag{B-91}$$

and

$$\mu''(t,\tau_c) = 2c^{-1}\exp(-\ell na - c(t-t_d)) \tag{B-92}$$

this becomes

$$\text{OUTPUT} = \sqrt{\frac{\pi c}{\beta}}\; e^{1/2(\ell na+c(t-t_d))}\, f(ae^{c(t-t_d)})\cos a(t) \tag{B-93}$$

where

$$a(t) = (\omega_o + 2\beta(a-t_o))t + \beta t^2 - 2\beta c^{-1}ae^{c(t-t_d)} + \phi_1 \tag{B-94}$$

and

$$\phi_1 = \beta t_o^{\,2} - \omega_o t_o + 2\beta c^{-1}a\ell na - 2\beta at_d - 2\beta c^{-1}a + \phi_o + C \tag{B-95}$$

Eq. (B-93) shows that the desired output can be obtained by multiplying this output by $(\beta/\pi C)^{1/2}\exp - 1/2(\ell na + c(t-t_d))$ and coherently detecting the envelope with a cosine having the phase variation given by Eq. (B-94) and constant phase given by Eq. (B-95) where C can be arbitrarily set to zero. The input signal f(t+a) is modulated by a cosine having the phase

variation given by Eq. (B-84). Since the entire valid output time interval should be utilized then

$$ae^{c(t-t_d)}\Big|_{t=t_o+b-a} = a \tag{B-96}$$

or

$$t_d = t_o + b - a \tag{B-97}$$

and

$$ae^{c(t-t_d)}\Big|_{t=t_o+T} = b \tag{B-98}$$

so that

$$c = \frac{\ell nb/a}{t-(b-a)} \tag{B-73}$$

as was previously specified. It should be noted that by following a similar procedure it is found that for an input given by

$$\text{INPUT} = f(t+a)\cos((\omega_o + 2\beta(t_d + a - t_o))t) \tag{B-99}$$

the output is given, using the stationary phase approximation, by

$$\text{OUTPUT} = \sqrt{\frac{\pi}{\beta}}\ f(t-t_d)\cos((\omega_o + 2\beta(t_d + a + t_o)t + \phi) \tag{B-100}$$

where

$$\phi = \beta t_o^2 - \beta t_d^2 - \beta a^2 - 2\beta a t_d - \omega_o t_o + \frac{\pi}{4} + \phi_o \tag{B-101}$$

For $t_d = t_o - a + t_D$, where t_D is some delay, then

$$\text{INPUT} = f(t+a)\cos((\omega_o+2\beta t_D)t) \tag{B-102}$$

and

$$\text{OUTPUT} = \sqrt{\frac{\pi}{\beta}}\ f(t + a - t_o - t_D)\cos(\omega_o+2\beta t_D)t + \phi) \tag{B-103}$$

Since the delay through a chirp filter is linearly proportional to frequency, by the chirp slope 2β, it can be seen from Eqs. (B-102) and (B-103) that the stationary phase approximation assumes that f(t) is a very narrowband signal (as Eq. (B-88) implies), otherwise the frequency components of this function will be greatly dispersed by the chirp filter, resulting in non-negligible distortion to this signal. Eq. (B-103) assumes that the signal is only delayed by the inherent delay of the chirp filter and the additional delay t_D that a component of frequency $2\beta t_D$ would have to undergo.